PREDICTING THE CYCLIC BEHAVIOR OF REINFORCED CONCRETE BEAMS

by

David L. Hanks
David Darwin
Steven L. McCabe

A Report on Research Sponsored by

THE NATIONAL SCIENCE FOUNDATION
Research Grant PFR 79-24696

and

THE UNIVERSITY OF KANSAS
General Research Fund Allocaions 3464-XO-0038 and 3064-XO-0038

UNIVERSITY OF KANSAS
LAWRENCE, KANSAS
March 1993

ABSTRACT

The effects of beam width on the cyclic behavior of reinforced concrete beam-to-column connections are investigated. A new procedure, which takes into consideration the influence of a member's strength, stiffness, and load history on cyclic performance, is developed to predict the number of cycles to failure and energy dissipation capacity per cycle in terms of beam design and load parameters. A parametric investigation is performed to quantify and evaluate the effect of changes in flexural and shear strength and geometry on the predicted number of cycles to failure.

Four lightly reinforced concrete cantilever beams, representing exterior beam-to-column connections in a moment resistant frame, were tested and compared to earlier tests to evaluate the effect of beam width on member response under severe cyclic loading. The overall dimensions of the specimens and the design strength of the columns were identical. The flexural reinforcement ratios of the beams were 0.34 or 0.51% and the maximum applied shear stress varied from 64 to 105 psi. The ratio of positive to negative moment beam reinforcement at the column face was 0.5 or 1.0. The size and spacing of the transverse reinforcement did not vary between specimens and provided a nominal stirrup shear capacity of 79 psi. The nominal concrete strength was 4,000 psi. The ratio of beam width-to-effective depth remained constant at 0.95.

Specimen response is evaluated based on the number of cycles to failure, energy dissipation capacity, and Energy Dissipation Index, D_i. Test results from the current study are compared to previous research results for narrow beams fabricated with the same reinforcement and subjected to the same load history. A rational procedure, based on a physical interpretation of the load-deflection hysteresis response of reinforced concrete beams, is developed to predict the number of cycles to failure and the energy dissipation capacity per cycle in terms of a beam's design and loading

parameters. A parametric investigation is performed to evaluate the effects of a change in flexural and shear strength and geometry on the predicted number of cycles to failure.

Based on the response of the beams investigated in the current study, an increase in the ratio of positive to negative moment reinforcement results in an increase in energy dissipated. For the wide beams with the same geometry and flexural and shear reinforcement, an increase in the displacement ductility factor decreases the number of cycles to failure and energy dissipation capacity.

A comparison of wide and narrow beam test results shows that an increase in width increases the number of cycles to failure and energy dissipation capacity.

An increase in the predicted number of cycles to failure is obtained with 1) a decrease in the maximum applied shear stress and root-mean-square displacement ductility factor, and 2) an increase in the nominal stirrup strength, ratio of positive to negative moment reinforcement, and ratio of beam width-to-stirrup spacing.

The findings of the parametric investigation show that, for the beam used in the case study, the least improvement in cyclic performance is obtained through an increase in concrete strength. The most effective means available to increase cyclic performance is to increase the amount of positive moment reinforcement within the hinging regions.

ACKNOWLEDGEMENTS

This report is based on a dissertation submitted by David L. Hanks to the Civil Engineering Department of the University of Kansas in partial fulfillment of the requirements for the PhD degree.

The research was supported by the National Science Foundation under NSF Grant No. PFR 79-24696 and the University of Kansas under General Research allocations No. 3464-XO-0038 and No. 3064-XO-0038. Sheffield Steel Corporation and Armco, Inc., donated the deformed bars and wire reinforcing steel, respectively.

Numerical calculations were performed on an Apollo DN 3500 workstation maintained by the Department of Civil Engineering at the University of Kansas.

TABLE OF CONTENTS

TABLE OF CONTENTS (continued)

LIST OF TABLES

LIST OF FIGURES

LIST OF FIGURES (continued)

Figures — Page

LIST OF FIGURES (continued)

Figures — Page

LIST OF FIGURES (continued)

LIST OF FIGURES (continued)

Figures — Page

LIST OF FIGURES (continued)

Figures — Page

LIST OF FIGURES (continued)

LIST OF FIGURES (continued)

Figures — Page

CHAPTER 1

INTRODUCTION

1.1 General

In regions of moderate to severe seismic loading, moment resistant frames designed with strong columns and weak beams dissipate seismic energy through the formation of plastic hinges in the beams. Tests of prototype beam-column connections indicate that the number of cycles to failure and the energy dissipated by the beam hinges are influenced by the maximum applied shear stress, stirrup spacing, ratio of positive to negative moment reinforcement, and concrete strength. Variations in test parameters, such as the amplitude of imposed displacement, have also been shown to affect hinge performance. Even though numerous studies have been undertaken to determine the influence of these parameters on member response, there is, to date, no consistent means with which to predict energy dissipation capacity or quantify hinge performance as a function of beam strength, stiffness, and load history.

The nonlinear cyclic response of a reinforced concrete frame subjected to earthquake excitations is highly dependent upon the parameters affecting the force-displacement relationship of the individual structural members. As seen from an experimental plot of load versus load-point deflection for a reinforced concrete beam (Fig. 1.1), the decrease in area bounded by each subsequent hysteresis loop indicates that a reduction in energy dissipation capacity and progressive hinge deterioration occurs with each cycle of load. Over the past twenty years, several measures of cyclic performance have been developed in an attempt to establish a relationship between the hysteretic response of reinforced concrete and the corresponding influence of design and test variables. These quantitative measures, or indices of cyclic performance, include the Energy Ratio (Brown & Jirsa 1971), the Work and Modified Work Index (Gosain, Brown & Jirsa 1977), the Normalized Energy Dissipation Ratio

(Scribner & Wight 1978, 1980), the Energy Index and Modified Energy Index (Hwang 1982), the Energy Dissipation Index (Nmai & Darwin 1984, 1986, Darwin & Nmai 1986, Hanks & Darwin 1988), and the Normalized Energy Index (Ehsani & Wight 1990). They are based upon the ductile behavior, or the energy dissipation capacity of a member, and represent a normalized form of cyclic performance that facilitates the comparison of results arising from specimens fabricated and tested with different parameters. Typically, these measures are plotted against a specified parameter, or combination of parameters, for reinforced concrete specimens subjected to severe inelastic loading. An evaluation of each design parameter's (i.e., independent variable) influence on the measure of cyclic performance (i.e., dependent variable) is based, in part, on a statistical analyses of available data. A reduction in the overall scatter of data relative to a best-fit line suggests an improved predictive capability of the parameters investigated (Fig. 1.2). Thus, member performance may be indirectly expressed in terms of the design and test parameters considered in the independent variable, provided there is reasonably good fit of the data.

More recently, analytic damage models have been developed as a means with which to predict the hysteretic response of reinforced concrete members (Banon, Biggs & Irvine 1981, Wang & Shah 1987, and Chung, Meyer & Shinozuka 1989). These models mathematically simulate the cyclic degradation in member strength and stiffness due to inelastic loading. Model formulation is based, in part, on the constitutive relationships for concrete and steel and "Takeda-type" hysteresis rules (Takeda, Sozen & Nielsen 1970) that specify the rate of change in pre- and post-yield stiffness. Reductions in member strength and stiffness are dependent upon the cumulative effect of inelastic deformations and experimentally determined modifiers and calibration factors. Damage, expressed as a function of selected specimen properties and response characteristics, is uniquely defined in each model. The use of these models to predict cyclic performance has been limited due to their complexity and inability to effectively express overall member response in terms of design and

test parameters.

Test results from studies that incorporate indirect measures of cyclic performance strongly indicate that the design parameter most significantly influencing cyclic performance is the maximum applied shear stress. Factors affecting the magnitude of shear stress include the effective depth, shear span, area of flexural reinforcement, and member width (Fig 1.3).

The influence of member width on the cyclic response of reinforced concrete has been recently investigated by Gentry & Wight (1992). Their research indicates that, for prototype beam-column connections, the ratio of beam width-to-column width (and the amount of flexural reinforcement anchored in the column) affects hinge performance. For specimens with ratios of beam width-to-column width greater than two, their findings show that a beams' ability to transmit forces to a column is dependent upon the torsional forces imposed upon the transverse beam in which part of the wide beams' longitudinal steel is anchored. However, the absence of test data for members with width-to-effective depth ratios near unity and fabricated with low amounts of flexural reinforcement limits the interpretative capabilities of existing correlations between measures of cyclic performance and the various beam parameters. A better understanding of the influence of beam width on cyclic performance is necessary to more accurately predict the nonlinear response of reinforced concrete members undergoing severe seismic loading.

1.2 Previous Work

The importance of maintaining adequate ductility in moment resistant reinforced concrete frames subjected to seismic forces is evident in current building code requirements (ACI 318-89, Recommended Lateral Force Requirements and Commentary 1980, and Uniform Building Code 1991). Progressive improvements in these design provisions have been the result of post-earthquake structural analysis and research directed at understanding the behavior of reinforced concrete members

undergoing severe inelastic cyclic loading. Several experimental investigations have been undertaken in an attempt to determine and quantify the influence of various parameters affecting cyclic performance. The majority of studies investigating the cyclic behavior of reinforced concrete involve test results of beam-to-column connections. These specimens typically represent an exterior beam-column subassembly in a moment resistant frame undergoing lateral displacements. Subassemblies are removed from the frame at column mid-height above and below the story and mid-span of the beam. The formation of plastic beam hinges in the structure is replicated by subjecting the free end of the cantilevered beam to repetitive cyclic loading. Numerous measures of cyclic performance have been developed in an effort to facilitate the determination of which factors, or design parameters, influence hinge response.

Existing measures of cyclic performance are generally a function of the cumulative energy dissipation capacity, as determined by the summation of the areas bounded by the load-deflection plot for the loading cycles. Numerous researchers have used energy dissipation as a means to indirectly evaluate the influence of different parameters on cyclic behavior (Brown & Jirsa 1971, Popov, Bertero & Krawinkler 1972, Bertero, Popov & Wang 1974, Ma, Bertero & Popov 1976, Gosain, Brown & Jirsa 1977, Scribner & Wight 1978 and 1980, Hwang 1982, Hwang & Scribner 1984, Nmai & Darwin 1984 and 1986, Darwin & Nmai 1986, Hanks & Darwin 1988, Ehsani & Wight 1990, Alameddine & Ehsani 1991). As discussed in the following paragraphs, results from several of these studies have provided significant insight as to which parameters affect the number of cycles to failure and influence the rate of hinge degradation.

Brown & Jirsa (1971) studied the cyclic inelastic response of twelve reinforced concrete beams to determine the influence of load history on strength, ductility, and failure mode. Cantilever beams with enlarged end blocks and flexural reinforcement ratios of 1.5 or 2.6% were fabricated with variable stirrup spacing and shear span.

Specimens were subjected to reversed cyclic loading corresponding to nominal beam-tip displacements of five or ten times the yield displacement. Deterioration and subsequent failure of the beams occurred along the interfaces of vertical and diagonal tension cracks. An evaluation of the load-deflection curves suggests that a reduced stirrup spacing provides additional confinement for the concrete, increases the number of cycles to failure, and improves energy dissipation capacity. A decrease in the shear span reduces the number of cycles to failure.

Brown & Jirsa developed the Energy Ratio as a means to predict the decrease in energy dissipation capacity with increased cyclic loading. They defined the Energy Ratio as the ratio of the area bounded by the experimental load-deflection curve to the area of an analytically computed curve for a member subjected to an identical deflection amplitude. Energy Ratios were calculated for specimens with the same flexural reinforcement, stirrup spacing, and shear span but subjected to different maximum displacements. For these specimens, the rate of degradation in the Energy Ratio shows that beams subjected to larger deflections decay and fail at a substantially faster rate. In addition, specimens with identical shear spans and tested to the same maximum displacement, but fabricated with smaller stirrup spacing, degrade at a slower rate and survive a larger number of cycles. Although the Energy Ratio provides a means to qualitatively evaluate the rate of decay in energy dissipation capacity, its use is limited. The lack of a means with which to calculate the actual energy dissipated per cycle prior to testing and the inability of the analytically computed load-deflection curves to model the effects of shear deformation restricts the "predictive" capabilities of the Energy Ratio.

Gosain, Brown & Jirsa (1977) analyzed the test results from six studies, representing sixty-five specimens. Primary test variables included the percentage of flexural and transverse reinforcement, stirrup spacing, level of axial load, and load history. In an effort to evaluate the shear requirements of hinging regions, they developed an index that provides a comparison of test results for specimens subjected

to different load histories. The index is based upon the work done, or energy dissipated by the member, and is normalized with respect to the load and deflection at first yielding of the longitudinal reinforcement, P_y and Δ_y, respectively. The Work Index I_w, is expressed as

$$I_w = \sum_{i=1}^{n} \left(\frac{P_i}{P_y}\right)\left(\frac{\Delta_i}{\Delta_y}\right) \tag{1.1}$$

in which P_i represents the maximum load during the i'th cycle and Δ_i is the displacement corresponding to P_i. The summation of terms in Eq. 1.1 is for all cycles in which $P_i \geq 0.75P_y$. The value of 0.75 was selected to ensure that I_w is representative of a member with substantial remaining energy dissipation capacity. Gosain, Brown & Jirsa observed that the ratio P_i/P_y is usually between 0.75 and 1.25 and could be approximated as 1.0. This simplification reduces the Work Index to the product of the number of cycles times the deflection ratio Δ_i/Δ_y for all cycles with $P_i \geq 0.75P_y$. Hence, I_w is calculated as

$$I_w = \sum_{i=1}^{n} \left(\frac{\Delta_i}{\Delta_y}\right) \tag{1.2}$$

I_w represents a normalized measure of energy dissipated in the hinging zone for specimens subjected to varying load schedules. Larger values of I_w reflect improvements in cyclic performance. The influence of load history on hinge performance was evaluated using plots of I_w versus the percentage of transverse reinforcement $\rho_w = A_v/(b_c s)$ (in which A_v = area of transverse reinforcement, b_c = concrete core width, and s = stirrup spacing), the measured ultimate shear stress normalized with respect to concrete strength $v_u/\sqrt{f'_c}$ [$v_u = V_m/(b_c d_c)$ (in which V_m = maximum shear force, d_c = concrete core depth)], and the ratio of stirrup capacity to maximum applied shear V_s/V_m [$V_s = (A_v f_y d_c)/s$ (in which f_y = stirrup yield strength)].

An evaluation of these plots suggests that there is no definitive relationship between ρ_w and I_w, specimens with lower ultimate shear stress produce higher values of I_w, and as the ratio V_s/V_m increases, I_w increases. Even though the calculation of I_w in accordance with Eq. 1.2 reflects variations in beam-tip displacement, the actual shape of the load-deflection curve, and thus energy dissipated, is not addressed and limits the use of I_w as a quantitative measure of cyclic performance. For example, at advanced stages of hinge degradation, the calculation of I_w does not reflect the true influence of shear deformation and subsequent reduction in energy dissipation due to pinching of the load-deflection hysteresis loops. Recognizing this limitation, Gosain, Brown & Jirsa (1977) improved the predictive capability of I_w by taking into consideration the influence of shear span and axial load on the load-deflection curve and thus the Work Index. This lead to the development of the Modified Work Index I'_w, which is calculated as

$$I'_w = I_w \left(1 - \frac{d_c}{a}\right)\left(1 + \frac{0.0005N}{A_{core}}\right) \tag{1.3}$$

in which a = shear span, N = axial load, and A_{core} = concrete core area. A plot of I'_w versus $v_u/\sqrt{f'_c}$ (Fig. 1.4) suggests a linear correlation between the two variables, with I'_w decreasing as $v_u/\sqrt{f'_c}$ increases, and shows much less scatter than a similar plot of I_w versus $v_u/\sqrt{f'_c}$. Although the fit of data is considerably better with I'_w than with I_w (i.e., Eq. 1.2), the results still exhibit significant scatter when using $v_u/\sqrt{f'_c}$ to predict cyclic performance. For example, at a shear stress of $6\sqrt{f'_c}$, the best-fit line for all sixty-five data points analyzed by Gosain et al. indicates a predicted value for I'_w of 37. However, the experimental spread in I'_w at $6\sqrt{f'_c}$ ranges from 16 to 340 and thus, limits the quantitative interpretation of test results.

Scribner & Wight (1978, 1980) investigated the influence of intermediate longitudinal reinforcement (i.e., flexural reinforcement placed near mid-depth on the beam perimeter) on reducing shear strength decay. Fourteen specimens (Scribner &

Wight 1980), representing beam-column subassemblies, were subjected to large scale reversed cyclic loading. Specimens were tested to different magnitudes of beam-tip deflection in the positive and negative directions. The overall loading history reflects a displacement ductility factor μ (defined as the ratio of maximum load-point displacement to yield displacement), of +4 and -3 for six cycles followed by +6 and -5 for six additional cycles. Termination of the test prior to the specified number of inelastic displacement cycles occurred when the specimen lost its load resisting capacity due to buckling of the compression reinforcement.

Scribner & Wight observed that specimens without intermediate reinforcement, and subjected to a shear stress of less than $3\sqrt{f'_c}$, respond in a ductile manner and do not suffer substantial shear strength deterioration. The addition of intermediate reinforcement does not significantly improve member performance for these specimens. For a shear stress between $3\sqrt{f'_c}$ and $6\sqrt{f'_c}$, beams with intermediate reinforcement dissipate an average of 27% more energy than specimens without intermediate reinforcement. Specimens with a shear stress greater than $6\sqrt{f'_c}$ suffer severe strength and stiffness deterioration. However, members with intermediate reinforcement dissipate 30% more energy than those containing only vertical shear reinforcement. The increase in energy dissipated by beams with intermediate reinforcement is attributed to the uniform distribution of cracks and restraint to crack opening throughout the hinging zone provided by the intermediate reinforcement.

To eliminate the influence of strength and size on specimen performance, Scribner & Wight developed the Normalized Energy Dissipation Ratio. This measure is defined as the ratio of "total" energy dissipated for all cycles to the energy dissipated during the first cycle. The parameter found to most significantly influence the Normalized Energy Dissipation Ratio is the maximum shear stress, $V_u/(bd)$ (in which V_u = maximum shear force, b and d = member width and effective depth, respectively). They observed that a plot of the Normalized Energy Dissipation Ratio versus the reciprocal of maximum shear stress, normalized with respect to $\sqrt{f'_c}$ (i.e.,

$\sqrt{f'_c}/v_u$) (Fig. 1.5), strongly indicates that cyclic performance is improved through 1) the inclusion of intermediate longitudinal reinforcement, and 2) a reduction in the maximum applied shear stress. Specimens with a reduced shear stress degrade at a slower rate and survive more cycles. The best-fit lines for specimens with and without intermediate reinforcement shown on the plot of the Normalized Energy Dissipation Ratio versus $\sqrt{f'_c}/v_u$ indicates that cyclic performance is better predicted by $\sqrt{f'_c}/v_u$ for the members with intermediate reinforcement than those without intermediate reinforcement. The inability to predetermine the energy dissipated by a member during the first cycle of loading restricts use of the Normalized Energy Dissipation Ratio as a predictive tool.

Hwang (1982) and Hwang & Scribner (1984) studied the influence of shear stress and variations in load history on the cyclic response of reinforced concrete flexural members. Eleven cantilever beams were fabricated and tested to facilitate the understanding of the relationship between load history and energy dissipation capacity. Identically reinforced specimens were subjected to four separate load histories. Magnitudes of beam tip displacement were 2% or 4% of the beam shear span. These percentages were chosen to represent displacements corresponding to specific values of story drift. Test results from beams subjected to alternating cycles of deflection amplitude (... two cycles at 2% followed by two cycles at 4% ...) were used to study the effect of loading sequence on member response. Testing terminated when a specimen lost its load resisting capability. Hwang & Scribner evaluated member behavior based on the number of cycles in which the maximum load was greater than 75% of the yield load (i.e., $P_i \geq 0.75P_y$), degree of shear deformation in the hinging zone, and energy dissipation capacity. They concluded that hinge degradation is dependent upon the magnitude of the applied shear stress and imposed displacement. Specimens subjected to a larger magnitude of displacement and higher shear stress decay at a faster rate, survive fewer cycles to failure, and dissipate less energy. Overall member response, as determined by the number of cycles where $P_i \geq 0.75P_y$,

is not significantly influenced by the sequence with which the alternating displacements are applied. Hwang (1982) developed the Energy Index I_E to evaluate the cyclic performance of specimens subjected to different load histories, stiffness degradation, and shear stress. The Energy Index is defined as

$$I_E = \sum_{i=1}^{n} E_i \left(\frac{K_i}{K_y}\right)\left(\frac{\Delta_i}{\Delta_y}\right)^2 = \sum_{i=1}^{n} \frac{E_i\ (P_i\Delta_i)}{(P_y\Delta_y)} \qquad (1.4)$$

in which n = number of cycles with $P_i \geq 0.75P_y$, E_i = energy dissipated during the i'th cycle, K_i/K_y = ratio of (P_i/Δ_i) to (P_y/Δ_y), P_i = maximum load in negative bending during the i'th cycle, Δ_i = displacement corresponding to P_i during the i'th cycle, and Δ_y = yield displacement. As a result of the limited range of load histories tested, Hwang included in the analysis results from the research by Lee, Hanson & Wight (1976) (8 specimens) and Scribner & Wight (1978) (12 specimens) as a test of the Energy Index's ability to predict cyclic performance. I_E was plotted against the maximum shear stress normalized with respect to concrete strength (i.e., $v_m/\sqrt{f'_c}$), the ratio of the stirrup shear capacity to the maximum applied shear V_s/V_m [$V_s = (A_v f_y d)/s$ in which A_v = area of transverse reinforcement, f_y = stirrup yield strength, d = effective depth, and s = stirrup spacing], and the ratio of shear span to effective depth, a/d. An overall evaluation of these plots indicates that improved cyclic performance is obtained with a lower shear stress and increased ratios of V_s/V_m and a/d. Even though Hwang concluded that the modifying term $P_i\Delta_i/P_y\Delta_y$ in Eq. 1.4 "compensated" for the effect of specimens with different displacement histories, the scatter of data relative to the best-fit line suggests that the correlation between I_E and the parameters investigated is qualitative at best.

Recognizing the influence of shear span and effective depth on the maximum shear stress, Hwang also proposed a Modified Energy Index, I'_E, defined as

$$I_E' = I_E \left(1 - \frac{d}{a}\right) \tag{1.5}$$

which provides a slightly improved fit of the data as compared to I_E. However, the correlation between I_E' and the parameter $v_m/\sqrt{f_c'}$ still exhibits significant scatter (Fig. 1.6). At a maximum shear stress of $6\sqrt{f_c'}$, the predicted value of I_E' based on the best-fit line is 780. The experimental spread of I_E' for the actual test results at $6\sqrt{f_c'}$ ranges from 380 to 2290 and suggests a qualitative interpretation of test results.

Nmai & Darwin (1984, 1986) tested seven lightly reinforced concrete beams to determine the affect of low amounts of flexural reinforcement on cyclic behavior. Test variables included the flexural reinforcement ratio, ρ, ratio of positive to negative reinforcement, A_s'/A_s, and stirrup spacing, s. Specimens were subjected to a constant displacement ductility factor, μ, ranging from 3.9 to 5.3. Testing terminated when the maximum load within a cycle P_i, dropped below 50% of the yield load, P_y, or when the longitudinal reinforcement fractured. Member performance was primarily based upon the summation of energy dissipated for all cycles in which $P_i \geq 0.75P_y$. Nmai & Darwin found that larger reinforcement ratios increase the maximum shear stress and therefore reduce the number of cycles to failure, and decrease energy dissipation. They also observed that an increase in A_s'/A_s increases the positive bending moment capacity, delays spalling of the compressed concrete, and increases energy dissipation capacity. A reduced stirrup spacing improves confinement of the concrete core, delays buckling of the compression reinforcement, and increases dissipated energy. Increases in the number of cycles to failure are obtained with reduced values of μ. Nmai & Darwin developed the Energy Dissipation Index as a measure of cyclic performance for specimens with different geometries, strengths, and load histories. The Energy Dissipation Index is defined as the energy dissipated by the specimen, normalized with respect to the elastic energy just prior to yielding for an equivalent full span beam, and is calculated as

$$D_i = \frac{\sum_{i=1}^{n} E_i}{\frac{1}{2} P_y \Delta_y \left[1 + \left(\frac{A_s'}{A_s} \right)^2 \right]} \tag{1.6}$$

in which n = number of cycles with $P_i \geq 0.75P_y$, and E_i = energy dissipated during the i'th cycle. The overall evaluation of D_i included data obtained from five additional studies, representing a total of forty-six specimens. A linear regression analysis was performed on data from twenty-six selected specimens from four of the six studies. A plot of D_i versus $[(v_s f_c')^{0.5}(v_m)^{-1.5}]$ (in which v_s = nominal stirrup strength, f_c' = concrete strength, and v_m = maximum applied shear stress) for the twenty-six specimens (Fig. 1.7) shows that improvements in cyclic performance are obtained by increasing v_s and f_c', and decreasing v_m. Darwin & Nmai (1986) suggested that, in terms of improving cyclic performance, it is more efficient to increase member width than increase transverse reinforcement. Darwin & Nmai also concluded that beams designed for D_i of at least 35 (corresponding to $v_u \approx 4.6\sqrt{f_c'}$ and $\phi V_s = V_u$, where v_u = maximum shear stress, V_s = nominal shear strength provided by shear reinforcement, V_u = factored shear force, and ϕ = strength reduction factor) would be able to sustain a minimum of five complete inelastic load cycles with $P_i \geq 0.75P_y$ and $3.9 \leq \mu \leq 6.0$. As compared to previous studies, the overall reduction in scatter of data relative to a best-fit line is obtained with $[(v_s f_c')^{0.5}(v_m)^{-1.5}]$. At a value of 0.25 for $[(v_s f_c')^{0.5}(v_m)^{-1.5}]$ (corresponding to $v_s / v_m = 1.0$ and $v_m / \sqrt{f_c'} = 4.0$), the best-fit predicted value of D_i is 38. The corresponding experimental spread for D_i ranges from approximately 20 to 55. Provided D_i is an accurate measure of cyclic performance, $[(v_s f_c')^{0.5}(v_m)^{-1.5}]$ appears to be a viable means for predicting inelastic response as function of the specified design parameters.

Hanks & Darwin (1988) investigated the effect of high strength concrete on the cyclic response of lightly reinforced beams. Four beam-to-column connections,

similar in design and detail to those tested by Nmai & Darwin (1984, 1986), were constructed with concrete strengths of approximately 12,000 psi. Specimens were subjected to a constant displacement ductility factor of five ($\mu = 5$) until fracture of the longitudinal beam reinforcement occurred or the maximum load within a cycle, P_i, dropped below 50% of the yield load, P_y. The influence of concrete strength on cyclic performance was based, in part, on a comparison of results from Hanks & Darwin's research to the normal concrete strength test results of Nmai & Darwin (1984, 1986). For beams with similar geometry, reinforcement and load history, Hanks & Darwin concluded that as the concrete strength increases, energy dissipation capacity also increases, and thus cyclic performance improves. The increase in energy dissipation capacity results from the fact that high strength concrete is subjected to a lower percentage of its compressive strength for a given steel percentage, and therefore degrades less rapidly under cyclic loading. High strength concrete appears to be more effective at dissipating energy as the reinforcement ratio increases.

In an effort to quantify the influence of concrete strength on cyclic performance, Hanks & Darwin performed a statistical analysis of the twenty-six specimens evaluated in Nmai & Darwin's study and the four specimens from their research. Based on an exponentially optimized correlation (Hanks & Darwin 1988) between D_i and the product of v_s, f'_c, & v_m (i.e., D_i versus $[(v_s)^{0.95}(f'_c)^{-0.01}(v_m)^{-2.02}]$), and the subsequent exponential influence of f'_c, they concluded that existing experimental results do not provide representative or sufficient test data over the full range of v_s, f'_c, and v_m, and additional parameters must be considered in the independent variable to adequately interpret the quantitative influence of v_s, f'_c, and v_m on cyclic performance. To improve the correlation of data and more accurately address the influence of stirrup spacing and beam width on member response, they developed and used the confinement ratio C_r (defined as the ratio of confined concrete volume between adjacent stirrups to the core volume) in subsequent analyses. An improved quantitative determination of the influence of concrete strength on cyclic

performance and reduction in scatter for the thirty test specimens relative to a best-fit line was obtained when the width to depth ratio, b/d, and C_r were added to the analysis. A plot of D_i versus the exponentially optimized products of v_s, f'_c, b/d, C_r, & v_m (i.e., $[(v_s)^{0.50}(f'_c)^{0.14}(b/d)^{0.47}(C_r)^{0.95}(v_m)^{-1.58}]$) (Fig. 1.8) indicates that, as observed in other studies, the maximum applied shear stress dominates cyclic performance. Concrete strength also influences performance, but to a much lesser degree than v_s, b/d, C_r, or v_m. As compared to the statistical analysis performed by Nmai & Darwin (Fig. 1.7), additional reductions in the overall scatter of data were obtained by Hanks & Darwin when using $[(v_s)^{0.50}(f'_c)^{0.14}(b/d)^{0.47}(C_r)^{0.95}(v_m)^{-1.58}]$ to predict member response (Fig. 1.8). At a value of 0.0051 for $[(v_s)^{0.50}(f'_c)^{0.14}(b/d)^{0.47}(C_r)^{0.95}(v_m)^{-1.58}]$ (corresponding to $v_s/v_m = 1.0$, $v_m/\sqrt{f'_c} = 4.0$, $f'_c = 4{,}000$ psi, b/d = 0.75, and $C_r = 0.71$), the predicted value of D_i based on the best-fit line is 50. The experimental spread for D_i at the same magnitude of $[(v_s)^{0.50}(f'_c)^{0.14}(b/d)^{0.47}(C_r)^{0.95}(v_m)^{-1.58}]$ ranges from 40 to 65. Hanks & Darwin concluded that the Energy Dissipation Index, D_i, provides a consistent measure of cyclic performance based on the range and number of parameters investigated.

Ehsani & Wight (1990) recognized the importance of maintaining ductile behavior in reinforced concrete frames subjected to severe lateral loading. Their research considered beam-column subassemblies under cyclic loading in which plastic hinges formed within the beam-to-column (joint) connection. Test results from eight studies (40 specimens) were investigated to further understand and predict joint response. They observed that variations in specimen size and scale could affect the interpretation of hinge performance when using the Energy Index I_E (Hwang 1982). In an effort to provide a non-dimensionalized measure of cyclic performance, they normalized I_E (Eq. 1.4) with respect to the yield load, P_y, and the yield displacement, Δ_y. The Normalized Energy Index I_{EN} is expressed as

$$I_{EN} = \sum_{i=1}^{n} \frac{E_i}{P_y \Delta_y} \left(\frac{K_i}{K_y}\right)\left(\frac{\Delta_i}{\Delta_y}\right)^2 = \sum_{i=1}^{n} \frac{E_i\,(P_i \Delta_i)}{(P_y \Delta_y)^2} \qquad (1.7)$$

in which n = number of cycles with $P_i \geq 0.75P_y$, E_i = energy dissipated during the i'th cycle, K_i/K_y = ratio of (P_i/Δ_i) to (P_y/Δ_y), P_i = maximum load in negative bending during the i'th cycle, Δ_i = displacement corresponding to P_i, and Δ_y = yield displacement. Based on a plot of I_{EN} versus joint shear stress (i.e., shear stress in the joint resulting from the nominal strengths of the members framing into the column) normalized with respect to $\sqrt{f'_c}$ and the subsequent evaluation of all forty specimens, Ehsani & Wight proposed a minimum acceptable lower limit of 60 for I_{EN}. They "inferred" from their analysis that a specimen having an I_{EN} of 60 or greater would possess sufficient ductility to satisfy the intent of recommendations made by ACI-ASCE Committee 352 (1985). Even though Ehsani & Wight discussed specimen performance as a function of the 1) flexural strength ratio, M_R (defined as the ratio of the flexural capacity of the columns to the flexural capacity of the beams at the intersection of a beam-column joint), 2) joint shear stress, 3) percentage of joint transverse reinforcement, 4) anchorage of longitudinal bars, 5) ratio of the beam tension and compression reinforcement, and 6) severity of loading, only the parameters of joint shear stress and concrete strength were used in the correlation of I_{EN} to member performance. The effect of too few parameters is readily observed when joint shear stress, expressed as a multiple of $\sqrt{f'_c}$, is used to predict I_{EN} (Fig. 1.9). For seventeen of the forty specimens, which represent members with $1.0 \leq M_R \leq 2.5$, the best-fit predicted value of I_{EN} at $8.8\sqrt{f'_c}$ is 280. The experimental spread of I_{EN} corresponding to a joint shear stress of $8.8\sqrt{f'_c}$ ranges from 60 to 640. Such a wide dispersion of data relative to a best-fit line makes the evaluation of member performance more qualitative than quantitative.

1.3 Evaluation of Previous Work

Existing measures of cyclic performance incorporate energy dissipation as a means to develop a correlation between member response and the various design parameters. Test results indicate that improvements in energy dissipation capacity and cyclic performance are obtained with (1) a decrease in shear stress, stirrup spacing, and displacement ductility factor, and (2) an increase in the ratio of positive to negative reinforcement, and concrete strength. Studies using indirect measures of cyclic performance clearly show that shear stress dominates cyclic behavior. Additional tests, investigating the effect of beam width on shear stress, may contribute to an improved correlation between measures of cyclic performance and the various design parameters.

A review of previous research indicates that the inclusion of several parameters in the statistical analysis of available data affects the quantitative interpretation of each parameter's influence on cyclic response (Hanks & Darwin 1988). The lack of a sufficient number of parameters in the independent variable to effectively model cyclic performance contributes to the scatter of test data relative to a best-fit line. These "latent" parameters (Draper & Smith 1981) severely restrict the interpretation of results. The research by Brown & Jirsa (1971), Hwang (1982), Hwang & Scribner (1984), and Nmai & Darwin (1984 and 1986) indicates that the amplitude of beam-tip displacement and the displacement ductility factor affects member response. Thus, it is reasonable to expect that the displacement ductility factor is a parameter that provides a viable contribution to the reduction of scatter in test data (i.e., an improvement in the prediction of cyclic performance). One additional factor that affects cumulative energy dissipation, and thus cyclic performance, is the number of cycles to failure. To date, the inability to predict the number of cycles to failure represents a common factor in the previous studies that inhibits both the development of an improved method for estimating energy dissipation capacity and more accurately predicting cyclic performance in concrete structures.

1.4 Object and Scope

The purpose of this study is to determine the effect of beam width on cyclic response and develop an improved procedure for predicting the nonlinear response of reinforced concrete beams subjected to severe inelastic loading. An experimental investigation is undertaken to supplement existing test results and gain further insight into the influence of beam width on cyclic performance. Four lightly reinforced concrete cantilever beams, representing exterior beam-to-column connections in a moment resistant frame undergoing inelastic cyclic loading, are fabricated and tested. The specimens have flexural reinforcement ratios of 0.34% and 0.51% and constant nominal effective depths and widths of 15.7 in. and 15 in., respectively. All beams are identical with respect to the overall subassembly dimensions. The displacement history reflects a constant cyclic beam-tip deflection, ranging from 4.3 to 8.5 of the yield deflection, throughout the tests. Specimen performance is evaluated based upon the number of cycles to failure and the energy dissipation capacity. The Energy Dissipation Index D_i is used to quantify and evaluate cyclic response.

Test results from this study, and those of other researchers, form the basis for a statistical analysis to predict the number of cycles to failure for specimens fabricated with varying strengths, geometric properties, and load histories. A rational procedure, based on a physical interpretation of the load-deflection hysteresis loops, is presented to predict the overall cyclic behavior of reinforced concrete beams. Recommendations are made for improving the cyclic performance of reinforced concrete members subjected to severe inelastic loading.

CHAPTER 2

EXPERIMENTAL INVESTIGATION

2.1 General

The influence of shear stress on the energy dissipation capacity and cyclic performance of reinforced concrete has been reported by many researchers (Bertero, Popov & Wang 1974, Ma, Bertero & Popov 1976, Gosain, Brown & Jirsa 1977, Scribner & Wight 1978, 1980, Hwang 1982, Hwang & Scribner 1984, Nmai & Darwin 1984, 1986, Darwin & Nmai 1986, Hanks & Darwin 1988, Alameddine & Ehsani 1989, 1991, and Ehsani & Wight 1990). These investigations show that beams subjected to lower levels of maximum applied shear stress respond in a ductile manner, survive more cycles to failure, and dissipate more energy than those specimens with a higher shear stress. Decreases in shear stress also postpone, or significantly reduce, the amount of shear deformation at advanced stages of hinge degradation. Excessive shear deformation results in pronounced pinching of load-deflection curves, a reduction in load resisting capability, and a substantial decrease in energy dissipation capacity. Delays in hinge degradation for specimens with relatively large magnitudes of shear stress and shear deformation are obtained by increasing the area of transverse reinforcement, decreasing the stirrup spacing, and increasing the concrete strength.

Although not specifically studied, analysis of existing test data (Nmai & Darwin 1984, Darwin & Nmai 1986, and Hanks & Darwin 1988) strongly indicate that improvements in hinge performance may be achieved by increasing member width. Specimens with a fixed amount of flexural steel and larger widths would be expected to exhibit improved cyclic behavior due to a reduction in both shear stress and compressive stress in the concrete. Lower levels of compressive stress reduce the rate of hinge degradation, improve confinement, and delay buckling of the

compression reinforcement. Thus, increased beam widths could contribute to an increase in the number of cycles to failure and energy dissipation capacity. For a given amount of flexural and shear reinforcement, increased widths also facilitate concrete placement.

The purpose of the experimental portion of this study was to fabricate and test four lightly reinforced concrete beams constructed with a width to depth ratio, b/d, near unity. The results from the experimental investigation are used in conjunction with those from previous research to determine the influence of beam width on energy dissipation capacity and inelastic response.

2.2 Test Specimens

For obvious reasons, experimental results from full-scale reinforced concrete structures subjected to earthquake-type loading cannot be economically obtained. Therefore, most research related to the cyclic behavior of reinforced concrete structures has been performed using specimens that represent beam-to-column connections in moment resisting frames. Idealized beam-column subassemblies consist of monolithically cast cantilever beams and column-stubs. Cyclic inelastic loading of the beam tip simulates member response under seismic loading. For specimens designed in accordance with the strong column-weak beam philosophy, the application of imposed displacement results in the formation of a plastic hinge in the beam, adjacent to the column face.

For this study, four lightly reinforced concrete specimens, representing an exterior beam-column subassembly, were fabricated and tested (Fig. 2.1). Reinforcement was designed and placed in accordance with ACI Committee 318 (1983). Specimens were cast in a vertical position to duplicate actual construction practice. The overall dimensions of the column were identical to those used by Nmai & Darwin (1984) and Hanks & Darwin (1988). The negative moment reinforcement ratio in the beam was 0.34% (Beams H-1, H-3 and H-4) or 0.51% (Beam H-2). The

nominal beam height, width, and shear span were 18, 15, and 60 in. respectively. Concrete compressive strength ranged from 4060 to 4400 psi. The displacement ductility factor, μ, defined as the ratio of maximum beam tip displacement to yield displacement, was constant during each test. The maximum applied shear stress, v_m, ranged from $0.99\sqrt{f'_c}$ to $1.58\sqrt{f'_c}$ in the four tests.

The negative moment reinforcement, A_s (top steel), consisted of two layers of #4 bars. The positive moment reinforcement, A'_s (bottom steel) also consisted of #4 bars and was placed in one layer for Beams H-1, H-2, & H-3 and two layers for Beam H-4. The beam flexural reinforcement was welded to a 3/4 x 13 x 16 in. bearing plate to prevent anchorage failure within the column (Fig. 2.1).

Transverse beam reinforcement was fabricated using smooth rods and welded to form a closed hoop. The first stirrup in all specimens was placed 1 in. from the vertical face of the column; subsequent stirrups were uniformly spaced at 3-5/8 in.. Three additional stirrups, fabricated using #3 bars and formed into a closed hoop, were continued at the same spacing into the column. A summary of the beam and reinforcement dimensions is presented in Table 2.1.

2.3 Materials

2.3.1 Reinforcement

Flexural reinforcement in the cantilever beams was fabricated from #4 deformed bars. A representative stress-strain curve for the #4 bars is presented in Fig. 2.2. The column reinforcement was fabricated using four #8 bars and four #6 bars as longitudinal reinforcement, and #3 bars as closed ties. The amount and spacing of column reinforcement was identical in all four specimens. Placement of the beam and column reinforcement is shown in Fig. 2.1.

Beam stirrups were fabricated from 7/32 in. nominal diameter smooth rod. 60 in. lengths were cut from a coil, straightened, and preyielded with a 2000 lb. maximum force to obtain a well-defined yield strength. A stress-strain curve for the

transverse reinforcement is shown in Fig. 2.3. Approximately four inches of smooth rod was overlapped and welded to form a closed hoop. The welded overlap was placed on the top of the reinforcing cage for all specimens.

2.3.2 Concrete

Concrete made with Type I portland cement, river sand and 3/4 in. nominal maximum size crushed limestone was supplied by a local ready-mix concrete plant. 1.5 cubic yards was purchased for each specimen's construction. Approximately twenty-four 6 x 12 in. concrete test cylinders were cast in steel molds, cured adjacent to the specimen, and tested periodically to monitor the concrete's strength gain for each test specimen. At least three test cylinders were used to determine concrete strength at the time of testing. Concrete mix proportions and properties are shown in Table 2.2.

2.4 Specimen Fabrication

Specimen fabrication procedures were similar to those employed by Nmai & Darwin (1984) and Hanks & Darwin (1988). Formwork for the 15 x 28 x 60 in. column (Fig. 2.1) and the cantilever beam support had been fabricated by Nmai & Darwin (1984). Modifications to the formwork to accommodate the 15 in. wide beam were made with Class I, 3/4 in. American Plywood Association grade B-B Plyform and 2 x 4 timber studs, joists, and wales. Form ties in the beam and column were fabricated from 3/8 and 1/4 in. diameter all-thread rod, respectively. Clear lacquer was applied to the Plyform to reduce moisture penetration and facilitate form removal. In addition, a form release agent was applied to the Plyform prior to installation of the assembled reinforcing cage.

Rigid metal bar supports were used to maintain the 1.0 and 1.5 in. nominal concrete cover in the beam and column, respectively. Each specimen was cast in a vertical position. Concrete was placed in maximum lifts of 9 in. in the beam and 12 in. in the column. The concrete was consolidated using a 1.5 in. flexible shaft

internal vibrator. When the level of concrete coincided with the top of the beam, placement was temporarily halted. The concrete in the beam was then screeded, floated, and covered with Plyform. The Plyform was secured to prevent concrete displacement in the beam due to the further addition of concrete in the column. At the conclusion of concrete placement, the specimen and test cylinders were covered with polyethylene. The formwork was removed within forty-eight hours and the specimen and cylinders were subsequently moist cured with wet burlap. When the test cylinders attained a compressive strength of approximately 3400 psi, the specimen was attached to a reusable column-stub (Fig. 2.4). A total post-tensioning force of 160 kips was used to connect the two columns together. The cantilever beam tip was then positioned beneath a hydraulic actuator and the entire assembly was post-tensioned to the structural floor with a total force of 200 kips (Fig. 2.5(a) & 2.5(b)). Diluted latex paint was applied to the specimen, and the location of the flexural and shear reinforcement was drawn on the vertical face of the beam. The beam tip was continuously supported until the start of testing.

2.5 Instrumentation

Twelve Micro-Measurements EA-06-060LZ-120 Option E electrical resistance foil gages were used to measure strains in the longitudinal and transverse beam reinforcement. For the beam flexural reinforcement, deformations in an area 1/2 in. long and 1/4 in. wide were filed smooth to permit bonding of the foil gage to the reinforcement. Surface filing was not required for the 7/32 in. nominal diameter smooth rod used as beam stirrups. Micro-Measurements M-Coat J was applied to the strain gages and adjacent reinforcement to prevent mechanical damage and provide a waterproof coating. Surface, gage, and leadwire preparation and installation were performed in accordance with Micro-Measurements Instruction Bulletins B-127-10 (Micro-Measurements 1979) and B-147-1 (Micro-Measurements 1986). Prior to concrete placement, all gages were tested to verify circuitry resistance. The relative

locations of the strain gages (Fig. 2.6) were identical to that used by Nmai & Darwin (1984) and Hanks & Darwin (1988).

Schaevitz DC-operated linear variable differential transformers (LVDT's) were used to control displacement of the beam tip, measure shear deformation in the hinging region, determine flexural rotation of the beam relative to the column, and measure rigid body rotation of the column-stub relative to the structural floor. A standard laboratory dial gage was positioned at the end of the cantilever to measure the change in beam length. The locations of the LVDT's and dial gage are shown in Fig. 2.7.

An MTS 110 kip capacity, 10 in. stroke actuator with a closed-loop servo-hydraulic control system applied the load to the beam tip. LVDT #1 (Fig. 2.7) provided the feedback signal for the MTS control system.

A potentiometric X-Y recorder provided a continuous plot of the actuator load versus beam tip displacement (LVDT #1). Strain gage, LVDT, and load cell output voltages were monitored and recorded using a Hewlett-Packard 3054 Data Acquisition System, which consisted of a 3456A Voltmeter, a 3497A Control Unit, and a 9825T calculator.

2.6 Test Procedures

Prior to testing, LVDT #1 was connected to the point of load application. The hydraulic actuator head was then bolted to the specimen. A uniform bearing surface between the actuator assembly and specimen was obtained using high strength gypsum cement (Hydrostone). After securing the actuator to the beam tip, the specimen was subjected to a 1 kip downward preload to verify instrumentation and then unloaded. Next the beam tip was displaced in the downward direction (corresponding to negative load and negative displacement) until a well-defined yield point was established based on the plot on the X-Y recorder. The specimen was then returned to the point of initial displacement and the servo-hydraulic control system was set to provide a

constant maximum beam-tip displacement. A representative displacement history is shown in Fig. 2.8.

Testing was terminated when the maximum load within a given cycle was less than 75% of the yield load, and (1) fracture of a positive moment reinforcing bar (bottom steel) occurred (Beams H-2 and H-3) or, (2) the specimen was subjected to 21 cycles (arbitrary cut off — no significant reduction was observed in load resisting capability compared to previous cycles) (Beams H-1 and H-4). All tests were terminated at the end of a full cycle.

At periodic intervals, testing was temporarily halted and recordings of strain, displacement, and load voltage outputs were made. An average of 30 data recordings were made for each cycle. The elapsed time to complete each of the first three cycles was approximately 30 minutes. After three cycles, cracking within the beam hinging zone was well-established; and the load rate was then doubled. Subsequent cycles took about 15 minutes to complete. Cracks were marked on the beam and column during each cycle at points of zero load. The maximum load obtained during the determination of the yield load and displacement and the load corresponding to the maximum negative displacement obtained during the first quarter of cycle #1 were also marked on the beam. Photographs of the hinging zone were taken at the end of each full cycle.

2.7 Test Results

The relationship between load and deflection provides a primary means to evaluate member performance. For specimens subjected to a constant maximum displacement amplitude, these plots reflect the rate of change in specimen strength and stiffness. Pinching of the load-deflection curve near the point of zero displacement indicates a reduction in shear stiffness. The area bounded by the load-deflection plot equals the energy dissipated by the specimen and is the principal measure of a specimen's ability to withstand cyclic loading. Figs. 2.9(a) - 2.9(d) show the

relationship between load and load-point deflection (LVDT #1) for each specimen throughout the test. A plot of load versus deflection, at a point equal to the effective beam depth from the column face (LVDT #2), is presented in Figs. 2.10(a) - 2.10(d).

Procedures used to calculate the magnitude of shear deformation and flexural rotation are presented in Appendix B. The relationships between load and flexural rotation in the region extending 1.0d from the column face (LVDT's #7 & #8) are presented in Figs. 2.11(a) - 2.11(d) for the four beams. Similarly, plots of load versus shear deformation extending 1.0d (LVDT's #3 & #4), and 1.0d to 2.0d (LVDT's #5 & #6) from the column face, are shown in Figs. 2.12(a) - 2.12(d) and Figs. 2.13(a) - 2.13(d), respectively. Rigid body rotation of the column, on the average, accounted for 2% of the total beam-tip deflection. Figs. 2.14(a) - 2.14(d) are plots of load versus rotation of the column-stub relative to the structural floor (LVDT's #9 & #10). The maximum rotation of the column-stub for Beams H-2, H-3, & H-4, ranged from −0.0002 to +0.0003 radians. In contrast, rotations in excess of +0.005 radians were measured for Beam H-1 (Fig. 2.14(a)). The measured rotations for Beam H-1 were the result of excessive LVDT movement (LVDT's #9 & #10) caused by splitting in the concrete cover of the column and therefore are not an accurate representation of the column rotation generated by the imposed beam-tip displacement.

Extensive cracking and splitting of the concrete and buckling of the longitudinal and transverse reinforcement within the beam hinging region resulted in failure of the strain gage circuitry prior to test termination. Plots of beam-tip load versus strain in the longitudinal beam reinforcement within the column (Gages #5 & #6) for the first five cycles for Beam H-1 are shown in Figs. 2.15(a) & 2.15(b). Similar plots of the first seven cycles for Beam H-4 are shown in Figs. 2.16(a) & 2.16(b). Representative plots of load versus strain for the transverse reinforcement (Gages #11 & #12) in Beam H-4 are presented in Figs. 2.17(a) & 2.17(b).

The computed and measured shears and principal experimental results are summarized in Tables 2.3 and 2.4.

2.8 Specimen Behavior

2.8.1 General

Initially, the beam tip was displaced in the downward (negative) direction to determine the yield load and the yield displacement. During this phase of loading, the application of the imposed displacement produced cracking in the concrete. Distinct, well-defined flexure cracks formed in the upper portion of the beam. In all specimens, one flexure crack formed at the beam-column interface. The remainder of the cracks were located in an area extending 1.0d from the column face (d is the effective beam depth in negative bending). The flexure cracks were perpendicular to the longitudinal beam axis and traversed the entire width. Further displacement required to determine the yield properties resulted in the development of flexure-shear cracks along the sides of the beam. Flexure-shear cracks adjacent to the first stirrup were nearly vertical and became more inclined with increased distance from the column. The majority of the flexure-shear cracks terminated near beam mid-height. Application of the initial downward displacement also produced near vertical tension cracks in the column adjacent to the upper and lower surface of the beam.

After determination of the yield load and deflection and upon reloading during the first quarter of cycle #1, displacements in excess of the yield deflection contributed to the formation of additional flexure cracks in the upper portion of the beam. At the maximum downward displacement, a uniform grid of flexure cracks developed. This pattern of cracking extended 1.0d from the column face. Flexure-shear cracks on the sides of the beam, and located within 1.0d of the column, terminated at the compression reinforcement. Flexure-shear cracks located in a region 1.0d to 1.5d from the column face, terminated near beam mid-height. At the maximum positive displacement during the cycle #1, flexure cracks formed in the lower portion of the beam within a region extending 1.0d from the column face. Diagonal flexure-shear cracks projected upward and terminated when they intersected existing cracks. Flexure-shear cracks located closer to the column were more vertical

than those nearer the beam tip. As a result of yielding of the negative moment reinforcement, cracks that had opened during determination of the yield load (downward displacement) failed to close completely when the load was reversed (upward displacement).

By the end of cycle #1, flexure and flexure-shear cracks were predominantly located in the region that extended 1.0d from the face of the column. The higher number and width of cracks in this region, relative to the remainder of the beam, delineated the plastic hinging zone. Cracks extended throughout the entire depth of the beam. Flexure-shear cracks located 1.0d from the column face were oriented at 45° with respect to the longitudinal beam axis. In the hinging zone, large uncracked blocks of concrete were present near the mid-height of the beam, while closely spaced cracks were present in the area adjacent to the flexural reinforcement. Vertical tension cracks developed in the column around the entire beam perimeter. The severity of cracking within the hinging zone appeared to be dependent upon the magnitude of the maximum applied shear stress.

The negative and positive displacements imposed during cycle #2 did not significantly contribute to the formation of new cracks. Existing crack widths decreased with increased distance from the column due to the reduction in applied moment and corresponding flexural stress. By the end of cycle #3, some spalling occurred at the intersection of the beam and column in the area adjacent to the lower flexural reinforcement.

During the remaining cycles, abrading and grinding of the concrete resulted in spalling along the flexure-shear cracks. The spalled concrete was primarily located near mid-height of the beam and within the hinging zone. Continued cycling resulted in additional cracking and spalling of the lower flexural reinforcement cover. Progressive buckling of the flexural reinforcement contributed to concrete spalling.

At the termination of the test, a fine grid of cracked concrete was present in the hinging zone adjacent to the positive and negative reinforcement. Spalling on the

lateral beam face was more severe in the region between the first and second stirrups. The following sections describe the individual behavior of each specimen in more detail:

2.8.2 Beam H-1 ($\rho = 0.34\%$, $b = 15$ in., $A_s = 0.8$ in.^{2}, $A_s' = 0.4$ in.^{2}, $v_m = 64$ psi, $v_s/v_m = 1.27$, $v_m/\sqrt{f_c'} = 0.99$, $\mu = 4.3$)

Compared to the other beams, this specimen had the smallest maximum applied shear stress, v_m, the largest ratio of nominal stirrup strength to maximum applied shear stress, v_s/v_m, and the smallest displacement ductility factor, μ.

Prior to testing, Beam H-1 developed shrinkage cracks on the lateral face (i.e., the face parallel to the longitudinal beam axis) of the column. The cracks propagated horizontally from all four beam corners. The imposed peak negative (downward) displacement during cycle #1 produced several primary flexure-shear cracks in the hinging zone. Cracks located between the first and second stirrup were nearly vertical. One primary flexure-shear crack, located 1.0d from the column face, was inclined with respect to the flexural reinforcement. This crack was centered on the fourth stirrup and terminated at the compression (bottom) reinforcement. In addition, one inclined flexure-shear crack developed 1.5d from the column face and terminated near beam mid-height. Vertical tension cracks were present in the column adjacent to the upper surface and sides of the beam (Fig. 2.18(a)).

At the peak positive (upward) displacement during cycle #1, additional flexure and flexure-shear cracks formed in the hinging zone. These cracks propagated upward from the lower surface of the beam and terminated upon intersection with existing cracks. Flexure-shear cracks closer to the column face were more vertically oriented than those nearer the beam-tip. As a result of yielding of the compression reinforcement during the maximum positive displacement, one primary crack was present at the end of cycle #1. This crack was approximately 1/8 in. in width and located on the side of the beam between the first and second stirrup, near the lower surface (Fig. 2.18(b)).

Continued inelastic cycling resulted in concrete spalling on the sides of the beam within the hinging zone. Spalling was primarily located along the interface of the flexure-shear cracks which developed between the first and second stirrups (Fig. 2.18(c)). Progressive spalling also continued on the longitudinal column face in the region adjacent to the lower surface of the beam.

During cycle #10, extensive spalling exposed the lower flexural reinforcement for a distance extending 0.25d from the column face. After cycle #12, the rate of decay in peak negative load appeared to decrease with additional inelastic cycling (Fig. 2.9(a)). Subsequent displacement reversals produced minor spalling above the lower flexural reinforcement. Buckling of the lower flexural reinforcement, between the first and second stirrup, occurred in cycle #17.

Even though this specimen maintained its load resisting capability, the test was terminated at the end of cycle #21. Damage appeared to be concentrated in the region surrounding the first stirrup and the lower flexural reinforcement. Between the second and third stirrup, a relatively large uncracked block of concrete remained intact at the conclusion of testing (Fig. 2.18(c)). Cracking within the beam was confined to a distance extending 1.5d from the column face. Although spalling occurred on the longitudinal column face (the face normal to the longitudinal beam axis) near the beam's lower flexural reinforcement, the column ties were not exposed.

2.8.3 Beam H-2 ($\rho = 0.51\%$, $b = 15$ in., $A_s = 1.2$ in.^{2}, $A_s' = 0.6$ in.^{2}, $v_m = 105$ psi, $v_s/v_m = 0.75$, $v_m/\sqrt{f_c'} = 1.58$, $\mu = 5.3$)

Beam H-2 was fabricated with 50% more negative moment reinforcement than the other three beams and 50% more positive reinforcement than Beams H-1 and H-3. This specimen had the largest maximum applied shear stress, v_m, and the smallest ratio of nominal stirrup strength to maximum applied shear stress, v_s/v_m.

During the application of the initial displacement to determine the yield load and displacement, flexure cracks formed in the upper portion of the beam over a distance extending 0.75d from the column face. In addition, one vertical flexure-shear

crack developed between the second and third stirrup. It extended from the upper surface of the beam to just above the compression reinforcement. At the maximum negative displacement in the first quarter of cycle #1, several flexure and flexure-shear cracks were present within the hinging zone. Flexure-shear cracks terminated near beam mid-height. Tension cracks were present on the lateral face of the column and extended above the upper surface of the beam (Fig. 2.19(a)).

By the end of cycle #1, a grid of intersecting flexure-shear cracks had developed over a region extending 1.0d from the column face. Cracks projected upward from the lower surface of the beam and terminated when they intersected existing cracks. Flexure-shear cracks on the sides of the beam were more vertically oriented when located closer to the column (Fig. 2.19(b)).

Spalling on the lower surface of the beam, near the first stirrup, occurred in cycle #2. Cyclic loading resulted in grinding along the flexure-shear cracks. The severity of spalling within the hinging zone increased with additional cycling. Crack widths increased as a result of abrasion along the crack interfaces. By the end of cycle #5, spalling on the sides of the beam was concentrated near mid-height, between the second and third stirrup. In cycle #6, the concrete cover spalled and exposed the lower flexural reinforcement for a distance extending 0.25d from the column face. By the end of cycle #7, the lower flexural reinforcement was exposed for a distance extending 0.75d from the column face. Concrete on the sides of the beam, between the third and fourth stirrup, spalled 0.25d up from the lower surface of the beam.

Buckling of the lower flexural reinforcement, between the second and third stirrup, occurred during cycle #8. At the end of cycle #9, spalling on the side of the beam had expanded upward 0.5d and was concentrated between the second and third stirrups. Continued cycling resulted in additional spalling of the concrete and pronounced buckling of the lower flexural reinforcement (Fig. 2.19(c)). In cycle #13, the lower flexural reinforcement fractured between the second and third stirrup, and the test was terminated.

2.8.4 Beam H-3 ($\rho = 0.34\%$, $b = 15$ in., $A_s = 0.8$ in.^{2}, $A_s' = 0.4$ in.^{2}, $v_m = 74$ psi, $v_s/v_m = 1.04$, $v_m/\sqrt{f_c'} = 1.15$, $\mu = 8.5$)

The negative moment reinforcement for this specimen was identical to Beam H-1 & H-4. Beam H-3 was subjected to the largest beam-tip deflection (Table 2.4) and displacement ductility factor, μ.

During determination of the yield load and displacement, one primary flexure-shear crack developed between the third and fourth stirrup. The crack was nearly vertical and terminated 0.75d below the upper surface of the beam. At the maximum negative displacement during the first quarter of cycle #1, this crack became inclined, propagated toward the compression reinforcement, and terminated below the first stirrup. In addition, other flexure-shear cracks developed over a region extending 1.5d from the column face. These flexure-shear cracks were inclined and oriented at 45° with respect to the longitudinal reinforcement. Vertical tension cracks developed in the column adjacent to the beam top and sides (Fig. 2.20(a)).

During the application of the maximum positive displacement of cycle #1, flexure-shear cracks developed and projected upward from the lower surface of the beam. These cracks appeared to be concentrated in the region adjacent to the third stirrup. The severity of the imposed positive displacement resulted in substantial cracking of the lower flexural reinforcement cover over a region extending 1.0d from the column face. At the end of cycle #1, a fine grid of closely spaced cracks formed in the hinging zone adjacent to the flexural reinforcement. Vertical tension cracks developed in the column around the beam perimeter (Fig. 2.20(b)). Fig. 2.20(c) (far side of the beam, adjacent to LVDT's #3 & #4) illustrates the full extent of the cracking over the depth and width of the hinging zone.

During cycle #2, splitting and spalling developed on the column corners directly beneath the beam. In addition, substantial spalling on the beam's sides and lower surface occurred between the third and fourth stirrup. Spalling projected upward 0.5d from the lower surface of the beam and exposed the lower flexural

reinforcement.

At the maximum positive displacement in cycle #3, increased spalling exposed the lower flexural reinforcement in the region extending 0.25d from the column face. Large uncracked blocks of concrete remained intact in the area adjacent to the second and third stirrups near beam mid-height. At the start of cycle #4, buckling of the bottom reinforcement occurred between the first and second stirrups. By the end of cycle #4, the lower flexural reinforcement was exposed for a distance extending 0.75d from the column face. The spalled concrete in this region projected upward 0.25d from the lower surface of the beam.

Testing was terminated at the end of cycle #5 (Fig. 2.20(d)) due to fatigue and fracture of the lower flexural reinforcement between the first and second stirrup.

2.8.5 Beam H-4 ($\rho = 0.34\%$, $b = 15$ in., $A_s = 0.8$ in.^{2}, $A'_s = 0.8$ in.^{2}, $v_m = 71$ psi, $v_s/v_m = 1.08$, $v_m/\sqrt{f'_c} = 1.11$, $\mu = 4.7$)

Beam H-4 was fabricated with the same negative reinforcement as Beams H-1 & H-3, but constructed with equal amounts of positive and negative moment reinforcement.

Two primary shear cracks developed in the hinging zone during application of the yield displacement. The first shear crack was nearly vertical and centered on the second stirrup. The second shear crack was inclined and located between the fourth and fifth stirrups. Both cracks started 0.25d below the upper surface of the beam and terminated at the lower layer of compression reinforcement. Vertical tension cracks were present in the lateral column face adjacent to the beam side. At the peak negative displacement in the first quarter of cycle #1, flexure-shear cracks in the beam were concentrated in a region extending 0.25d from the column face. Inclined flexure-shear cracks terminated at the compression reinforcement. Cracks located closer to the column were more vertically oriented than those nearer the beam tip. A fine grid of cracks was present in the area adjacent to the tension reinforcement and extended 0.75d from the column. At a distance of 2.0d from the

column face, a separate group of flexure-shear and shear cracks was present.

At the maximum positive displacement in cycle #1, flexure-shear cracks propagated upward from the lower surface of the beam. The majority of these cracks formed in a region extending 0.75d from the column face and terminated when they intersected an existing crack. In addition, one shear crack, near beam mid-height, had developed beyond the hinging zone (Fig. 2.21(a)).

At the end of cycle #1, a fine grid of closely spaced cracks had formed adjacent to the flexural reinforcement. Large uncracked blocks of concrete were present in the hinging zone. Shear cracks further from the column were oriented at 45° with respect to the longitudinal beam reinforcement.

Continued cycling resulted in abrading of the flexure-shear cracks and contributed to spalling on the beam's lateral face. Movement along the concrete interfaces appeared to be more prominent between the second and third stirrup at beam mid-height. By the end of cycle #6, cracking over the entire beam depth was concentrated in the region extending 0.5d from the column. Spalling in cycle #6 exposed the lower layer of positive moment reinforcement from the column face to the second stirrup. Vertical tension cracks in the column were present in the area adjacent to the beam perimeter. During cycle #12, spalling on the lateral beam face exposed both layers of the lower flexural reinforcement. The spalled concrete extended 0.25d upward from the lower surface of the beam (Fig. 2.21(b)).

Buckling of bars in the lower layer of the positive moment reinforcement, between the first and second stirrup, occurred in cycle #14. By the end of cycle #15, spalling had exposed the second stirrup over the entire beam depth. Spalling within the hinging zone was primarily concentrated on the sides of the beam, adjacent to the positive and negative moment reinforcement. Spalling occurred over a distance extending 0.25d from the column face. By the end of cycle #18, buckling occurred in both layers of the positive and negative moment reinforcement. Spalling and buckling was most prominent between the first and second stirrup.

Although there was no significant reduction in the positive and negative load resisting capacity during cycles #20 and #21, testing was terminated at the end of cycle #21. Within the hinging zone, large uncracked blocks of concrete were present near beam mid-height, while substantial cracking occurred in the area surrounding the positive and negative moment reinforcement. Beam H-4 exhibited substantially greater cracking [Figs. 2.21(c) & 2.21(d)] than Beam H-1 [Fig. 2.18(b)] which had the same negative moment reinforcement but 50% less positive moment reinforcement. In cycle #21, the peak negative loads for Beams H-4 & H-1 were 9.1 and 8.1 kips, respectively. The apparent severity of cracking in Beam H-4 may be due, in part, to the increase in positive moment reinforcement and subsequent corresponding increase in positive bending shear stress. The increase in positive moment reinforcement for Beam H-4 also results in a higher compressive force during negative bending and thus, may contribute to the larger peak negative load.

CHAPTER 3

DISCUSSION AND EVALUATION OF TEST RESULTS

3.1 General

Reinforced concrete structures designed to resist earthquakes must possess a sufficient amount of energy dissipation capacity to meet the applied energy demand. In moment resistant frames, energy dissipation primarily occurs through the inelastic deformation of the lateral force resisting elements. These deformations should occur within beams, rather than columns, if the overall stability of the structure is to be maintained throughout the duration of an earthquake. The seismic design of reinforced concrete structures must reflect an understanding of the demands that will be placed upon the structure.

For moment resistant concrete frames undergoing lateral loading, beam elements are subjected to high stresses near their supports. Current ACI design provisions (ACI 318-89 - Chapter 21) reduce the possibility of sudden beam shear failures in regions of high stress by establishing minimum detailing requirements. These provisions are aimed at improving confinement of the flexural reinforcement and concrete where the formation of a plastic hinge is likely to occur. To achieve this, the ACI code requires that transverse reinforcement, in the form of closed or overlapping hoops, be provided over a distance equal to twice the beam's effective depth, measured from the face of the support. In the hinging regions, the maximum hoop spacing must not to exceed 1) one-fourth of the effective depth of the beam, 2) eight times the diameter of the smallest longitudinal bar, 3) twenty-four times the hoop diameter, or 4) 12 in.. These requirements are intended to maintain the integrity of the beam hinge throughout the earthquake oscillations and compensate for an inability to accurately determine the ductility demand imposed upon the member. The inclusion of these provisions in the ACI code is based on field and laboratory

experience and is meant to provide a minimum acceptable level of cyclic performance.

Test results from several experimental studies suggest that shear stress significantly influences, or dominates, the inelastic response of reinforced concrete beams undergoing reversed cyclic loading (Bertero, Popov & Wang 1974, Ma, Bertero & Popov 1976, Gosain, Brown & Jirsa 1977, Scribner & Wight 1978 and 1980, Hwang 1982, Hwang & Scribner 1984, Nmai & Darwin 1984 and 1986, Darwin & Nmai 1986, Hanks & Darwin 1988). Test specimens with increased magnitudes of shear stress exhibit 1) an increase in the amount of shear deformation, and 2) a decrease in load carrying capacity, number of cycles to failure, and energy dissipation capacity. These observations are valid over a wide range of shear stress for members with different flexural reinforcing ratios, ρ, and shear span-to-effective depth ratios, a/d. Some researchers (Darwin & Nmai 1986, and Hanks & Darwin 1988) have suggested that improvements in cyclic performance are possible with an increase in beam width, because greater widths reduce the magnitude of the shear stress and potentially increase the confinement of the core concrete. Improved confinement delays buckling of the compression reinforcement, and thus, decreases the rate of hinge degradation. While test results reflecting a relatively wide range of flexural reinforcement and shear span-to-effective depth ratios are available, the effect of beam width on cyclic behavior has received little attention.

Attempts to quantify the influence of shear stress on the inelastic behavior of reinforced concrete have been primarily based upon statistical analyses of test data that use various measures of cyclic performance (Brown & Jirsa 1977, Scribner & Wight 1978 and 1980, Hwang 1982, Nmai & Darwin 1984 and 1986, Darwin & Nmai 1986, Hanks & Darwin 1988, Ehsani & Wight 1990). These measures are related to the energy dissipated by the specimen and represent the experimental response of the members undergoing repetitive inelastic loading. Increased measures of cyclic performance indicate improved inelastic behavior. Parameters, such as the maximum shear stress, are used to "predict" the experimental response of the member. For

example, specimens with lower amounts of shear stress have been shown to dissipate more energy, and thus, exhibit improved cyclic response. Therefore, shear stress is a parameter that indirectly predicts cyclic performance. Typically, the choice of which parameters to use in the prediction of member response is based on an evaluation of a plot representing the correlation between a dependent variable (i.e., measure of cyclic performance) and the independent variable [i.e., parameter(s)]. The resulting scatter of data points relative to a best-fit line, provides one means with which to evaluate the relationship between the dependent and independent variables investigated. This allows the measure of cyclic performance to be expressed in terms of a specimen's design parameters, provided there is reasonably good fit of the data.

Results from experimental studies have also shown that, in addition to shear stress, parameters such as the displacement ductility factor, μ, stirrup spacing, s, ratio of positive to negative moment reinforcement, A'_s/A_s, and concrete strength, f'_c, influence the nonlinear response of reinforced concrete (Brown & Jirsa 1971, Bertero, Popov & Wang 1974, Ma, Bertero & Popov 1976, Nmai & Darwin 1986, Darwin & Nmai 1986, and Hanks & Darwin 1988). For example, specimens with a reduced stirrup spacing dissipate more energy than those with a larger spacing due to the increase in concrete confinement. In addition, a reduced stirrup spacing delays buckling of the compression reinforcement which also increases the energy dissipation capacity of the member. For a member undergoing negative bending, an increase in the ratio of positive to negative reinforcement reduces the concrete compressive stress, delays concrete spalling, increases the number of cycles to failure, and, subsequently, increases the member's energy dissipation capacity for each cycle of loading. Specimens fabricated with increased concrete strengths also dissipate more energy than those with lower concrete strengths, since higher strength concretes are subjected to a lower percentage of their compressive strength for a given steel percentage and thus survive more cycles until failure.

Results from statistical analyses which correlate measures of cyclic

performance with specimen parameters are highly dependent upon the choice of which measure is used to quantify experimental response. Previous research, by Nmai & Darwin (1984 and 1986), Darwin & Nmai (1986), and Hanks & Darwin (1988), indicates that one measure of cyclic performance that provides a reasonably consistent correlation between test results and a relatively wide range of parameters is the Energy Dissipation Index, D_i. D_i represents a normalized form of energy dissipation capacity and provides a non-dimensionalized basis for comparing the test results of specimens with different strengths, stiffnesses, and load histories.

The purpose of this experimental investigation was to determine the influence of beam width on cyclic response. In addition, the results from this study, which represent specimens fabricated with low amounts of flexural reinforcement and relatively large widths, will be used to evaluate the effect of the displacement ductility factor and ratio of positive to negative moment reinforcement on cyclic response. The Energy Dissipation Index is used to quantify experimental results and correlate test data to selected beam parameters. A statistical analysis of results from this research program and those of other studies (Wight & Sozen 1973, Scribner & Wight 1976, Hwang 1982, Hwang & Scribner 1984, Nmai & Darwin 1984 and 1986, Darwin & Nmai 1986, and Hanks & Darwin 1988) is performed to more accurately quantify the influence of beam width on the cyclic behavior of reinforced concrete.

3.2 Energy Dissipation

A comparison of dissipated energy is one means with which to evaluate the influence of width on the cyclic response of reinforced concrete beams. For cantilevered specimens, the energy dissipation capacity is readily determined by summing the area enclosed by the load versus load-point displacement hysteresis loops for all applicable load cycles. Factors affecting the energy dissipation capacity include the maximum displacement amplitude, the member strength, and the number of cycles to failure. An increase in the energy dissipation capacity of a member

implies improved cyclic performance. At advanced stages of hinge degradation, "pinching" of the load-deflection loops near the point of zero displacement suggests an increase in the amount of shear deformation and a reduction in the energy dissipation capacity. From a design perspective, the selection of parameters that postpone buckling of the compression reinforcement, maintain the integrity of the concrete core, and decrease the amount of shear deformation provides a means to improve the earthquake resistance of the structure.

The effect of beam width on cyclic response may be determined by comparing the energy dissipation capacity of beams fabricated with different widths, provided that the test specimens 1) have the same load history (i.e., similar displacement ductility factor, μ, which is defined as the ratio of the maximum beam-tip displacement to the yield displacement), 2) have similar flexural and concrete strengths, effective depths, stirrup spacing, and 3) there exists a consistent method to quantify failure. Several studies (Gosain, Brown & Jirsa 1977, Scribner & Wight 1978 and 1980, Hwang 1982, Hwang & Scribner 1984, Nmai & Darwin 1984 and 1986, Darwin & Nmai 1986, and Hanks & Darwin 1988) have defined "failure" as the point at which the maximum load, P_i, for a given hysteresis loop is less than 75% of the yield load, P_y. Subsequently, the energy dissipated per cycle is summed for all cycles with $P_i \geq 0.75P_y$ and represents the energy dissipation capacity, E, of the member.

The influence of member width on cyclic response can be evaluated by comparing the energy dissipation capacities, E, of two specimens from this study (i.e., Beams H-1 & H-2) with two specimens tested by Nmai & Darwin (1984, 1986) (i.e., Beams F-3 & F-2). Beams H-1 and F-3 were fabricated with widths of 15 in. and 7.5 in., respectively. Beam H-1 (μ = 4.3, A_s' = 2#4, A_s = 4#4, f_c' = 4200 psi, d = 15.69 in., s = 3.6 in., and E = 245 kip-in.) dissipated 18% more energy than Beam F-3 (μ = 4.4, A_s' = 2#4, A_s = 4#4, f_c' = 4260 psi, d = 15.38 in., s = 3.8 in., and E = 208 kip-in.). The increase in E for Beam H-1 is directly attributed to the 100% increase in

member width. Beams H-2 and F-2 were also fabricated with widths of 15 in. and 7.5 in., respectively. A comparison of the energy dissipated by Beam H-2 (μ = 5.3, A_s' = 3#4, A_s = 6#4, f_c' = 4400 psi, d = 15.81 in., s = 3.6 in., and E = 315 kip-in.) and Beam F-2 (μ = 5.1, A_s' = 3#4, A_s = 6#4, f_c' = 4220 psi, d = 15.38 in., s = 3.8 in., and E = 184 kip-in.) shows that the 71% increase in E is the result of the larger width for Beam H-2.

Beams H-1 and H-2 were subjected to only 50% of the shear stress of Beams F-3 and F-2, respectively, and provided more confinement for the concrete core than did the narrower beams. These two factors resulted in reduced shear deformation and delayed buckling of the bottom reinforcement, which, in turn, contributed to an increase in the number of cycles to failure, n, and the energy dissipation capacity, E. Graphically, the improvement in cyclic performance for the wide beams can be seen in a plot of the cumulative energy dissipated per cycle versus the number of cycles to failure. Such a plot for Beams F-2, H-2, F-3, and H-1 is presented in Fig. 3.1. For beams with similar effective depths, flexural strength, and load history, this figure shows that an increase in width (and a corresponding reduction in shear stress) results in a decrease in the energy dissipated per load cycle, but, an increase in n. The net effect of the increase in the number of cycles to failure is an increase in energy dissipation capacity, E, for the wide beams.

The 4 specimens shown in Fig. 3.1 represent two values of flexural strength (i.e., A_s = 6#4 & A_s' = 3#4 for Beams F-2 and H-2 and A_s = 4#4 & A_s' = 2#4 for Beams F-3 and H-1). The relationship between energy dissipation capacity and flexural strength for Beams F-2 & H-2 and Beams F-3 & H-1 strongly suggests that an increase in width is more effective in improving cyclic performance as the amount of beam reinforcement increases.

The beneficial influence of an increase in member width on energy dissipation capacity may also be seen in a plot of the energy dissipation capacity, E, versus the maximum applied shear stress in negative bending, v_m, for Beams H-1, H-2, F-2, and

F-3. Fig. 3.2 graphically depicts the decrease in E accompanying an increase in v_m from 105 psi for Beam H-2 to 215 psi for Beam F-2 and an increase in v_m from 64 psi for Beam H-1 to 145 psi for Beam F-3. The negative slope of the lines for Beams H-2 & F-2 and H-1 & F-3 represents the reduction in E due to a decrease in member width and subsequent increase in v_m.

Although Fig. 3.2 illustrates the adverse influence of shear stress on energy dissipation capacity, shear stress by itself, is clearly not a reliable indicator of member response. A comparison of E for Beams F-2 (v_m = 215 psi) and F-3 (v_m = 145 psi) indicates that a reduction in v_m results in an increase in E, while a comparison of E for Beams H-2 (v_m = 105 psi) and H-1 (v_m = 64 psi) shows a reduction in E even though v_m is reduced substantially. Thus, additional considerations are needed to develop a consistent correlation of the data.

Some further insight into the effects of the displacement ductility factor, μ, and the ratio of positive to negative moment reinforcement, A_s'/A_s, on cyclic response may be gained by considering the test results for Beams H-3 and H-4 (like H-1 and H-2, fabricated with widths of 15 in.). A comparison of the energy dissipated by Beams H-3 (μ = 8.5, A_s' = 2#4, A_s = 4#4, f_c' = 4120 psi, d = 15.63 in., s = 3.6 in., and E = 178 kip-in.) and H-1 (E = 245 kip-in.) shows that the 98% increase in μ decreased the energy dissipated by 27% and decreased the number of cycles to failure by 69%. The net effect of the increase in μ for Beam H-3 was a reduction in both the energy dissipation capacity and the number of cycles to failure (n = 4 for Beam H-3 and n = 13 for Beam H-1). Similarly, the test results for Beams H-4 (μ = 4.7, A_s' = 4#4, A_s = 4#4, f_c' = 4060 psi, d = 15.75 in., s = 3.6 in., and E = 507 kip-in.) and H-1 show that an increase in A_s'/A_s from 0.5 to 1.0 resulted in a 107% increase in E and a 31% increase in n (n = 17 for Beam H-4).

3.3 Energy Dissipation Index, D_i

3.3.1 Background

A number of researchers (Gosain, Brown & Jirsa 1977, Scribner & Wight 1978 and 1980, Hwang 1982, Nmai & Darwin 1984 and 1986, Darwin & Nmai 1986, Hanks & Darwin 1988, and Ehsani & Wight 1990) have developed measures of cyclic response that normalize a member's energy dissipation capacity with respect to the member's elastic energy at initial yield (e.g., the product of P_y and Δ_y). The advantage of using elastic energy can be explained in terms of the energy demand imposed upon the member. For a given displacement ductility factor, members with increased moment capacities dissipate more energy during the first load cycle. However, this increase in energy dissipation is offset by a proportional increase in shear force. Thus, the energy demand is greater in members with increased moment capacities. Using a normalized form of the energy dissipation capacity allows the cyclic performance of members with different flexural strengths to be compared.

As previously discussed, one measure of cyclic performance which provides a consistent means to evaluate the influence of different design and test parameters on cyclic response is the Energy Dissipation Index, D_i (Nmai & Darwin 1984, 1986). The development of D_i was based on a statistical analysis of selected test results from six experimental studies (Wight & Sozen 1973, Bertero, Popov & Wang 1974, Ma, Bertero & Popov 1976, Scribner & Wight 1978, Hwang & Scribner 1984, and Nmai & Darwin 1984). Nmai & Darwin (1984 and 1986) and Darwin & Nmai (1986) observed that D_i was significantly influenced by the 1) nominal stirrup strength, v_s [$v_s = A_v f_{vy}/(bs)$, A_v = total cross-sectional area of shear reinforcement, f_{vy} = yield strength of shear reinforcement, b = beam width, and s = stirrup spacing], 2) concrete strength, f'_c, and 3) maximum applied shear stress, v_m [$v_m = V_m/(bd)$, V_m = maximum shear force and d = effective beam depth in negative bending]. An analysis of test results from Wight & Sozen (1973), Scribner & Wight (1978), Hwang & Scribner (1984), and Nmai & Darwin (1984) indicates that D_i is reasonably well predicted by

v_s, f'_c, and v_m when expressed in the form $[(v_s f'_c)^{0.5}(v_m)^{-1.5}]$. Hanks & Darwin (1988) obtained an improved fit of experimental data by comparing their test results for high strength concrete specimens (11310 psi $\leq f'_c \leq$ 12860 psi) with the results for the normal concrete strength specimens (3750 psi $\leq f'_c \leq$ 5880 psi) analyzed by Nmai & Darwin (1984, 1986) and Darwin & Nmai (1986) and correlating the values of D_i with $(v_s)^{0.50}(f'_c)^{0.14}(b/d)^{0.47}(C_r)^{0.95}(v_m)^{-1.58}$ (C_r is defined as the ratio of confined concrete volume between adjacent stirrups to the core volume). They concluded that $(v_s)^{0.50}(f'_c)^{0.14}(b/d)^{0.47}(C_r)^{0.95}(v_m)^{-1.58}$ provides a means to quantify cyclic response as a function of variations in design parameters (e.g., a change in stirrup spacing, beam width, effective depth).

3.3.2 Current Study

The effect of an increase in beam width on cyclic performance may be evaluated by comparing the values of the Energy Dissipation Index, D_i, for Beams H-1 (b = 15 in., and D_i = 102), F-3 (b = 7.5 in., and D_i = 52), H-2 (b = 15 in., and D_i = 71), and F-2 (b = 7.5 in., and D_i = 28). A 100% increase in width resulted in a 96% increase in D_i for Beam H-1, compared to Beam F-3, and a 154% increase in D_i for Beam H-2, compared to Beam F-2. These changes represent greater improvements in cyclic performance than indicated by the increases in E, 18 and 71%, respectively.

The influence of the displacement ductility factor, μ, and the ratio of positive to negative moment reinforcement, A'_s/A_s, on cyclic performance, as measured by D_i, is demonstrated by two comparisons: For Beams H-1 (μ = 4.3, A'_s/A_s = 0.5, and D_i = 102) and H-3 (μ = 8.5, A'_s/A_s = 0.5, and D_i = 91), the 98% increase in μ from Beam H-1 to Beam H-3 resulted in a 11% decrease in D_i, which matches the earlier observations based on E. However, for Beams H-1 (μ = 4.3, A'_s/A_s = 0.5, and D_i = 102) and H-4 (μ = 4.7, A'_s/A_s = 1.0, and D_i = 93) the conclusions based on E and D_i do not match. Although a 100% increase in A'_s/A_s from Beam H-1 to Beam H-4 resulted in a substantial increase in energy dissipation capacity (E = 507 kip-in. and 245 kip-in. for Beams H-4 and H-1, respectively), D_i decreased by 9%. Clearly, an

increase in the ratio of positive to negative moment reinforcement at the face of a support does not ensure a marked improvement in the cyclic performance of a reinforced concrete beam (Nmai & Darwin 1986). In this case, the net decrease in D_i (which is dependent upon the approximated elastic energy of a full span beam) for Beam H-4 resulted from an increase in shear force in the prototype beam due to the addition of positive reinforcement as represented by the terms in the denominator of D_i (note, as seen in Eq. 1.6, there is an inverse relationship between D_i and A_s'/A_s).

Comparing the effects of increases in width and A_s'/A_s on D_i shows that improvements in cyclic performance may be more readily obtained through an increase in member width than through an increase in A_s'/A_s. This conclusion is based on the fact that for a given design, an increase in width reduces the shear stress in both positive and negative bending (an increase in width also increases the moment capacity of a section, but only nominally), while an increase in the ratio of positive to negative moment reinforcement decreases the concrete compressive stresses in negative bending but increases the shear force (and stress) in positive bending.

Graphically, the beneficial effect of an increase in width on cyclic performance for Beams H-1 thru H-4 can be seen in a plot of D_i versus $(v_s)^{0.50}(f_c')^{0.14}(b/d)^{0.47}(C_r)^{0.95}(v_m)^{-1.58}$ (Fig. 3.3). The overall trend of the data in Fig. 3.3 suggests that there is a linear relationship between D_i $(v_s)^{0.50}(f_c')^{0.14}(b/d)^{0.47}(C_r)^{0.95}(v_m)^{-1.58}$. Furthermore, a standard regression analysis (least squares method) of the data in Fig. 3.3 results in a best-fit equation of

$$D_i = 29 + 2501\left[(v_s)^{0.50}(f_c')^{0.14}(b/d)^{0.47}(C_r)^{0.95}(v_m)^{-1.58}\right] \qquad (3.1)$$

with the coefficient of determination $r^2 = 0.945$. Eq. 3.1 is also plotted in Fig. 3.3 and, as shown in this figure, the small scatter of data relative to the best-fit line indicates a linear correlation between D_i and $(v_s)^{0.50}(f_c')^{0.14}(b/d)^{0.47}(C_r)^{0.95}(v_m)^{-1.58}$.

When the results of this study are combined with the 30 test results analyzed by Hanks & Darwin (1988) (see Table 3.1), a considerably different best-fit equation

is obtained,

$$D_i = 28 + 3327\left[(v_s)^{0.50}(f_c')^{0.14}(b/d)^{0.47}(C_r)^{0.95}(v_m)^{-1.58}\right] \quad (3.2)$$

with a much poorer correlation, $r^2 = 0.578$ (Fig. 3.4). As seen in Fig. 3.4, two distinct trends are apparent. The first trend, characterized by the solid line, represents Eq. 3.2. The test results of the current study dominate the data at values of $(v_s)^{0.50}(f_c')^{0.14}(b/d)^{0.47}(C_r)^{0.95}(v_m)^{-1.58}$ greater than 0.01. This is primarily due to the low values of shear stress (obtained through the use of increased widths) for Beams H-1 thru H-4 (64 psi $\leq v_m \leq$ 105 psi) compared to the other 30 specimens (141 psi $\leq v_m \leq$ 528 psi). The second trend is characterized by the dashed line which represents the best-fit line for the 30 specimens analyzed by Hanks & Darwin (1988). These test results dominate the data at values of $(v_s)^{0.50}(f_c')^{0.14}(b/d)^{0.47}(C_r)^{0.95}(v_m)^{-1.58}$ less than 0.01. The disparity between the two lines shown in Fig 3.4 suggests that $(v_s)^{0.50}(f_c')^{0.14}(b/d)^{0.47}(C_r)^{0.95}(v_m)^{-1.58}$ does not provide a consistent means to quantify member response. Thus, an improved method for evaluating the nonlinear response of reinforced concrete beams subjected to cyclic loading is required.

CHAPTER 4

PREDICTING CYCLIC RESPONSE

4.1 General

The Energy Dissipation Index, D_i, developed by Nmai & Darwin (1984, 1986), provides a means to quantify the experimental response of a reinforced concrete beam subjected to severe inelastic loading. Statistical analyses (Nmai & Darwin 1984, 1986, Darwin & Nmai 1986, and Hanks & Darwin 1988) indicate that D_i may be effectively modeled as the product of design variables such as the maximum applied shear stress, v_m, the nominal stirrup strength, v_s, and the concrete strength, f'_c. The product of multiple variables represents an indirect characterization of D_i, and thus, provides a means to predict cyclic response in terms of geometric, material, and loading (predictor) parameters. Although the statistical model developed by Hanks & Darwin (1988) provides a better fit of data for a wider range of test results (including specimens fabricated with high strength concrete) than the model developed by Nmai & Darwin (1984, 1986), it does not adequately predict the experimental response of available test results when the specimens of this study are included in a statistical analysis of data (see Chapter 3).

The inability of the earlier (Hanks & Darwin 1988) model to consistently predict D_i may be related to the analytical characterization of D_i (i.e., using the product of design parameters to predict experimental response). As previously discussed (Chapter 1), D_i is dependent upon a member's energy dissipation capacity, E. Two factors that affect E are the number of cycles in which the maximum load, P_i, is at least 75% of the yield load, P_y, and the energy dissipated per cycle. To date, analytical expressions for D_i have not addressed or formulated specimen response in terms of these fundamental factors.

In an effort to improve the method by which the cyclic response of reinforced

concrete is predicted, a new procedure will be developed that 1) quantifies the number of cycles a reinforced concrete member sustains when subjected to severe cyclic loading (i.e., $\mu > 2$), and 2) analytically characterizes the Energy Dissipation Index, D_i, as a function of member properties and loading parameters that affect the energy dissipation capacity of the member.

4.2 Cycles to "Failure"

Defining the "failure" of reinforced concrete test specimens in terms of their ability to resist a percentage of the initial yield load provides a means to reduce some of the ambiguity in quantifying experimental response. From this perspective, equating "failure" to the point at which the maximum load within a cycle is less than 75% of the yield load has merit. Several researchers (Gosain et al. 1977, Scribner & Wight 1978 and 1980, Hwang 1982, Hwang & Scribner 1984, Nmai & Darwin 1984 and 1986, Darwin & Nmai 1986, and Hanks & Darwin 1988) have used this criterion (number of cycles with $P_i \geq 0.75P_y$) to quantify the total useable energy dissipation capacity of a specimen and have obtained moderate-to-reasonably good correlations between measures of cyclic performance and selected specimen parameters (Chapter 1). While the specific results from these correlations are dependent upon the test specimens included in the analysis of data, collectively they provide a basis for developing a statistical relationship between the number of cycles with $P_i \geq 0.75P_y$ and parameters known to influence cyclic performance.

4.2.1 Factors Influencing the Number of Cycles with $P_i \geq 0.75P_y$, n

Test results from research by Scribner & Wight (1978, 1980), Hwang (1982), Hwang & Scribner (1984), Nmai & Darwin (1984, 1986), Darwin & Nmai (1986), Hanks & Darwin (1988), and those of the current study indicate that several factors influence the number of inelastic load cycles a reinforced concrete member sustains. These factors represent variables that are used to design the specimen and define the loading regime. They include the maximum applied shear stress, v_m, nominal stirrup

strength, v_s, ratio of positive to negative moment reinforcement, A_s'/A_s, concrete strength, f_c', stirrup spacing, s (relative to effective beam depth, d), beam width-to-effective depth ratio, b/d, the Confinement Ratio, C_r (defined in Chapter 3), and the displacement ductility factor, μ. The ability to predict n, the number of cycles with $P_i \geq 0.75P_y$, in terms of multiple parameters requires 1) an appropriate statistical model and 2) the best selection of parameters to be included in the model. In an effort to minimize the number of parameters, yet maximize the correlation of available experimental data, five parameters are selected.

4.2.1.1 Maximum Applied Shear Stress, $(v_m/\sqrt{f_c'})[1 + (A_s'/A_s)^2]$

Research by Gosain, Brown & Jirsa (1977), Scribner & Wight (1980), Hwang (1982), and Hwang & Scribner (1984) has shown that the ratio of maximum applied shear stress (in negative bending) to the square root of the concrete strength, $v_m/\sqrt{f_c'}$, is a reasonable predictor of cyclic performance for a relatively wide range of specimen strengths and load histories. For a given specimen and loading regime, the effect of an increase in $v_m/\sqrt{f_c'}$ (obtained either through an increase in v_m or a decrease in f_c') is a reduction in cyclic performance (number of load cycles with $P_i \geq 0.75P_y$). Thus, the parameter $v_m/\sqrt{f_c'}$ is chosen to represent the influence of shear stress and concrete strength on the number of cycles with $P_i \geq 0.75P_y$. In addition, research by Scribner & Wight (1980), Hwang (1982), and Hwang & Scribner (1984) suggests that member response is dependent upon the magnitude of beam-tip displacement in both the negative and the positive directions. Therefore, the influence of shear stress in positive bending is also considered to be a factor influencing the number of load cycles with $P_i \geq 0.75P_y$. To account for the influence of shear stress in both directions of displacement, a parameter must be developed that characterizes the effect of the negative and the positive maximum applied shear stress on cyclic performance.

For beams designed to resist earthquakes, the design shear force (based on ACI 318-89 requirements) is dependent upon gravity loads, end moments, and clear span.

However, for cantilever beams tested in the laboratory, the applied shear force is primarily a function of the member's moment capacity and shear span. Thus, for beam-column specimens subjected to inelastic loading, the maximum shear forces in negative and positive bending can be approximated as

$$V_m^- = V_m \approx \frac{1.25 A_s f_y \left(d - \frac{a}{2}\right)}{\text{shear span}} \tag{4.1a}$$

and

$$V_m^+ \approx \frac{1.25 A_s' f_y \left(d_1 - \frac{a}{2}\right)}{\text{shear span}} \tag{4.1b}$$

in which A_s and A_s' are the areas of negative and positive moment reinforcement, d and d_1 are the effective beam depths in negative and positive bending, respectively, and a is the depth of the concrete compression block. Since a/2 is usually small with respect to d and d_1, the maximum applied shear force (and shear stress) is dependent upon the product of flexural reinforcement and effective depth ($A_s d$ or $A_s' d_1$). Thus, in positive bending, the maximum applied shear stress, v_m^+, is approximately proportional to the product of the maximum applied shear stress in negative bending, v_m, and the ratio of $A_s' d_1$ to $A_s d$ ($v_m^+ \approx v_m[(A_s' d_1/A_s d)]$). For reinforced concrete beams with nearly-equal effective depths in positive and negative bending, v_m^+ can be approximated as $v_m(A_s'/A_s)$. Subsequently, a parameter that accounts for the influence of shear stress in both directions of displacement may be expressed as

$$\frac{v_m}{\sqrt{f_c'}} \left[1 + \left(\frac{A_s'}{A_s}\right)\right] \tag{4.2a}$$

Although Eq. 4.2(a) represents a viable characterization of the influence of

shear stress on the number of load cycles, an analysis of available experimental results (presented in more detail in the following sections) indicates that improvements in the correlation of data (i.e., the correlation between n and the five predictor parameters) are obtained when v_m^+ is approximated as $v_m(A_s'/A_s)^2$. The improved correlation (indicated by an increase in the coefficient of determination, r^2) obtained with $(A_s'/A_s)^2$, compared to (A_s'/A_s), suggests that 1) the shear stress in positive bending is a contributing factor that improves the fit of the data between the predictor parameters and the experimentally determined number of cycles to failure, and 2) the influence of shear stress in positive bending on n, is disproportionately smaller than the influence of the shear stress in negative bending. Therefore, a parameter that represents the combined influence of shear stress in both directions of displacement, and thus, the net effect of the maximum applied shear stress (and the concrete strength) on the number of cycles with $P_i \geq 0.75P_y$ can be expressed as

$$\frac{v_m}{\sqrt{f_c'}}\left[1 + \left(\frac{A_s'}{A_s}\right)^2\right] \qquad (4.2b)$$

Based on the adverse influence of shear stress on cyclic performance (Gosain, Brown & Jirsa 1977, Scribner & Wight 1978 and 1980, Hwang 1982, Hwang & Scribner 1984, Nmai & Darwin 1984 and 1986, and Hanks & Darwin 1988), it is reasonable to expect that an increase in Eq. 4.2(b) will have a "negative" influence on the number of cycles with $P_i \geq 0.75P_y$ (i.e., for a given specimen and loading regime, an increase in Eq. 4.2(b) results in an increase in the rate of cyclic degradation and a decrease in n).

4.2.1.2 Nominal Stirrup Strength, $v_s/\sqrt{f_c'}$

In regions of high seismic risk, current ACI code provisions (ACI 318-89 - Chapter 21) require that the transverse reinforcement in frame members be designed to resist the earthquake-induced shear forces, neglecting any contribution by the

concrete. This requirement reflects the role of transverse reinforcement in maintaining adequate shear strength under severe cyclic loading. Thus, the nominal shear contribution of beam stirrups, v_s, is a significant factor in the response (cycles with $P_i \geq 0.75P_y$) of reinforced concrete beams subjected to seismic forces. To maintain dimensional consistency with the influence of shear stress, v_m, on the number of load cycles [Eq. 4.2(b)], the nominal stirrup strength is normalized with respect to concrete strength and expressed as $v_s/\sqrt{f'_c}$. For beams undergoing severe inelastic loading, an increase in v_s improves confinement of the core concrete and delays buckling of the compression reinforcement. Thus, the parameter $v_s/\sqrt{f'_c}$ has a "positive" influence on the number of cycles with $P_i \geq 0.75P_y$.

4.2.1.3 Ratio of Positive to Negative Moment Reinforcement, A'_s/A_s

Research by Ma, Bertero, & Popov (1976) and Nmai & Darwin (1984, 1986) indicates that the ratio of positive to negative moment reinforcement, A'_s/A_s, affects the response of reinforced concrete beams subjected to reversed cyclic loading. For example, a comparison of test results for Beam F-6 ($A'_s/A_s = 0.75$) versus Beam F-3 ($A'_s/A_s = 0.50$) (Nmai & Darwin 1984, 1986) shows that an increase in A'_s/A_s increases the number of cycles with $P_i \geq 0.75P_y$. Similar results were obtained for Beams H-4 ($A'_s/A_s = 1.0$) and H-1 ($A'_s/A_s = 0.5$) of the current study. An increase in A'_s/A_s decreases the concrete compressive stresses in negative bending and delays spalling. Thus, for a given specimen and loading regime, A'_s/A_s has a "positive" influence on the number of cycles with $P_i \geq 0.75P_y$. Note that an increase in A'_s/A_s increases the shear stress in positive bending as indicated in Eq. 4.2(b). Therefore, the net effect of A'_s/A_s on n is also dependent upon the "negative" influence of $(v_m/\sqrt{f'_c})[(A'_s/A_s)^2]$.

4.2.1.4 Ratio of Beam Width to Stirrup Spacing, b/s

The statistical analysis performed by Hanks & Darwin (1988) indicates that beam width-to-depth ratio, b/d, affects the inelastic response of reinforced concrete. The ACI code (ACI 318-89 - Chapter 21) requires that the width-to-depth ratio of

frame members shall not be less than 0.3. Hanks & Darwin concluded that square-shaped beams should exhibit better cyclic performance than rectangular beams due to an increase in confinement of the core concrete. This point is emphasized by the current experimental study. Although beam shape appears to be an important factor influencing member response, a better characterization of confinement is possible using the stirrup spacing, s, in lieu of effective depth, d. Results of the research by Nmai & Darwin (1984, 1986) indicate that a reduction in stirrup spacing improves confinement of the core concrete and postpones buckling of the compression reinforcement which increases the number of load cycles and energy dissipation capacity. Therefore, the parameter b/s is selected as a parameter influencing n. An increase in b/s (obtained either through an increase in beam width or decrease in stirrup spacing) should have a "positive" influence on the number of cycles with $P_i \geq 0.75P_y$.

4.2.1.5 Root-Mean-Square Displacement Ductility Factor, μ_{rms}

Tests by Hwang (1982) and Hwang & Scribner (1984) indicate that an increase in the maximum amplitude of beam-tip displacement, and thus μ, adversely affects the number of cycles with $P_i \geq 0.75P_y$. Since some studies use loading regimes in which μ in the negative and positive directions change during the test, an alternate representation of μ is required to capture the overall effects of displacement ductility. The root-mean-square of the displacement ductility is, therefore, used to represent μ up to the point of failure (i.e., $P_i \geq 0.75P_y$) and is calculated as follows:

$$\mu_{rms} = \sqrt{\frac{\sum_{j=1}^{n} \left(\frac{\mu^- + \mu^+}{2} \right)_j^2}{n}} \qquad (4.3)$$

An increase in μ_{rms} is expected to increase the rate of degradation, and thus, have a "negative" effect on the number of cycles with $P_i \geq 0.75P_y$.

Based on the availability of experimental data in which $(\mu^-)_j$ and $(\mu^+)_j$ are well defined, specimens from the research by Wight & Sozen (1973), Scribner & Wight (1978), Hwang (1982), Nmai & Darwin (1984), Hanks & Darwin (1988), and the current study provide a data base with which to evaluate a statistical model which predicts the number of cycles with $P_i \geq 0.75P_y$ (see Table 4.1 for $(\mu^-)_j$ and $(\mu^+)_j$ for $j \leq n$ and μ_{rms}).

4.2.2 Modeling the Number of Cycles with $P_i \geq 0.75P_y$, n

In general, the choice of an appropriate model to predict n is subjective, but ultimately the model must provide a balance between one that 1) accurately predicts the response variable, and 2) sufficiently describes the quantitative influence of each parameter on n (i.e., the model must not just fit the data). Even though $(v_m/\sqrt{f'_c})[1 + (A'_s/A_s)^2]$, $v_s/\sqrt{f'_c}$, and b/s, are correlated (e.g., v_m, v_s, and b/s are a function of beam width, b, and therefore correlated), the lack of interaction between A'_s/A_s, b/s, and μ_{rms} indicates an additive (linear) effect of these parameters on n. Thus, a viable statistical model of the form

$$Y_i = \beta_0 + \beta_1(X_{i1}) + \beta_2(X_{i2}) + \ldots + \beta_{p-1}(X_{i,p-1}) \qquad (4.4)$$

is considered to be appropriate.

Eq. 4.4 is referred to as a general first-order (linear) model with p-1 independent variables (Neter & Wasserman 1974). The model is linear in both the regression coefficients and the parameters investigated (β's and X's, respectively). Higher-order, or multiplicative models, can also be expressed in the form of Eq. 4.4 by performing a transformation of variables, such as the logarithmic transformation of variables used by Hanks & Darwin (1988) to develop a multiplicative model.

Substituting the five parameters and response variable n into Eq. 4.4 results in

$$n = \beta_0 + \beta_1 \frac{v_m}{\sqrt{f_c'}}\left[1 + \left(\frac{A_s'}{A_s}\right)^2\right] + \beta_2 \frac{v_s}{\sqrt{f_c'}} + \beta_3 \frac{A_s'}{A_s} + \beta_4 \frac{b}{s} + \beta_5 \mu_{rms} \qquad (4.5)$$

Although the relationship between n and $(v_m/\sqrt{f_c'})[1 + (A_s'/A_s)^2]$, $v_s/\sqrt{f_c'}$, A_s'/A_s, b/s, and μ_{rms} in Eq. 4.5 appears to be a viable expression, it should be noted that the parameter μ_{rms} may also be a function of n, the response variable. For test specimens with constant values of $(\mu^-)_j$ and $(\mu^+)_j$ $(1 \le j \le n)$, the value of μ_{rms} does not depend on n. However, for specimens with variable magnitudes of $(\mu^-)_j$ or $(\mu^+)_j$ [e.g., Specimen 5 from Scribner & Wight (1980) (Table 4.1)], the experimental value of n used to calculate μ_{rms} will not, in general, correspond to the value of n predicted by Eq. 4.5. Thus, for these specimens an alternate method to predict n is necessary, as will be discussed in more detail. However, in the following section the experimental value of n is initially used to define μ_{rms} for specimens with and without variable magnitudes of $(\mu^-)_j$ or $(\mu^+)_j$.

4.2.3 Predicting the Number of Cycles with $P_i \ge 0.75P_y$, n

An evaluation of the relationship between n and the five parameters is possible by performing a statistical analysis of available test data and determining the coefficient of determination, r^2, which quantifies the goodness of fit for the proposed model. A perfect correlation results in $r^2 = 1.0$. Applying standard multiple regression solution techniques (i.e., the least squares method) results in the determination of the least squares estimators for β_0 thru β_5. Test results from Wight & Sozen (1973), Scribner & Wight (1978), Hwang & Scribner (1984), Nmai & Darwin (1984, 1986), Hanks & Darwin (1988), and the current study are selected for inclusion in the analysis and presented in Table 4.1. A multiple regression analysis of this data results in a linear regression equation of

$$n = 8.17 - 1.89\frac{v_m}{\sqrt{f_c'}}\left[1+\left(\frac{A_s'}{A_s}\right)^2\right] + 0.80\frac{v_s}{\sqrt{f_c'}}$$

$$+ 16.74\frac{A_s'}{A_s} + 1.43\frac{b}{s} - 2.10\mu_{rms} \qquad (4.6)$$

where the coefficient of determination $r^2 = 0.914$. Eq. 4.6 and the 90% confidence limits relative to the regression equation (i.e., Eq. 4.6) are plotted in Fig. 4.1. The small scatter of data relative to the best-fit line, as shown in this plot, and the relatively high value of r^2 indicates that the model in Eq. 4.5 provides a good fit of the data. The algebraic sign of the regression coefficients in Eq. 4.6 also correspond to the anticipated influence of each parameter on the number of cycles with $P_i \geq 0.75P_y$ such that 1) estimators for β_1 and β_5 are negative and indicate that an increase in n is obtained with a reduction in $(v_m/\sqrt{f_c'})[1+(A_s'/A_s)^2]$ and μ_{rms}, and 2) estimators for β_2, β_3, and β_4 are positive and indicate that an increase in n is obtained with an increase in $(v_s/\sqrt{f_c'})$, A_s'/A_s, and b/s. However, the estimated value of +8.17 for β_0 implies that the model fits the data rather than the true response (i.e., β_0 is zero when the correlation between the independent and dependent variables is perfect). An improved correlation (i.e., an increase in r^2 and reduction in β_0) between n and the five predictor parameters can be obtained by using a model that is still linear in the coefficients but nonlinear in the selected parameters.

One means available to select the appropriate linear or nonlinear influence of each parameter on n is to apply a modified "all possible regressions" procedure (Draper & Smith 1981). This procedure requires that, initially, a range of exponential influence is selected for each parameter (e.g., the exponential influence of μ_{rms} on n may range from 0.10 to 1.00 in increments of 0.05). Starting at the lower limit of the exponential influence for one parameter, the exponential influences of the remaining

parameters are held constant and a multiple regression analysis is performed. Additional analyses are performed by incrementing each parameter's exponent until all desired combinations of exponents have been investigated. Comparing the results of all analyses provides a means to determine a "locally" constrained optimized solution. Based on this procedure, an improved correlation of test results is obtained with $(A_s'/A_s)^{0.20}$, $(b/s)^{0.20}$, and $(\mu_{rms})^{0.15}$ [the optimization of Eq. 4.6 results in the exponential influence of the parameters $(v_m/\sqrt{f_c'})[1 + (A_s'/A_s)^2]$ and $v_s/\sqrt{f_c'}$ remaining linear]. Using these parameters and performing a multiple regression analysis for the same specimens used to develop Eq. 4.6 results in a best-fit equation of

$$n = 3.75 - 2.06\frac{v_m}{\sqrt{f_c'}}\left[1 + \left(\frac{A_s'}{A_s}\right)^2\right] + 0.85\frac{v_s}{\sqrt{f_c'}}$$

$$+ 67.55\left(\frac{A_s'}{A_s}\right)^{0.20} + 14.53\left(\frac{b}{s}\right)^{0.20} - 55.07(\mu_{rms})^{0.15} \qquad (4.7)$$

with $r^2 = 0.938$. Eq. 4.7 and the 90% confidence limits relative to the regression equation are plotted in Fig. 4.2. By reducing the exponential influence of A_s'/A_s, b/s, and μ_{rms} in Eq. 4.7, as compared to Eq. 4.6, the coefficient of determination increases while the scatter in the data and the estimator for β_0 decrease. Thus, Eq. 4.7 provides an improved fit of the data. For the specimens analyzed, the statistical prediction of n in terms of the selected parameters facilitates an evaluation of the cyclic response of reinforced concrete beams by quantifying the influence of the parameters investigated. Both Eqs. 4.6 and 4.7 exhibit similar relative orders of magnitude (and thus significance) for the least squares estimators. Thus, the ranking or influence of the five parameters on n is not affected by the nonlinearity of A_s'/A_s, b/s, and μ_{rms}.

Although Eq. 4.7 provides a means to predict the number of cycles with $P_i \geq 0.75P_y$ in terms of the predictor parameters, it should be noted that, for non-constant

values of $(\mu^-)_j$ or $(\mu^+)_j$, μ_{rms} is not constant for all j, $j \leq n$, and the determination of μ_{rms} requires a prior knowledge of n. Thus, for specimens with variable magnitudes of $(\mu^-)_j$ or $(\mu^+)_j$, a direct prediction of n in terms of the five parameters in Eq. 4.7 is not possible since n appears on both sides of Eq. 4.7.

Three methods are potentially available with which to predict n for specimens tested with non-constant values of $(\mu^-)_j$ or $(\mu^+)_j$. The first and most direct method is to use the experimental or test value of n, n_{test}, in the calculation of μ_{rms} (Eq. 4.3) (this method is used to define the value of μ_{rms} in Eqs. 4.6 and 4.7). However, the value of μ_{rms} based on the predicted value of n, n_{pre}, will not in general match the value of μ_{rms} (from the test) used to calculate n_{pre}.

The second method involves a reformulation of the model so that the dependent variable completely characterizes the interaction between specimen response and μ_{rms}. In essence, the interdependency between μ_{rms} and the predicted value of n necessitates a reparameterization of the net effect of a variation in $(\mu^-)_j$ or $(\mu^+)_j$. This procedure is not pursued in this study.

The third method (which acknowledges the presence of n on both sides of Eq. 4.7) uses an iterative procedure to obtain a unique value of n_{pre}. This method, using Eq. 4.7 without modification of the regression coefficients, is described next.

Initially, μ_{rms} is calculated in accordance with Eq. 4.3 such that $[(\mu^+ + \mu^-)/2]_j^2$ is summed over, and divided by, the experimentally determined number of cycles with $P_i \geq 0.75P_y$ (n_{test}). The resulting value of μ_{rms} is then substituted into Eq. 4.7 and the predicted number of cycles with $P_i \geq 0.75P_y$, n_{pre}, determined [note that n_{pre} is a real number with integer and fractional components (n_i and n_f, respectively)]. If n_{pre} differs from n_{test}, then a modified value of the root-mean-square displacement ductility factor, μ'_{rms}, is calculated such that

$$\mu'_{rms} = \sqrt{\frac{\Gamma_1 + \Gamma_2}{n_{pre}}} \tag{4.8a}$$

in which

$$\Gamma_1 = \sum_{j=1}^{(n)_i} \left(\frac{\mu^- + \mu^+}{2} \right)_j^2 \tag{4.8b}$$

and

$$\Gamma_2 = (n)_f \left[\sum_{j=1}^{(n)_i+1} \left(\frac{\mu^- + \mu^+}{2} \right)_j^2 - \sum_{j=1}^{(n)_i} \left(\frac{\mu^- + \mu^+}{2} \right)_j^2 \right] \tag{4.8c}$$

n_{pre} is recalculated using the new value of μ'_{rms}. The solution continues until convergence is obtained. The predicted value of n, which was dependent upon μ_{rms}, is now calculated using μ'_{rms} in accordance with Eqs. 4.8(a) - 4.8(c). For the specimens with non-constant values of $(\mu^-)_j$ or $(\mu^+)_j$, the value of μ'_{rms} is presented in Table 4.1. A comparison of μ_{rms} (Eq. 4.3) and μ'_{rms} [Eqs. 4.8(a) - 4.8(c)] indicates that the use of an iterative solution procedure results in relatively small changes in μ_{rms}. The substitution of μ'_{rms} for μ_{rms} in Eq. 4.7 results in

$$n = 3.75 - 2.06\frac{v_m}{\sqrt{f'_c}}\left[1 + \left(\frac{A'_s}{A_s}\right)^2\right] + 0.85\frac{v_s}{\sqrt{f'_c}}$$

$$+ 67.55\left(\frac{A'_s}{A_s}\right)^{0.20} + 14.53\left(\frac{b}{s}\right)^{0.20} - 55.07(\mu'_{rms})^{0.15} \tag{4.9}$$

When the specimens with and without constant values of $(\mu^-)_j$ or $(\mu^+)_j$ (Table 4.1) are statistically re-evaluated using Eq. 4.9 (i.e., a multiple regression analysis is

performed using the converged value of μ'_{rms} in lieu of μ_{rms}), the coefficient of determination, r^2, increases from 0.938 to 0.948. Thus, the net effect of applying the convergence technique is a reduction in the scatter of the data (see Fig. 4.3). For the specimens investigated, the relationship between the experimentally determined number of cycles with $P_i \geq 0.75P_y$ and the linear combination of terms shown in Eq. 4.9 indicates that there is reasonably good fit of the data. Further insight into the appropriateness of Eq. 4.9 to predict n is provided by statistically analyzing the ratio of n_{test} to n_{pre} for the specimens presented in Table 4.1. The mean and coefficient of variation of n_{test}/n_{pre} for these beams are 1.00 and 14.0%, respectively. Based on these results, an increase in the number of cycles with $P_i \geq 0.75P_y$ is obtained with 1) decreases in the maximum applied shear stress and the root-mean-square displacement ductility factor (μ'_{rms}), and 2) increases in the nominal stirrup strength, ratio of positive to negative moment reinforcement, and ratio of beam width-to-stirrup spacing.

Since the derivation of Eq. 4.9 is largely empirical, its application should be strictly limited to members that fall within the limits of the geometric and material properties of the specimens used to establish the equation. The limits of these properties are: $1.0 \leq v_m/\sqrt{f'_c} \leq 7.4$, $0.5 \leq A'_s/A_s \leq 1.0$, $1.2 \leq v_s/\sqrt{f'_c} \leq 11.8$, $1.2 \leq b/s \leq 4.7$, $2.5 \leq \mu'_{rms} \leq 8.5$, 3,980 psi $\leq f'_c \leq$ 12,860 psi, 52,700 psi $\leq f_y \leq$ 73,800 psi, 32,300 psi $\leq f_{vy} \leq$ 75,300 psi, and $0.48 \leq b/d \leq 0.96$.

4.3 Predicting Energy Dissipation Capacity, E

As previously discussed, the Energy Dissipation Index, D_i, is a measure of cyclic performance and dependent upon a member's energy dissipation capacity, E. However, to date, the prediction of D_i has been characterized by models represented by a product of design variables (Nmai & Darwin 1984, 1986, Darwin & Nmai 1986, and Hanks & Darwin 1988). These models (and the parameters in the models) do not directly account for the energy dissipated by a member subjected to cyclic loading.

Therefore, an analytical development of E is proposed in an effort to express the cyclic response of a reinforced concrete member in terms of geometric, material, and loading parameters. The ability to predict E in terms of a specimen's parameters provides a means to analytically predict D_i for specimens not yet tested.

For reinforced concrete frames, the negative moment in beams at the face of the support due to gravity loads results in designs with more top steel than bottom steel. This provides greater moment capacity in negative rather than positive bending. Because of the greater moment capacity, prototype cantilever beam specimens are loaded in the downward, or negative direction at the initiation of a test. Cantilever specimens that are reinforced with different amounts of negative and positive flexural reinforcement (A_s and A_s', respectively) generally exhibit initial (cycle #1) load versus load-point deflection behavior of the type depicted by the solid curve in Fig. 4.4. For these specimens, the energy dissipated in a cycle is dependent upon the energy dissipated in both the negative and positive bending directions. Each component of energy is equivalent to the respective area bounded by the load-deflection plot. An approximation of the area bounded by an experimental load-deflection curve can be obtained by using a rectilinear characterization of response as shown by the dashed line in Fig. 4.4. Two points on the load versus load-point deflection plot are of particular interest: the points representing the maximum loads and deflections in negative and positive bending [$(P_{max},\Delta_{max})^-$ and $(P_{max},\Delta_{max})^+$, respectively]. Using these points as "delineators of response", the energy dissipated in the first complete load cycle can be expressed as

$$E_1 = K_1 \left[(P_{max}\Delta_{max})^- + (P_{max}\Delta_{max})^+\right]_1 \qquad (4.10)$$

in which K_1 = a proportionality factor for cycle #1. For specimens subjected to multiple cycles of inelastic loading, the energy dissipated during subsequent cycles may be expressed in a general form such that

$$E_j = K_j \left[(P_{max}\Delta_{max})^- + (P_{max}\Delta_{max})^+ \right]_j \tag{4.11}$$

in which j is the index defining the individual cycle number.

Although K_j is not explicitly defined in Eq. 4.11, some of its "characteristics" may be anticipated. When a reinforced concrete beam is subjected to inelastic loading at constant amplitudes of displacement, the energy dissipated per cycle decreases as the number of cycles increases. Therefore, it is reasonable to expect a continual decrease in K_j (i.e., $K_j \geq K_{j+1} \geq K_{j+2} \geq \ldots$). In addition, for those specimens exhibiting significant deformation as a result of severe reversed cyclic loading (i.e., $\mu > 2$), it is reasonable to expect a nonlinear relationship between the K_j's and cycle number, j.

The cumulative dissipated energy for a reinforced concrete beam, E, is determined by summing Eq. 4.11 for all j's over n cycles such that

$$E = \sum_{j=1}^{n} K_j \left[(P_{max}\Delta_{max})^- + (P_{max}\Delta_{max})^+ \right]_j \tag{4.12}$$

and n = the number of load cycles with $P_i \geq 0.75P_y$. Noting that the displacement ductility factor, μ, is defined as the ratio of maximum beam-tip displacement to yield displacement (i.e., Δ_{max}/Δ_y), Eq. 4.12 may be alternatively expressed by substituting $(\mu\Delta_y)^-$ and $(\mu\Delta_y)^+$ for $(\Delta_{max})^-$ and $(\Delta_{max})^+$, respectively. The resulting equation, which expresses the energy dissipated by a reinforced concrete beam as a function of the maximum load, displacement ductility factor, and yield displacement in the negative and positive directions, becomes

$$E = \sum_{j=1}^{n} K_j \left[P^-_{max}(\mu\Delta_y)^- + P^+_{max}(\mu\Delta_y)^+ \right]_j \tag{4.13}$$

Rearranging terms in Eq. 4.13 results in

$$E = \sum_{j=1}^{n} K_j \left[(P_{max}\Delta_y)^- \right]_j \left[(\mu^-) + \left(\frac{(P_{max}\Delta_y)^+}{(P_{max}\Delta_y)^-} \right) (\mu^+) \right]_j \tag{4.14}$$

Two additional modifications can be made to simplify Eq. 4.14.

The first modification is related to $(P_{max})^-$, the maximum negative load obtained during testing. Current ACI code provisions (ACI 318-89 - Chapter 21) require that, in regions of high seismic risk, the forces acting at the face of a joint must be based on a stress in the flexural tensile reinforcement of $1.25f_y$. The 25% increase in yield stress accounts for the effects of strain hardening, as depicted by the experimental curve in Fig. 4.4. Thus, a reasonable estimation for $(P_{max})^-$ is $1.25(P_y)^-$.

The second modification pertains to the ratio of $(P_{max}\Delta_y)^+$ to $(P_{max}\Delta_y)^-$. Both P_{max} and Δ_y are dependent upon the area of flexural reinforcement (Nmai & Darwin 1984). Therefore, the ratio of $(A_s')^2/(A_s)^2$ might be used as an approximation of $(P_{max}\Delta_y)^+/(P_{max}\Delta_y)^-$. An analysis of the available test results (presented in more detail in the following sections) indicates that an improved correlation between experimental and analytical values of D_i is obtained when $(A_s')/(A_s)$ is used in lieu of $(A_s')^2/(A_s)^2$. Substituting $1.25(P_y)^-$ for $(P_{max})^-$ and A_s'/A_s for $(P_{max}\Delta_y)^+/(P_{max}\Delta_y)^-$ and rearranging terms in Eq. 4.14 results in

$$E = (P_y\Delta_y)^- \sum_{j=1}^{n} K_j \left[(\mu^-)_j + \left(\frac{A_s'}{A_s} \right) (\mu^+)_j \right] \tag{4.15}$$

in which K_j now includes the constant 1.25.

Eq. 4.15 indicates that the cumulative energy dissipated by a reinforced concrete beam can be approximated based on: 1) $(P_y\Delta_y)^-$, the yield load and deflection in the primary, or negative, bending direction, 2) n, the number of cycles with $P_i \geq 0.75P_y$, 3) K_j, the proportionality factors for cycles 1 thru n, and 4) (A_s'/A_s) and μ, design and load parameters, respectively. The term $[(\mu^-)_j + (A_s'/A_s)(\mu^+)_j]$ is a function

of both the negative and positive displacement ductility factor and, therefore, characterizes the ductility range for the j'th cycle.

4.4 D_i versus the Normalized Ductility Range, NDR

To obtain an expression relating the experimentally determined value of D_i and the parameters $(\mu^-)_j$, $(\mu^+)_j$, and (A_s'/A_s), both sides of Eq. 4.15 are normalized with respect to the expression originally used by Nmai & Darwin (1984, 1986) to approximate the elastic energy at yield of an equivalent full span beam, $0.5(P_y\Delta_y)^-[1 + (A_s'/A_s)^2]$.

$$D_i = \frac{E}{\frac{1}{2}(P_y\Delta_y)^-\left[1 + \left(\frac{A_s'}{A_s}\right)^2\right]} = \sum_{j=1}^{n} K_j \frac{\left[(\mu^-)_j + \left(\frac{A_s'}{A_s}\right)(\mu^+)_j\right]}{\left[1 + \left(\frac{A_s'}{A_s}\right)^2\right]} \qquad (4.16)$$

In Eq. 4.16, K_j now includes the factor 1/0.5 = 2.0. The ratio of $[(\mu^-)_j + (A_s'/A_s)(\mu^+)_j]$ to $[1 + (A_s'/A_s)^2]$ is referred to as the Normalized Ductility Range (NDR) for cycle j. Substituting the NDR into Eq. 4.16 results in

$$D_i = \sum_{j=1}^{n} K_j\,(NDR)_j \qquad (4.17)$$

The values of K_j correlate a measure of the loading and section properties, $[(\mu^-) + (A_s'/A_s)(\mu^+)_j]$, to the actual dissipated energy, $[(E)_j]$, on a per cycle basis. The existence of a unique set of K_j is now investigated by examining the relationship between the contribution to D_i by each cycle, $(D_i)_j$, and the corresponding value of $(NDR)_j$.

4.4.1 $(D_i)_j$ versus $(NDR)_j$

For each cycle, the relationship between $(D_i)_j$ and $(NDR)_j$ may be written as

$$(D_i)_j = K_j\,(NDR)_j \tag{4.18}$$

in which

$$(D_i)_j = \frac{(E)_j}{\frac{1}{2}(P_y\Delta_y)\left[1 + \left(\frac{A_s'}{A_s}\right)^2\right]} \tag{4.19}$$

and $(E)_j$ is the energy dissipated during the j'th cycle.

$(E)_j$ has been determined for specific test specimens from the research by Wight & Sozen (1973), Scribner & Wight (1978), Hwang & Scribner (1984), Nmai & Darwin (1984, 1986), Hanks & Darwin (1988), and the current study (Appendix C describes the method by which the experimental values of $(E)_j$ are determined). The values of $(E)_j$ and $(D_i)_j$ for these specimens (for $1 \le j \le n$) are listed in Tables 4.2 and 4.3, respectively.

Statistically, Eq. 4.18 is a first-order (linear) model of the form $Y_i = \beta_0 + \beta_1(X_i)$, with $\beta_0 = 0$ [i.e., for all j, when $(NDR)_j$ is zero, $(D_i)_j$ must also be zero]. For the specimens presented in Tables 4.2 and 4.3, a plot of $(D_i)_j$ versus $(NDR)_j$ provides a means with which to evaluate the implied linearity of Eq. 4.18. For these specimens, the relationship between $(D_i)_j$ and $(NDR)_j$ is presented in Figs. 4.5(a) - 4.5(d) for j = 1, 4, 7, and 10 (cycles 1, 4, 7, and 10), respectively. A regression analysis [using the least squares method and the model $Y_i = \beta_1(X_i)$] is performed on the data in each figure to empirically determine K_j for each cycle. The resulting best-fit equations are

$$(D_i)_1 = 2.47\,(NDR)_1 \tag{4.20a}$$

$$(D_i)_4 = 1.40(NDR)_4 \tag{4.20b}$$

$$(D_i)_7 = 1.28(NDR)_7 \tag{4.20c}$$

$$(D_i)_{10} = 1.08(NDR)_{10} \tag{4.20d}$$

with $r^2 = 0.504$, 0.452, 0.318, and 0.327, respectively. Eqs. 4.20(a) - 4.20(d) are plotted in Figs. 4.5(a) - 4.5(d), respectively. As implied by the low values of r^2 for these equations, the lack of correlation suggests that a linear model $Y_i = \beta_1(X_i)$ is not an appropriate characterization of the relationship between $(D_i)_j$ and $(NDR)_j$. However, the data in Figs. 4.5(a) - 4.5(d) does indicate that K_j is dependent upon both the cycle number and the magnitude of $(NDR)_j$. The dependency of K_j on $(NDR)_j$ suggests that the relationship between $(D_i)_j$ and $(NDR)_j$ may be more appropriately characterized with a higher-order model obtained through an alternate expression for K_j. This expression may be written as

$$K_j = [K_{j1} + K_{j2}(NDR)_j] \tag{4.21}$$

When Eq. 4.21 is substituted into Eq. 4.18, the relationship between $(D_i)_j$ and $(NDR)_j$ becomes

$$(D_i)_j = K_{j1}(NDR)_j + K_{j2}(NDR)_j^2 \tag{4.22}$$

Statistically, Eq. 4.22 is a second-order model of the form $Y_i = \beta_0 + \beta_1(X_i) + \beta_2(X_i)^2$, with $\beta_0 = 0$. The appropriateness of Eq. 4.22 to model the relationship between $(D_i)_j$ and $(NDR)_j$ may be evaluated by again performing a regression analysis on the data in Figs. 4.5(a) - 4.5(d). Using this incomplete second-order model, the resulting best-fit equations for j = 1, 4, 7, and 10 are

$$(D_i)_1 = 1.48(NDR)_1 + 0.17(NDR)_1^2 \quad (4.23a)$$

$$(D_i)_4 = 0.93(NDR)_4 + 0.08(NDR)_4^2 \quad (4.23b)$$

$$(D_i)_7 = 0.14(NDR)_7 + 0.20(NDR)_7^2 \quad (4.23c)$$

$$(D_i)_{10} = 0.66(NDR)_{10} + 0.08(NDR)_{10}^2 \quad (4.23d)$$

with $r^2 = 0.975$, 0.877, 0.813, and 0.695, respectively. Eqs. 4.23(a) - 4.23(d) are also plotted in Figs. 4.5(a) - 4.5(d), respectively. As seen from a comparison of these figures, 1) the trend of the best-fit equations is to slightly overpredict $(D_i)_j$ at low values of NDR and underpredict at high values of NDR, and 2) the number of available test results decreases as j increases, and thus, the reliability of the relationship between K_{j1}, K_{j2}, $(NDR)_j$, and $(D_i)_j$ appears to diminish (r^2 decreases as j increases). Graphical summaries of K_{j1} and K_{j2} are presented in Figs. 4.6 and 4.7, respectively, for integer values of j for the first 13 load cycles. After 13 cycles only one experimental data point is available for $(NDR)_j$, and a unique second order curve through the origin and this point is unobtainable. Specific values of K_{j1} and K_{j2} for a given cycle are clearly dependent upon the availability of experimental evidence. Thus, the discrete values of K_{j1} and K_{j2} presented in Figs. 4.6 and 4.7 represent statistical approximations. The reasonably good correlation of available data obtained with Eqs. 4.23(a) - 4.23(d) suggests that, for the specimens analyzed, $K_{j1}(NDR)_j + K_{j2}(NDR)_j^2$ is a viable predictor of $(D_i)_j$.

4.4.2 Predicting D_i in Terms of K_{j1}, K_{j2}, and $(NDR)_j$

The prediction of the Energy Dissipation Index, D_i, in terms of K_{j1}, K_{j2}, and $(NDR)_j$ requires the summation of $(D_i)_j$ for all j's over n cycles. Therefore, D_i may

be expressed as

$$D_i = \sum_{j=1}^{n} (D_i)_j = \sum_{j=1}^{n} \left[K_{j1} (NDR)_j + K_{j2} (NDR)_j^2 \right] \tag{4.24}$$

The prediction of D_i also requires the quantification of K_{j1}, K_{j2}, and $(NDR)_j$ for n cycles.

The development of the relationships between K_{j1} and K_{j2} and j provides a viable means to determine intermediate values for K_{j1} and K_{j2}. For the first 8 cycles ($1 \leq j \leq 8$), functional relationships between K_{j1} and K_{j2} and j, shown in Figs. 4.6 and 4.7, may be obtained by performing a regression analysis on the discrete values of K_{j1} and K_{j2} and using a complete second-order model ($Y_i = \beta_0 + \beta_1(X_i) + \beta_2(X_i)^2$, $\beta_0 \neq 0$). The resulting best-fit equations are

$$K_{j1} = 1.604 - 0.246(j) + 0.004(j)^2 \tag{4.25}$$

$$K_{j2} = 0.197 - 0.042(j) + 0.006(j)^2 \tag{4.26}$$

For cycles 9 through 13, the relatively inconsistent variations in K_{j1} and K_{j2} restrict the development of similar meaningful functional relationships for these cycles. However, an alternate representation of K_{j1} and K_{j2} for $j > 8$ may be obtained by evaluating Eqs. 4.24 and 4.25 at $j = 8$ and using the resulting value of K_{j1} and K_{j2} to characterize the response for the remaining cycles. Thus, for $j \geq 8$, $K_{j1} = -0.113$ and $K_{j2} = 0.257$. The continuous representations of K_{j1} and K_{j2} for any real value of $j \geq 1$ are plotted in Figs. 4.6 and 4.7, respectively.

When Eq. 4.9 is used to predict the number of cycles with $P_i \geq 0.75P_y$, the resulting value is a real number with integral and fractional components, $(n)_i$ and $(n)_f$, respectively. A linear interpolation is used to calculate $(NDR)_{j=n}$ such that

$$(NDR)_{j=n} = \Lambda_1 + \Lambda_2 \tag{4.27a}$$

in which

$$\Lambda_1 = \frac{\left[(\mu^-)_{j=(n)_i} + \left(\frac{A_s'}{A_s}\right)(\mu^+)_{j=(n)_i} \right]}{\left[1 + \left(\frac{A_s'}{A_s}\right)^2 \right]} \tag{4.27b}$$

and

$$\Lambda_2 = \frac{(n)_f\left[(\mu^-)_{j=(n)_i+1} + \left(\frac{A_s'}{A_s}\right)(\mu^+)_{j=(n)_i+1} \right]}{\left[1 + \left(\frac{A_s'}{A_s}\right)^2 \right]}$$

$$- \frac{(n)_f\left[(\mu^-)_{j=(n)_i} + \left(\frac{A_s'}{A_s}\right)(\mu^+)_{j=(n)_i} \right]}{\left[1 + \left(\frac{A_s'}{A_s}\right)^2 \right]} \tag{4.27c}$$

The appropriateness of $\sum[K_{j1}(NDR)_j + K_{j2}(NDR)_j^2]$ to analytically predict the Energy Dissipation Index, D_i, can be evaluated by statistically analyzing the relationship between the experimental and predicted values of D_i [$(D_i)_{test}$ and $(D_i)_{pre}$, respectively] for the specimens in Table 4.4. It should be noted that, as compared to the beams listed in Tables 4.2 [$(E)_j$] and 4.3 [$(D_i)_j$], Specimen 1-2 from the research

by Hwang & Scribner (1984) is excluded from Table 4.4. The exclusion of this specimen from the following statistical analyses is based on the fact that the predicted value of n (Eq. 4.9) for Specimen 1-2 lies outside the upper 90% confidence limit in Fig. 4.3. Therefore, the response of this specimen is considered to be "non-representative", and thus, omitted from further statistical evaluation. For the beams presented in Table 4.4, the mean and coefficient of variation of $(D_i)_{test}/(D_i)_{pre}$ [where $K_{j1}(NDR)_j + K_{j2}(NDR)_j^2$ is summed over n_{pre} cycles to obtain $(D_i)_{pre}$] are 0.949 and 14.8%, respectively.

Using the experimental value of D_i and $\sum[K_{j1}(NDR)_j + K_{j2}(NDR)_j^2]$ as the dependent and independent variables, respectively, a regression analysis of the specimens in Table 4.4 results in a best-fit equation of

$$D_i = -4.79 + 1.07 \sum_{j=1}^{n} \left[K_{j1}(NDR)_j + K_{j2}(NDR)_j^2\right] \tag{4.28}$$

with $r^2 = 0.925$. Eq. 4.28 and the 90% confidence limits relative to the regression equation are plotted in Fig. 4.8. As shown in this figure, Eq. 4.28 overestimates D_i at low values of $\sum[K_{j1}(NDR)_j + K_{j2}(NDR)_j^2]$ and underestimates D_i at high values of $\sum[K_{j1}(NDR)_j + K_{j2}(NDR)_j^2]$. This is related to the fact that Eqs. 4.23(a) - 4.23(d) generally overpredict and underpredict $(D_i)_j$ at low and high values of $(NDR)_j$, respectively. Although Eq. 4.28 has a negative intercept, this equation provides a reasonably consistent fit of the data as indicated by the relatively high value of r^2.

4.5 D_i versus the Cumulative Normalized Ductility Range, CNDR

Recent research involving models designed to predict the hysteretic behavior of reinforced concrete members (Chung, Meyer, & Shinozuka 1989, 1990) suggests that formulating cyclic response in terms of "cumulative damage" is a viable means to study the effects of variations in strength, stiffness, and load history. The concept of "cumulative damage" may be extended to the analytical prediction of D_i by

examining the relationship between the cumulative contribution to D_i for a given number of cycles [a summation of $(D_i)_j$] and the corresponding cumulative value of the Normalized Ductility Range [a summation of $(NDR)_j$].

4.5.1 $(D_i)_s$ versus $(CNDR)_s$

As seen in Eq. 4.18, the analytical contribution to D_i for each cycle, $(D_i)_j$, is defined as the product of the modification factor, K_j, and the Normalized Ductility Range for that cycle, $(NDR)_j$. This product may be extended to characterize the cumulative relationship between $(D_i)_j$ and $(NDR)_j$ by summing the individual terms of D_i $[(D_i)_j]$ and $(NDR)_j$ over s cycles. Defining the cumulative ratio, $\Sigma[(\mu^-)_j + (A_s'/A_s)(\mu^+)_j]/[1 + (A_s'/A_s)^2]$, as the Cumulative Normalized Ductility Range, CNDR, and summing both sides of Eq. 4.18 over s cycles gives

$$(D_i)_s = K_s\ (CNDR)_s \tag{4.29}$$

in which

$$(D_i)_s = \frac{\sum_{j=1}^{s} (E)_j}{\frac{1}{2}(P_y\Delta_y)^-\left[1 + \left(\frac{A_s'}{A_s}\right)^2\right]} = \sum_{j=1}^{s} (D_i)_j \tag{4.30}$$

$$(CNDR)_s = \sum_{j=1}^{s} \frac{\left[(\mu^-)_j + \left(\frac{A_s'}{A_s}\right)(\mu^+)_j\right]}{\left[1 + \left(\frac{A_s'}{A_s}\right)^2\right]} \tag{4.31}$$

and K_s is a proportionality constant that correlates $(CNDR)_s$ with $(D_i)_s$.

Eq. 4.29 quantifies the cumulative experimental response of a reinforced concrete beam for s cycles. For example, in the current study, Beam H-1 survived 13 cycles with $P_i \geq 0.75P_y$. Thirteen specific values of $(D_i)_s$ may be calculated, one corresponding to each value of s [$(D_i)_{s=13}$ is numerically equivalent to D_i]. The values of $(D_i)_s$ for the specimens listed in Table 4.3 are listed in Table 4.5.

Analogous to Eq. 4.18, Eq. 4.29 represents a first-order model (linear) such that $Y_i = \beta_0 + \beta_1(X_i)$, with $\beta_0 = 0$ (for all j, when $(CNDR)_s$ is zero, $(D_i)_s$ must also be zero). The implied linearity of Eq. 4.29 may be examined by plotting $(D_i)_s$ versus $(CNDR)_s$ for the specimens listed in Table 4.5. Figs. 4.9(a) - 4.9(d) graphically depict the relationship between $(D_i)_s$ and $(CNDR)_s$ for s = 1, 4, 7, and 10 (cycles 1, 4, 7, and 10), respectively. It should be noted that the same specimens are plotted in Fig. 4.5(a) and 4.9(a), but presented at different scales, since the relationship between $(D_i)_j$ and $(NDR)_j$ is identical to $(D_i)_s$ and $(CNDR)_s$ at j = s = 1. As for K_j, an empirical determination of K_s may be obtained by performing a regression analysis of the data in each figure. Using the least squares method, the resulting best-fit equations are

$$(D_i)_1 = 2.47(CNDR)_1 \tag{4.32a}$$

$$(D_i)_4 = 1.18(CNDR)_4 \tag{4.32b}$$

$$(D_i)_7 = 1.57(CNDR)_7 \tag{4.32c}$$

$$(D_i)_{10} = 1.39(CNDR)_{10} \tag{4.32d}$$

with $r^2 = 0.504$, 0.466, 0.443, and 0.239, respectively. Eqs. 4.32(a) - 4.32(d) are plotted in Figs. 4.9(a) - 4.9(d), respectively. As compared to Eqs. 4.20(a) - 4.20(c), the larger values of r^2 for Eqs. 4.32(a) - 4.32(c) suggest that the relationship between $(D_i)_s$ and $(CNDR)_s$ is more linear than the relationship between $(D_i)_j$ and $(NDR)_j$.

However, the values of r^2 are still low, which indicates that the model $Y_i = \beta_1(X_i)$ is not appropriate for the relationship between $(D_i)_s$ and $(CNDR)_s$. Analogous to the development of Eqs. 4.21 and 4.22, an improved correlation between $(D_i)_s$ and $(CNDR)_s$ may be obtained with an alternate expression for K_s such that

$$K_s = [K_{s1} + K_{s2}(CNDR)_s] \tag{4.33}$$

and

$$(D_i)_s = K_{s1}(CNDR)_s + K_{s2}(CNDR)_s^2 \tag{4.34}$$

The appropriateness of Eq. 4.34 to characterize the relationship between $(D_i)_s$ and $(CNDR)_s$ may be evaluated by performing a regression analysis on the data in Figs. 4.9(a) - 4.9(d). Using a second-order model of the form $Y_i = \beta_1(X_i) + \beta_2(X_i)^2$, the resulting best-fit equations are

$$(D_i)_1 = 1.48(CNDR)_1 + 0.17(CNDR)_1^2 \tag{4.35a}$$

$$(D_i)_4 = 1.07(CNDR)_4 + 0.03(CNDR)_4^2 \tag{4.35b}$$

$$(D_i)_7 = 0.55(CNDR)_7 + 0.03(CNDR)_7^2 \tag{4.35c}$$

$$(D_i)_{10} = -0.14(CNDR)_{10} + 0.03(CNDR)_{10}^2 \tag{4.35d}$$

with $r^2 = 0.975$, 0.954, 0.951, and 0.864, respectively. Eqs. 4.35(a) - 4.35(d), which define the values of K_{s1} and K_{s2}, are plotted in Fig. 4.9(a) - 4.9(d), respectively. As compared to the fit of the data obtained with Eqs. 4.32(a) - 4.32(d), Eqs. 4.35(a) - 4.35(d) more appropriately characterize the trend of the experimental data. Figs. 4.10 and 4.11 provide a graphical summary of the values of K_{s1} and K_{s2}, respectively, for

the first 13 cycles of the data shown in Table 4.5. The larger values of r^2 obtained with Eqs. 4.35(b) - 4.35(d), compared to those obtained with Eqs. 4.23(b) - 4.23(d), suggest that the CNDR characterizes the cyclic performance of reinforced concrete beams more consistently than the NDR. As compared to the NDR, which characterizes energy dissipation in terms of a given cycle, the CNDR characterizes energy dissipation through a given cycle, and thus, reflects the effects of a member's prior load history. Further, when the cumulative dissipated energy and displacement ductility factors are used to correlate cyclic response, the impact of relatively large changes in specific values of $(E)_j$, $(\mu^-)_j$, or $(\mu^+)_j$, become less significant. Subsequently, K_{s1} and K_{s2} exhibit less variation than K_{j1} and K_{j2}.

Analogous to the evaluation of results using the NDR, the number of available test specimens decreases as s increases. Thus, less reliability is implied for the relationship between K_{s1}, K_{s2}, $(CNDR)_s$, and $(D_i)_s$ as the number of load cycles increases.

4.5.2 Predicting D_i in Terms of K_{s1}, K_{s2}, and $(CNDR)_s$

When s = n, the analytical value of D_i given by Eq. 4.34 may be expressed as

$$D_i = (D_i)_{s=n} \tag{4.36}$$

Quantifying $(D_i)_s$ (and thus D_i) in terms of K_{s1}, K_{s2}, and $(CNDR)_s$ also requires the determination of n, the number of cycles with $P_i \geq 0.75P_y$ (again, n is a real number when calculated in accordance with Eq. 4.9). Thus, the contribution of $(D_i)_s$ to D_i that corresponds to a non-integer number of cycles must be determined. The method used to calculate the value of K_{s1}, K_{s2} and $(CNDR)_s$ which corresponds to s = n is described next.

A continuous functional relationship between K_{s1} and s may be developed by performing a regression analysis on the 13 discrete data points shown in Fig. 4.10 and using a complete second-order model [i.e. $Y_i = \beta_0 + \beta_1(X_i) + \beta_2(X_i)^2$]. The resulting best-fit equation is given by

$$K_{s1} = 1.585 - 0.167(s) + 0.002(s)^2 \tag{4.37}$$

and will be used for all values of s (even though Eq. 4.37 is based on the discrete data for 13 cycles, it will be used to extrapolate the value of K_{s1} for $s \leq 17.6$, where 17.6 is the maximum predicted value of n using the current data). A similar expression may be developed for K_{s2}. However, the discrete data shown in Fig. 4.11 suggests that the characterization of K_{s2} for $1 \leq s \leq 4$ is markedly different than the characterization of K_{s2} for $s > 4$. Thus, two separate models are chosen to represent the mathematical expressions for K_{s2}. Based on the data shown in Fig. 4.11, a second-order model is selected for specimens with $s \leq 4$. The discrete data points for the fourth and thirteenth cycle are used to define a first-order model for specimens with $s > 4$. The resulting best-fit equations are

$$K_{s2} = 0.278 - 0.132(s) + 0.018(s)^2 \tag{4.38}$$

and

$$K_{s2} = 0.034 - 0.001(s) \tag{4.39}$$

The slope of Eq. 4.38 is positive (concave up) for $s > 3.67$, and thus, a smooth characterization of K_{s2} is not obtained (Eq. 4.38 does not continuously decrease in the interval $3.67 \leq s \leq 4$). In an effort to improve the overall prediction of K_{s2} for non-integer values of s (as s increases, K_{s2} should continually decrease in the interval $3.67 \leq s \leq 4$), the maximum and minimum values of s for Eqs. 4.38 and 4.39, respectively, are chosen to correspond to the value of s where the slopes of these two equations are the same (i.e., $s = 3.7$). Thus, the range of s corresponding to Eqs. 4.38 and 4.39 becomes $1 \leq s \leq 3.7$ and $3.7 \leq s \leq 17.6$, respectively. The resulting continuous functional relationships between K_{s1}, K_{s2}, and s are plotted in Figs. 4.10 and 4.11.

Analogous to the determination of $(NDR)_j$ for $j = n$ (where n is a non-integer

number), a linear interpolation for $(CNDR)_{s=n}$ is used such that

$$(CNDR)_{s=n} = \Xi_1 + \Xi_2 \tag{4.40a}$$

in which

$$\Xi_1 = \frac{\sum_{j=1}^{(n)_i} \left[(\mu^-)_j + \left(\frac{A_s'}{A_s} \right) (\mu^+)_j \right]}{\left[1 + \left(\frac{A_s'}{A_s} \right)^2 \right]} \tag{4.40b}$$

and

$$\Xi_2 = \frac{(n)_f \left\{ \sum_{j=1}^{(n)_i+1} \left[(\mu^-)_j + \left(\frac{A_s'}{A_s} \right) (\mu^+)_j \right] - \sum_{j=1}^{(n)_i} \left[(\mu^-)_j + \left(\frac{A_s'}{A_s} \right) (\mu^+)_j \right] \right\}}{\left[1 + \left(\frac{A_s'}{A_s} \right)^2 \right]} \tag{4.40c}$$

The continuous mathematical relationships between K_{s1}, K_{s2}, and s, and the ability to calculate $(CNDR)_s$ for a non-integer number of cycles permits the analytical quantification of the Energy Dissipation Index, D_i. The appropriateness of $K_{s1}(CNDR)_s + K_{s2}(CNDR)_s^2$ for s = n to predict D_i may be evaluated by performing a linear regression analysis on the same specimens used to define the Normalized Ductility Range presented in Table 4.5 (see Table 4.6 for the corresponding values of CNDR). For the beams in Table 4.6, the ratio of $(D_i)_{test}/(D_i)_{pre}$ (where $[K_{s1}(CNDR)_s + K_{s2}(CNDR)_s^2]$ defines the analytical value of D_i) is statistically evaluated. The resulting mean and coefficient of variation of this ratio are 0.964 and 14.2%, respectively. Thus, as compared to the previous values of 0.949 and 14.8% (which

are based on the NDR formulation), a slightly improved fit of the data (the ratio of experimental D_i to predicted D_i) is obtained using the CNDR.

Using D_i and $[K_{s1}(CNDR)_s + K_{s2}(CNDR)_s^2]_{s=n}$ as the dependent and independent variables, respectively, a regression analysis for the specimens in Table 4.6 results in a best-fit equation of

$$D_i = -2.94 + 1.04\left[K_{s1}(CNDR)_s + K_{s2}(CNDR)_s^2\right]_{s=n} \tag{4.41}$$

with $r^2 = 0.922$. Eq. 4.41 and the 90% confidence limits relative to the regression equation are plotted in Fig. 4.12. Analogous to Fig. 4.8, Fig. 4.12 shows that the relationship between D_i and $[K_{s1}(CNDR)_s + K_{s2}(CNDR)_s^2]_{s=n}$ is linear and that Eq. 4.41 overpredicts D_i at low values of CNDR and underpredicts D_i at high values of CNDR. As compared to Eq. 4.28, the slope and intercept of Eq. 4.41 are closer to unity and zero, respectively, while the values of r^2 are nearly identical. This further supports the observation that a formulation expressed in terms of CNDR will provide a better prediction of D_i than a formulation expressed in terms of NDR.

Possibly an improvement in the prediction of D_i could be obtained by recalculating K_{s1} and K_{s2} where a refined relationship between $(D_i)_s$ and $(CNDR)_s$ [Figs. 4.9(a) - 4.9(d)] incorporates the predicted value of $(CNDR)_s$ and only those specimens which fail during cycle s. However, the limited amount of experimental data restricts a meaningful interpretation of K_{s1} and K_{s2} using this "re-calibration" procedure. Clearly, additional specimen results will facilitate an improved correlation between K_{s1}, K_{s2}, CNDR, and D_i.

CHAPTER 5

DESIGN IMPLICATIONS

5.1 Introduction

For flexural members in earthquake resistant frames, the anticipated amplitude of displacement and the number of cycles to failure are important design considerations. As previously discussed, the ability to quantify the number of load cycles (and the energy dissipation capacity) in terms of a member's design parameters provides a means to evaluate cyclic response for a wide range of beams that are designed with different geometries and strengths. In this chapter, the methods developed in Chapter 4 are applied to a beam design from the current research program to study the effect of a change in displacement ductility on cyclic response. The Cumulative Normalized Ductility Range, CNDR, (rather than the Normalized Ductility Range, NDR) is used to quantify the Energy Dissipation Index, D_i, since 1) the CNDR provides a more consistent fit of existing experimental results (less scatter relative to the best-fit line), and 2) the results of the previous statistical analysis (Chapter 4 — mean and coefficient of variation of $(D_i)_{test}/(D_i)_{pre}$) imply that D_i is somewhat more accurately characterized with the CNDR than the NDR. In addition, a parametric investigation is undertaken, using a beam proportioned to resist a seismic event (Uniform Building Code 1988 and ACI Building Code), to evaluate the effects of changes in flexural and shear reinforcement (v_m and v_s, respectively), concrete strength, and beam width on the predicted number of cycles to failure. Based on these analyses, design guidance is provided for improving the response of reinforced concrete beams subjected to earthquake loading.

5.2 Application of Analytical Procedure

The response of a reinforced concrete structure to earthquake loading is highly

dependent upon the magnitude of the lateral displacement. For reinforced concrete beams, the sensitivity of n (the number of cycles with $P_i \geq 0.75P_y$), CNDR, and D_i to changes in the root-mean-square displacement ductility factor, μ'_{rms}, can be evaluated by investigating the change in cyclic response that results from a change in μ'_{rms}. Beam H-1 from the current study is used for this investigation. As indicated in Table 4.1, the test value of μ'_{rms} for Beam H-1 is 4.3. The experimental values of n and D_i for Beam H-1 are 13 and 102, respectively (Table 4.5).

Using the test value of v_m and the values of v_s, f'_c, A'_s/A_s, b, and s shown in Table 3.1, and Eqs. 4.9, 4.31, and 4.36 to calculate n, CNDR, and D_i, respectively, the cyclic response of Beam H-1 is evaluated as μ'_{rms} increases from 4.3 to 8.5 (8.5 corresponds to the value of μ'_{rms} for Beam H-3, which had the same geometry and reinforcement as Beam H-1).

For $\mu'_{rms} = 4.3$, the predicted values of n and D_i are 11.9 and 87, 8.5 and 14.7% below the experimental values, respectively. The differences between the test and predicted values of D_i are primarily due to the underprediction of n.

The adverse effect of an increase in displacement ductility on cyclic response is shown in Fig. 5.1, a plot of n versus μ'_{rms}. In this case, n decreases from 11.9 to 4.5 cycles as μ'_{rms} increases from 4.3 to 8.5. As seen in Fig. 5.1, for the range of μ'_{rms} investigated ($4.3 \leq \mu'_{rms} \leq 8.5$), the relationship between n and μ'_{rms} is nearly linear.

Using the procedure developed in Chapter 4 to calculate CNDR for s = n cycles, the effect of a change in μ'_{rms} on CNDR and D_i may also be studied. The relationships between CNDR and D_i and μ'_{rms} are shown in Fig. 5.2. This figure shows that an increase in μ'_{rms} (and thus, a decrease in n) results in a decrease in CNDR for values of $\mu'_{rms} > 4.9$ (there is a 0.9% increase in CNDR as μ'_{rms} increases from 4.3 to 4.9). In addition, Fig. 5.2 shows that the maximum dissipated energy does not occur at the lowest value of μ'_{rms}. For example, with $\mu'_{rms} = 4.3$, the predicted value of D_i is 87. However, the maximum predicted value of D_i, 123, occurs at $\mu'_{rms} = 6.7$. Similar results are obtained (i.e., maximum energy dissipation

capacity does not correspond to the lowest value of μ'_{rms}) when the NDR is used to predict D_i. Although the maximum energy dissipation capacity for Beam H-1 does not correspond to the minimum value of μ'_{rms}, maximum energy dissipation and a maximum value of D_i do not ensure maximum cyclic performance, at least for an individual beam. For a reinforced concrete beam by itself, the maximum cyclic performance is achieved by maximizing n. However, maximizing the energy dissipated may be of greater importance for the structure as a whole. For Beam H-1, the nonlinear relationship between D_i and μ'_{rms} in Fig. 5.2 suggests that, for the range of μ'_{rms} investigated, an "optimum" combination of design and loading parameters exists that maximizes D_i.

5.3 Parametric Investigation

In the following sections, a parametric investigation is undertaken that examines the effect of changes in the flexural and shear strengths of a reinforced concrete beam on member response. In addition, a change in beam width is also investigated to study the effects of a change in geometry on the number of cycles to failure.

The parametric investigation is carried out using a beam design presented in Part 31 - Special Provisions for Seismic Design of the PCA notes on ACI 318-89 (Portland Cement Association 1990). The beam (Fig. 5.3) represents a typical flexural member from an interior frame in a multistory frame-shearwall structure that has been designed and detailed in accordance with the seismic provisions specified in Chapter 21 of ACI 318-89. The earthquake induced forces are calculated in accordance with the Uniform Building Code (1988) — Seismic Zone 4.

As shown in Chapter 4, the prediction of n requires the determination of the maximum applied shear stress, v_m. For beams designed in accordance with the ACI Building Code, this necessitates the determination of the maximum applied shear force, V_m (the ACI code uses the notation V_e in lieu of V_m), where the calculation of

V_m is based on 1) gravity loading, and 2) the probable moment strength, M_{pr}, of the beam at the joint faces, obtained using $f_s = 1.25f_y$. The design shear force at each joint face, V_m, is therefore dependent upon the summation of M_{pr} for both ends of the beam divided by the clear span. For the analysis, $v_m = V_m/(bd)$.

The transverse reinforcement, shear strength = ϕV_s ($\phi = 0.85$), is designed to resist V_m. Thus, the required nominal shear strength is determined such that $V_s \geq V_m/\phi$, with a maximum value of $V_s = 4\sqrt{f'_c}(b_w d)$ (b_w = beam web width and d = effective depth in negative bending).

The unfactored dead and live loads for the beam are 2.56 and 0.88 kips/ft, respectively. The concrete design strength is 4,000 psi, and the yield strength of the flexural and shear reinforcement is 60,000 psi. The clear span is 18.17 ft. The negative moment reinforcement, A_s, at the exterior and interior joint faces is comprised of 5 #8 bars ($\rho = 0.0092$) and 5 #9 bars ($\rho = 0.0116$), respectively. The positive moment reinforcement, A'_s, is comprised of 3 #8 bars ($\rho' = 0.0055$) and is continuous over the entire length of the span. The transverse reinforcement in the beam hinging regions consists of #3 closed stirrups plus one #3 crosstie, extending 2h (h = 24 in.) from the faces of the supports at a spacing of 4.5 in.. The details of this beam are presented in Fig. 5.3.

In the analyses that follow, the quantification of the number of cycles to failure assumes that a strong column-weak beam response prevails throughout the duration of an earthquake and that opposite ends of a span are simultaneously subjected to negative and positive bending as a frame deflects laterally. Thus, both the negative and the positive moment reinforcement (at different ends of the span), A_s and A'_s, respectively, contribute to the earthquake induced shear force. It is also assumed that the displacement ductility factor is unaffected by changes in beam strength and geometry.

The analysis of n_{test}/n_{pre} for the beams in Table 4.1 shows that, statistically, Eq. 4.9 is a viable predictor of the number of cycles to failure, and thus,

$$n = 3.75 - 2.06\frac{v_m}{\sqrt{f_c'}}\left[1+\left(\frac{A_s'}{A_s}\right)^2\right] + 0.85\frac{v_s}{\sqrt{f_c'}}$$

$$+ 67.55\left(\frac{A_s'}{A_s}\right)^{0.20} + 14.53\left(\frac{b}{s}\right)^{0.20} - 55.07(\mu'_{rms})^{0.15} \qquad (4.9)$$

provides one means with which to quantitatively evaluate performance as a function of variations in design and loading parameters. However, for the beam used in the case study, the ability to calculate the maximum shear stress in negative and positive bending at each end of the span suggests that a slight modification to the shear stress term in Eq. 4.9 is appropriate.

The parameter in Eq. 4.9 that represents the effect of the maximum applied shear stress in positive bending, v_m^+, is $v_m(A_s'/A_s)^2$ (the ratio of A_s' to A_s is used due to the fact that v_m^+ can not be experimentally measured for cantilevered specimens that are initially loaded in the "negative bending" direction). The improved correlation of test results obtained with $v_m(A_s'/A_s)^2$ in lieu of $v_m(A_s'/A_s)$ (see Chapter 4), indicates that the influence of the maximum applied shear stress in positive bending on n is less than the design value of v_m^+. Thus, for a reinforced concrete beam with a specified loading, the relative effect of v_m^+ is approximated by $v_m(v_m^+/v_m)^2$. Substituting this expression into the shear stress term of Eq. 4.9 results in

$$n = 3.75 - 2.06\frac{v_m}{\sqrt{f_c'}}\left[1 + \left(\frac{v_m^+}{v_m}\right)^2\right] + 0.85\frac{v_s}{\sqrt{f_c'}}$$

$$+ 67.55\left(\frac{A_s'}{A_s}\right)^{0.20} + 14.53\left(\frac{b}{s}\right)^{0.20} - 55.07(\mu'_{rms})^{0.15} \qquad (5.1)$$

When Eq. 5.1 is used to predict the number of cycles to failure for the beam in Fig. 5.3, the values of n at the exterior joint are 13.3 and 5.9 for $\mu'_{rms} = 4$ and 8, respectively. Likewise, the values of n predicted at the interior joint are 10.5 and 3.0 for $\mu'_{rms} = 4$ and 8, respectively.

In the following sections, the effects of changes in the amount of flexural reinforcement, area and spacing of transverse reinforcement, concrete strength, and beam width on the number of cycles to failure are studied to evaluate their influence on the cyclic performance of a reinforced concrete beam subjected to severe cyclic loading. For each parameter investigated, response is examined at displacement ductility factors of $\mu'_{rms} = 4$ and 8.

5.3.1 Negative Moment Reinforcement, A_s

For prismatic reinforced concrete beams designed to resist severe seismic loading, the shear force at a joint face is primarily dependent upon the amount of flexural reinforcement. An increase in A_s (and to a lesser degree A_s') results in an increase in the negative bending moment capacity of the section, and thus, an increase in the maximum applied shear stress. Since both ends of a span contribute to the maximum applied shear stress, a change in A_s at one face affects the predicted number of cycles to failure at both faces. To study the effect of an increase in A_s on n for the beam shown in Fig. 5.3, yet maintain the as designed proportions of the

beam, the increase in shear stress due to an increase in A_s is calculated such that 1) a constant ratio of A_s'/A_s at the exterior and interior joint faces [$(A_s'/A_s)_{ext} = 0.60$ and $(A_s'/A_s)_{int} = 0.474$] is maintained, and 2) A_s' is continuous along the entire span length. Thus, an increase in A_s at the exterior or interior joint face has the net effect of increasing A_s at the opposite joint face.

For the exterior joint of the beam shown in Fig. 5.3, the maximum applied shear stresses in negative (v_m^-) and positive (v_m^+) bending are 172 and 41 psi, respectively. The increase in shear stress due to an increase in A_s at the exterior joint face (and subsequently an increase in A_s at the interior joint face) is illustrated in the plot of shear stress versus $\rho = A_s/(bd)$ in Fig. 5.4. The maximum value of ρ investigated for the exterior joint is 0.0197, which corresponds to $\rho = 0.025$ for the interior joint (Chapter 21 of ACI 318-89 restricts ρ for flexural members to a maximum of 0.025). At $\rho = 0.0197$, the values of v_m^- and v_m^+ for the exterior joint are 262 and 137 psi, respectively.

A similar plot of the relationship between shear stress and ρ at the interior joint is presented in Fig. 5.5. The as designed values of v_m^- and v_m^+ are 186 and 27 psi, respectively. At $\rho = 0.025$, v_m^- and v_m^+ are 283 and 118 psi, respectively.

The effect of an increase in A_s on the cyclic response of the exterior and interior joints is evaluated based on changes in n (Eq. 5.1). For the exterior joint, an increase in ρ from 0.0092 to 0.0197 results in a net decrease of 3.5 cycles (for both values of μ_{rms}' investigated). Likewise, for $\mu_{rms}' = 4$ and 8, an increase in ρ from 0.0116 to 0.025 for the interior joint results in a decrease of 3.1 cycles. Although the minimum and maximum values of ρ are different for the two joints investigated, the net decrease in n is nearly identical (3.5 versus 3.1 cycles). For the exterior and interior joints, the decrease in n resulting from an increase in A_s is shown in Figs. 5.6 and 5.7, respectively.

For the interior joint, the relationship between n and ρ shown in Fig. 5.7 indicates that, at $\mu_{rms}' = 8$, $n < 2$ for values of $\rho \geq 0.016$. Since the derivation of Eq.

4.9, and thus Eq. 5.1, is based on test results for specimens with $2 \leq n_{test} \leq 17$ (n = 2 and 17 define the applicable range for the prediction of n), reinforced concrete beams with predicted values of $n < 2$ should be presumed to perform poorly under cyclic loading, although the exact behavior is uncertain. In addition, $\rho = 0.016$, which corresponds to n = 2, is based on the best-fit line obtained from a regression analysis of available data. Therefore, an equal probability exists that n is overpredicted or underpredicted. A conservative estimate of n would be more appropriately predicted using the lower 90% confidence limit in Fig. 4.3.

A comparison of Figs. 5.6 and 5.7 for a given value of μ'_{rms} and ρ shows that the predicted value of n is greater for the exterior joint than the interior joint. For example, at $\mu'_{rms} = 4$ and $\rho = 0.015$, the number of cycles to failure for the exterior and interior joints are 11.3 and 9.7, respectively. The larger value of n for the exterior joint is primarily attributed to the fact that the exterior joint has a larger ratio of A'_s/A_s than the interior joint, and thus, exhibits improved cyclic performance.

5.3.2 Positive Moment Reinforcement, A'_s

For doubly reinforced concrete beams with a constant area of negative moment reinforcement, an increase in A'_s results in an increase in the positive bending moment capacity, and thus, an increase in shear stress. The effect of a change in A'_s on shear stress (and n) for the beam shown in Fig. 5.3 is determined based on constant values of A_s at both joints (A_s = 5 #8 bars and 5 #9 bars for the exterior and interior joints, respectively), and A'_s continuous along the entire span length. The increase in shear stress resulting from an increase in A'_s is shown in Figs. 5.8 and 5.9 for the exterior and interior joints, respectively (A'_s/A_s is used as the independent variable in both figures).

As shown in Fig. 5.8 for the exterior joint, the shear stress in negative bending, v_m^-, increases from 172 to 195 psi and the shear stress in positive bending, v_m^+, increases from 41 to 63 psi as A'_s/A_s increases from 0.6 to 1.0 Similarly, as shown in Fig. 5.9 for the interior joint, v_m^- increases from 186 to 223 and v_m^+ increases

from 27 to 63 psi as A'_s/A_s increases from 0.474 to 1.0.

The relationship between n and A'_s/A_s is shown in Figs. 5.10 and 5.11 for the exterior and interior joints, respectively. However, unlike the relationships between n and the negative moment reinforcement (i.e., ρ) shown in Figs. 5.6 and 5.7, the relationships in Figs. 5.10 and 5.11 show that n increases as the positive moment reinforcement increases. For the exterior joint, the net increase in n is 5.8 cycles (for both values of μ'_{rms} investigated) as A'_s/A_s increases from 0.6 to 1.0. For the interior joint, the net increase is 8.3 cycles (for both values of μ'_{rms} investigated) as A'_s/A_s increases from 0.474 to 1.0. The difference between the increase in n for the two joints is due to the greater increase in A'_s/A_s for the interior joint (i.e., the range of A'_s/A_s is larger for the interior joint than the exterior joint). In both cases, the increase in n is attributed to the decrease in concrete compressive stresses obtained with an increase in A'_s, which postpones spalling of the concrete around A'_s and subsequent buckling of the compression reinforcement.

Figs. 5.10 and 5.11 show that, as A'_s/A_s increases, the slope of the curves decreases (i.e., the effectiveness of an increase in A'_s on improving cyclic performance decreases at A'_s/A_s increases). Presumably the change in n at lower values of A'_s/A_s reflects the beneficial influence of an increase in A'_s which reduces the concrete compressive stresses. As the ratio of A'_s/A_s increases, the maximum applied shear stress in positive bending, v^+_m, increases, and thus, the contribution of A'_s to v^+_m becomes more influential in reducing n.

5.3.3 Shear Reinforcement

For reinforced concrete beams undergoing reversed loading, an improvement in cyclic performance is achieved by increasing the shear capacity of the section and confinement of the concrete core. In this section, the effect of a change in shear strength on the predicted number of cycles to failure is studied. Three parameters are investigated: 1) an increase in the area of transverse reinforcement at a constant spacing, 2) a decrease in spacing at a constant area of transverse reinforcement, and

3) a decrease in spacing at a constant nominal stirrup strength. For these analyses, the yield strength of the transverse reinforcement, f_{vy}, and beam width, b, remain constant at 60,000 psi and 20 in., respectively.

5.3.3.1 Increased Area of Transverse Reinforcement, A_v, at Constant Spacing

For the beam in Fig. 5.3, an increase in the area of transverse reinforcement, A_v, at a constant stirrup spacing, s, provides an increase in the nominal stirrup strength, $v_s = A_v f_{vy}/(bs) = \rho_v f_{vy}$, and number of cycles to failure. The prediction of n in accordance with Eq. 5.1 reflects the positive effects of an increase in A_v on cyclic response. As designed, v_s and ρ_v (where $A_v = 0.33$ in.^{2} and $s = 4.5$ in.) are 220 psi and 0.0037 for both joints of the beam in Fig. 5.3 (both joints have the identical shear reinforcement and stirrup spacing). An increase in A_v from 0.33 to 0.77 in.^{2} ($v_s = 510$ psi and $\rho_v = 0.0084$) ($A_v = 0.77$ in.^{2} corresponds to the maximum limit of $v_s = 8\sqrt{f'_c}$ as specified in Chapter 11 of ACI 318-89), results in a net increase of 3.9 cycles for both values of μ'_{rms} investigated. The increase in A_v from 0.33 to 0.77 in.^{2} corresponds to an increase in the transverse reinforcement from 1 #3 closed stirrup plus 1 #3 crosstie to ≈ 1 #5 closed stirrup plus 1 #3 crosstie. For the interior joint, the relationship between n and ρ_v is presented in Fig. 5.12.

A comparison of the results illustrated in Figs. 5.11 and 5.12 provides a relative measure of the effects of increasing A'_s/A_s and area of transverse reinforcement. The increase in n of 8.3 cycles, obtained as A'_s/A_s increases from 0.474 to 1.0, is substantially greater than the increase in n of 3.9 cycles as A_v increases from 0.33 to 0.77 in.^{2}.

5.3.3.2 Decreased Spacing of Transverse Reinforcement, s, at Constant Area

An increase in the shear capacity of a reinforced concrete beam, and thus, an increase in cyclic performance, is obtained with a decrease in stirrup spacing, s. In addition, for prismatic members, a decrease in s reduces buckling of the compression reinforcement, delays spalling of the concrete cover, and improves confinement of the concrete core. This also contributes to an increase in the number of cycles to failure.

The effect of stirrup spacing on cyclic performance is studied by examining the change in n resulting from a change in s. For this investigation, A_v remains constant.

For the interior joint of the beam in Fig. 5.3, a decrease in s from 4.5 (v_s = 220 psi and ρ_v = 0.0037) to 2 in. (v_s = 495 psi and ρ_v = 0.0084) (s = 2 in. corresponds to $v_s = 8\sqrt{f'_c}$) results in a net increase of 7.4 cycles for both values of μ'_{rms} investigated. The relationship between n and s for this joint is shown in Fig. 5.13, a plot of n versus ρ_v. As compared to Fig. 5.12 which illustrates the change in n resulting from a change in A_v, Fig. 5.13 shows that larger increases in n are obtained through a decrease in s (where A_v is constant) than an increase in A_v (where s is constant). For example, in Figs. 5.12 and 5.13 at $\mu'_{rms} = 4$ and $\rho_v = 0.006$, the number of cycles predicted by Eq. 5.1 for the interior joint are 12.4 cycles for $A_v = 0.54$ in.^{2} and s = 4.5 in. versus 14.4 cycles for $A_v = 0.33$ in.^{2} and s = 2.75 in..

5.3.3.3 Decreased Spacing of Transverse Reinforcement, s, at Constant v_s

One additional means with which to study the effect of stirrup spacing on cyclic performance is possible by examining the relationship between a change in s and n for a member with a constant value of v_s. For this study, the ratio of A_v to s does not vary from the as designed condition (i.e., $A_v/s = 0.073$ in. remains constant). Thus, a decrease in s results in a proportional decrease in A_v.

For the interior joint of the beam in Fig. 5.3, a decrease in s from 4.5 (ρ_v = 0.0037) to 2 in. (ρ_v = 0.0037), which corresponds to a decrease in A_v from 0.33 to 0.15 in.^{2}, results in a net increase of 3.5 cycles for both values of μ'_{rms} investigated. The relationship between the number of cycles to failure and stirrup spacing is shown in Fig. 5.14, a plot of n versus d/s (d/s is used as the independent variable since d is constant at 21.5 in.). The net increase in n of 3.5 cycles, which is due to the decrease in s from 4.5 to 2 in. at a constant v_s, is nearly identical to the increase in n of 3.9 cycles obtained from an increase in A_v from 0.33 to 0.77 in.^{2} at a constant s. At the maximum allowable value of v_s ($8\sqrt{f'_c}$), the sum of the number of cycles resulting from 1) the decrease in s at a constant v_s (3.5 cycles), and 2) the increase in A_v at a

constant s (3.9 cycles), equals the number of cycles resulting from the decrease in s at a constant A_v (7.4 cycles).

Fig. 5.14 shows that the slope of the curve decreases slightly as d/s increases. This change in slope is also reflected in Fig. 5.13 and is due to the relationship between n and s in Eqs. 4.9 and 5.1, in which changes in n are proportional to v_s and $(b/s)^{0.20}$. Although Fig. 5.14 illustrates the beneficial effect of a reduction in stirrup spacing on cyclic response, it should be noted that a decrease in s (which also requires a decrease in A_v for this comparison) is not a practical means to increase n since the beam is already designed with the minimum size stirrup (i.e., #3 bar).

5.3.4 Concrete Strength, f'_c

For the purpose of designing transverse reinforcement, Chapter 21 of ACI 318-89 states that, if the contribution to V_m from the earthquake-induced shear force is $\geq V_m/2$, the shear strength provided by the concrete, V_c, is assumed to be zero. Therefore, for the beam in Fig. 5.3, $V_c = 0$ for design purposes. However, as indicated in Eq. 5.1, concrete strength, f'_c, is a design parameter that influences the number of cycles to failure. The effect of an increase in f'_c on the cyclic response of the exterior and interior joints is evaluated by comparing the change in n resulting from a change in f'_c. As f'_c increases from 4 to 12 ksi, n increases 1.1 and 1.2 cycles for the exterior and interior joints, respectively, for both values of μ'_{rms} investigated.

The relationship between n and f'_c is shown in Figs. 5.15 and 5.16 for the exterior and interior joints, respectively. As seen in both figures, the increase of 8 ksi for f'_c from the as designed condition ($f'_c = 4$ ksi) does not significantly increase n. Thus, an increase in f'_c does not appear to be an efficient means with which to improve the cyclic performance of this member. This observation agrees with earlier observations by Hanks & Darwin (1988) on the influence of concrete strength on energy dissipation capacity.

5.3.5 Beam Width, b

In general, an increase in the width of a flexural member results in a nominal

increase in moment capacity and a proportional increase in beam weight (both factors are taken into consideration in the following calculations). An increase in width, b, also reduces the shear stress (v_m^- and v_m^+) and improves the confinement of the concrete core. Therefore, cyclic performance is also improved.

For the beam in Fig. 5.3, the affect of an increase in b on n cannot be directly evaluated since the as designed ratio of b/d is 0.93 (i.e., Eq. 5.1 is based on $0.48 \leq b/d \leq 0.96$). However, the influence of a change in b may be evaluated by investigating the change in shear stress and n that result from a decrease in b.

As previously noted, the design values of v_m^- and v_m^+ for the exterior and interior joints are 172 & 41 psi and 186 & 27 psi, respectively. The effects of b on shear stress are examined as b decreases from 20 in. ($\rho_{ext} = 0.0092$ and $\rho_{int} = 0.0116$) to 10 in. ($\rho_{ext} = 0.0184$ and $\rho_{int} = 0.0233$) (b = 10 in. is the minimum width permitted in Chapter 21 of ACI 318-89 for structures in regions of high seismic risk). Thus, at b = 10 in., the values of v_m^- and v_m^+ for the exterior and interior joints are 319 & 61 psi and 338 & 41 psi, respectively. The relationship between shear stress and beam width is shown in Figs. 5.17 and 5.18 for the exterior and interior joints, respectively. Both figures show that the relative increase in shear stress is much greater for v_m^- than v_m^+ as b drops from 20 to 10 in.. The reason is that the increases in shear stress due to a decrease in b are mitigated by decreases in the probable moment strength, M_{pr}. The percentage mitigation is greater for positive shears because the positive shear forces induced by M_{pr} are reduced by gravity loads (which do not change much) while the negative shear forces are increased by gravity loads; thus the mitigating drop in shear force represents a greater percentage of the positive shear force than it does the negative shear force.

The effect of a change in b on n is shown in Figs. 5.19 and 5.20 for the exterior and interior joints, respectively. These figures show that a reduction in beam width has a significant effect on the cyclic performance of the beam. For the exterior and interior joints, the decrease in b from 20 to 10 in. results in a net decrease of 5.1

and 5.2 cycles, respectively. For $\mu'_{rms} = 4$, this corresponds to a decrease in n from 13.3 to 8.2 cycles for the exterior joint and from 10.5 to 5.3 cycles for the interior joint. However, for $\mu'_{rms} = 8$, the decrease in n is somewhat different. For the exterior and interior joints, n decreases from 5.9 to 0.8 cycles and 3.0 to -2.2 cycles, respectively, as b decreases from 20 to 10 in.. As previously mentioned, the experimental range of available data is $2 \leq n_{test} \leq 17$. At $\mu'_{rms} = 8$, widths less than 11.6 in. for the exterior joint and 17.0 in. for the interior joint result in $n < 2$, and thus, imply exceptionally poor performance under cyclic loading.

Figs. 5.19 and 5.20 show that, as b increases, the slope of the curves decrease. Thus, the effectiveness of an increase in width on improving cyclic performance appears to diminish as b increases (a similar observation can be made for the relationship between n and A'_s/A_s shown in Figs. 5.10 and 5.11).

5.3.6 Evaluation of Parametric Investigation

As discussed in Chapter 1, several investigations have been undertaken to study the influence of design and loading parameters on the cyclic performance of reinforced concrete beams. The results of these investigations show that improvements in beam response are obtained with 1) a decrease in the maximum applied shear stress, stirrup spacing, and displacement ductility factor, and 2) an increase in the ratio of positive to negative moment reinforcement and concrete strength. The findings of this investigation show that these improvements are quantified in Eq. 5.1.

The parametric investigation demonstrates that changes in the number of cycles to failure, n, result from changes in the flexural and shear strength of the member and in the amplitude of imposed displacement. The presumption that reinforced concrete beams proportioned with $\phi v_s/v_m \geq 1.0$ are adequately designed to resist severe seismic loading is supported only in part by the findings of this investigation. For the beam in Fig. 5.3, the as designed values of $\phi v_s/v_m$ (where $v_m = \bar{v_m}$) are 1.09 and 1.0 for the exterior and interior joints, respectively. At $\mu'_{rms} = 4$, the beam exhibits good

cyclic performance (n = 13.3 and 10.5 cycles for the exterior and interior joints, respectively). At μ'_{rms} = 8, the exterior joint exhibits good performance (n = 5.9 cycles). However, the interior joint exhibits somewhat poorer performance (n = 3.0 cycles). This implies that, for regions of high seismic risk, the ratio of nominal stirrup strength to maximum applied shear stress, v_s/v_m, by itself is not a sufficient indication of adequate cyclic performance. Clearly, the amplitude of the imposed displacement must be an important design consideration.

For the beam used in the case study, at μ'_{rms} = 8, improvements in the performance of the interior joint are necessary to ensure good response under severe cyclic loading. Assuming that the negative moment reinforcement and the geometry of the beam remain constant, these improvements are possible with an increase in the positive moment reinforcement, A'_s, and nominal stirrup strength of the section, v_s.

One means available with which to evaluate the relative efficiency of the influence of the change in A'_s and v_s on cyclic response is to compare the change in n (Eq. 5.1) for the range of parameter investigated. For the interior joint, a summary of the preceding investigations shows that, relative to the as designed condition, the number of cycles 1) decreases by 3.1 cycles as ρ increases from 0.0116 to 0.025 (which corresponds to an increase in A_s from 5.0 to 10.75 in.^{2}), 2) increases by 8.3 cycles as A'_s/A_s increases from 0.474 to 1.0 (which corresponds to an increase in A'_s from 2.37 to 5.0 in.^{2}), 3) increases by 3.9 cycles as A_v increases from 0.33 to 0.77 in.^{2} (constant spacing), 4) increases by 7.4 cycles as s decreases from 4.5 to 2 in. (constant A_v), and 5) increases by 3.5 cycles as s decreases from 4.5 to 2 in. (constant v_s where A_v/s = 0.073 in.). As A_s and A'_s increase from 5.0 to 10.75 in^2. and 2.37 to 5.0 in^2., respectively, the increase in weight of the flexural reinforcement (excluding splices) is 19.6 and 8.9 lb per foot of beam length, respectively. If the stirrup configuration shown in Fig. 5.3 does not vary and the extension of the standard hooks remains constant at 3 in., the increase in weight of the transverse reinforcement as A_v increases from 0.33 to 0.77 in^2. (at a constant spacing of 4.5 in.) is 38.3 lb/ft

(2.67 stirrups are located within a linear foot of the beam hinging region). Similarly, the increase in stirrup weight as s decreases from 4.5 to 2 in. (at a constant area of 0.33 in^2.) is 35.9 lb/ft (6 stirrups within a linear foot). When A_v/s remains constant (0.073 in.) and s decreases from 4.5 to 2 in., there is no increase in weight from the as designed condition. As previously mentioned, it is not practical to decrease s at a constant value of A_v/s in an effort to increase n since the beam is already designed with the minimum size stirrup.

A direct cost comparison based on the preceding material weights is difficult since pricing is somewhat dependent upon national and regional conditions. However, some guidance in selecting the most effective means with which to improve cyclic response is provided by comparing cost extras (Means Building Construction Cost Data 1992). For example, reinforcing bar extras are a function of size, bending, quantity, and grade. Extras due to size are \$5, \$2, \$1.5, \$1.25, and \$1 per 100 lb for #3, #4, #5, #6, #7 thru #11 bars, respectively. Extras due to bending are \$4 for light bending (i.e., all stirrups) per 100 lb (light bending is defined in Chapter 4 of ACI 315-80). Clearly, cost extras resulting from an increase in the size of a straight bar (e.g., an increase in A_s'), as compared to extras resulting from an increase in light bending (e.g., an increase in A_v), are substantially less.

Based on the increase in material weight within the hinging zone and corresponding cost of reinforcement extras, an increase in A_s' appears to be more effective at improving the cyclic performance of the beam (an increase of 8.3 cycles is obtained with an increase of 8.9 lb/ft) as compared to an increase in A_v at a constant s (an increase of 3.9 cycles is obtained with an increase of 38.3 lb/ft). Although a reduction in stirrup spacing is not a practical means to increase the inelastic response of this beam, the decrease in s at a constant A_v is more effective (an increase of 7.4 cycles is obtained with an increase of 35.9 lb/ft) than the increase in A_v at a constant s (it should be noted that a decrease in s increases the difficulty in which concrete is placed and consolidated, and thus, increases labor costs).

For the parameters investigated, an increase in concrete strength is the least effective means to improve cyclic performance. Moderate improvements in performance are possible with an increase in the area of transverse reinforcement at a constant spacing, decrease in stirrup spacing of the transverse reinforcement at a constant v_s, and increase in beam width. The most effective means to improve performance of this beam is to increase the amount of positive moment reinforcement within the hinging regions.

CHAPTER 6

SUMMARY AND CONCLUSIONS

6.1 Summary

The effects of beam width on the cyclic behavior of reinforced concrete beam-to-column connections are investigated. A new procedure, which takes into consideration the influence of a member's strength, stiffness, and load history on cyclic performance, is developed to predict the number of cycles to failure and energy dissipation capacity per cycle in terms of beam design and load parameters. A parametric investigation is performed to quantify and evaluate the effect of changes in flexural and shear strength and geometry on the predicted number of cycles to failure.

To study the effect of beam width on cyclic performance, four cantilever beams were fabricated with flexural reinforcement ratios of 0.34 or 0.51% and nominal effective depths and widths of 15.7 and 15 in., respectively. The nominal stirrup shear strength, v_s = 79 psi, and spacing, s = 3.6 in., were constant for all specimens. The maximum applied shear stress ranged from 64 to 105 psi. The ratio of nominal stirrup strength to maximum applied shear stress, v_s/v_m, varied between 0.75 and 1.27. The nominal concrete strength was 4,000 psi. Cyclic beam-tip displacements ranged from 4.3 to 8.5 times the yield deflection. The amplitude of beam-tip displacement for each specimen was constant throughout testing.

The number of cycles to failure was defined as the summation of all cycles in which the maximum load was at least 75% of the yield load. The number of cycles to failure was used to quantify the total useable energy dissipated. Beam response was evaluated based on the number of cycles to failure and energy dissipation capacity.

Two analytical procedures were developed to quantify energy dissipation

capacity in terms of a Normalized Ductility Range, NDR, or a Cumulative Normalized Ductility Range, CNDR. The NDR and CNDR are developed based on a physical interpretation of the load-deflection hysteresis loops.

Recommendations were made for improving the performance of a reinforced concrete beam subjected to severe seismic loading.

6.2 Conclusions

Based on the experimental and analytical findings of this study, the following conclusions are obtained:

1. For reinforced concrete beams with the same effective depth, longitudinal and transverse reinforcement, and load history, an increase in width improves cyclic performance.
2. Wide beams (beams with width-to-depth ratios near unity) have lower shear stress and better confinement of the concrete core than narrow beams. Thus, under severe cyclic loading, wide beams exhibit less shear deformation, spalling of the concrete surrounding the flexural reinforcement, and buckling of the compression reinforcement. These factors contribute to an increase in the number of cycles to failure and energy dissipation capacity.
3. For the specimens with the same geometry and flexural and shear strength, an increase in the displacement ductility factor, μ, results in a decrease in the number of cycles to failure, energy dissipation capacity, and Energy Dissipation Index, D_i.
4. For the specimens with the same geometry, area of negative moment reinforcement, shear strength, and load history, an increase in the ratio of positive to negative moment reinforcement results in an increase in the number of cycles to failure and energy dissipation capacity.
5. An increase in beam width is more effective at increasing energy dissipation capacity as the amount of flexural reinforcement increases.

6. An increase in the predicted number of cycles to failure is obtained with a decrease in the maximum applied shear stress and displacement ductility factor, and an increase in the nominal stirrup strength, ratio of positive to negative moment reinforcement, and ratio of beam width-to-stirrup spacing.
7. Statistically, the CNDR provides a slightly better characterization of D_i than the NDR. Therefore, based on available experimental data, the CNDR represents a better means to predict D_i.
8. For the beam used in the parametric investigation, the interior joint exhibits good cyclic performance at $\mu = 4$ ($n = 10.5$ cycles) but poorer performance at $\mu = 8$ ($n = 3.0$ cycles). The least improvement in beam performance is obtained with an increase in concrete strength. Moderate increases in performance are possible with an increase in the area of transverse reinforcement at constant spacing. Although not a practical solution for this beam, improvements in performance are possible with a decrease in stirrup spacing at constant v_s, and an increase in beam width. The most effective means available to increase the cyclic performance is to increase the amount of positive moment reinforcement.

6.3 Recommendations for Future Study

As discussed in Chapter 4, the derivation of the equation that predicts the number of cycles to failure is largely empirical. Thus, its use is limited to those specimens whose geometric and material properties are within the range of parameters used to develop the equation. Future experimental studies designed to broaden the range of beam properties investigated provides a means to further evaluate the appropriateness of this equation.

In general, a better understanding of the inelastic response of reinforced concrete beams would also be possible if future research would address the following questions:

1. For a given beam design, what is the relationship between response (e.g., the number of cycles to failure and energy dissipation) and μ? How do changes in flexural and shear strength and geometry affect this relationship?
2. Is there a "threshold" value of μ that results in a significant change in beam response? How do changes in a member's design parameters affect this value?
3. If the predicted response of a relatively wide range of reinforced concrete beams is now quantifiable, should a minimum number of inelastic displacements be proposed for inclusion into seismic code provisions?
4. Considering the beneficial effect of an increase in beam width on cyclic response, is the use of high strength concrete to reduce member size an appropriate design practice in regions of high seismicity?
5. Should the minimum width of 10 in. specified in ACI 318-89 Section 21.3 be increased? Would it be appropriate for the ACI Code to specify a minimum beam width equal to the column width?
6. For a beam with a given depth and area of negative moment reinforcement, what combination of A_s'/A_s, A_v, s, and b provides the "optimum" response?
7. Is the influence of beam width on cyclic performance significantly affected by changes in the flexural strength of a reinforced concrete beam?
8. Can the influence of axial load on cyclic performance be realistically quantified when trying to predict the number of cycles to failure?

REFERENCES

Abdel-Fattah, B. A., and Wight, J. K. (1985). "Experimental Study of Moving Beam Plastic Hinging Zones for Earthquake Resistant Deign of R/C Buildings," *Report* No. UMCE 85-11, Department of Civil Engineering, University of Michigan, Ann Arbor, MI, December, 291 pp.

Abdel-Fattah, B., and Wight, J. K. (1987). "Study of Moving Beam Plastic Hinging Zones for Earthquake-Resistant Design of R/C Buildings," *ACI Structural Journal*, Vol. 84, No. 1, January- February, pp. 31-39.

ACI Committee 315 (1986). "Details and Detailing of Concrete Reinforcement (ACI 315-86)," *American Concrete Institute*, Detroit, Michigan, 57 pp.

ACI Committee 318 (1983). "Building Code Requirements for Reinforced Concrete (ACI 318-83)," *American Concrete Institute*, Detroit, Michigan, 111 pp.

ACI Committee 318 (1983). "Commentary on Building Code Requirements for Reinforced Concrete (ACI 318-83) (ACI 318R-83)," *American Concrete Institute*, Detroit, MI, 155 pp.

ACI Committee 318 (1989). "Building Code Requirements for Reinforced Concrete (ACI 318-89) and Commentary (ACI 318R-89)," *American Concrete Institute*, Detroit, MI, 353 pp.

ACI-ASCE Committee 352 (1985). "Recommendations for Design of Beam-Column Joints in Monolithic Reinforced Concrete Structures (ACI 352 R-85)," *American Concrete Institute*, Detroit, MI, 18 pp.

Alameddine, F., and Ehsani, M. R. (1989). "Behavior of Ductile High-Strength Concrete Connections," *Report* No. CEEM-89-105, Department of Civil Engineering and Engineering Mechanics, University of Arizona, Tucson, AZ, November, 258 pp.

Alameddine, F., and Ehsani, M. R. (1991). "High-Strength RC Connections Subjected to Inelastic Cyclic Loading," *Journal of Structural Engineering*, ASCE, Vol. 117, No. 3, March, pp. 829-850.

Banon, H., Biggs, J. M., and Irvine, H. M. (1981). "Seismic Damage in Reinforced Concrete Frames," *Journal of Structural Engineering*, ASCE, Vol. 107, No. 9, September, pp. 1713-1729.

Bertero, V. V., Popov, E. P., and Wang, T. Y. (1974). "Hysteretic Behavior of Reinforced Concrete Flexural Members with Special Web Reinforcement," Earthquake Engineering Research Center, University of California, Berkeley, *Report* No. EERC 74- 9, August, 126 pp.

Brown, R. H., and Jirsa, J. O. (1971). "Reinforced Concrete Beams Under Load Reversals," *Journal of the American Concrete Institute*, Vol. 68, No. 5, May, pp. 380-390.

Chung, Y. S., Meyer, C., and Shinozuka, M. (1989). "Modeling of Concrete Damage," *ACI Structural Journal*, Vol. 86, No. 3, May-June, pp. 259-271.

Darwin, D. and Nmai, C. K. (1986). "Energy Dissipation in RC Beams Under Cyclic Load," *Journal of Structural Engineering*, ASCE, Vol. 112, No. 8, August, pp. 1829-1846.

Draper, N. R., and Smith, H. (1981). *Applied Regression Analysis*, John Wiley & Sons, Inc., New York, NY, 709 pp.

Ehsani, M. R., Moussa, A. E., and Vallenilla, C. R. (1987). "Comparison of Inelastic Behavior of Reinforced Ordinary- and High- Strength Concrete Frames," *ACI Structural Journal,* Vol. 84, No. 2, March-April, pp. 161-169.

Ehsani, M. R., and Wight, J. K. (1982). "Behavior of External Reinforced Concrete Beam to Column Connections Subjected to Earthquake Type Loading," *Report* No. UMEE 82R5, Department of Civil Engineering, University of Michigan, Ann Arbor, MI, July, 243 pp.

Ehsani, M. R., and Wight, J. K. (1985). "Effect of Transverse Beams and Slab on Behavior of Reinforced Concrete Beam-to-Column Connections," *Journal of the American Concrete Institute*, Vol. 82, No. 2, March-April, pp. 188-195.

Ehsani, M. R., and Wight, J. K. (1985). "Exterior Reinforced Concrete Beam-to-Column Connections Subjected to Earthquake-Type Loading," *Journal of the American Concrete Institute*, Vol. 82, No. 4, July-August, pp. 492-499.

Ehsani, M. R., and Wight, J. K. (1990). "Confinement Steel Requirements for Connections in Ductile Frames," *ACI Structural Journal*, Vol. 116, No. 3, March, pp. 751-767.

Gentry, T. R., and Wight, J. K. (1992). "Reinforced Concrete Wide Beam-Column Connections Under Earthquake-Type Loading," *Report* No. UMCEE 92-12, Department of Civil and Environmental Engineering, The University of Michigan, Ann Arbor, MI, June, 203 pp.

Gosain, N. K., Brown, R. H., and Jirsa, J. O. (1977). "Shear Requirements for Load Reversals on RC Members," *Journal of the Structural Division*, ASCE, Vol. 103, No. ST7, July, pp. 1461-1476.

Hanks, D. L., and Darwin, D. (1988). "Cyclic Behavior of High Strength Concrete Beams," *SM Report* No. 21, University of Kansas Center for Research, Inc., Lawrence, KS, August, 120 pp.

Hwang, T. H. (1982). "Effects of Variation in Load History on Cyclic Response of Concrete Flexural Members," Thesis submitted to the University of Illinois at Urbana-Champaign in partial fulfillment of the requirements for the degree of Doctor of Philosophy, July, 232 pp.

Hwang, T. H., and Scribner, C. F. (1984). "R/C Member Cyclic Response During Various Loadings," *Journal of Structural Engineering*, ASCE, Vol. 110, No. 3, March, pp. 477-489.

Lee, D. L. N., Hanson, R. D., and Wight, J. K. (1976). "Original and Repaired Reinforced Concrete Beam-Column Subassemblages Subjected to Earthquake Type Loading," *Report* No. UMEE 76R4, Department of Civil Engineering, University of Michigan, Ann Arbor, MI, April, 206 pp.

Ma, S. M., Bertero, V. V., and Popov, E. P. (1976). "Experimental and Analytical Studies on the Hysteretic Behavior of Reinforced Concrete Rectangular and T-Beams," Earthquake Engineering Research Center, University of California, Berkeley, *Report* No. EERC 76-2, May, 254 pp.

Means Building Construction Cost Data (1992), 50th Annual Edition, Construction Consultants & Publishers, Kingston, MA, 552 pp.

Micro-Measurements (1979). "Strain Gage Installations with M-Bond 200 Adhesive," *Instruction Bulletin* B-127-10, Measurements Group, Inc., Raleigh, NC, 4 pp.

Micro-Measurements (1986). "Application of M-Coat J and JL Protective Coatings," *Instruction Bulletin* B-147-1, Measurements Group, Inc., Raleigh, NC, 2 pp.

Neter, J., and Wasserman, W. (1974). *Applied Linear Statistical Models*, Richard D. Irwin, Inc., Homewood, IL, 842 pp.

Nmai, C. K., and Darwin, D. (1984). "Cyclic Behavior of Lightly Reinforced Concrete Beams," *SM Report* No. 12, University of Kansas Center for Research, Inc., Lawrence, KS, June, 139 pp.

Nmai, C. K., and Darwin, D. (1986). "Lightly Reinforced Concrete Beams under Cyclic Load," *Journal of the American Concrete Institute*, Vol. 83, No. 5, September-October, pp. 777-783.

Popov, E. P., Bertero, V. V., and Krawinkler, H. (1972). "Cyclic Behavior of Three R. C. Flexural Members with High Shear," Earthquake Engineering Research Center, University of California, Berkeley, *Report* No. EERC 72-5, October, 82 pp.

Portland Cement Association (1990). "Notes on ACI 318-89," *Portland Cement Association*, Skokie, IL, pp. 31.1-31.81.

Recommended Lateral Force Requirements and Commentary (1980), Seismology Committee Structural Engineers Association of California, San Francisco, CA, 172 pp.

Scribner, C. F., and Wight, J. K. (1978). "Delaying Shear Strength Decay in Reinforced Concrete Flexural Members Under Large Load Reversals," *Report* No. UMEE 78R2, Department of Civil Engineering, University of Michigan, Ann Arbor, MI, May, 221 pp.

Scribner, C. F., and Wight, J. K. (1980). "Strength Decay in R/C Beams Under Load Reversals," *Journal of the Structural Division*, ASCE, Vol. 106, No. ST4, April, pp. 861-876.

Sheikh, S. A., and Uzumeri, S. M. (1980). "Strength and Ductility of Tied Concrete Columns," *Journal of the Structural Division*, ASCE, Vol. 106, No. ST5, May, pp. 1079-1102.

Takeda, T., Sozen, M. A., and Nielsen, N. N. (1970). "Reinforced Concrete Response to Simulated Earthquakes," *Journal of the Structural Division*, ASCE, Vol. 96, No. ST12, December, pp. 2557-2573.

Uniform Building Code (1988), International Conference of Building Officials, Whittier, CA, 926 pp.

Wang, M., and Shah, S. P. (1987). "Reinforced Concrete Hysteresis Model Based on the Damage Concept," *Earthquake Engineering and Structural Dynamics*, Vol. 15, pp. 993-1003.

Wight, J. K., and Sozen, M. A. (1973). "Shear Strength Decay in Reinforced Concrete Columns Subjected to Large Deflection Reversals," *Civil Engineering Studies*, SRS No. 403, University of Illinois at Urbana-Champaign, August, 290 pp.

Wight, J. K., and Sozen, M. A. (1975). "Strength Decay of RC Columns Under Shear Reversals," *Journal of the Structural Division*, ASCE, Vol. 101, No. ST5, May, pp. 1053-1065.

Table 2.1 Beam and Reinforcement Properties

	BEAM			
	H-1	H-2	H-3	H-4
PROPERTY:				
Height, h (in.)	18	18	18	18
Width, b (in.)	15	15	15	15
Effective depth, d (in.)	15.69	15.81	15.63	15.75
Effective depth, d_1 (in.)	16.81	16.88	16.69	15.75
Core Width, b_c (in.)	13.0	13.0	13.0	13.0
Core Depth, d_c (in.)	15.91	16.03	15.85	15.97
Shear Span, a (in.)	60	60	60	60
a/d	3.8	3.8	3.8	3.8
Reinforcement Ratio, ρ (%)	0.34	0.51	0.34	0.34
Top Reinforcement, A_s	4#4	6#4	4#4	4#4
Bottom Reinforcement, A_s'	2#4	3#4	2#4	4#4
A_s'/A_s	0.5	0.5	0.5	1.0
f_y (ksi)	66.4	66.4	66.4	71.7
Stirrup diameter (in.)	0.222	0.222	0.222	0.222
Stirrup spacing, s (in.)	3.6	3.6	3.6	3.6
f_{vy} (ksi)	56.6	55.5	54.3	54.3

Table 2.2 Concrete Mix Proportions and Properties

Mix Proportions[1]

Water	Cement	FA[2] (SSD)	CA[3] (SSD)
267	517	1490	1490

Concrete Properties

Beam	Slump (in.)	Air Content (%)	f'_c[4] (psi)	Age At Testing (days)
H-1	3 1/4	2.6	4200	7
H-2	4	2.8	4400	21
H-3	2	3.5	4120	5
H-4	4	3.3	4060	19

(1) Pounds per cubic yard

(2) Kansas River Sand: Lawrence Sand Company
Bulk specific gravity = 2.62
Absorption = 0.5%
Fineness modulus = 3.0

(3) Crushed Limestone: Hamm's Quarry, Perry, KS
Bulk specific gravity = 2.52
Absorption = 3.5%
Maximum size = 3/4 in.
Unit weight = 97 lb/ft^3

(4) Compressive strength from 6 x 12 in. cylinders

Table 2.3 Computed and Measured Shears

	BEAM			
	H-1	H-2	H-3	H-4
Nominal Stirrup Capacity:				
$V_s = A_v f_{vy} d/s$ (kips)	19.1	18.9	18.2	18.4
$v_s = A_v f_{vy}/(bs)$ (psi)	81	79	77	77
Calculated Shears:				
V_y (1) (kips)	13.5	20.1	13.4	14.5
V_c (2) (kips)	30.5	31.5	30.1	30.1
V_m (3) (kips)	49.6	50.4	48.3	48.5
Test Shears:				
V_y (kips)	12.8	20.9	13.0	14.8
V_m (kips)	15.1	24.8	17.4	16.8
Maximum Shear Stress:				
v_m (psi)	64	105	74	71
$v_m/\sqrt{f'_c}$	0.99	1.58	1.15	1.11

(1) V_y = Shear force at yielding of beam flexural reinforcement
(2) $V_c = 2\sqrt{f'_c} b_w d$
(3) V_m = Maximum shear force = $V_c + V_s$

Table 2.4 Principal Experimental Results

	BEAM			
	H-1	H-2	H-3	H-4
Yield Load (kips)	12.8	20.9	13.0	14.8
Maximum Load (kips)	15.1	24.8	17.4	16.8
Yield Deflection (in.)	0.30	0.34	0.24	0.37
Maximum Deflection (in.)	1.29	1.80	2.04	1.74
μ[(1)]	4.3	5.3	8.5	4.7
Maximum Growth (in.)	0.289	0.408	0.424	0.409
Number of Cycles:				
$P_i \geq 0.75P_y$	13	7	4	17
Maximum[(2)]	21	13	5	21

(1) μ = Displacement ductility factor
= Ratio of maximum beam-tip deflection to yield deflection

(2) Testing terminated after fracture of A_s' or 21 cycles

Table 3.1 Test Results of Experimental Research

Reference	Beam	b (in.)	s (in.)	v_s (psi)	f'_c (psi)	b/d
Current Study	H - 1	15	3.6	81	4,200	0.96
	H - 2	15	3.6	79	4,400	0.95
	H - 3	15	3.6	77	4,120	0.96
	H - 4	15	3.6	77	4,060	0.95
Hanks & Darwin (1988)	G - 1	7.5	3.6	169	11,610	0.48
	G - 2	7.5	3.6	168	11,310	0.48
	G - 3	7.5	3.6	176	12,860	0.48
	G - 4	7.5	3.6	168	12,700	0.48
Nmai & Darwin (1984)	F - 1	7.5	3.8	161	4,260	0.49
	F - 2	7.5	3.8	161	4,220	0.49
	F - 3	7.5	3.8	160	4,260	0.49
	F - 4	7.5	1.6	158	4,330	0.49
	F - 5	7.5	2.1	121	4,370	0.49
	F - 6	7.5	3.8	160	4,320	0.49
	F - 7	7.5	3.8	133	4,220	0.49
Scribner & Wight (1978)	1	8	2	268	4,970	0.93
	5	8	2	268	3,980	0.93
	9	10	3	394	4,940	0.83
	11	10	3	394	4,940	0.83
Wight & Sozen (1973)	00.033W	6	5	166	4,640	0.60
	00.048W	6.1	3.5	235	3,750	0.61
	00.067W	6.1	2.5	327	4,610	0.61
	00.105E	6.1	3.5	473	4,850	0.61
	00.105W	6	3.5	482	4,850	0.60
	00.147E	6	2.5	675	4,900	0.60
	00.147W	5.9	2.5	690	4,900	0.59
Hwang & Scribner (1984)	1 - 2	8	2.5	267	5,880	0.79
	1 - 4	8	2.5	291	4,980	0.81
	2 - 2	8	2.5	267	5,390	0.83
	2 - 3	8	2.5	291	4,710	0.82
	2 - 4	8	2.5	267	4,780	0.83
	3 - 2	8	2.5	830	4,970	0.82
	3 - 3	8	2.5	830	4,980	0.83
	3 - 4	8	2.5	830	5,060	0.82

Table 3.1 Test Results of Experimental Research (continued)

Reference	Beam	C_r	v_m (psi)	A_s'/A_s	Yield Load (kips)	Yield Deflection (in.)
Current Study	H - 1	0.77	64	0.5	12.8	0.3
	H - 2	0.77	105	0.5	20.9	0.34
	H - 3	0.77	74	0.5	13.0	0.24
	H - 4	0.77	71	1.0	14.8	0.37
Hanks & Darwin (1988)	G - 1	0.61	145	0.5	13.7	0.33
	G - 2	0.62	208	0.5	20.8	0.37
	G - 3	0.61	151	0.5	14.1	0.37
	G - 4	0.61	210	0.5	20.8	0.37
Nmai & Darwin (1984)	F - 1	0.52	197	0.5	18.2	0.656
	F - 2	0.59	215	0.5	19.7	0.533
	F - 3	0.59	145	0.5	13.5	0.467
	F - 4	0.81	141	0.5	13.0	0.4
	F - 5	0.75	143	0.5	13.0	0.447
	F - 6	0.59	145	0.75	13.3	0.383
	F - 7	0.59	144	0.5	13.3	0.4
Scribner & Wight (1978)	1	0.71	144	0.69	8.9	0.39
	5	0.71	212	0.69	11.6	0.43
	9	0.70	342	0.77	34.2	1.1
	11	0.70	426	0.77	41.0	0.72
Wight & Sozen (1973)	00.033W	0.41	293	1.0	17.3	0.44
	00.048W	0.51	319	1.0	16.3	0.5
	00.067W	0.62	336	1.0	15.2	0.44
	00.105E	0.52	386	1.0	18.4	0.5
	00.105W	0.64	383	1.0	18.4	0.53
	00.147E	0.64	382	1.0	17.0	0.44
	00.147W	0.64	388	1.0	18.1	0.47
Hwang & Scribner (1984)	1 - 2	0.66	270	0.69	18.6	0.41
	1 - 4	0.65	242	0.69	17.2	0.4
	2 - 2	0.65	383	0.73	24.6	0.37
	2 - 3	0.65	406	0.73	25.9	0.44
	2 - 4	0.65	390	0.73	25.9	0.37
	3 - 2	0.66	506	0.73	34.4	0.25
	3 - 3	0.65	495	0.73	35.5	0.25
	3 - 4	0.66	528	0.73	36.1	0.25

Table 3.1 Test Results of Experimental Research (continued)

Reference	Beam	E (kip - in.)	D_i
Current Study	H - 1	245	102
	H - 2	315	71
	H - 3	178	91
	H - 4	507	93
Hanks & Darwin (1988)	G - 1	225	79
	G - 2	229	48
	G - 3	231	71
	G - 4	227	47
Nmai & Darwin (1984)	F - 1	297	40
	F - 2	184	28
	F - 3	208	52
	F - 4	310	95
	F - 5	269	73
	F - 6	329	83
	F - 7	215	65
Scribner & Wight (1978)	1	* 366	143
	5	275	75
	9	1267	42
	11	625	27
Wight & Sozen (1973)	00.033W	119	16
	00.048W	* 175	22
	00.067W	* 230	34
	00.105E	178	19
	00.105W	* 215	22
	00.147E	* 298	40
	00.147W	* 326	38
Hwang & Scribner (1984)	1 - 2	342	61
	1 - 4	240	47
	2 - 2	163	23
	2 - 3	169	19
	2 - 4	149	20
	3 - 2	152	23
	3 - 3	196	29
	3 - 4	182	26

Table 4.1 Displacement Ductility Factor in the Negative (i.e., primary) & Positive Directions for all Cycles with $P_i \geq 0.75P_y$

Reference	Beam	Cycle 1 (-)/(+)	Cycle 2 (-)/(+)	Cycle 3 (-)/(+)	Cycle 4 (-)/(+)	Cycle 5 (-)/(+)	Cycle 6 (-)/(+)	Cycle 7 (-)/(+)
Current Study	H - 1	4.3 / 4.3	4.3 / 4.3	4.3 / 4.3	4.3 / 4.3	4.3 / 4.3	4.3 / 4.3	4.3 / 4.3
	H - 2	5.3 / 5.3	5.3 / 5.3	5.3 / 5.3	5.3 / 5.3	5.3 / 5.3	5.3 / 5.3	5.3 / 5.3
	H - 3	8.5 / 8.5	8.5 / 8.5	8.5 / 8.5	8.5 / 8.5			
	H - 4	4.7 / 4.7	4.7 / 4.7	4.7 / 4.7	4.7 / 4.7	4.7 / 4.7	4.7 / 4.7	4.7 / 4.7
Hanks & Darwin (1988)	G - 1	5 / 5	5 / 5	5 / 5	5 / 5	5 / 5	5 / 5	5 / 5
	G - 2	5 / 5	5 / 5	5 / 5	5 / 5	5 / 5		
	G - 3	5 / 5	5 / 5	5 / 5	5 / 5	5 / 5	5 / 5	5 / 5
	G - 4	5 / 5	5 / 5	5 / 5	5 / 5	5 / 5		
Nmai & Darwin (1984)	F - 1	3.9 / 3.9	3.9 / 3.9	3.9 / 3.9	3.9 / 3.9	3.9 / 3.9		
	F - 2	5.1 / 5.1	5.1 / 5.1					
	F - 3	4.4 / 4.4	4.4 / 4.4	4.4 / 4.4	4.4 / 4.4	4.4 / 4.4	4.4 / 4.4	
	F - 4	5.1 / 5.1	5.1 / 5.1	5.1 / 5.1	5.1 / 5.1	5.1 / 5.1	5.1 / 5.1	5.1 / 5.1
	F - 5	4.6 / 4.6	4.6 / 4.6	4.6 / 4.6	4.6 / 4.6	4.6 / 4.6	4.6 / 4.6	4.6 / 4.6
	F - 6	5.3 / 5.3	5.3 / 5.3	5.3 / 5.3	5.3 / 5.3	5.3 / 5.3	5.3 / 5.3	5.3 / 5.3
	F - 7	5.1 / 5.1	5.1 / 5.1	5.1 / 5.1	5.1 / 5.1	5.1 / 5.1	5.1 / 5.1	
Scribner & Wight (1978)	5	4 / 3	4 / 3	4 / 3	4 / 3	4 / 3	4 / 3	6 / 5
	9	4 / 3	4 / 3	4 / 3	4 / 3	4 / 3	4 / 3	6 / 5
	11	4 / 3	4 / 3	4 / 3	4 / 3			
Wight & Sozen (1973)	00.033W	2 / 2	2 / 2	2 / 2	2 / 2	2 / 2	2 / 2	4 / 4
	00.105E	4 / 4	4 / 4	4 / 4				
	00.105W	4 / 4	4 / 4	4 / 4	4 / 4			
Hwang & Scribner (1984)	1 - 4	4 / 4	4 / 4	2 / 2	2 / 2	4 / 4	4 / 4	2 / 2
	2 - 2	4 / 4	4 / 4	4 / 4	4 / 4			
	2 - 3	2 / 2	2 / 2	4 / 4	4 / 4	2 / 2	2 / 2	4 / 4
	2 - 4	4 / 4	4 / 4	2 / 2	2 / 2	4 / 4		
	3 - 2	4 / 4	4 / 4	4 / 4	4 / 4			
	3 - 3	2 / 2	2 / 2	4 / 4	4 / 4	2 / 2	2 / 2	4 / 4
	3 - 4	4 / 4	4 / 4	2 / 2	2 / 2	4 / 4	4 / 4	

Table 4.1 Displacement Ductility Factor in the Negative (i.e., primary) & Positive Directions for all Cycles with $P_i \geq 0.75P_y$ (continued)

Reference	Beam	Cycle 8 (-)/(+)	Cycle 9 (-)/(+)	Cycle 10 (-)/(+)	Cycle 11 (-)/(+)	Cycle 12 (-)/(+)	Cycle 13 (-)/(+)	Cycle 14 (-)/(+)
Current Study	H - 1	4.3 / 4.3	4.3 / 4.3	4.3 / 4.3	4.3 / 4.3	4.3 / 4.3	4.3 / 4.3	
	H - 2							
	H - 3							
	H - 4	4.7 / 4.7	4.7 / 4.7	4.7 / 4.7	4.7 / 4.7	4.7 / 4.7	4.7 / 4.7	4.7 / 4.7
Hanks & Darwin (1988)	G - 1	5 / 5	5 / 5					
	G - 2							
	G - 3							
	G - 4							
Nmai & Darwin (1984)	F - 1							
	F - 2							
	F - 3							
	F - 4	5.1 / 5.1	5.1 / 5.1					
	F - 5	4.6 / 4.6						
	F - 6	5.3 / 5.3	5.3 / 5.3					
	F - 7							
Scribner & Wight (1978)	5	6 / 5	6 / 5	6 / 5				
	9							
	11							
Wight & Sozen (1973)	00.033W							
	00.105E							
	00.105W							
Hwang & Scribner (1984)	1 - 4	2 / 2	4 / 4	4 / 4	2 / 2	2 / 2	4 / 4	
	2 - 2							
	2 - 3							
	2 - 4							
	3 - 2							
	3 - 3	4 / 4						
	3 - 4							

Table 4.1 Displacement Ductility Factor in the Negative (i.e., primary) & Positive Directions for all Cycles with $P_i \geq 0.75P_y$ (continued)

Reference	Beam	Cycle 15 (-)/(+)	Cycle 16 (-)/(+)	Cycle 17 (-)/(+)	μ_{rms} (Eq. 4.3)	μ'_{rms} (Eq. 4.8)	$n_{pre}(\mu'_{rms})$ (Eq. 4.9)	n_{pre}/n_{test}
Current Study	H - 1				4.3	4.3	11.9	1.10
	H - 2				5.3	5.3	8.1	0.86
	H - 3				8.5	8.5	4	1.00
	H - 4	4.7 / 4.7	4.7 / 4.7	4.7 / 4.7	4.7	4.7	17.6	0.97
Hanks & Darwin (1988)	G - 1				5	5	7.1	1.26
	G - 2				5	5	5.6	0.90
	G - 3				5	5	7.2	0.98
	G - 4				5	5	5.7	0.87
Nmai & Darwin (1984)	F - 1				3.9	3.9	6	0.84
	F - 2				5.1	5.1	2.5	0.81
	F - 3				4.4	4.4	6.8	0.88
	F - 4				5.1	5.1	8.5	1.05
	F - 5				4.6	4.6	8	0.99
	F - 6				5.3	5.3	8.4	1.07
	F - 7				5.1	5.1	4.9	1.22
Scribner & Wight (1978)	5				4.41	4.43	10.2	0.98
	9				3.85	3.96	7.4	0.94
	11				3.5	3.5	4.8	0.84
Wight & Sozen (1973)	00.033W				2.39	2.52	7.5	0.94
	00.105E				4	4	2.7	1.13
	00.105W				4	4	2.9	1.38
Hwang & Scribner (1984)	1 - 4				3.23	3.18	12.3	1.05
	2 - 2				4	4	4.3	0.93
	2 - 3				3.02	2.84	6	1.16
	2 - 4				3.35	3.34	5	1.01
	3 - 2				4	4	5	0.79
	3 - 3				3.16	3.15	7.9	1.01
	3 - 4				3.46	3.43	5.7	1.05
							Mean =	1.00
							COV =	14.0 %

Table 4.2 Energy Dissipated per Cycle, $(E)_j$

Reference	Beam	Cycle 1 (kip - in.)	Cycle 2 (kip - in.)	Cycle 3 (kip - in.)	Cycle 4 (kip - in.)	Cycle 5 (kip - in.)	Cycle 6 (kip - in.)	Cycle 7 (kip - in.)
Current Study	H - 1	32.2	23.1	20.7	19.0	18.5	17.7	17.6
	H - 2	72.4	51.4	45.1	41.1	38.1	35.3	31.2
	H - 3	61.2	46.9	39.2	31.0			
	H - 4	63.3	46.3	40.2	36.2	34.0	31.8	30.2
Hanks & Darwin (1988)	G - 1	41.0	30.2	27.3	25.6	24.6	22.6	20.7
	G - 2	65.0	47.4	43.5	39.2	34.2		
	G - 3	48.5	36.6	32.9	30.8	29.4	27.7	25.4
	G - 4	66.8	47.2	42.2	38.4	32.0		
Nmai & Darwin (1984)	F - 1	78.3	64.0	58.2	53.4	43.1		
	F - 2	108.8	75.2					
	F - 3	51.1	38.5	35.5	32.1	28.8	22.1	
	F - 4	52.4	39.1	35.9	33.7	32.3	30.8	30.0
	F - 5	50.6	37.1	33.8	31.6	30.8	29.9	28.9
	F - 6	59.8	46.2	42.1	39.4	35.6	32.3	29.8
	F - 7	55.7	39.9	36.9	32.5	28.4	21.2	
Scribner & Wight (1978)	5	33.9	25.7	22.2	19.7	18.4	17.6	42.2
	9	232.0	184.0	166.0	154.0	145.0	139.0	247.0
	11	205.0	160.0	142.0	118.0			
Wight & Sozen (1973)	00.033W	24.0	14.1	12.1	10.6	9.8	9.0	39.7
	00.105E	76.5	54.6	46.9				
Hwang & Scribner (1984)	1 - 2	52.5	34.7	29.4	27.3	25.9	24.6	24.1
	1 - 4	54.6	37.1	6.1	4.9	28.8	28.4	3.9
	2 - 2	64.0	41.3	32.4	25.5			
	2 - 3	21.0	12.7	53.1	40.9	6.2	3.5	31.7
	2 - 4	66.2	43.8	6.0	3.4	29.5		
	3 - 2	61.8	37.8	28.7	23.3			
	3 - 3	23.9	13.3	51.5	37.8	6.1	4.5	30.0
	3 - 4	67.2	42.3	6.6	4.5	32.8	28.6	

Table 4.2 Energy Dissipated per Cycle, $(E)_j$ (continued)

Reference	Beam	Cycle 8 (kip - in.)	Cycle 9 (kip - in.)	Cycle 10 (kip - in.)	Cycle 11 (kip - in.)	Cycle 12 (kip - in.)	Cycle 13 (kip - in.)	Cycle 14 (kip - in.)
Current Study	H - 1	17.1	16.7	16.3	15.7	15.4	15.1	
	H - 2							
	H - 3							
	H - 4	28.5	27.1	25.7	24.7	23.5	22.0	20.8
Hanks & Darwin (1988)	G - 1	18.8	13.7					
	G - 2							
	G - 3							
	G - 4							
Nmai & Darwin (1984)	F - 1							
	F - 2							
	F - 3							
	F - 4	28.4	26.9					
	F - 5	26.1						
	F - 6	25.0	18.8					
	F - 7							
Scribner & Wight (1978)	5	37.6	31.2	26.3				
	9							
	11							
Wight & Sozen (1973)	00.033W							
	00.105E							
Hwang & Scribner (1984)	1 - 2	23.3	21.7	21.2	20.2	19.0	17.8	
	1 - 4	3.3	24.3	24.2	2.2	2.1	20.4	
	2 - 2							
	2 - 3							
	2 - 4							
	3 - 2							
	3 - 3	28.6						
	3 - 4							

Table 4.2 Energy Dissipated per Cycle, $(E)_j$ (continued)

Reference	Beam	Cycle 15 (kip - in.)	Cycle 16 (kip - in.)	Cycle 17 (kip - in.)	$\Sigma (E)_j$ (kip - in.)
Current Study	H - 1				245
	H - 2				315
	H - 3				178
	H - 4	19.1	16.7	16.6	507
Hanks & Darwin (1988)	G - 1				225
	G - 2				229
	G - 3				231
	G - 4				227
Nmai & Darwin (1984)	F - 1				297
	F - 2				184
	F - 3				208
	F - 4				310
	F - 5				269
	F - 6				329
	F - 7				215
Scribner & Wight (1978)	5				275
	9				1267
	11				625
Wight & Sozen (1973)	00.033W				119
	00.105E				178
Hwang & Scribner (1984)	1 - 2				342
	1 - 4				240
	2 - 2				163
	2 - 3				169
	2 - 4				149
	3 - 2				152
	3 - 3				196
	3 - 4				182

Table 4.3 Contributions to D_i per Cycle, $(D_i)_j$

Reference	Beam	Cycle 1	Cycle 2	Cycle 3	Cycle 4	Cycle 5	Cycle 6	Cycle 7
Current Study	H - 1	13.4	9.6	8.6	7.9	7.7	7.4	7.3
	H - 2	16.3	11.6	10.2	9.2	8.6	8.0	7.0
	H - 3	31.4	24.0	20.1	15.9			
	H - 4	11.6	8.5	7.3	6.6	6.2	5.8	5.5
Hanks & Darwin	G - 1	14.5	10.7	9.6	9.1	8.7	8.0	7.3
(1988)	G - 2	13.5	9.9	9.0	8.1	7.1		
	G - 3	14.9	11.2	10.1	9.4	9.0	8.5	7.8
	G - 4	13.9	9.8	8.8	8.0	6.6		
Nmai & Darwin	F - 1	10.4	8.5	7.8	7.1	5.7		
(1984)	F - 2	16.7	11.5					
	F - 3	12.9	9.7	8.9	8.1	7.3	5.6	
	F - 4	16.1	12.0	11.0	10.4	9.9	9.5	9.2
	F - 5	13.8	10.1	9.2	8.6	8.4	8.2	7.9
	F - 6	15.2	11.7	10.7	10.0	9.0	8.2	7.6
	F - 7	16.7	12.0	11.1	9.8	8.5	6.4	
Scribner &	5	9.2	7.0	6.0	5.4	5.0	4.8	11.5
Wight (1978)	9	7.7	6.1	5.5	5.1	4.8	4.6	8.2
	11	8.7	6.8	6.0	5.0			
Wight &	00.033W	3.2	1.9	1.6	1.4	1.3	1.2	5.2
Sozen (1973)	00.105E	8.3	5.9	5.1				
Hwang &	1 - 2	9.3	6.2	5.2	4.8	4.6	4.4	4.3
Scribner (1984)	1 - 4	10.8	7.3	1.2	1.0	5.7	5.6	0.8
	2 - 2	9.2	5.9	4.6	3.6			
	2 - 3	2.4	1.5	6.1	4.7	0.7	0.4	3.6
	2 - 4	9.0	6.0	0.8	0.5	4.0		
	3 - 2	9.4	5.7	4.3	3.5			
	3 - 3	3.5	2.0	7.6	5.6	0.9	0.7	4.4
	3 - 4	9.7	6.1	0.9	0.7	4.7	4.1	

Table 4.3 Contributions to D_i per Cycle, $(D_i)_j$ (continued)

Reference	Beam	Cycle 8	Cycle 9	Cycle 10	Cycle 11	Cycle 12	Cycle 13	Cycle 14
Current Study	H - 1	7.1	6.9	6.8	6.5	6.4	6.3	
	H - 2							
	H - 3							
	H - 4	5.2	5.0	4.7	4.5	4.3	4.0	3.8
Hanks & Darwin (1988)	G - 1	6.7	4.8					
	G - 2							
	G - 3							
	G - 4							
Nmai & Darwin (1984)	F - 1							
	F - 2							
	F - 3							
	F - 4	8.7	8.3					
	F - 5	7.1						
	F - 6	6.3	4.8					
	F - 7							
Scribner & Wight (1978)	5	10.2	8.5	7.1				
	9							
	11							
Wight & Sozen (1973)	00.033W							
	00.105E							
Hwang & Scribner (1984)	1 - 2	4.1	3.9	3.8	3.6	3.4	3.2	
	1 - 4	0.6	4.8	4.8	0.4	0.4	4.0	
	2 - 2							
	2 - 3							
	2 - 4							
	3 - 2							
	3 - 3	4.2						
	3 - 4							

Table 4.3 Contributions to D_i per Cycle, $(D_i)_j$ (continued)

Reference	Beam	Cycle 15	Cycle 16	Cycle 17	$\Sigma (D_i)_j$
Current Study	H - 1				102
	H - 2				71
	H - 3				91
	H - 4	3.5	3.0	3.0	93
Hanks & Darwin (1988)	G - 1				79
	G - 2				48
	G - 3				71
	G - 4				47
Nmai & Darwin (1984)	F - 1				40
	F - 2				28
	F - 3				52
	F - 4				95
	F - 5				73
	F - 6				83
	F - 7				65
Scribner & Wight (1978)	5				75
	9				42
	11				27
Wight & Sozen (1973)	00.033W				16
	00.105E				19
Hwang & Scribner (1984)	1 - 2				61
	1 - 4				47
	2 - 2				23
	2 - 3				19
	2 - 4				20
	3 - 2				23
	3 - 3				29
	3 - 4				26

Table 4.4 Normalized Ductility Range for all Cycles with $P_i \geq 0.75P_y$, $(NDR)_j$

Reference	Beam	Cycle 1	Cycle 2	Cycle 3	Cycle 4	Cycle 5	Cycle 6	Cycle 7
Current Study	H - 1	5.2	5.2	5.2	5.2	5.2	5.2	5.2
	H - 2	6.4	6.4	6.4	6.4	6.4	6.4	6.4
	H - 3	10.2	10.2	10.2	10.2			
	H - 4	4.7	4.7	4.7	4.7	4.7	4.7	4.7
Hanks & Darwin (1988)	G - 1	6.0	6.0	6.0	6.0	6.0	6.0	6.0
	G - 2	6.0	6.0	6.0	6.0	6.0		
	G - 3	6.0	6.0	6.0	6.0	6.0	6.0	6.0
	G - 4	6.0	6.0	6.0	6.0	6.0		
Nmai & Darwin (1984)	F - 1	4.7	4.7	4.7	4.7	4.7		
	F - 2	6.1	6.1					
	F - 3	5.3	5.3	5.3	5.3	5.3	5.3	
	F - 4	6.1	6.1	6.1	6.1	6.1	6.1	6.1
	F - 5	5.5	5.5	5.5	5.5	5.5	5.5	5.5
	F - 6	5.9	5.9	5.9	5.9	5.9	5.9	5.9
	F - 7	6.1	6.1	6.1	6.1	6.1	6.1	
Scribner & Wight (1978)	5	4.1	4.1	4.1	4.1	4.1	4.1	6.4
	9	4.0	4.0	4.0	4.0	4.0	4.0	6.2
	11	4.0	4.0	4.0	4.0			
Wight & Sozen (1973)	00.033W	2.0	2.0	2.0	2.0	2.0	2.0	4.0
	00.105E	4.0	4.0	4.0				
Hwang & Scribner (1984)	1 - 4	4.6	4.6	2.3	2.3	4.6	4.6	2.3
	2 - 2	4.5	4.5	4.5	4.5			
	2 - 3	2.3	2.3	4.5	4.5	2.3	2.3	4.5
	2 - 4	4.5	4.5	2.3	2.3	4.5		
	3 - 2	4.5	4.5	4.5	4.5			
	3 - 3	2.3	2.3	4.5	4.5	2.3	2.3	4.5
	3 - 4	4.5	4.5	2.3	2.3	4.5	4.5	

Table 4.4 Normalized Ductility Range for all Cycles with $P_i \geq 0.75P_y$, $(NDR)_j$ (continued)

Reference	Beam	Cycle 8	Cycle 9	Cycle 10	Cycle 11	Cycle 12	Cycle 13	Cycle 14
Current Study	H - 1	5.2	5.2	5.2	5.2	5.2	5.2	
	H - 2							
	H - 3							
	H - 4	4.7	4.7	4.7	4.7	4.7	4.7	4.7
Hanks & Darwin (1988)	G - 1	6.0	6.0					
	G - 2							
	G - 3							
	G - 4							
Nmai & Darwin (1984)	F - 1							
	F - 2							
	F - 3							
	F - 4	6.1	6.1					
	F - 5	5.5						
	F - 6	5.9	5.9					
	F - 7							
Scribner & Wight (1978)	5	6.4	6.4	6.4				
	9							
	11							
Wight & Sozen (1973)	00.033W							
	00.105E							
Hwang & Scribner (1984)	1 - 4	2.3	4.6	4.6	2.3	2.3	4.6	
	2 - 2							
	2 - 3							
	2 - 4							
	3 - 2							
	3 - 3	4.5						
	3 - 4							

Table 4.4 Normalized Ductility Range for all Cycles with $P_i \geq 0.75P_y$, $(NDR)_j$ (continued)

Reference	Beam	Cycle 15	Cycle 16	Cycle 17	$(D_i)_{pre}$	$(D_i)_{test}/(D_i)_{pre}$
Current Study	H - 1				84	1.22
	H - 2				85	0.84
	H - 3				99	0.92
	H - 4	4.7	4.7	4.7	101	0.92
Hanks & Darwin (1988)	G - 1				69	1.15
	G - 2				57	0.84
	G - 3				69	1.03
	G - 4				58	0.81
Nmai & Darwin (1984)	F - 1				41	0.96
	F - 2				31	0.90
	F - 3				54	0.97
	F - 4				84	1.14
	F - 5				67	1.10
	F - 6				78	1.06
	F - 7				53	1.21
Scribner & Wight (1978)	5				74	1.00
	9				45	0.94
	11				28	0.95
Wight & Sozen (1973)	00.033W				18	0.86
	00.105E				18	1.05
Hwang & Scribner (1984)	1 - 4				48	0.98
	2 - 2				31	0.75
	2 - 3				23	0.85
	2 - 4				27	0.75
	3 - 2				35	0.66
	3 - 3				32	0.91
	3 - 4				30	0.86
					Mean =	0.949
					COV =	14.8%

Table 4.5 Cumulative Contributions to D_i per Cycle, $(D_i)_s$

Reference	Beam	Cycle 1	Cycle 2	Cycle 3	Cycle 4	Cycle 5	Cycle 6	Cycle 7
Current Study	H - 1	13.4	23.0	31.7	39.6	47.3	54.7	62.0
	H - 2	16.3	27.9	38.0	47.3	55.9	63.8	70.8
	H - 3	31.4	55.4	75.5	91.4			
	H - 4	11.6	20.0	27.4	34.0	40.2	46.0	51.5
Hanks & Darwin (1988)	G - 1	14.5	25.2	34.8	43.9	52.6	60.6	68.0
	G - 2	13.5	23.4	32.4	40.5	47.7		
	G - 3	14.9	26.1	36.2	45.6	54.6	63.1	70.9
	G - 4	13.9	23.7	32.5	40.5	47.1	47.1	
Nmai & Darwin (1984)	F - 1	10.4	19.0	26.7	33.8	39.6		
	F - 2	16.7	28.2					
	F - 3	12.9	22.6	31.5	39.6	46.9	52.4	
	F - 4	16.1	28.2	39.2	49.6	59.5	69.0	78.2
	F - 5	13.8	24.0	33.2	41.9	50.3	58.5	66.4
	F - 6	15.2	26.9	37.5	47.5	56.5	64.7	72.2
	F - 7	16.7	28.7	39.8	49.6	58.1	64.5	
Scribner & Wight (1978)	5	9.2	16.2	22.2	27.6	32.6	37.3	48.8
	9	7.7	13.9	19.4	24.6	29.4	34.0	42.3
	11	8.7	15.5	21.6	26.6			
Wight & Sozen (1973)	00.033W	3.2	5.0	6.6	8.0	9.3	10.4	15.7
	00.105E	8.3	14.3	19.3				
Hwang & Scribner (1984)	1 - 2	9.3	15.5	20.7	25.6	30.2	34.5	38.8
	1 - 4	10.8	18.1	19.2	20.2	25.9	31.5	32.2
	2 - 2	9.2	15.1	19.7	23.4			
	2 - 3	2.4	3.9	9.9	14.6	15.3	15.7	19.4
	2 - 4	9.0	15.0	15.8	16.2	20.3		
	3 - 2	9.4	15.1	19.5	23.0			
	3 - 3	3.5	5.5	13.0	18.6	19.5	20.1	24.6
	3 - 4	9.7	15.8	16.8	17.4	22.2	26.3	

Table 4.5 Cumulative Contributions to D_i per Cycle, $(D_i)_s$ (continued)

Reference	Beam	Cycle 8	Cycle 9	Cycle 10	Cycle 11	Cycle 12	Cycle 13	Cycle 14
Current Study	H - 1	69.1	76.1	82.9	89.4	95.8	102.1	
	H - 2							
	H - 3							
	H - 4	56.7	61.6	66.3	70.9	75.1	79.2	83.0
Hanks & Darwin (1988)	G - 1	74.6	79.4					
	G - 2							
	G - 3							
	G - 4							
Nmai & Darwin (1984)	F - 1							
	F - 2							
	F - 3							
	F - 4	86.9	95.2					
	F - 5	73.4						
	F - 6	78.6	83.3					
	F - 7							
Scribner & Wight (1978)	5	59.0	67.5	74.6				
	9							
	11							
Wight & Sozen (1973)	00.033W							
	00.105E							
Hwang & Scribner (1984)	1 - 2	43.0	46.8	50.6	54.2	57.5	60.7	
	1 - 4	32.9	37.7	42.4	42.9	43.3	47.3	
	2 - 2							
	2 - 3							
	2 - 4							
	3 - 2							
	3 - 3	28.8						
	3 - 4							

Table 4.5 Cumulative Contributions to D_i per Cycle, $(D_i)_s$ (continued)

Reference	Beam	Cycle 15	Cycle 16	Cycle 17	$\Sigma (D_i)_{s=n}$
Current Study	H - 1				102
	H - 2				71
	H - 3				91
	H - 4	86.4	89.5	92.5	93
Hanks & Darwin (1988)	G - 1				79
	G - 2				48
	G - 3				71
	G - 4				47
Nmai & Darwin (1984)	F - 1				40
	F - 2				28
	F - 3				52
	F - 4				95
	F - 5				73
	F - 6				83
	F - 7				65
Scribner & Wight (1978)	5				75
	9				42
	11				27
Wight & Sozen (1973)	00.033W				16
	00.105E				19
Hwang & Scribner (1984)	1 - 2				61
	1 - 4				47
	2 - 2				23
	2 - 3				19
	2 - 4				20
	3 - 2				23
	3 - 3				29
	3 - 4				26

Table 4.6 Cumulative Normalized Ductility Range for all Cycles with $P_i \geq 0.75P_y$, $(CNDR)_s$

Reference	Beam	Cycle 1	Cycle 2	Cycle 3	Cycle 4	Cycle 5	Cycle 6	Cycle 7
Current Study	H - 1	5.2	10.3	15.5	20.6	25.8	31.0	36.1
	H - 2	6.4	12.7	19.1	25.4	31.8	38.2	44.5
	H - 3	10.2	20.4	30.6	40.8			
	H - 4	4.7	9.4	14.1	18.8	23.5	28.2	32.9
Hanks & Darwin	G - 1	6	12	18	24	30	36	42
(1988)	G - 2	6	12	18	24	30		
	G - 3	6	12	18	24	30	36	42
	G - 4	6	12	18	24	30		
Nmai & Darwin	F - 1	4.7	9.4	14.0	18.7	23.4		
(1984)	F - 2	6.1	12.2					
	F - 3	5.3	10.6	15.8	21.1	26.4	31.7	
	F - 4	6.1	12.2	18.4	24.5	30.6	36.7	42.8
	F - 5	5.5	11.0	16.6	22.1	27.6	33.1	38.6
	F - 6	5.9	11.9	17.8	23.7	29.7	35.6	41.6
	F - 7	6.1	12.2	18.4	24.5	30.6	36.7	
Scribner &	5	4.1	8.2	12.3	16.4	20.6	24.7	31.1
Wight (1978)	9	4.0	7.9	11.9	15.8	19.8	23.8	30.0
	11	4.0	7.9	11.9	15.8			
Wight &	00.033W	2	4	6	8	10	12	16
Sozen (1973)	00.105E	4	8	12				
Hwang &	1 - 4	4.6	9.2	11.4	13.7	18.3	22.9	25.2
Scribner (1984)	2 - 2	4.5	9.0	13.5	18.1			
	2 - 3	2.3	4.5	9.0	13.5	15.8	18.1	22.6
	2 - 4	4.5	9.0	11.3	13.5	18.1		
	3 - 2	4.5	9.0	13.5	18.1			
	3 - 3	2.3	4.5	9.0	13.5	15.8	18.1	22.6
	3 - 4	4.5	9.0	11.3	13.5	18.1	22.6	

Table 4.6 Cumulative Normalized Ductility Range for all Cycles with $P_i \geq 0.75P_y$, $(CNDR)_s$ (continued)

Reference	Beam	Cycle 8	Cycle 9	Cycle 10	Cycle 11	Cycle 12	Cycle 13	Cycle 14
Current Study	H - 1	41.3	46.4	51.6	56.8	61.9	67.1	
	H - 2							
	H - 3							
	H - 4	37.6	42.3	47.0	51.7	56.4	61.1	65.8
Hanks & Darwin (1988)	G - 1	48	54					
	G - 2							
	G - 3							
	G - 4							
Nmai & Darwin (1984)	F - 1							
	F - 2							
	F - 3							
	F - 4	49.0	55.1					
	F - 5	44.2						
	F - 6	47.5	53.4					
	F - 7							
Scribner & Wight (1978)	5	37.5	43.9	50.3				
	9							
	11							
Wight & Sozen (1973)	00.033W							
	00.105E							
Hwang & Scribner (1984)	1 - 4	27.5	32.1	36.6	38.9	41.2	45.8	
	2 - 2							
	2 - 3							
	2 - 4							
	3 - 2							
	3 - 3	27.1						
	3 - 4							

Table 4.6 Cumulative Normalized Ductility Range for all Cycles with $P_i \geq 0.75P_y$, $(CNDR)_s$ (continued)

Reference	Beam	Cycle 15	Cycle 16	Cycle 17	$(D_i)_{pre}$	$(D_i)_{test}/(D_i)_{pre}$
Current Study	H - 1				87	1.17
	H - 2				93	0.76
	H - 3				91	1.01
	H - 4	70.5	75.2	79.9	81	1.14
Hanks & Darwin (1988)	G - 1				74	1.08
	G - 2				57	0.83
	G - 3				74	0.96
	G - 4				59	0.80
Nmai & Darwin (1984)	F - 1				42	0.95
	F - 2				31	0.90
	F - 3				57	0.93
	F - 4				91	1.04
	F - 5				72	1.03
	F - 6				85	0.98
	F - 7				52	1.24
Scribner & Wight (1978)	5				75	1.00
	9				45	0.94
	11				27	1.00
Wight & Sozen (1973)	00.033W				17	0.91
	00.105E				18	1.07
Hwang & Scribner (1984)	1 - 4				38	1.24
	2 - 2				29	0.80
	2 - 3				22	0.89
	2 - 4				24	0.84
	3 - 2				34	0.68
	3 - 3				31	0.94
	3 - 4				28	0.93
					Mean =	0.965
					COV =	14.2%

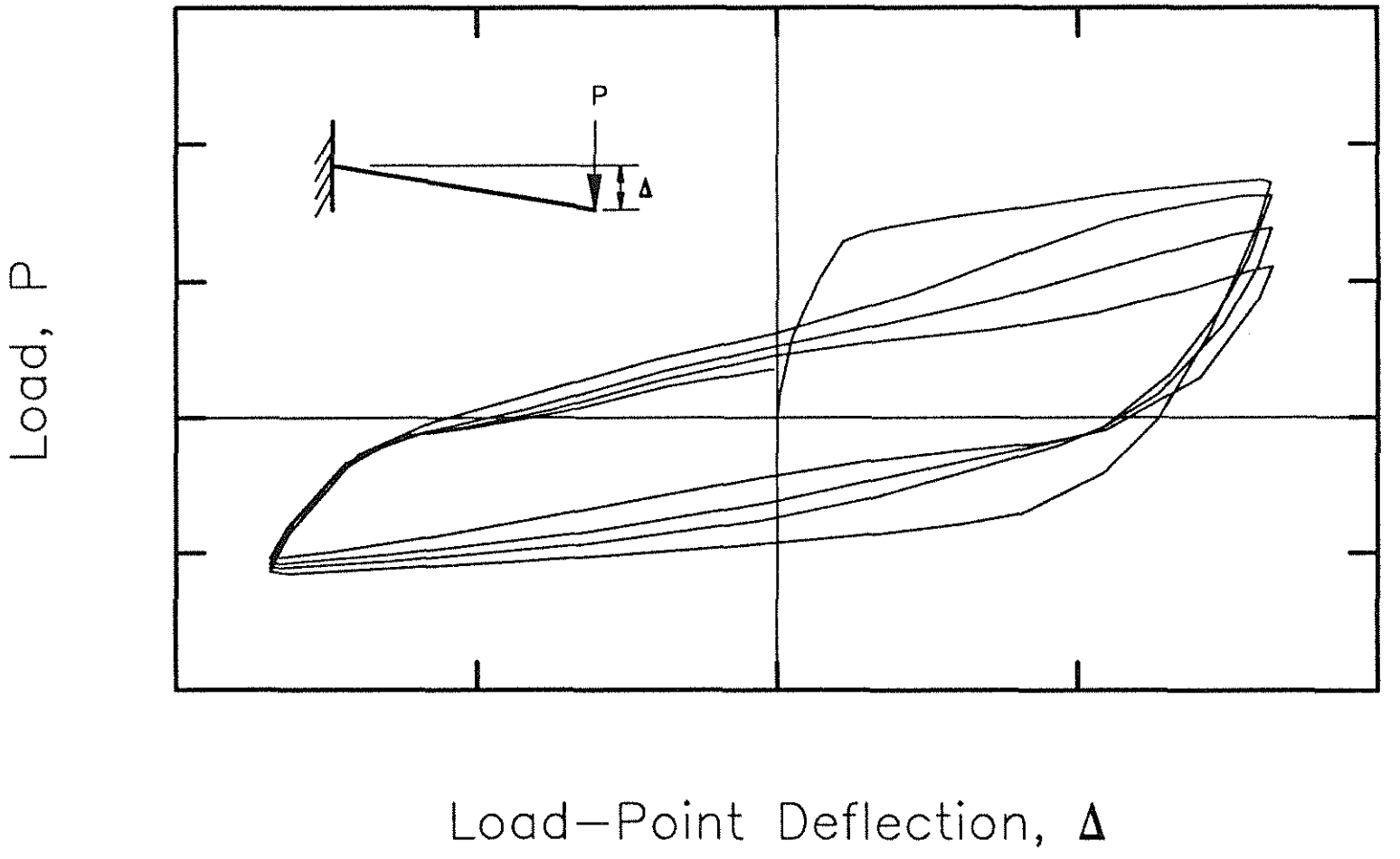

Fig. 1.1 Load versus Load-Point Deflection for a reinforced concrete beam (taken in part from Beam H-3 of the current study)

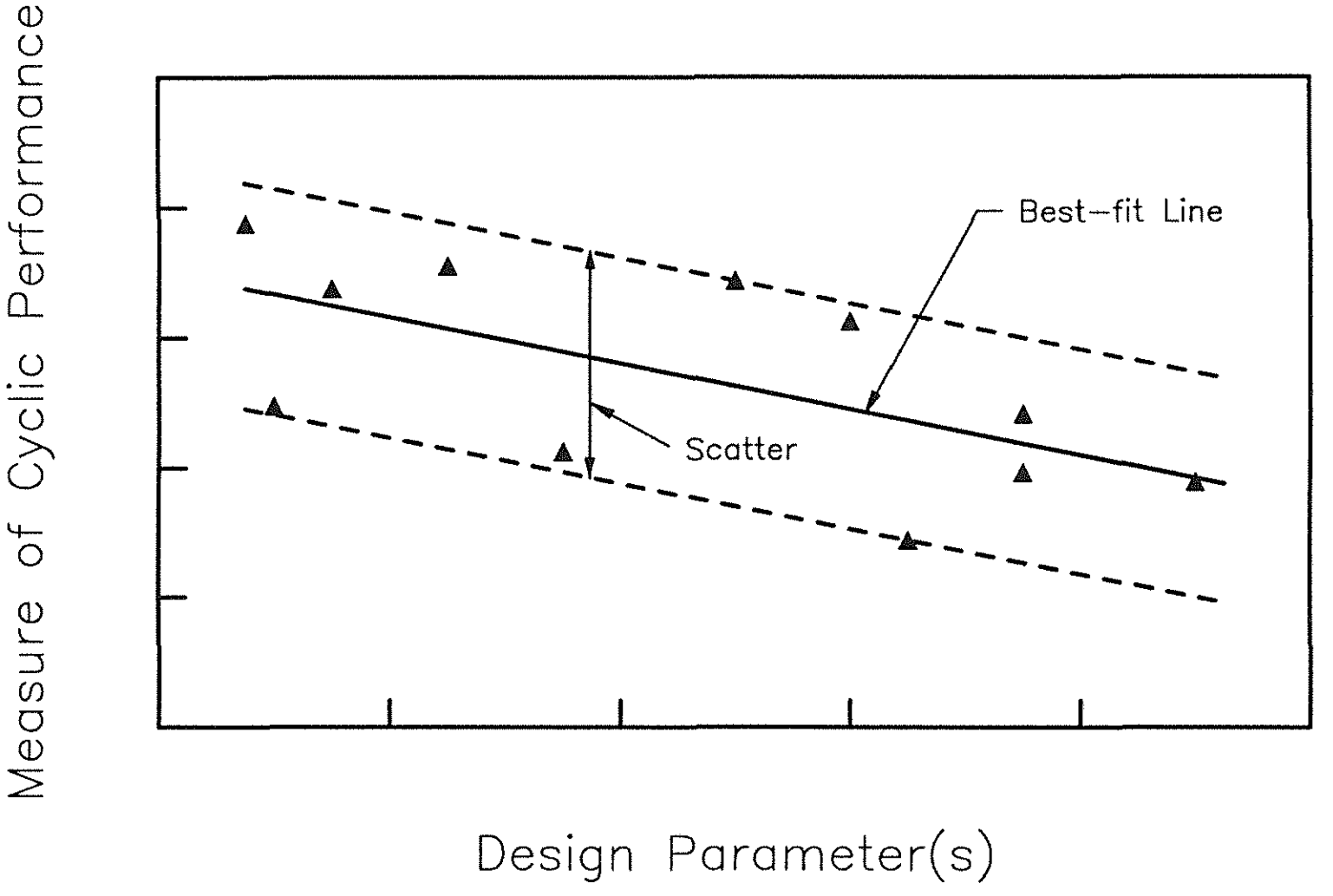

Fig. 1.2 Measure of Cyclic Performance versus Design Parameter(s)

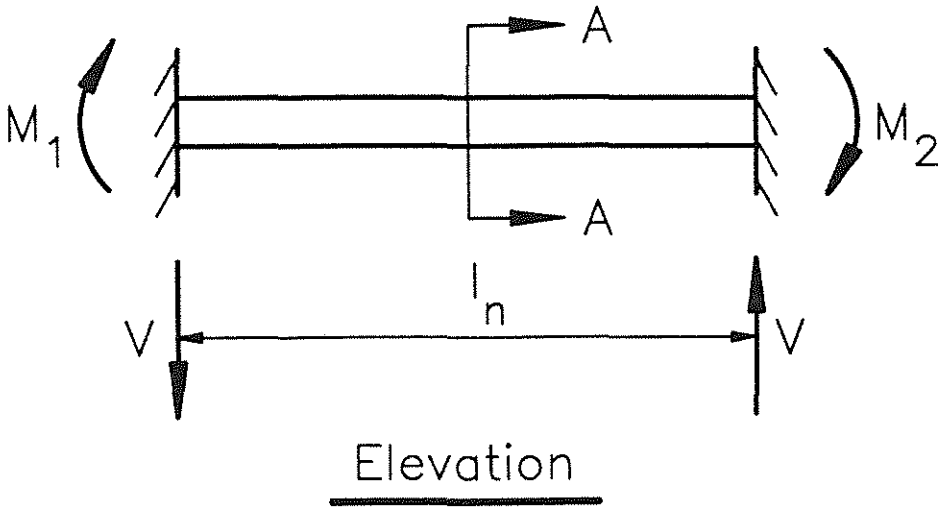

Elevation

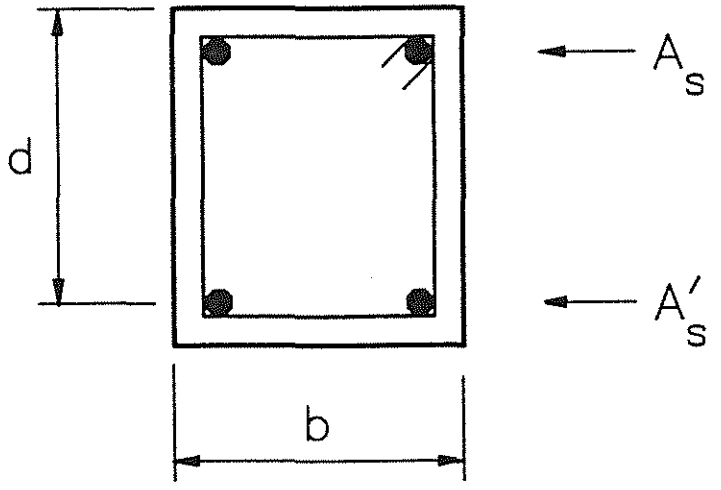

Section A–A

$$\text{Beam Shear Force} = V = (M_1 + M_2)/l_n$$

$$\text{Beam Shear Stress} = V/(bd)$$

Fig. 1.3 Parameters Affecting Beam Shear Stress

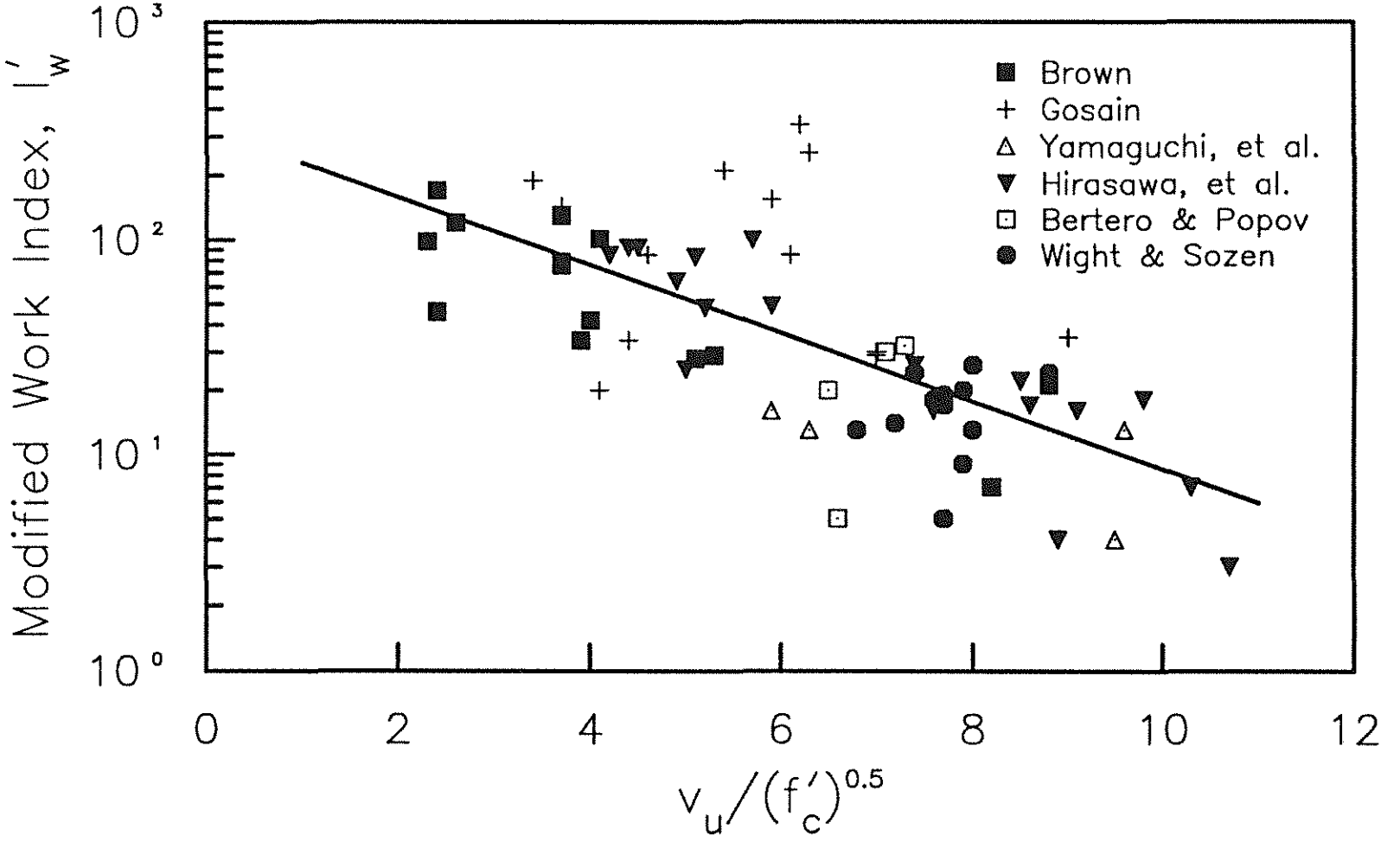

Fig. 1.4 Modified Work Index versus $v_u/(f'_c)^{0.5}$, Gosain et. al (1977)

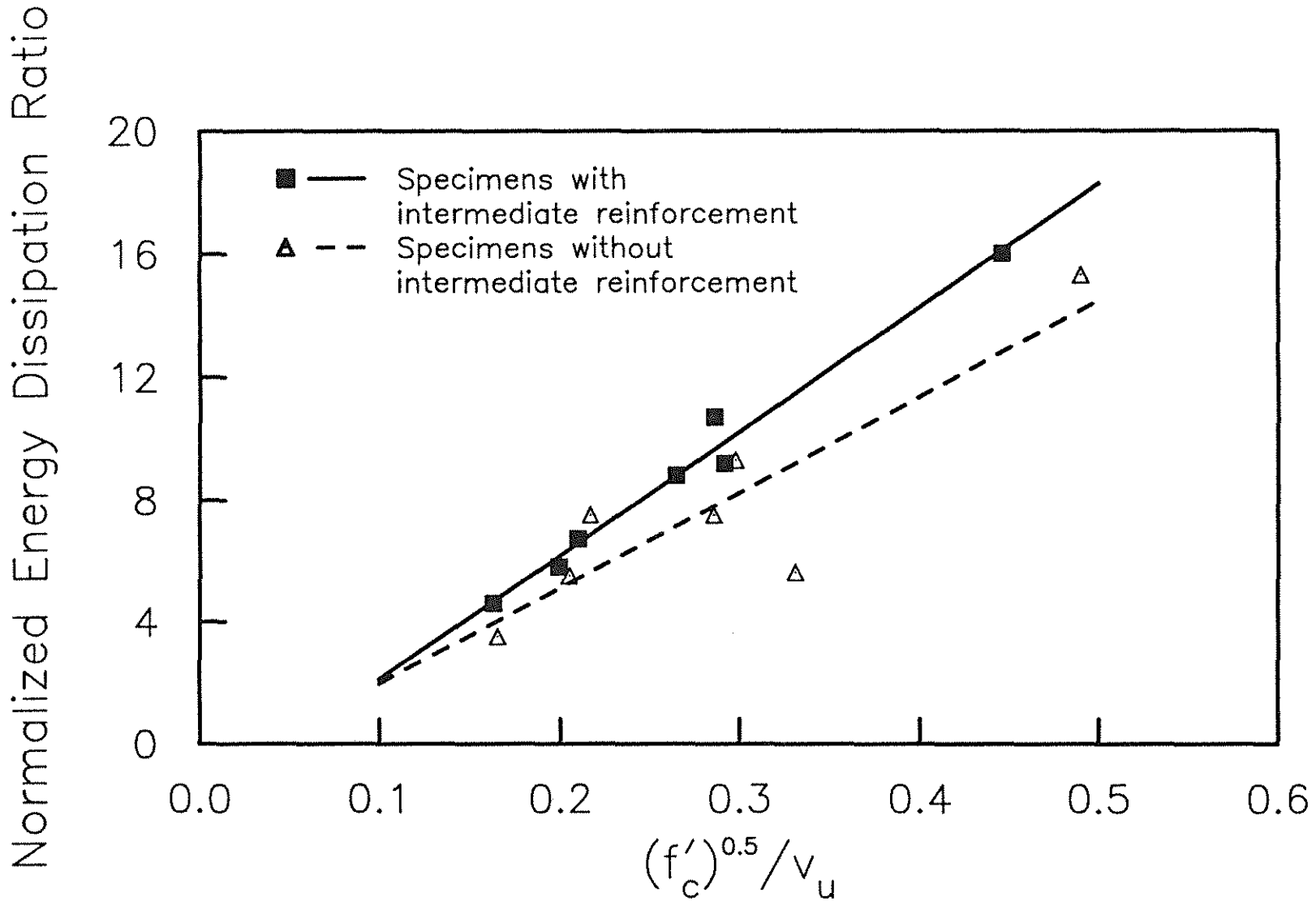

Fig. 1.5 Normalized Energy Dissipation Ratio versus $(f'_c)^{0.5}/v_u$, Scribner & Wight (1980)

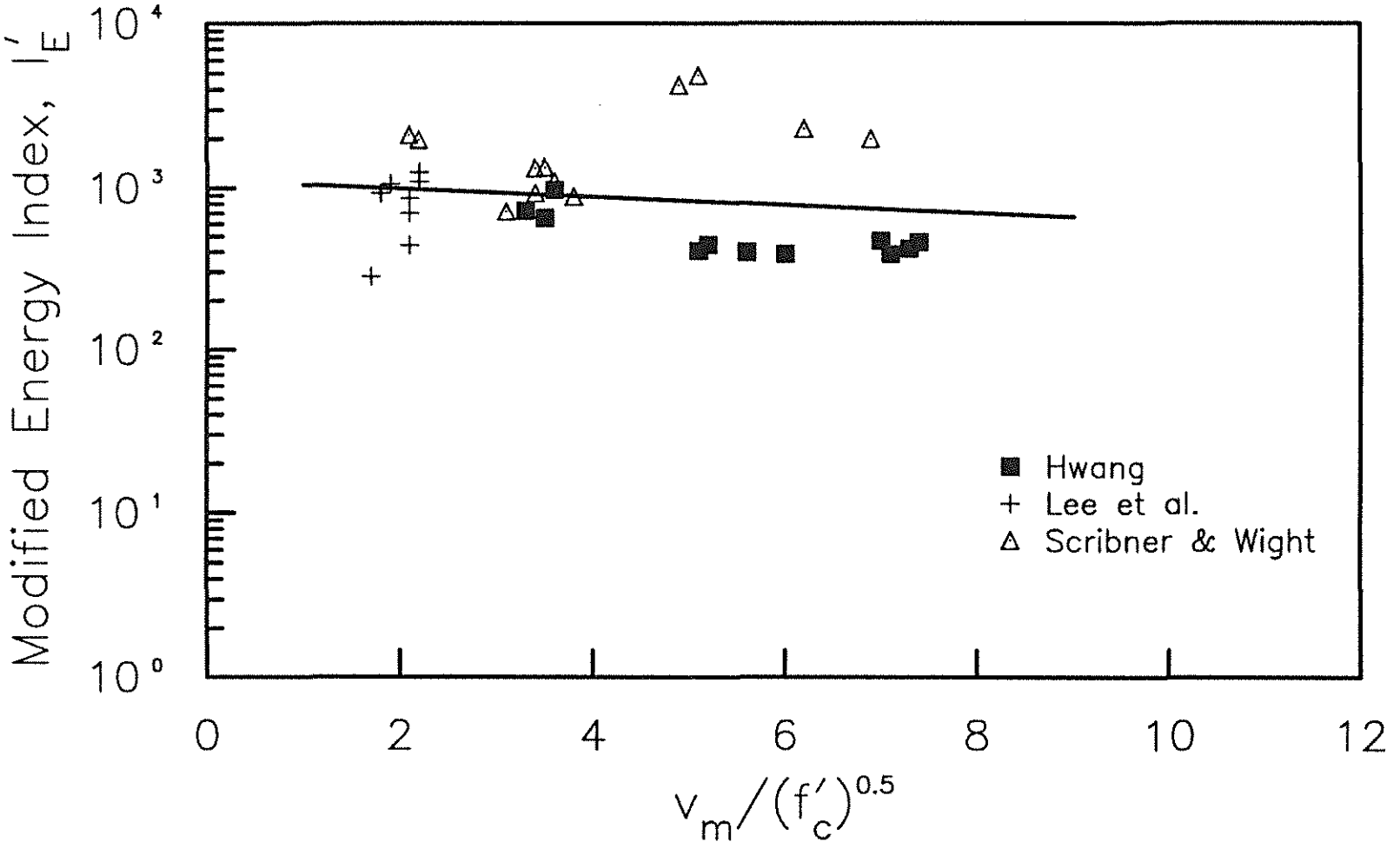

Fig. 1.6 Modified Energy Index versus $v_m/(f'_c)^{0.5}$, Hwang (1982)

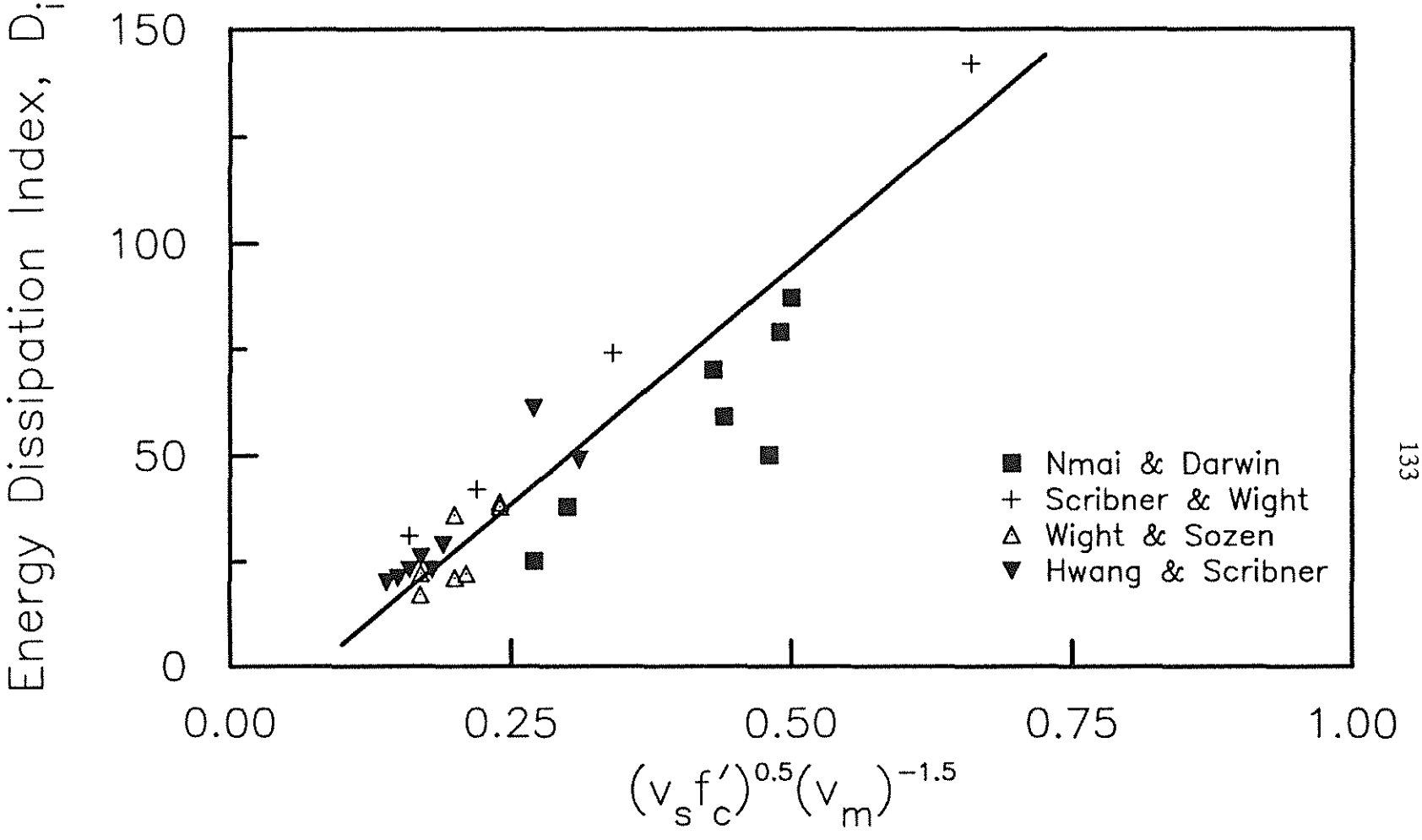

Fig. 1.7 Energy Dissipation Index versus $(v_s f'_c)^{0.5}(v_m)^{-1.5}$, Nmai & Darwin (1984, 1986)

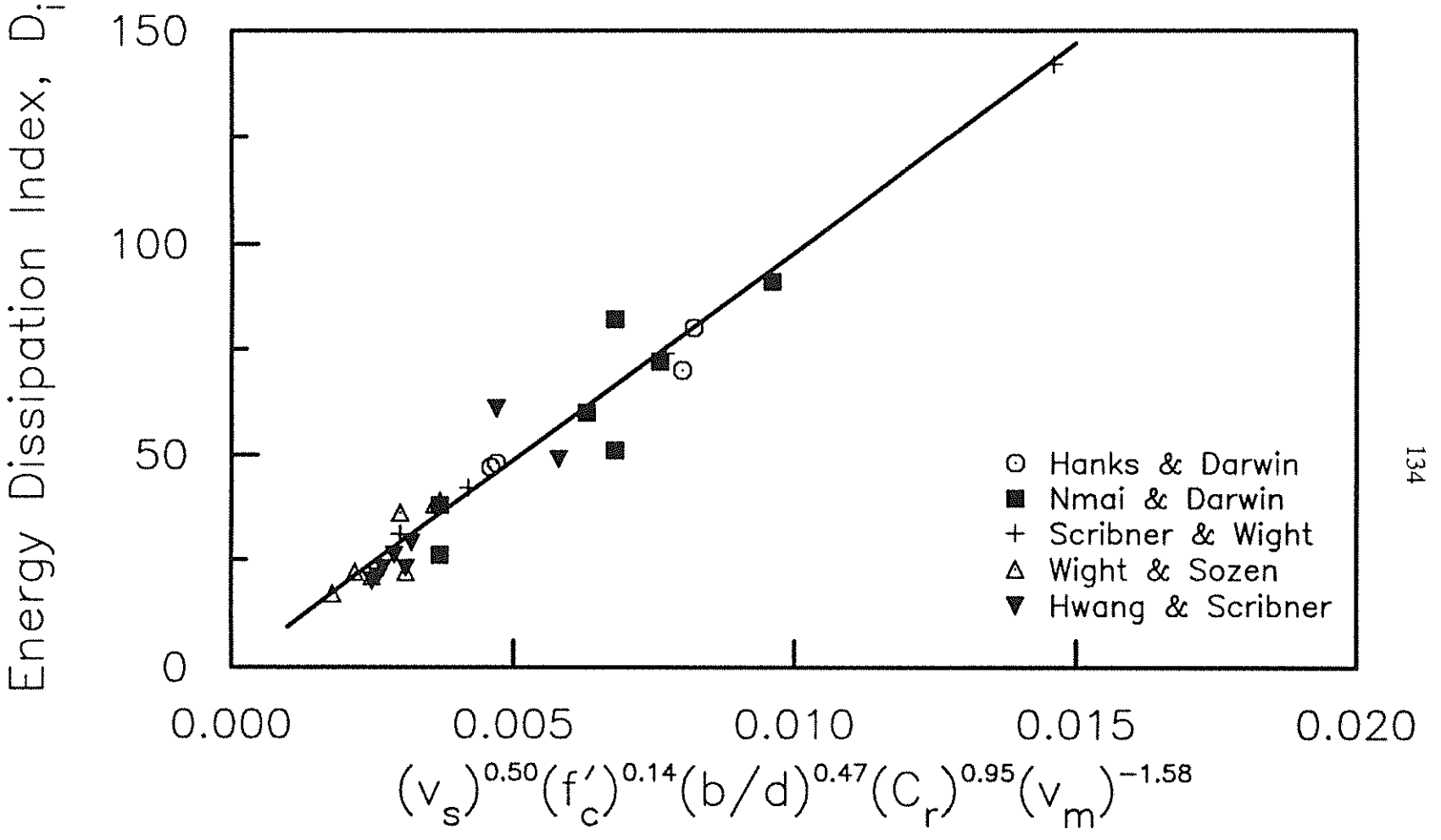

Fig. 1.8 Energy Dissipation Index versus $(v_s)^{0.50}(f'_c)^{0.14}(b/d)^{0.47}(C_r)^{0.95}(v_m)^{-1.58}$, Hanks & Darwin (1988)

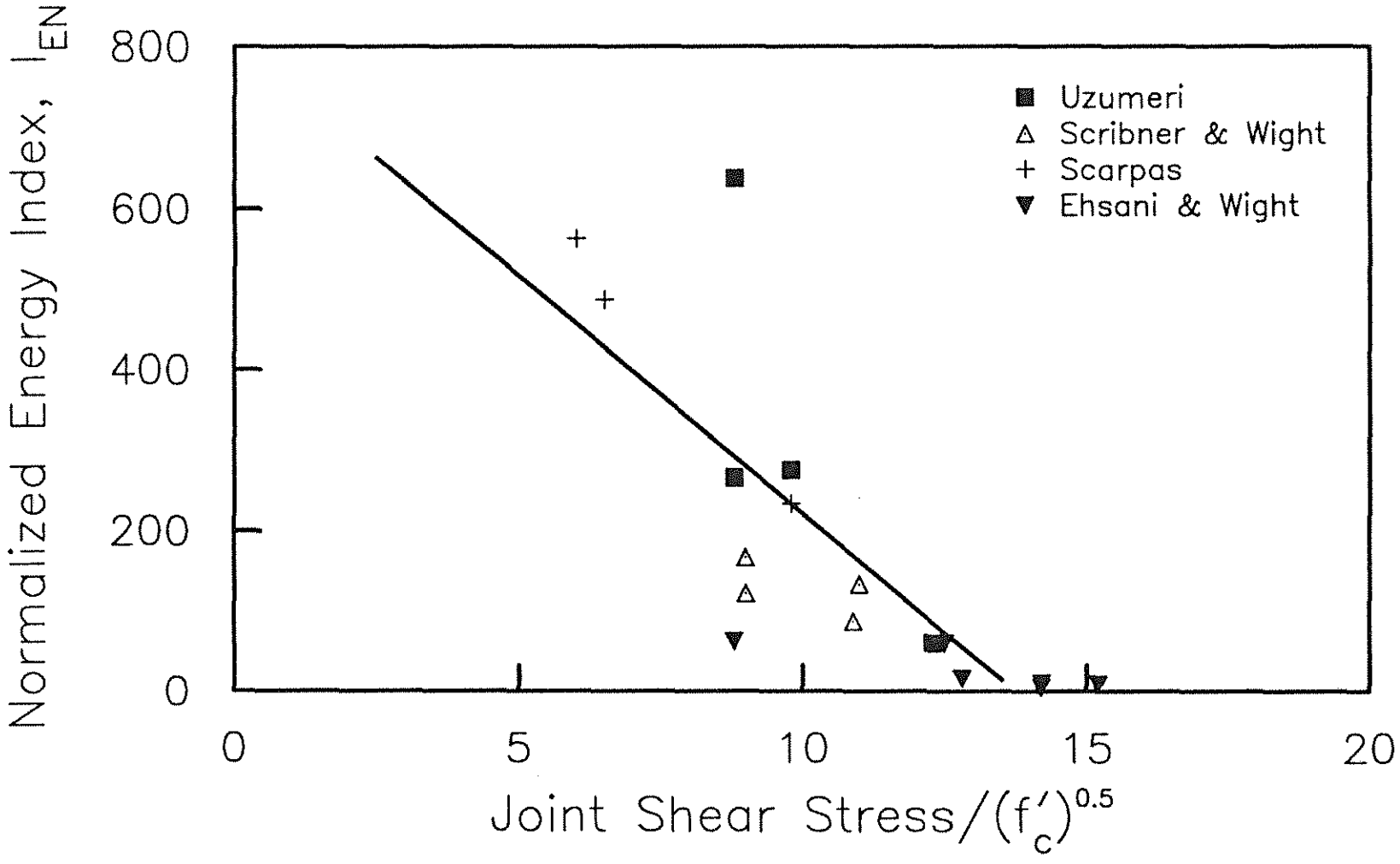

Fig. 1.9 Normalized Energy Index versus Joint Shear Stress/$(f'_c)^{0.5}$, Ehsani & Wight (1990)

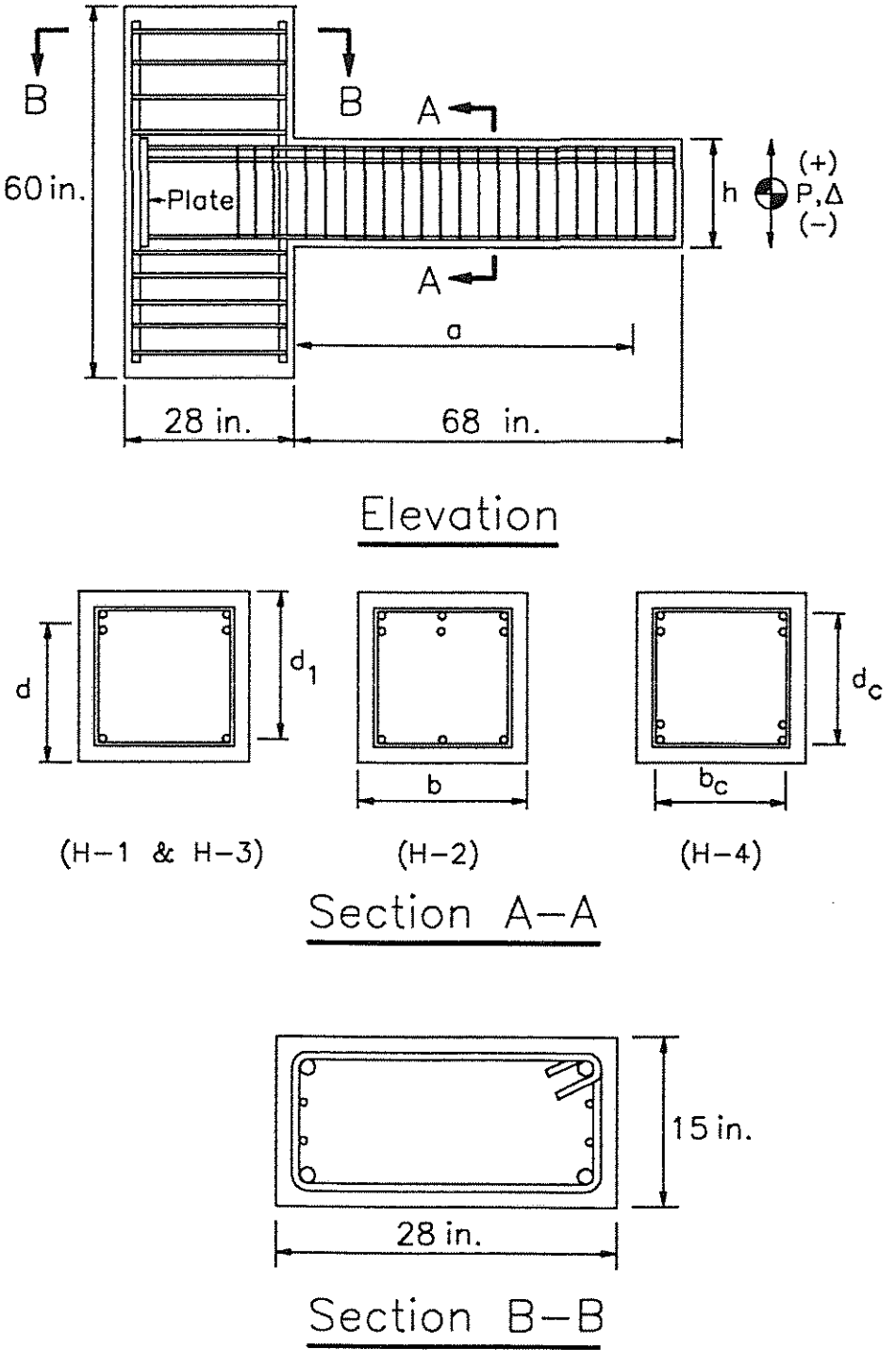

Fig. 2.1 Test Specimen and Reinforcing Details

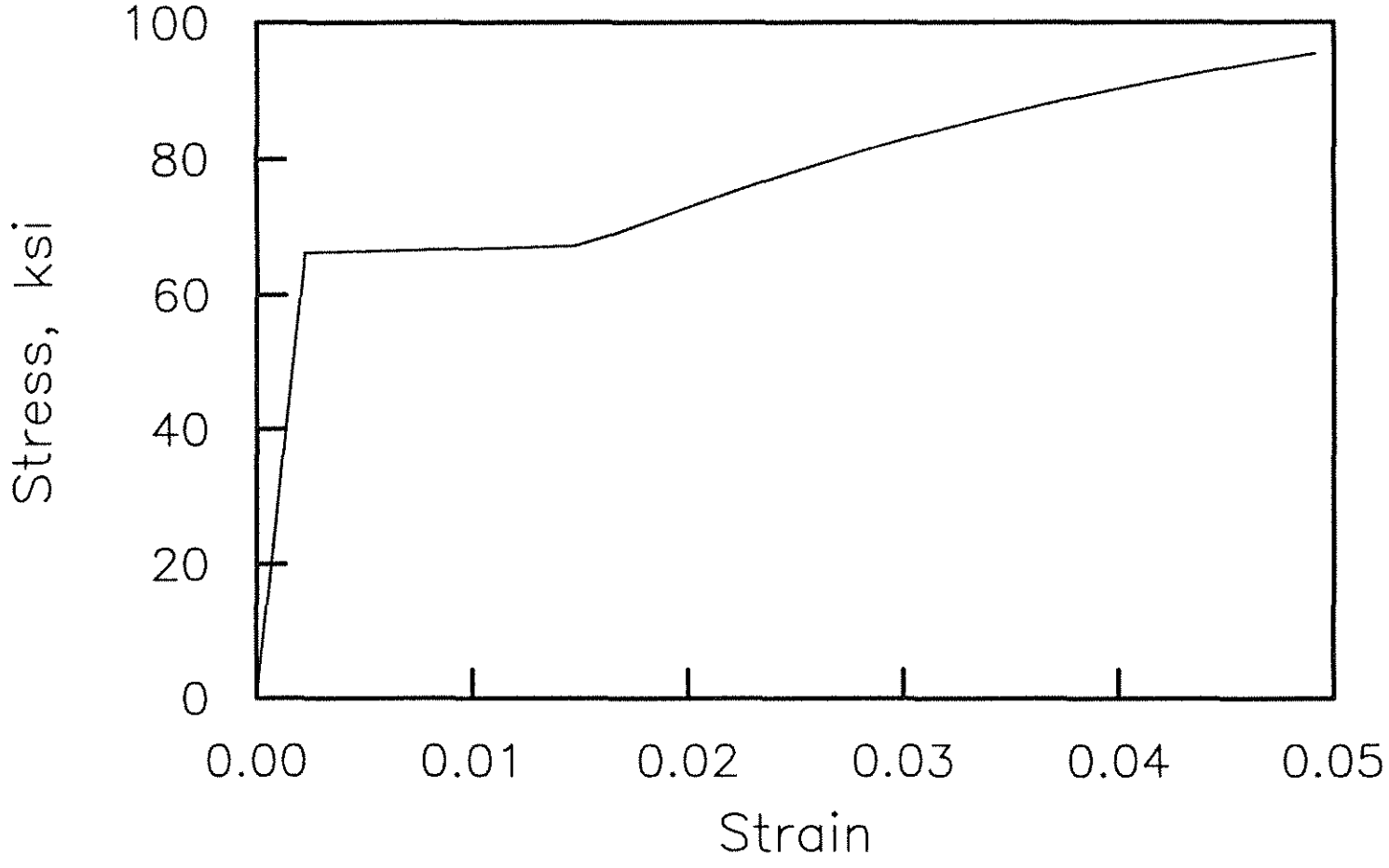

Fig. 2.2 Stress versus Strain for the beam flexural reinforcement (#4 bars)

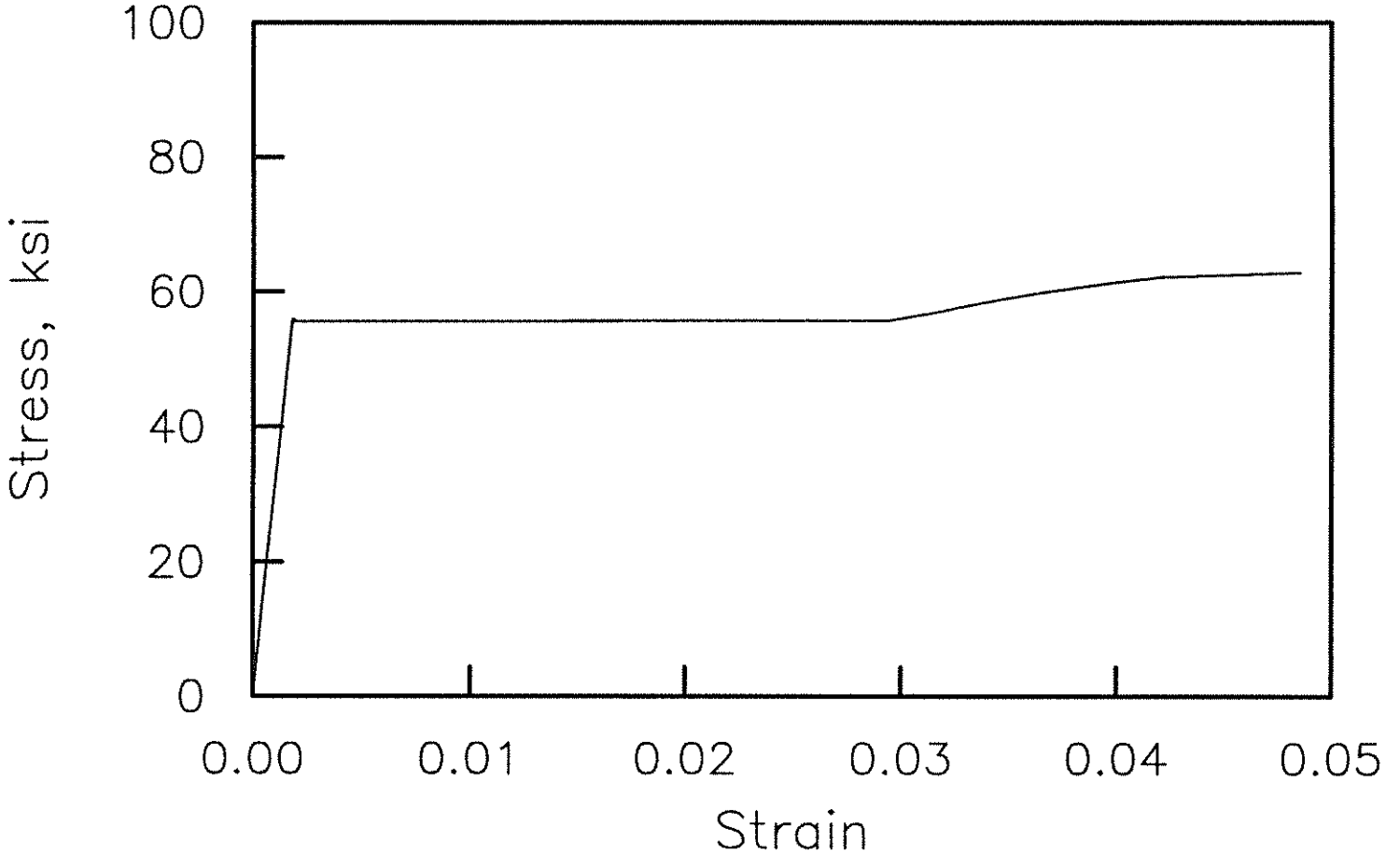

Fig. 2.3 Stress versus Strain for the beam transverse reinforcement (7/32 in. nominal diameter smooth rod)

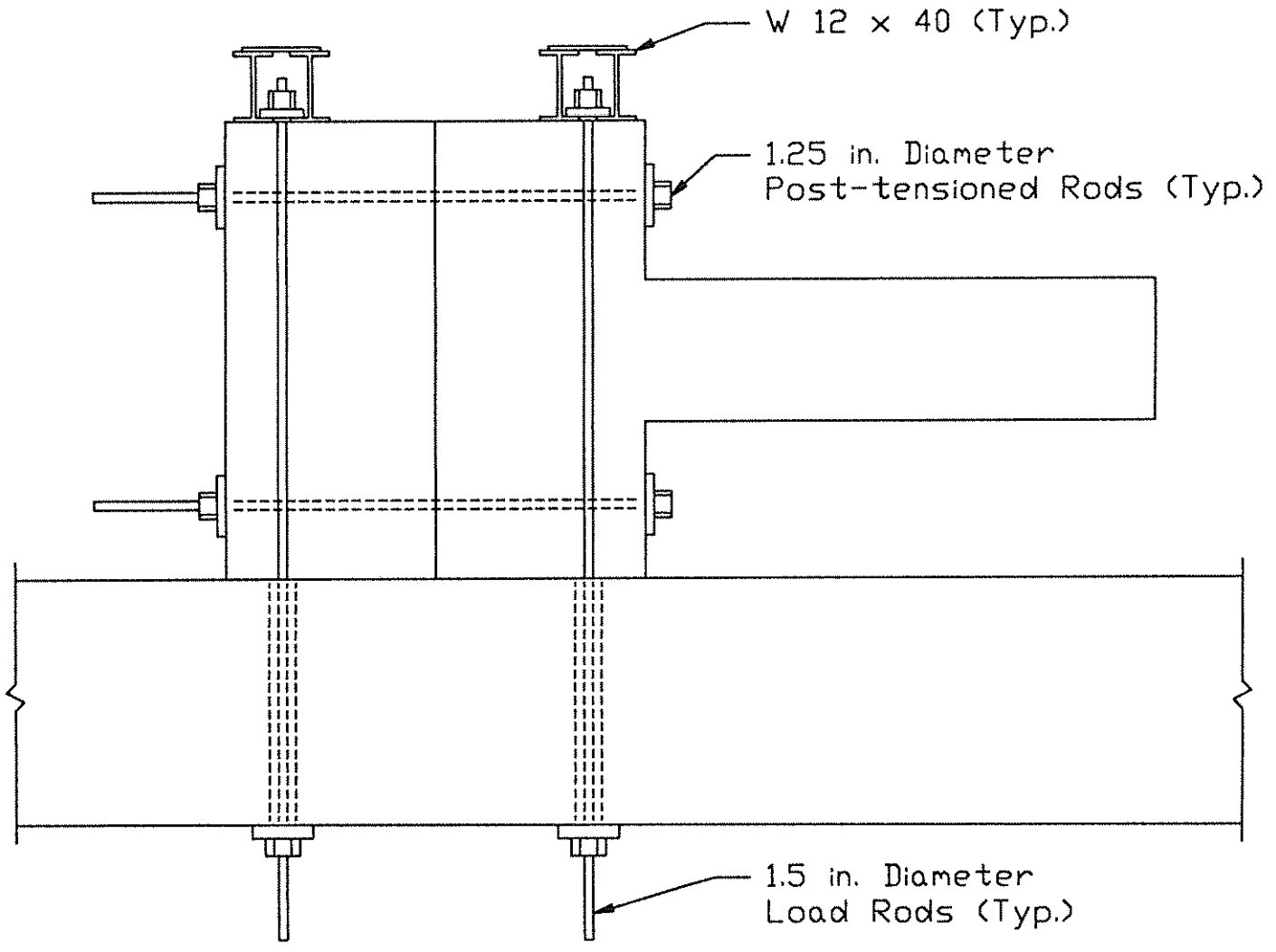

Fig. 2.4 Beam-Column Subassembly

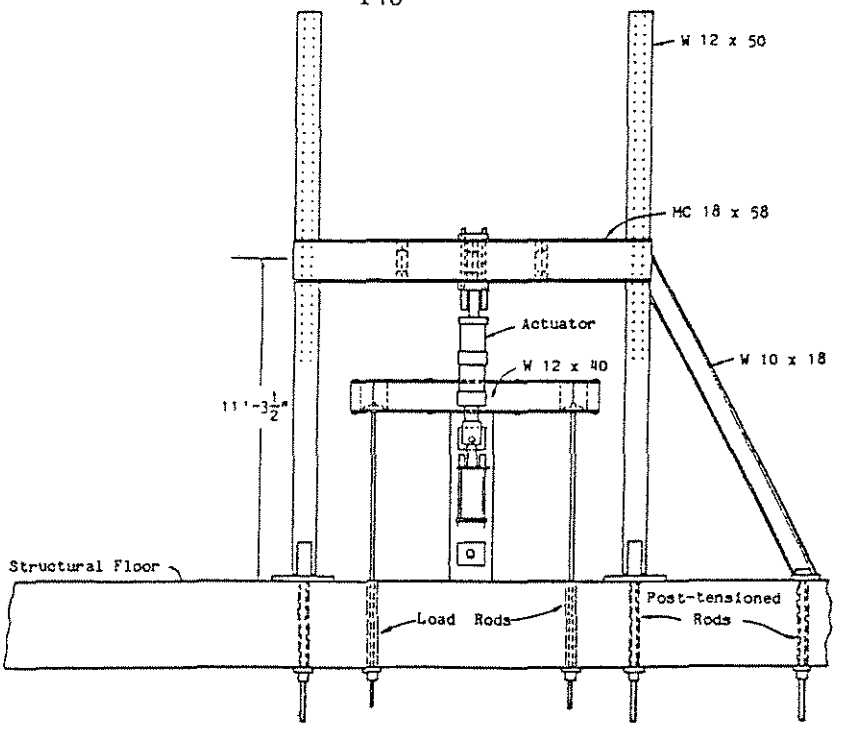

Fig. 2.5(a) Specimen in Test Position, End View (Nmai & Darwin 1984)

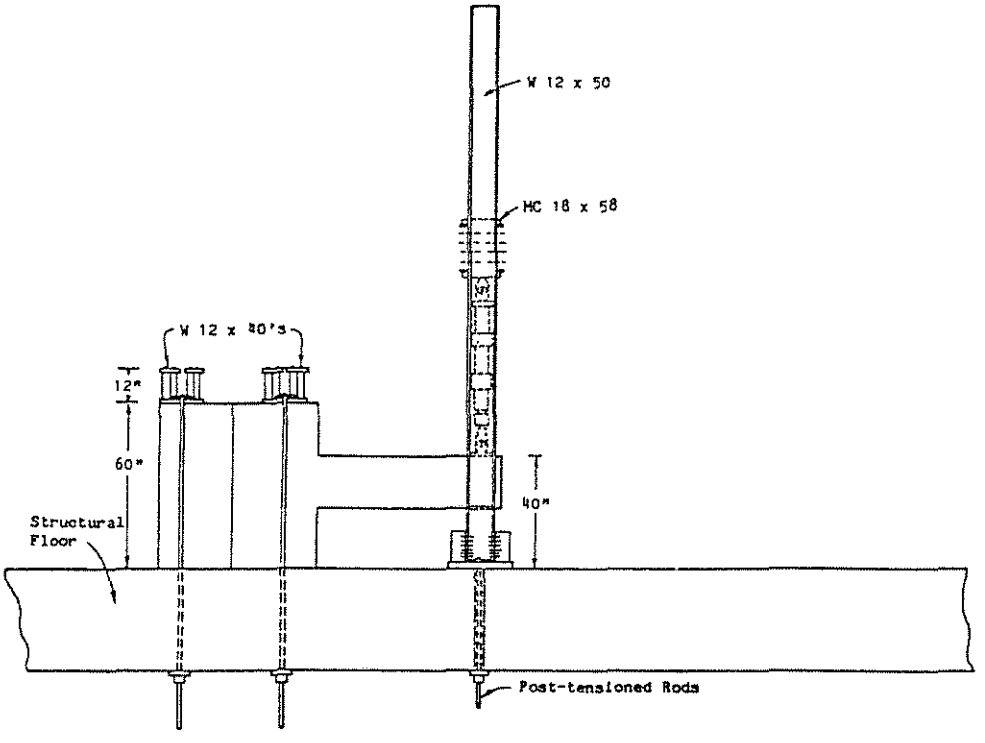

Fig. 2.5(b) Specimen in Test Position, Side View (Nmai & Darwin 1984)

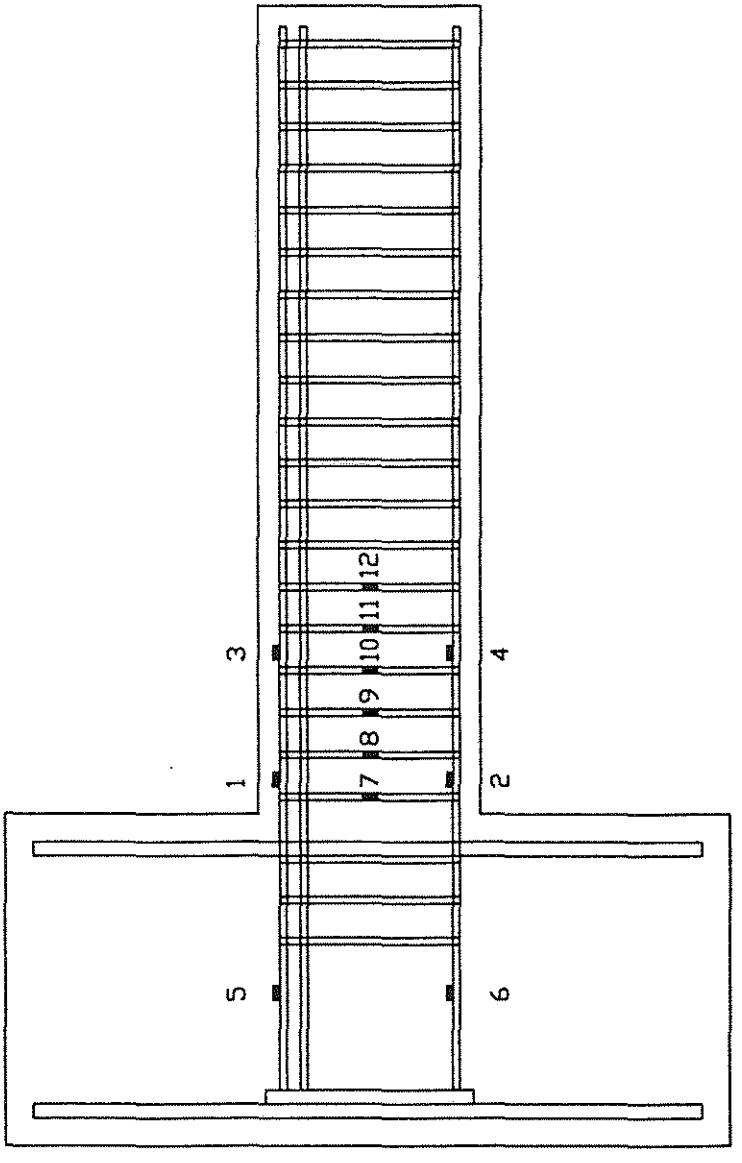

Fig. 2.6 Location of Strain Gages

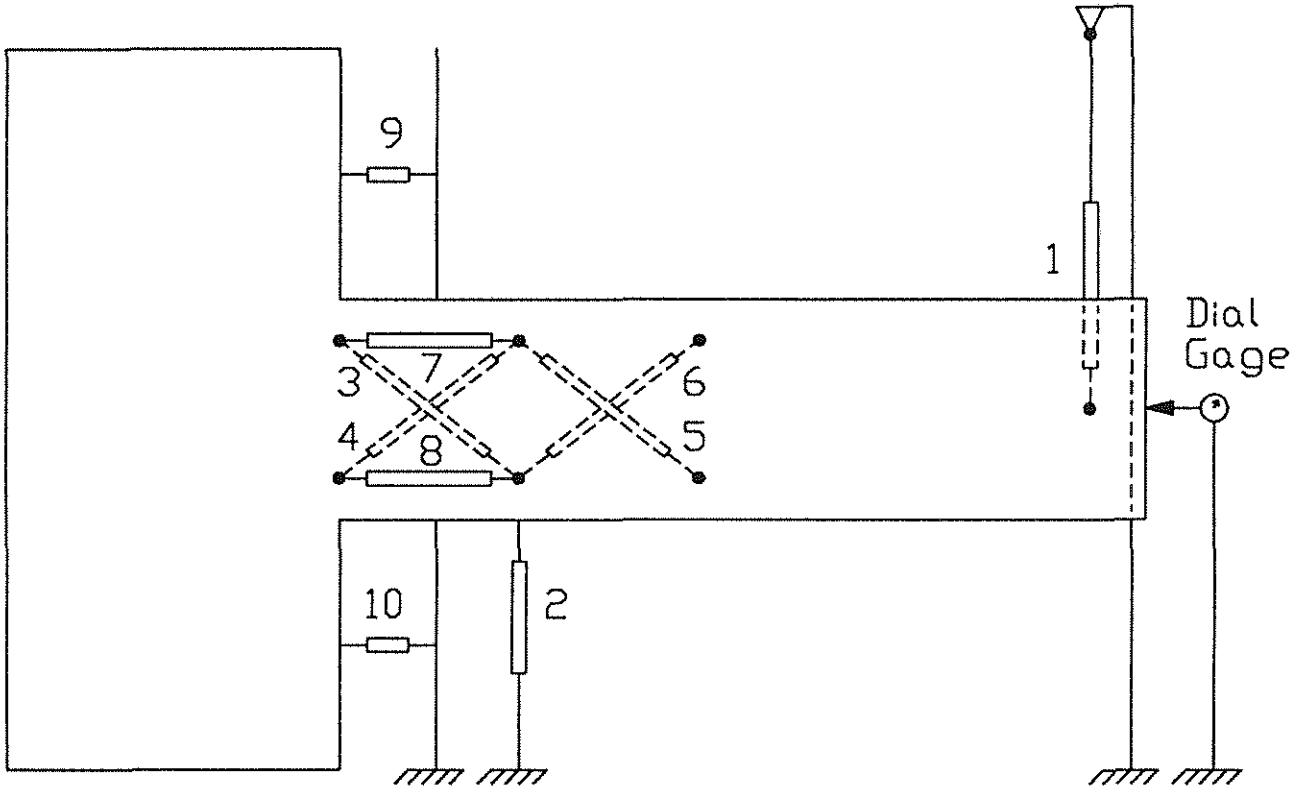

Fig. 2.7 Location of LVDT's and Dial Gage

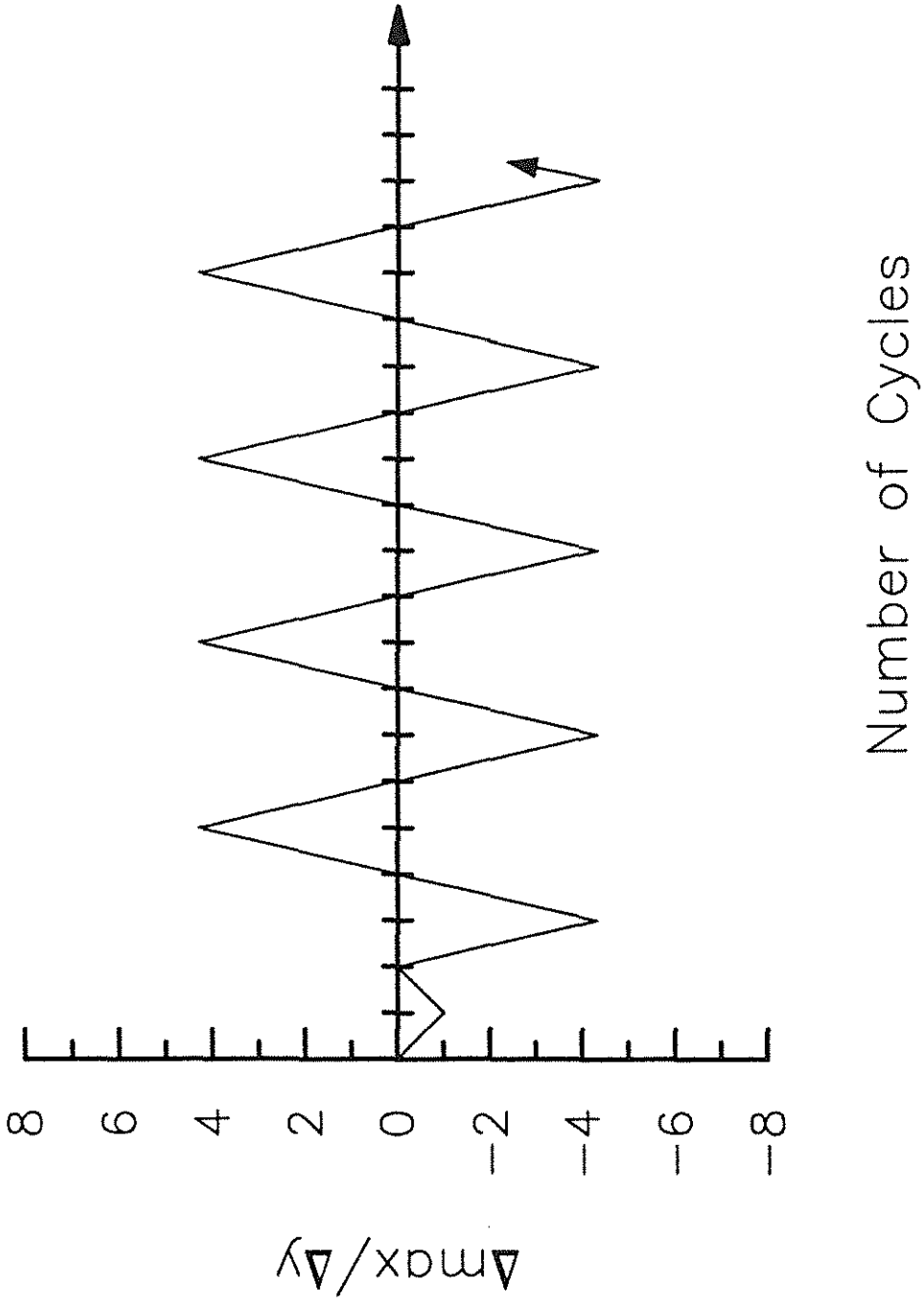

Fig. 2.8 Displacement Schedule

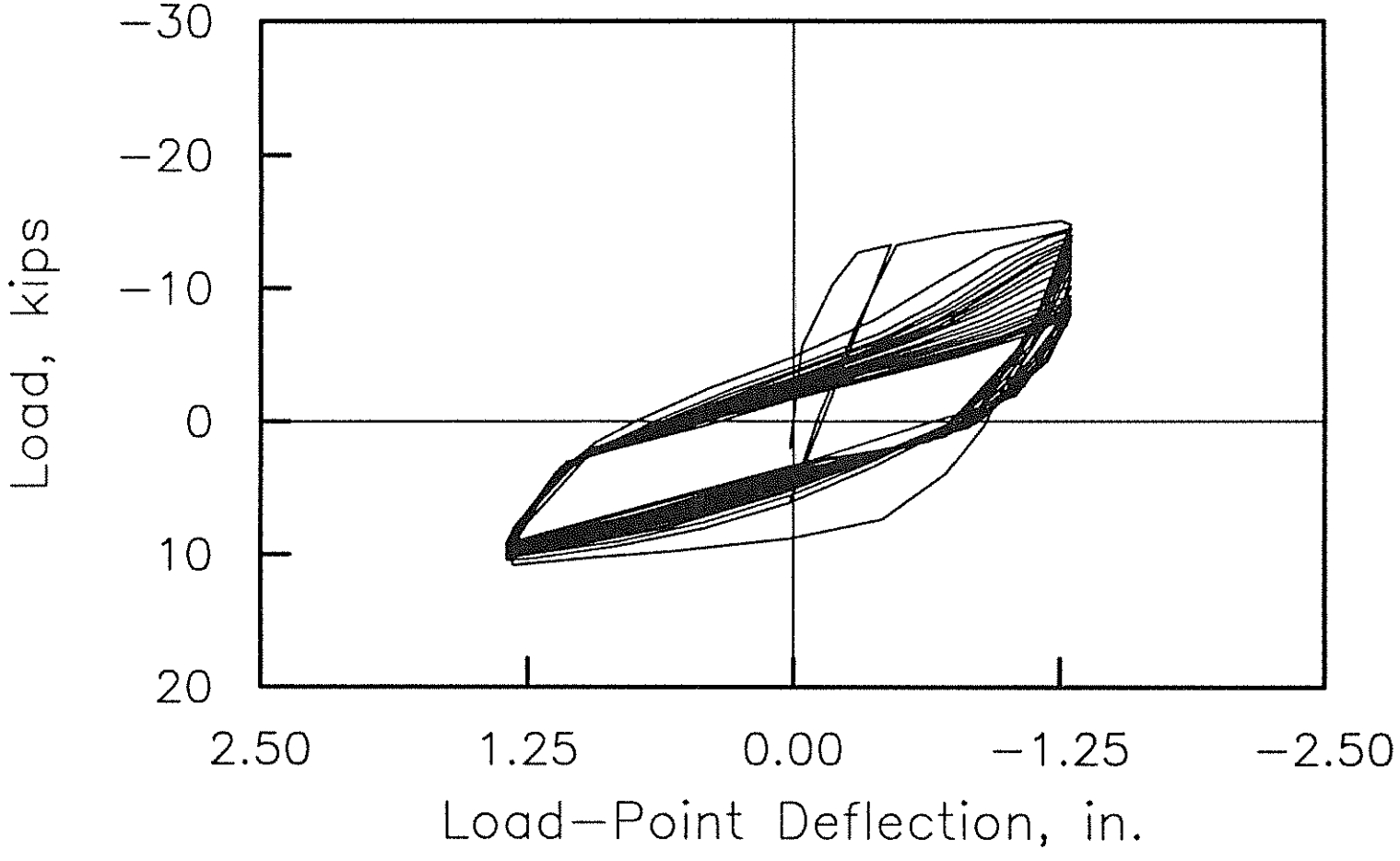

Fig. 2.9(a) Load versus Load-Point Deflection (LVDT #1), Beam H-1

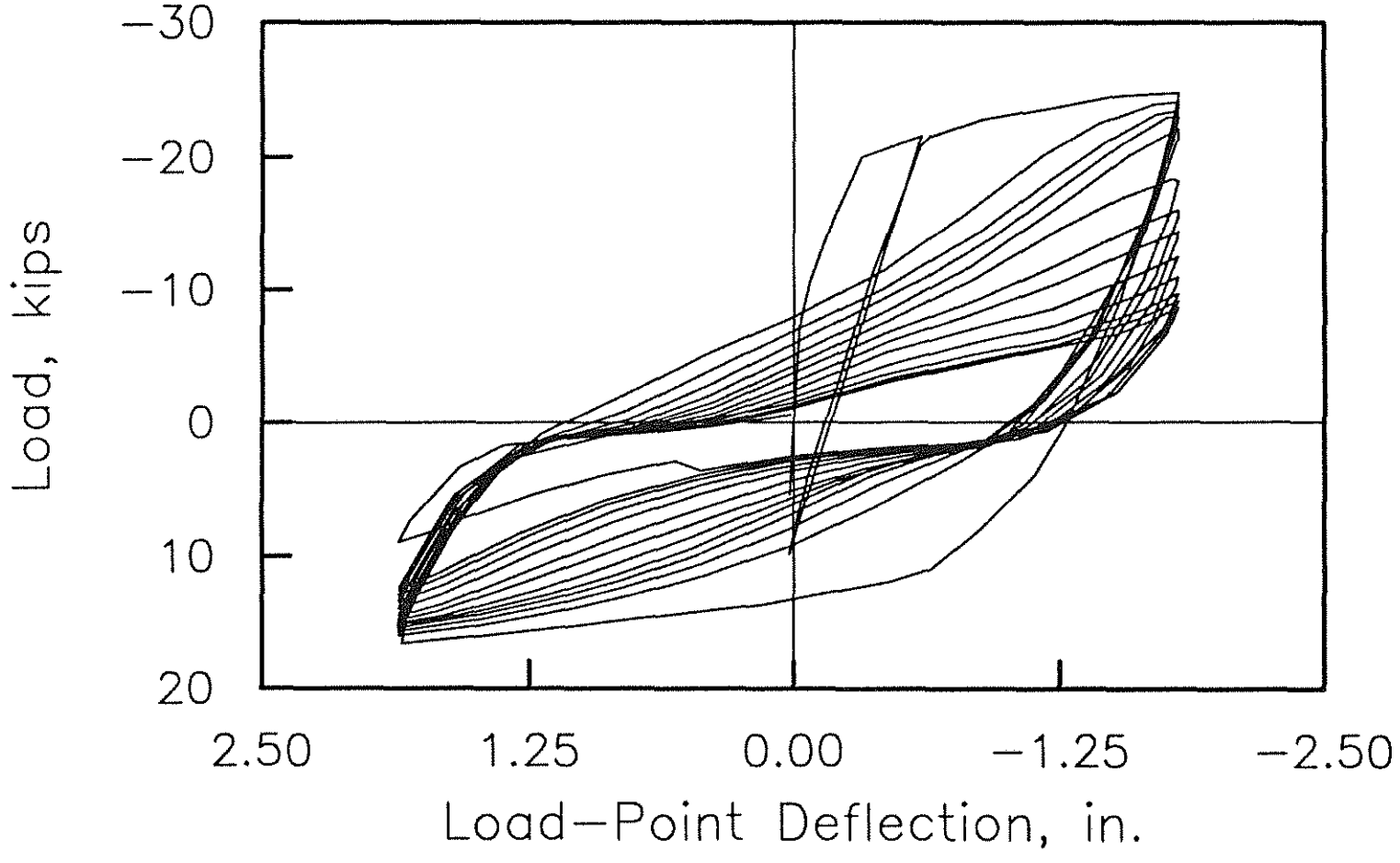

Fig. 2.9(b) Load versus Load-Point Deflection (LVDT #1), Beam H-2

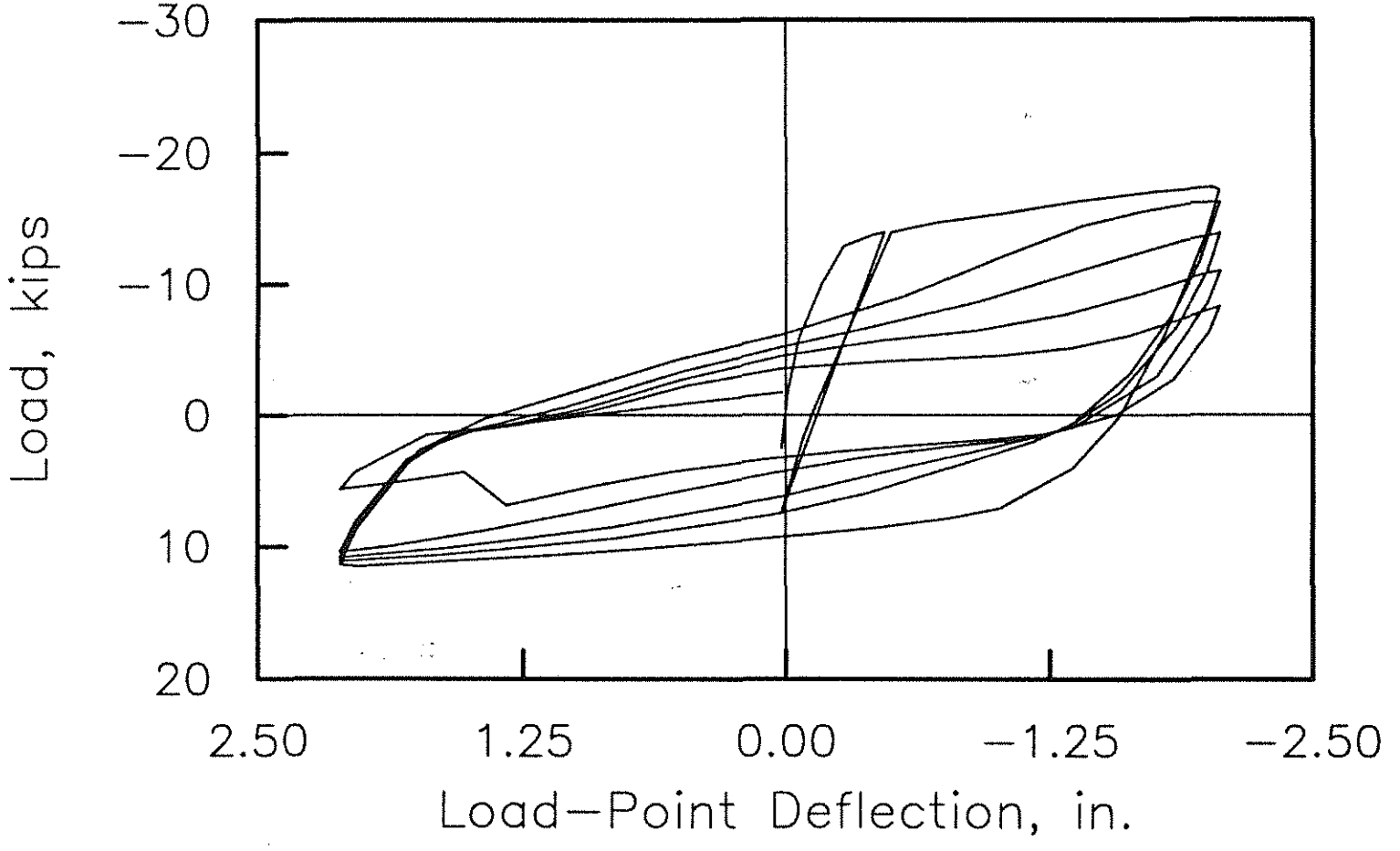

Fig. 2.9(c) Load versus Load-Point Deflection (LVDT #1), Beam H-3

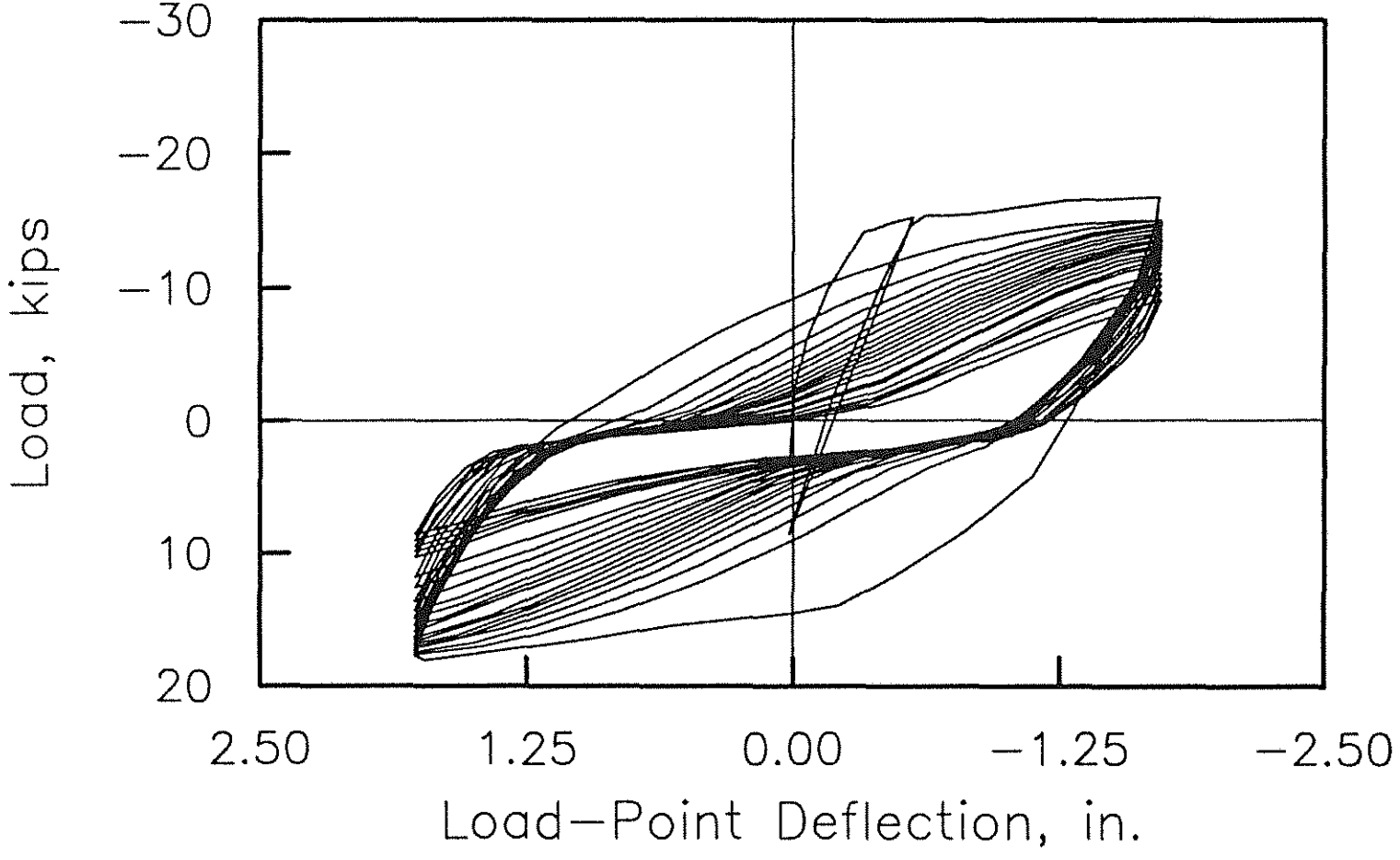

Fig. 2.9(d) Load versus Load-Point Deflection (LVDT #1), Beam H-4

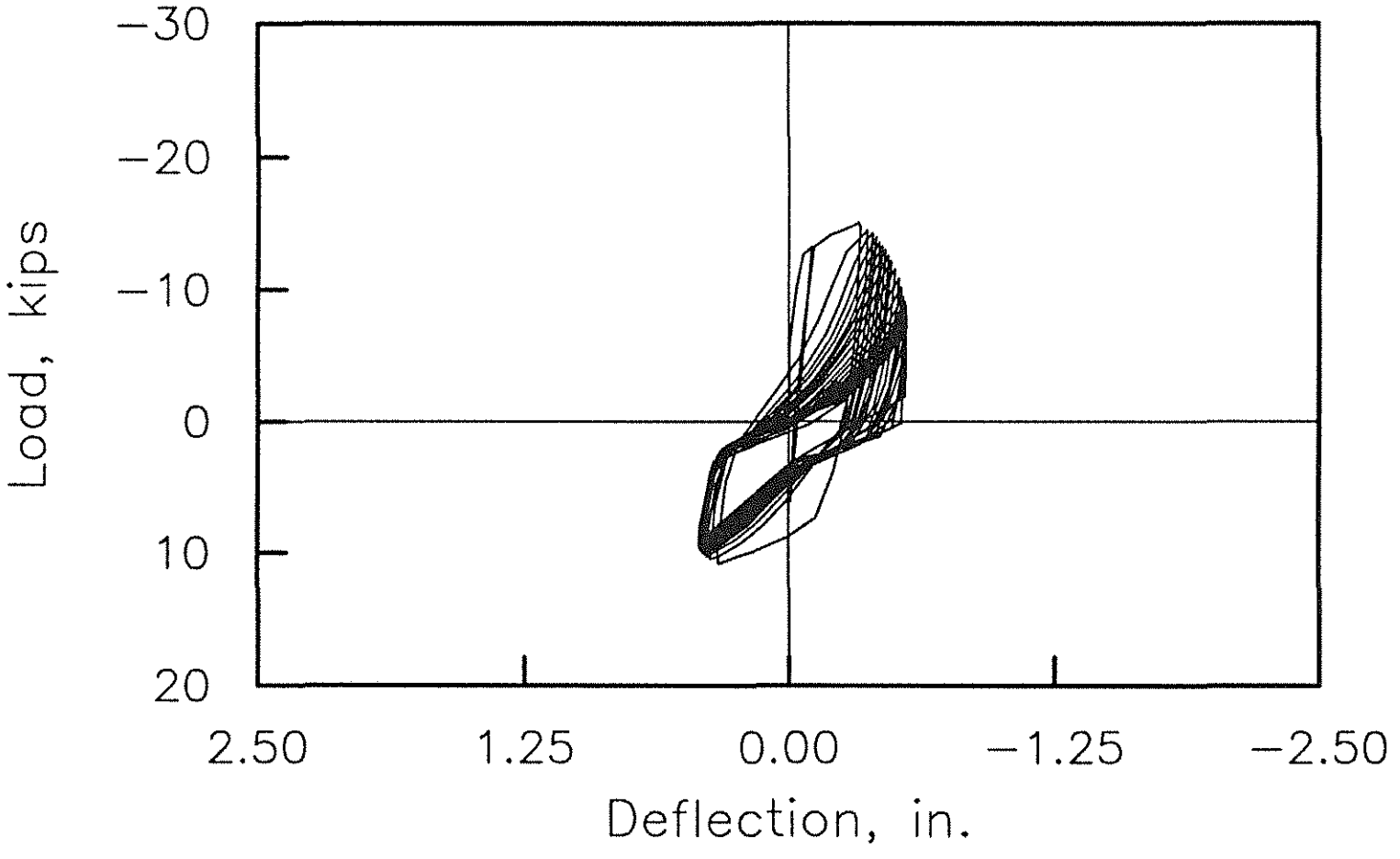

Fig. 2.10(a) Load versus Deflection at d from the column face (LVDT #2), Beam H-1

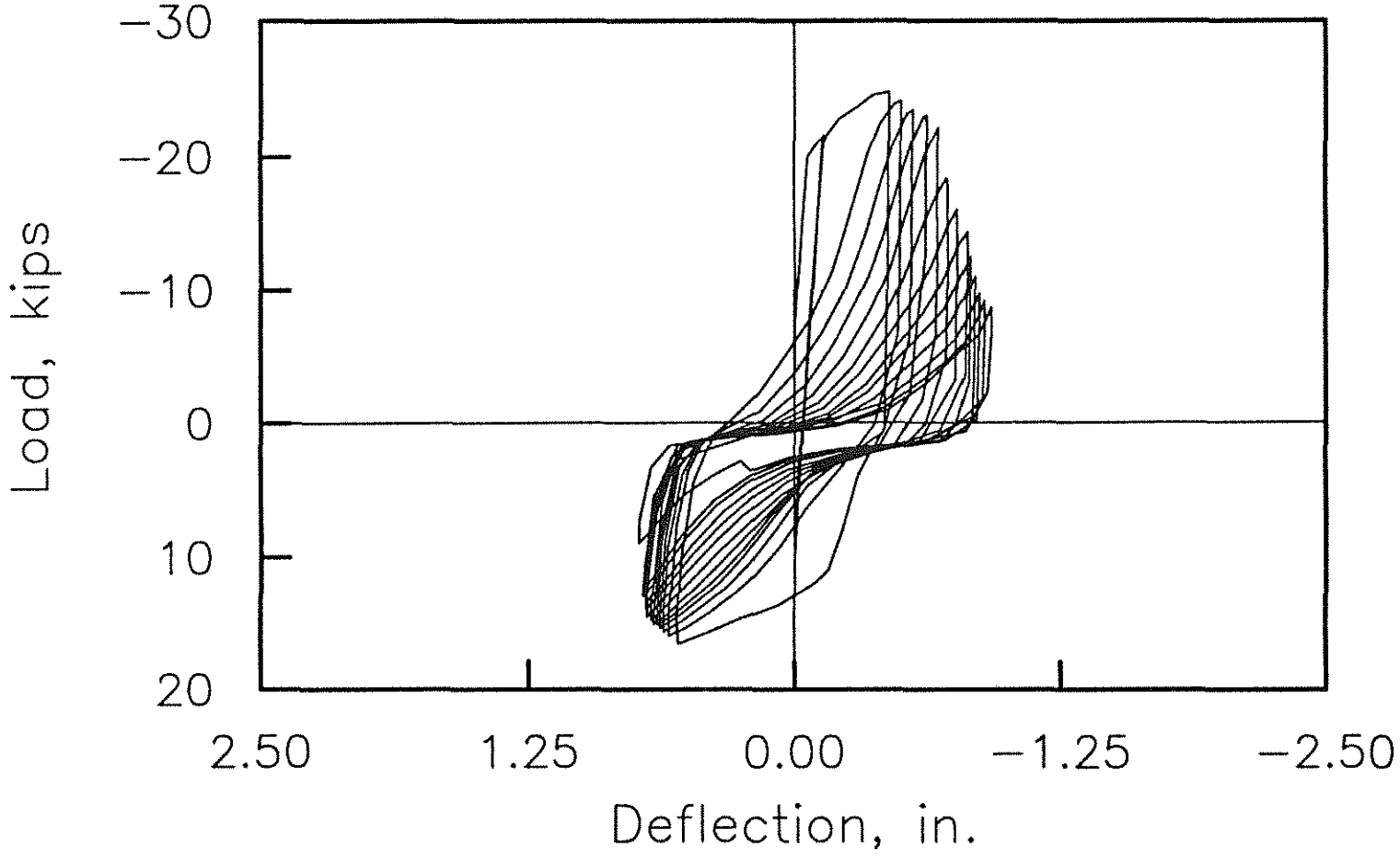

Fig. 2.10(b) Load versus Deflection at d from the column face (LVDT #2), Beam H-2

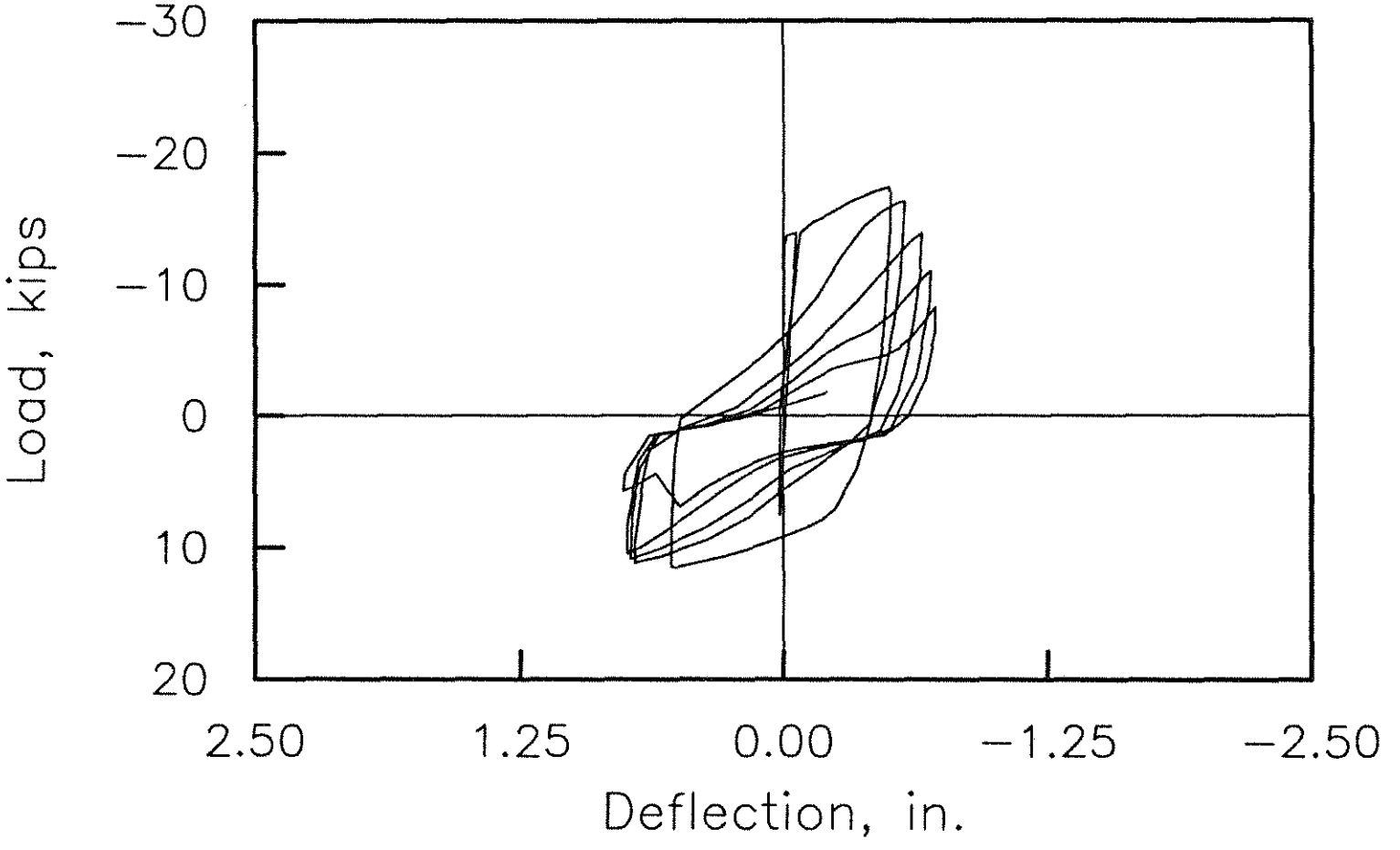

Fig. 2.10(c) Load versus Deflection at d from the column face (LVDT #2), Beam H-3

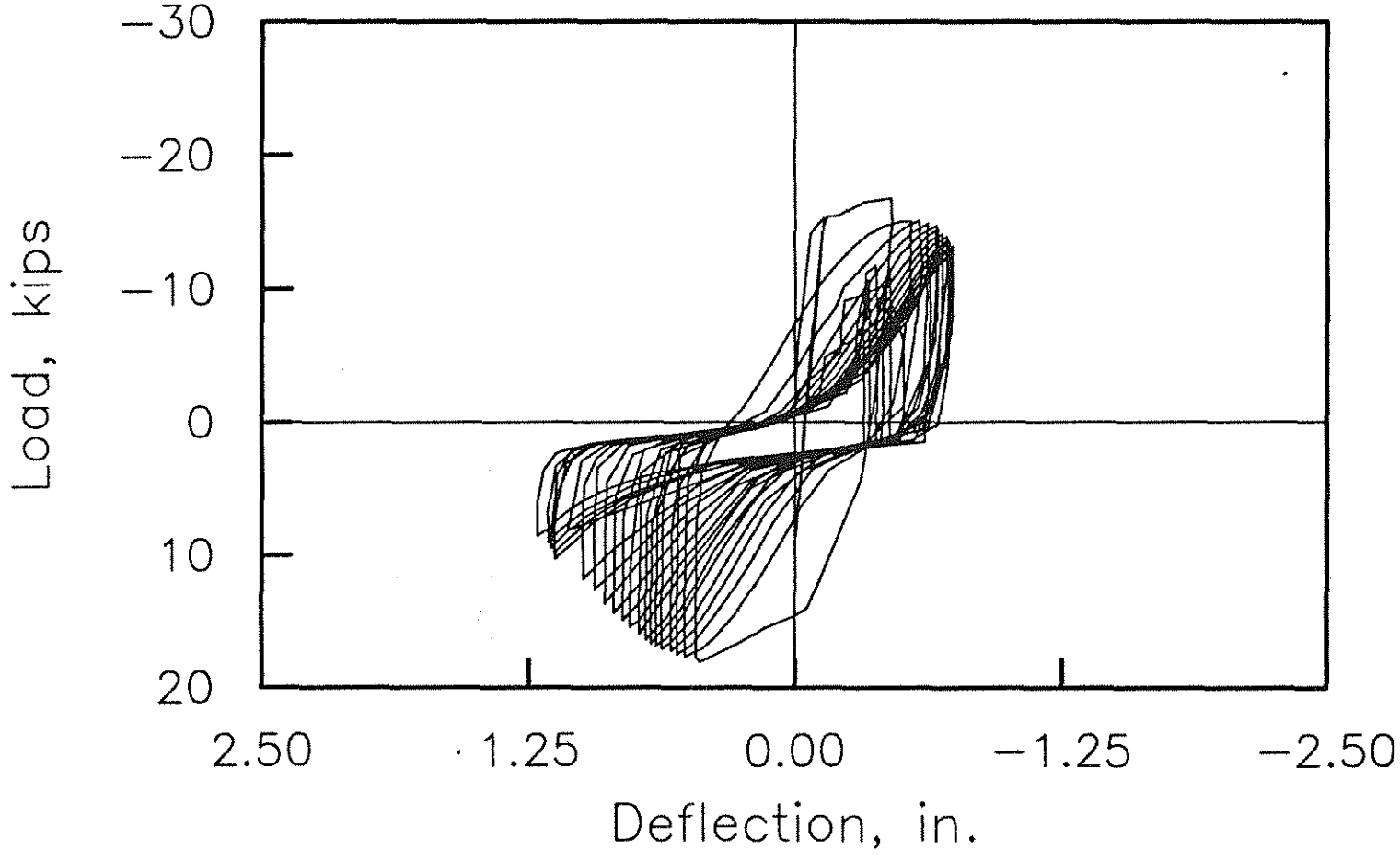

Fig. 2.10(d) Load versus Deflection at d from the column face (LVDT #2), Beam H-4

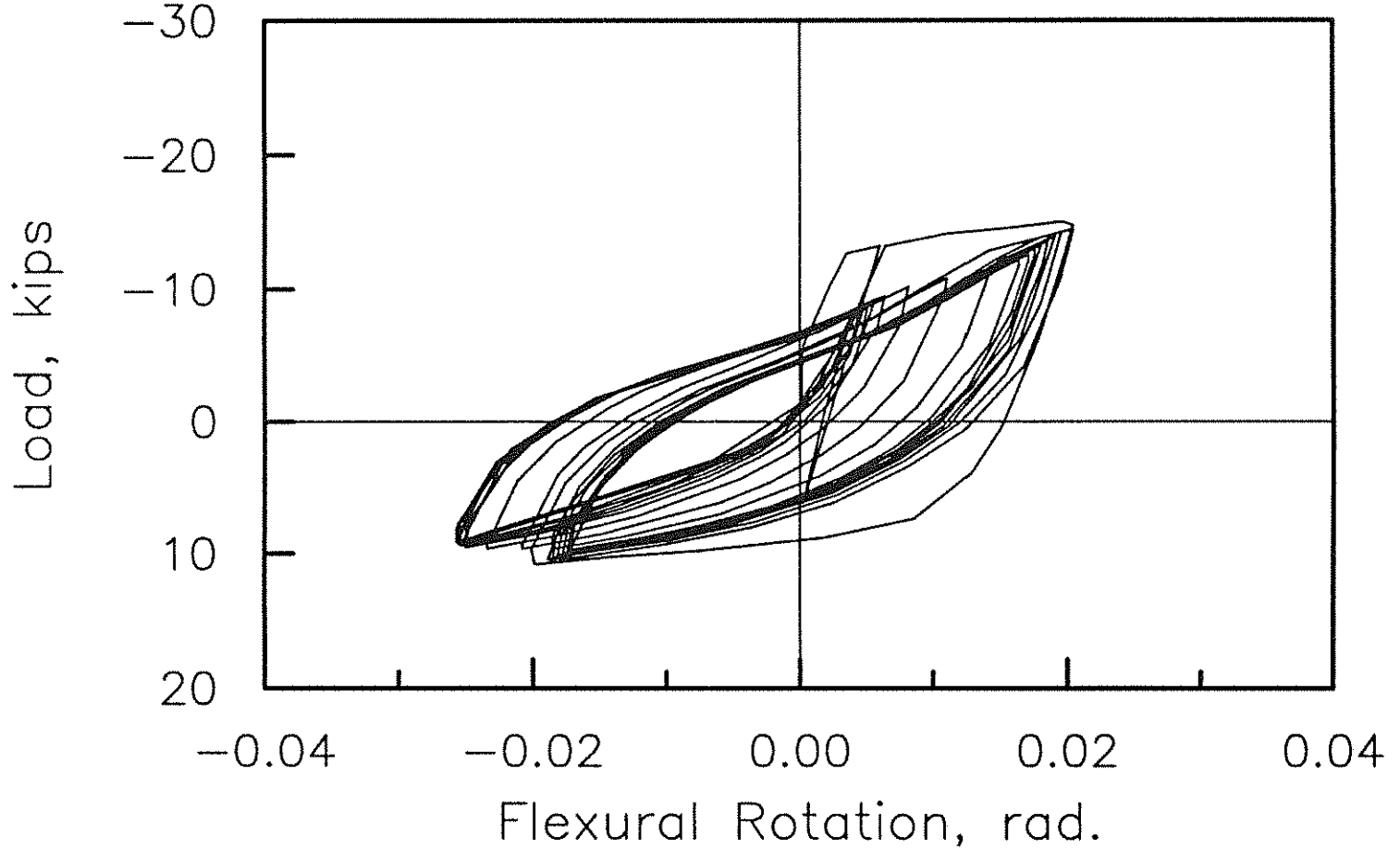

Fig. 2.11(a) Load versus Hinging Zone Flexural Rotation over the region extending d from the column face (LVDT #7 & #8), Beam H-1

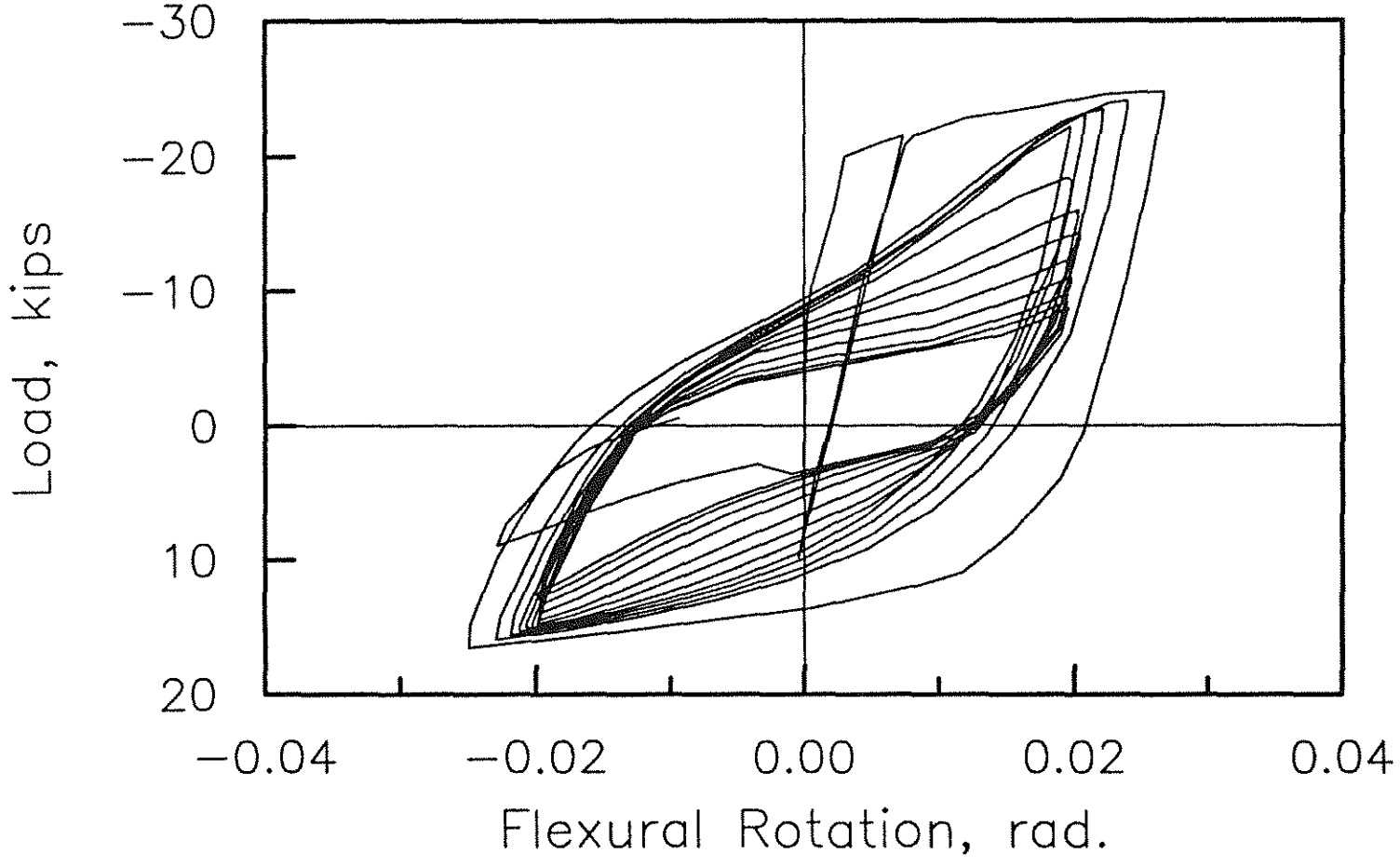

Fig. 2.11(b) Load versus Hinging Zone Flexural Rotation over the region extending d from the column face (LVDT #7 & #8), Beam H-2

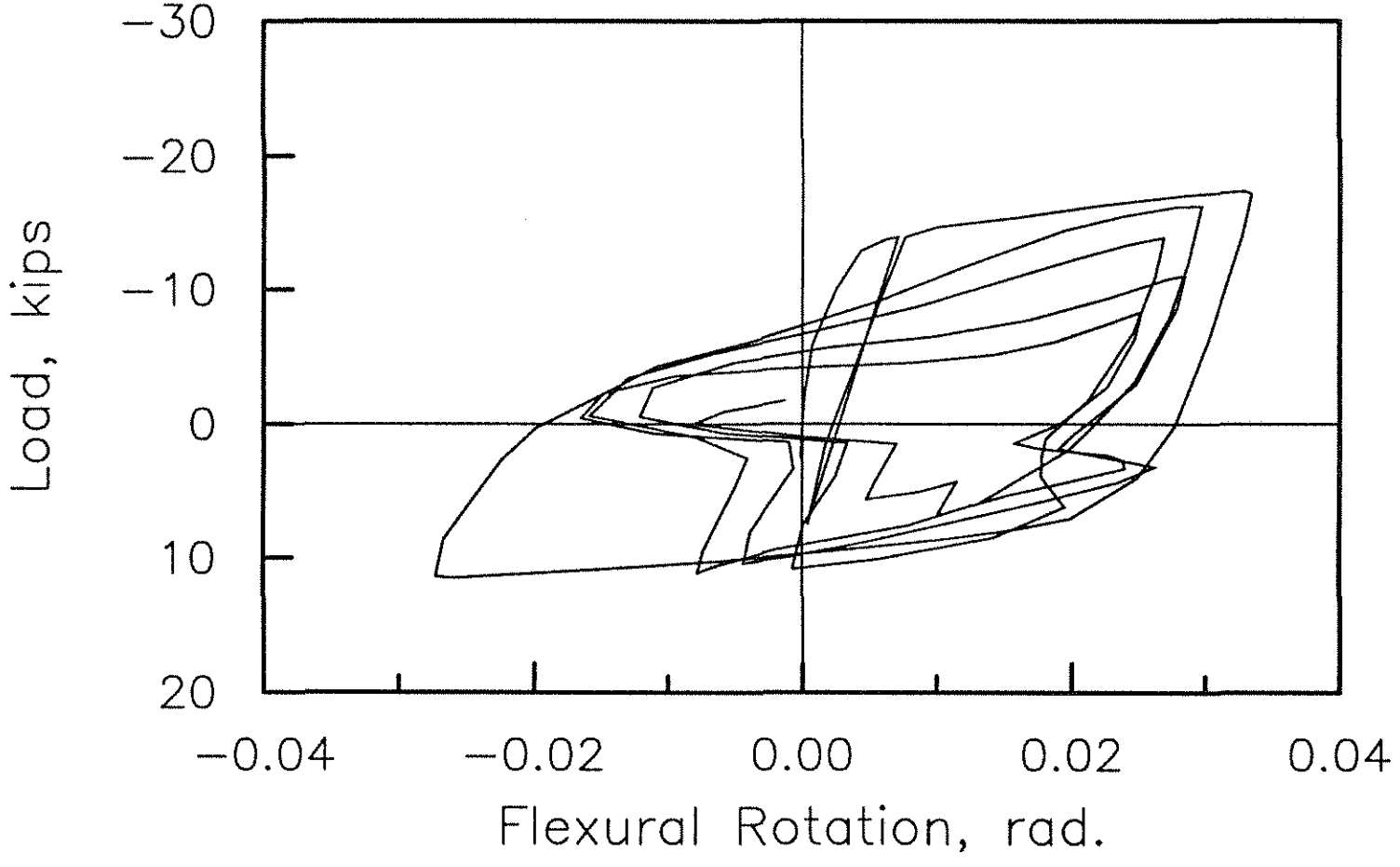

Fig. 2.11(c) Load versus Hinging Zone Flexural Rotation over the region extending d from the column face (LVDT #7 & #8), Beam H-3

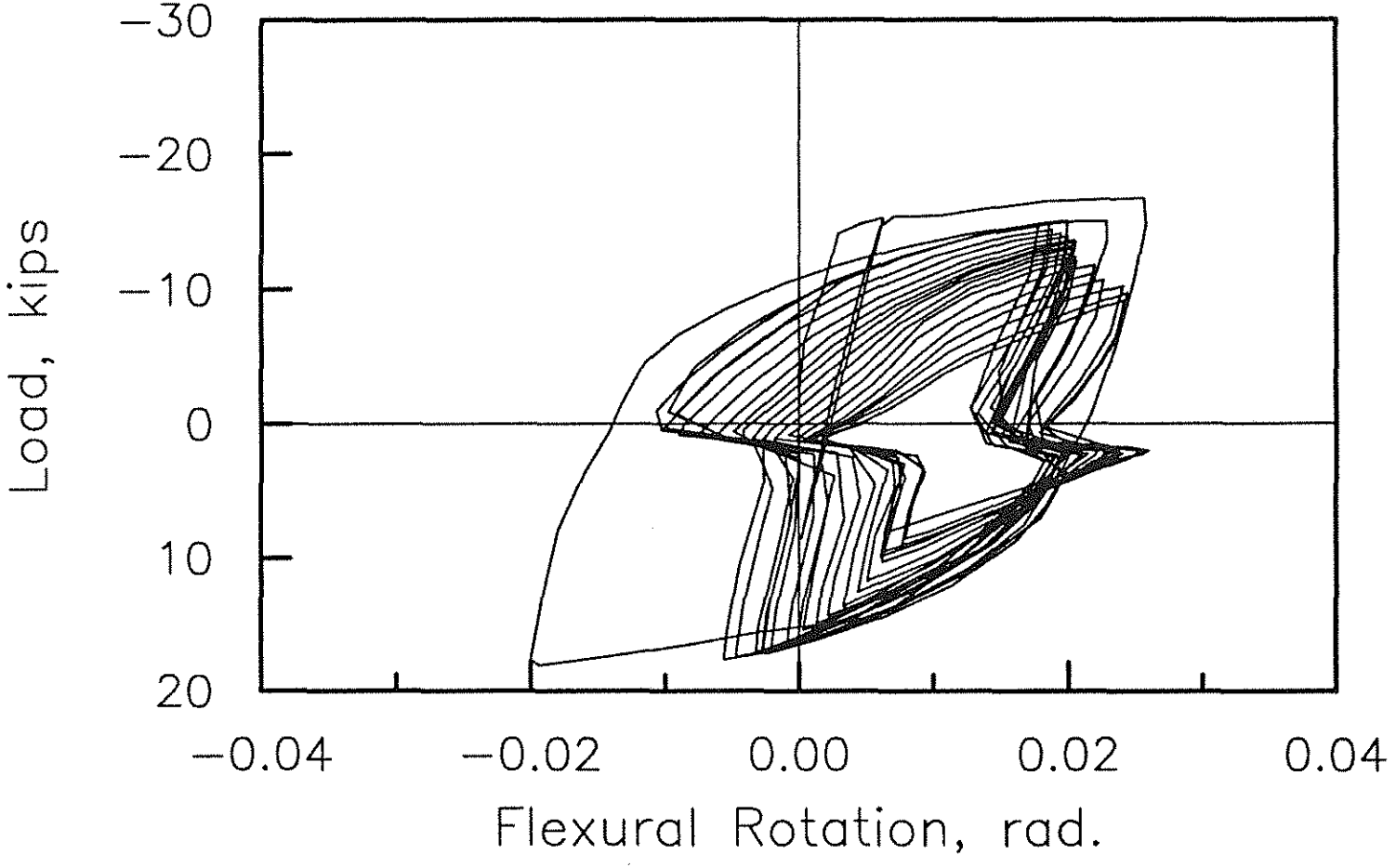

Fig. 2.11(d) Load versus Hinging Zone Flexural Rotation over the region extending d from the column face (LVDT #7 & #8), Beam H-4

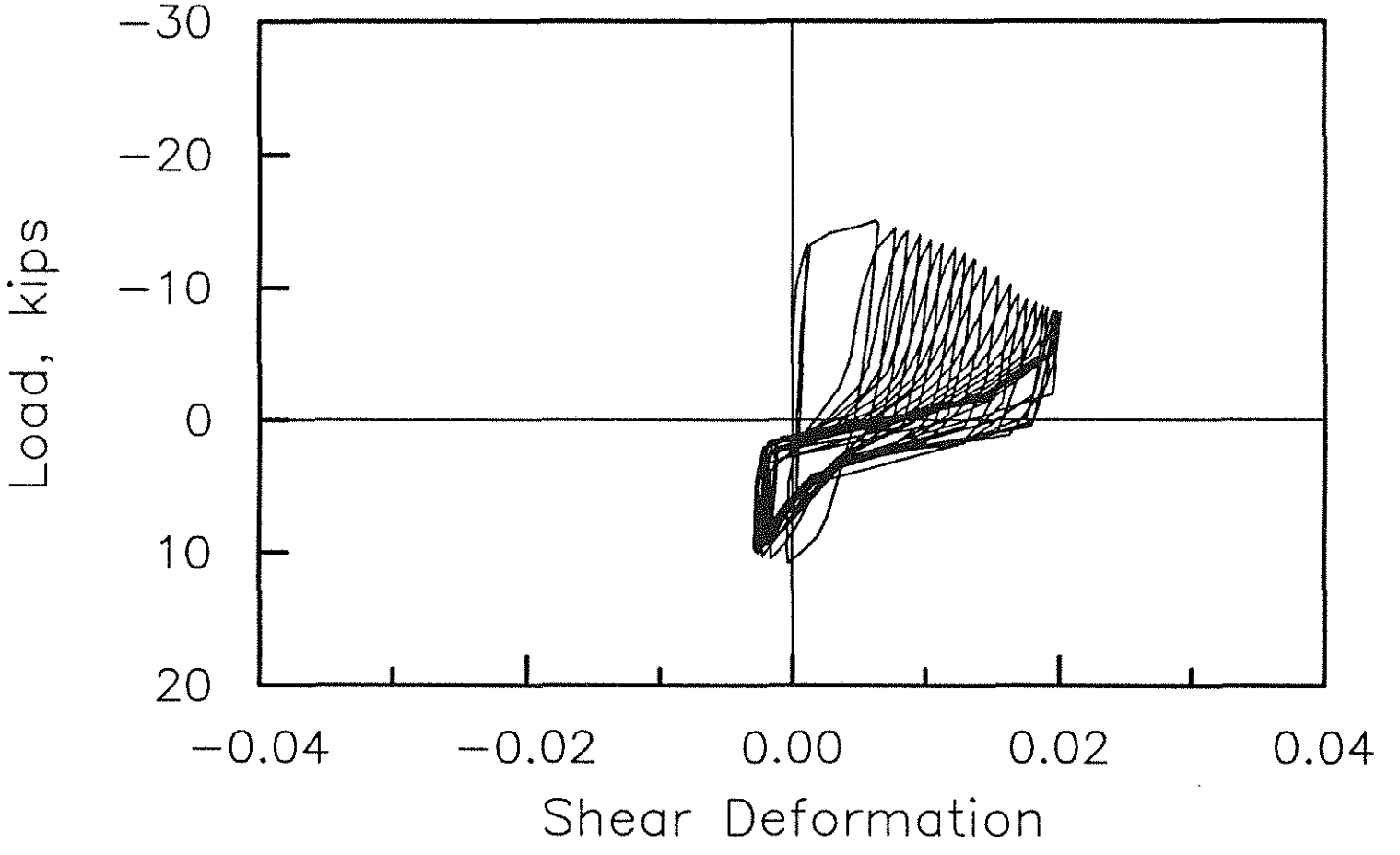

Fig. 2.12(a) Load versus Hinging Zone Shear Deformation over the region extending d from the column face (LVDT #3 & #4), Beam H-1

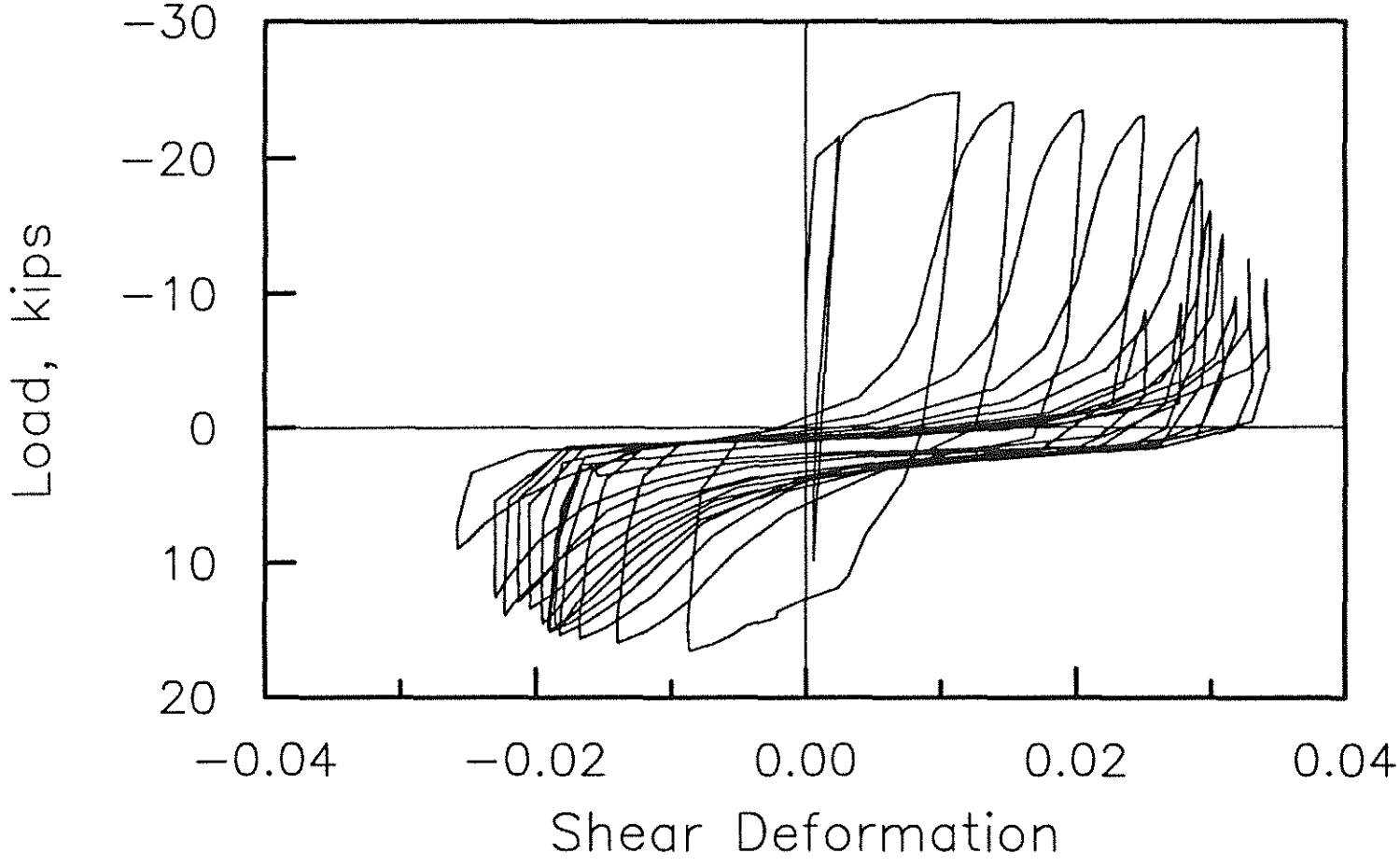

Fig. 2.12(b) Load versus Hinging Zone Shear Deformation over the region extending d from the column face (LVDT #3 & #4), Beam H-2

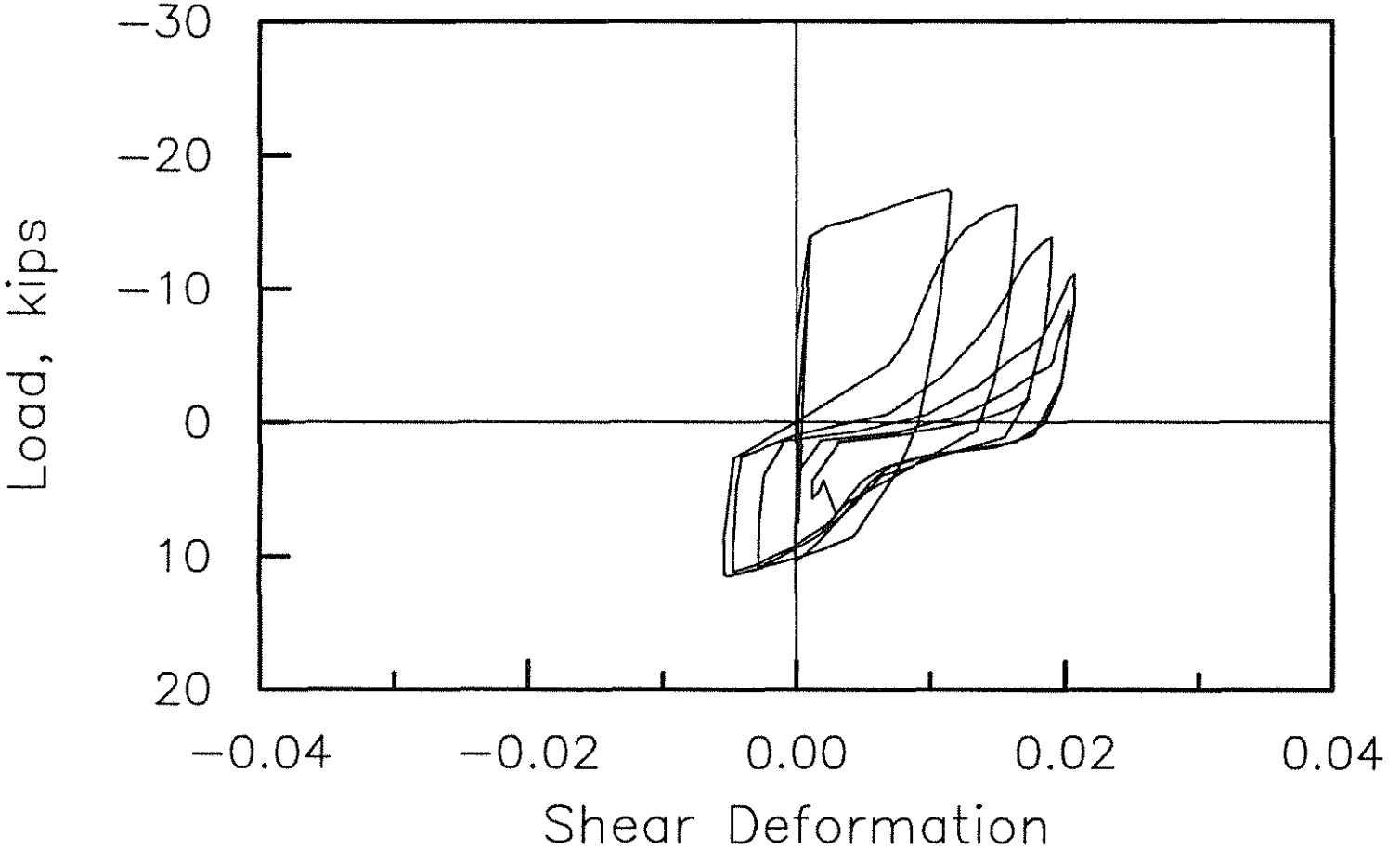

Fig. 2.12(c) Load versus Hinging Zone Shear Deformation over the region extending d from the column face (LVDT #3 & #4), Beam H-3

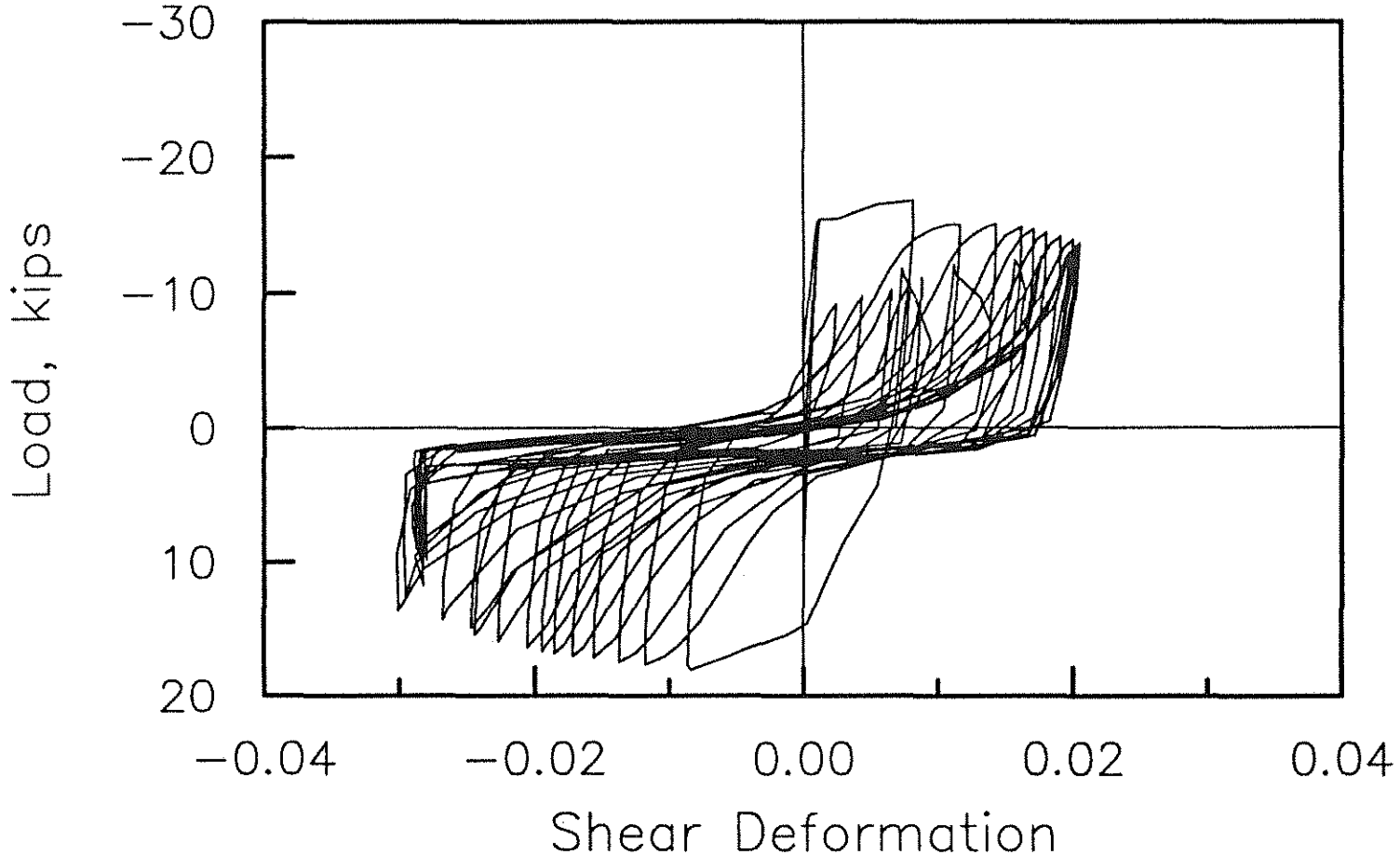

Fig. 2.12(d) Load versus Hinging Zone Shear Deformation over the region extending d from the column face (LVDT #3 & #4), Beam H-4

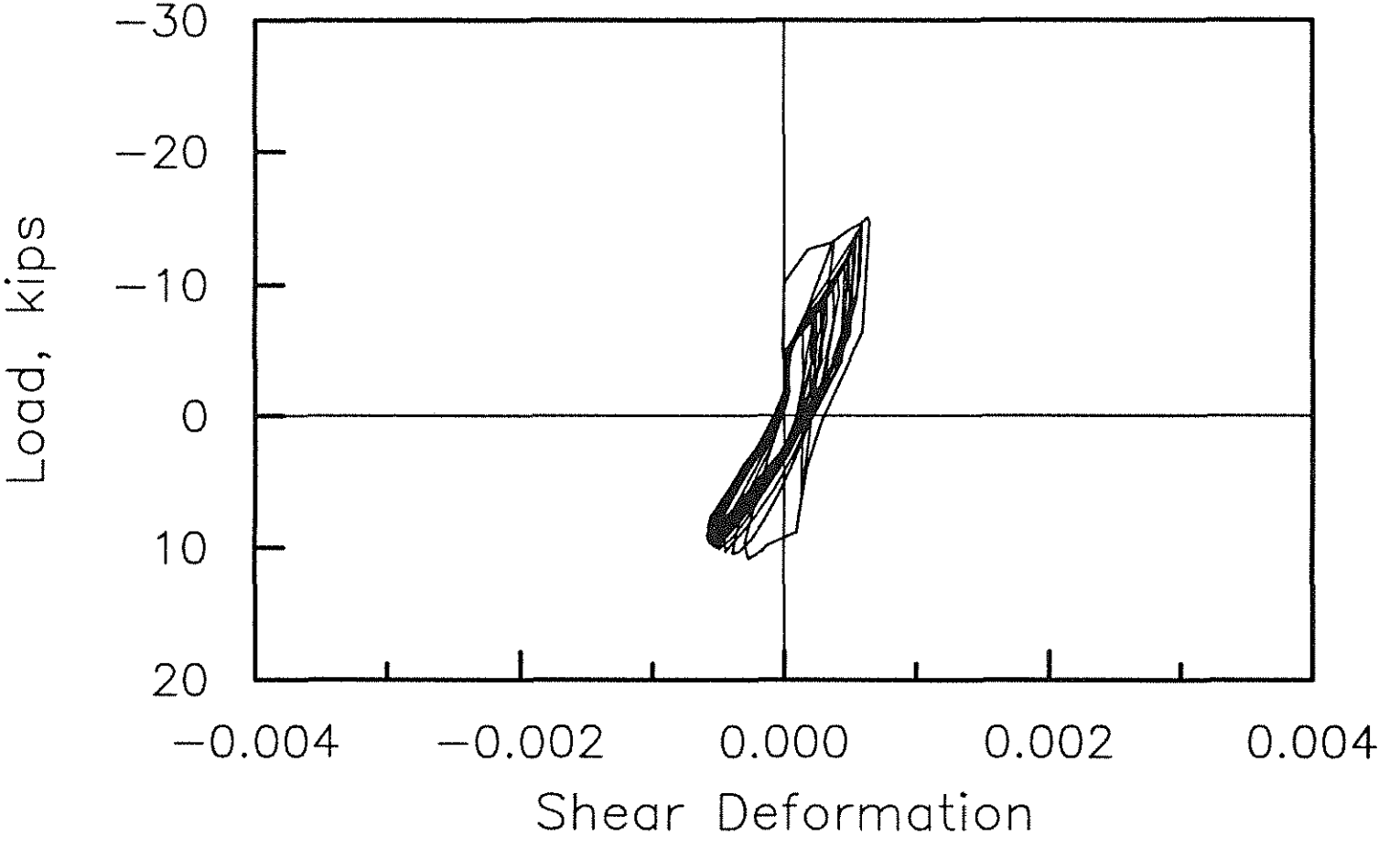

Fig. 2.13(a) Load versus Shear Deformation over the region extending 1.0d to 2.0d from the column face (LVDT #5 & #6), Beam H-1

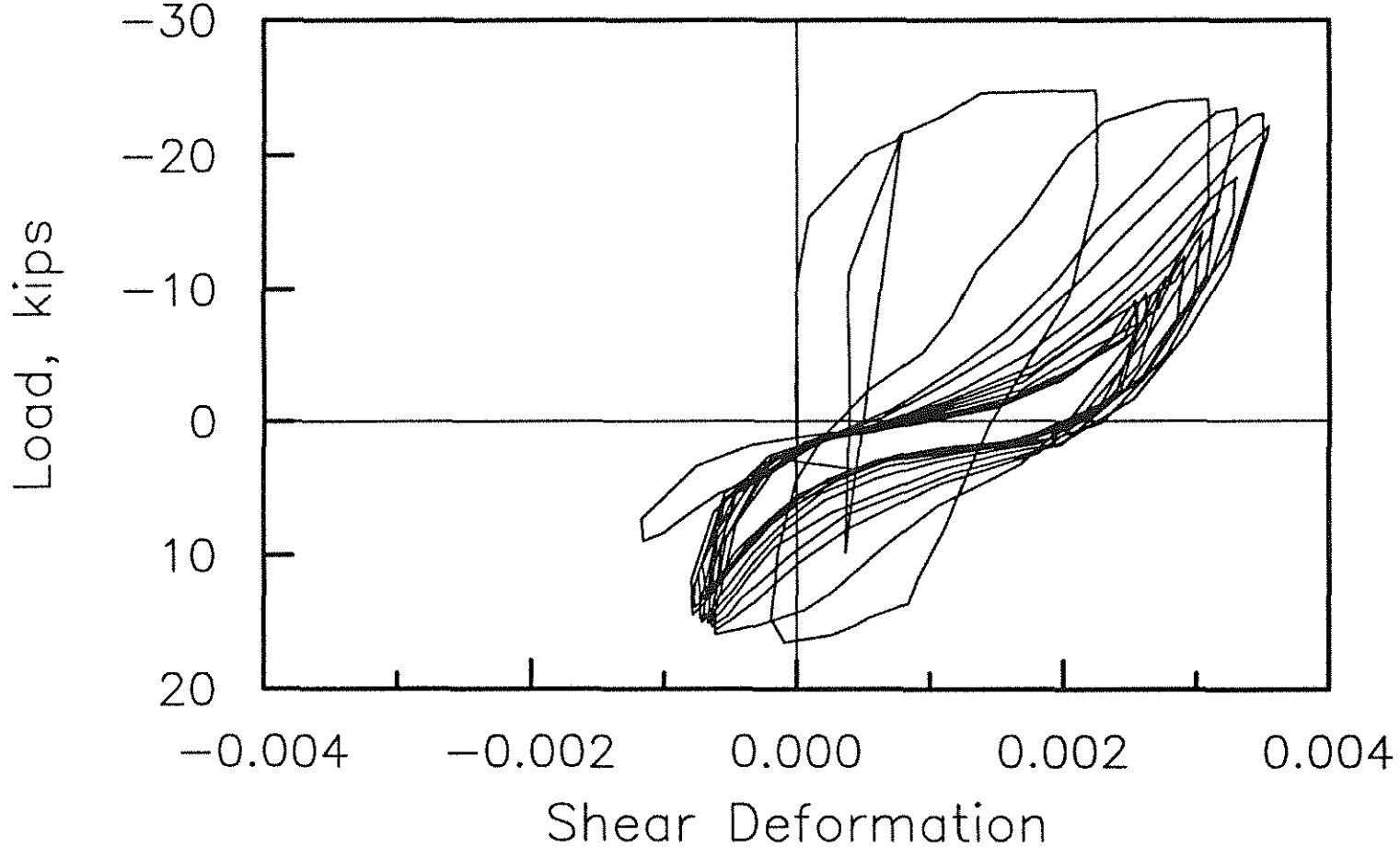

Fig. 2.13(b) Load versus Shear Deformation over the region extending 1.0d to 2.0d from the column face (LVDT #5 & #6), Beam H-2

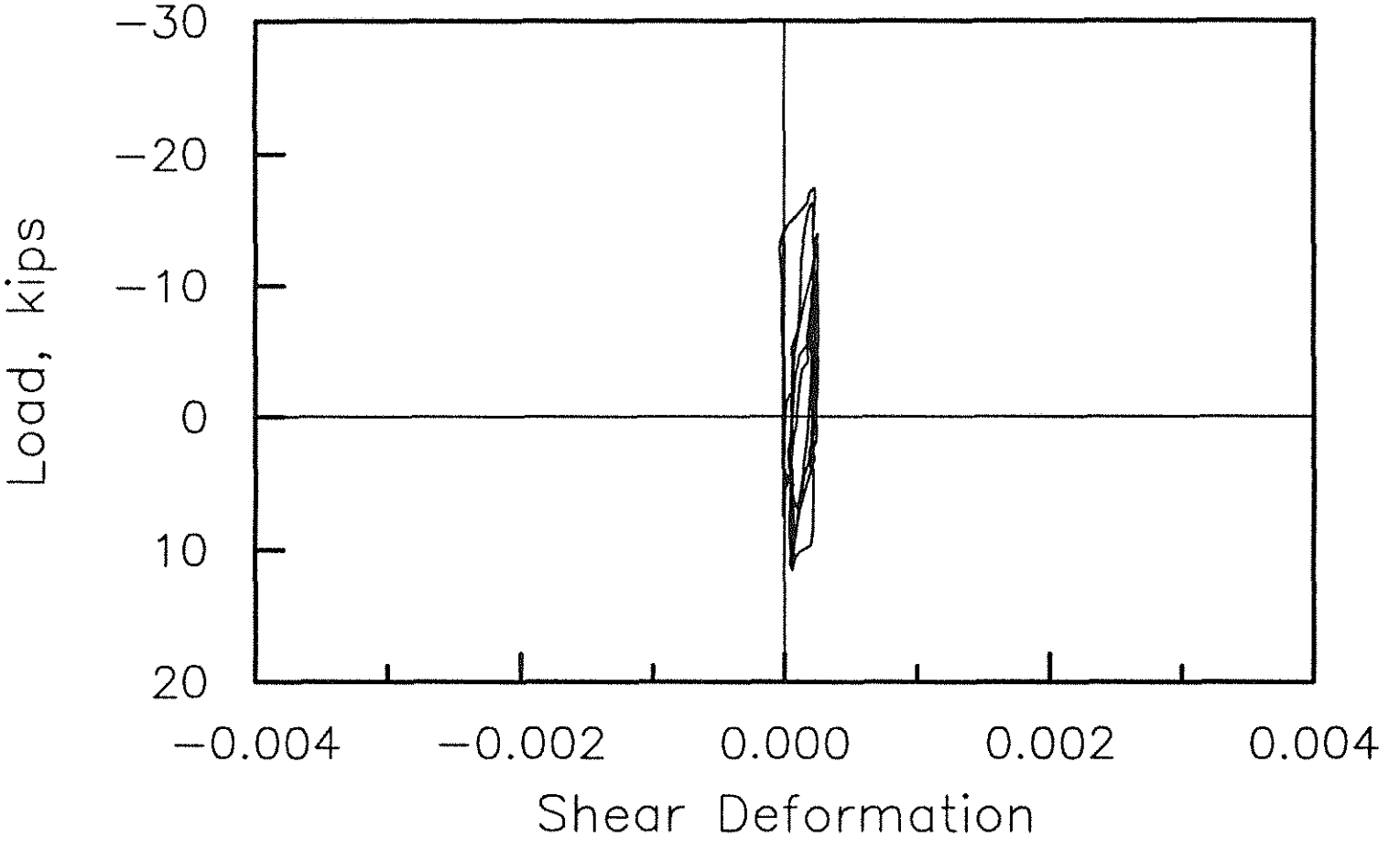

Fig. 2.13(c) Load versus Shear Deformation over the region extending 1.0d to 2.0d from the column face (LVDT #5 & #6), Beam H-3

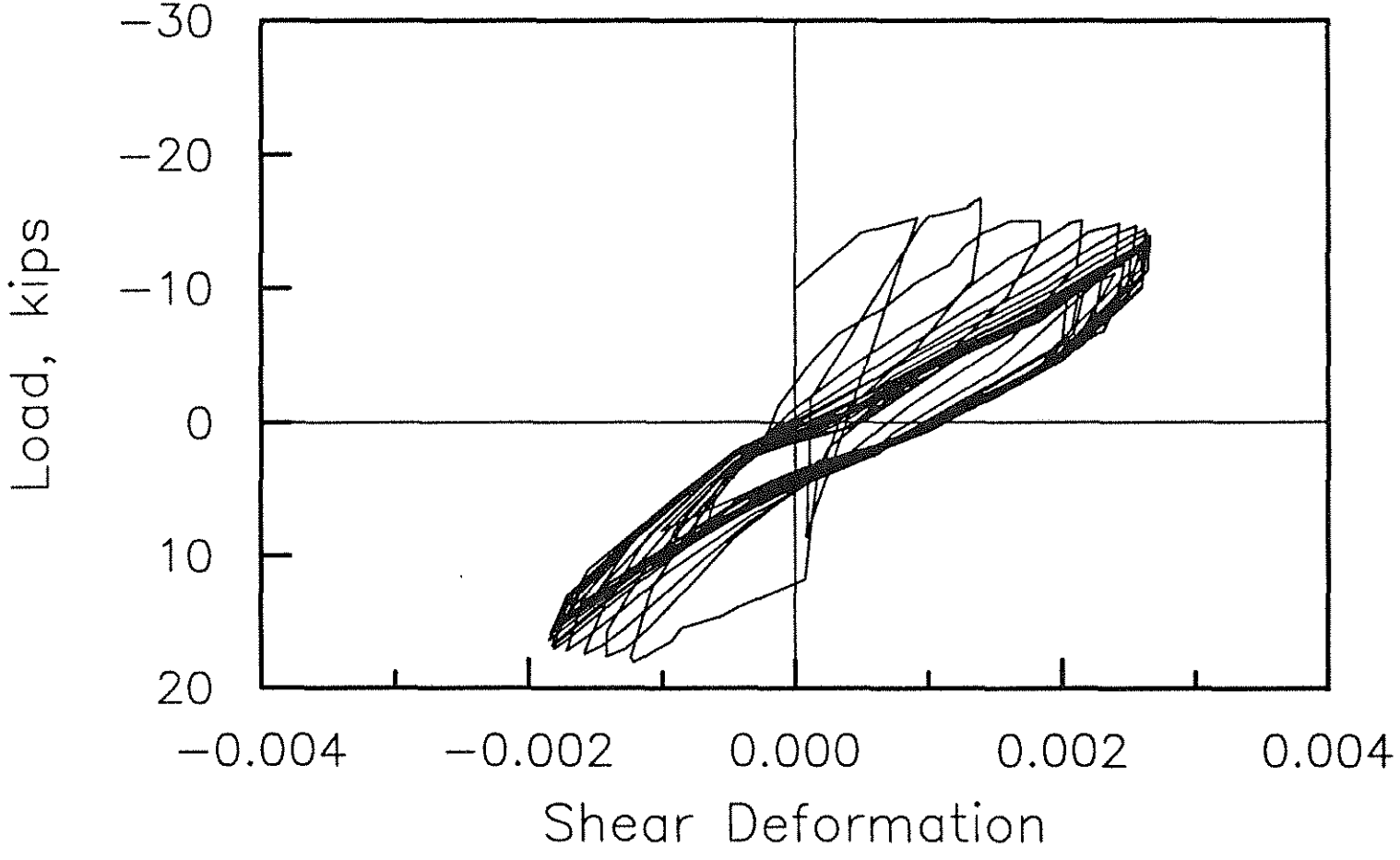

Fig. 2.13(d) Load versus Shear Deformation over the region extending 1.0d to 2.0d from the column face (LVDT #5 & #6), Beam H-4

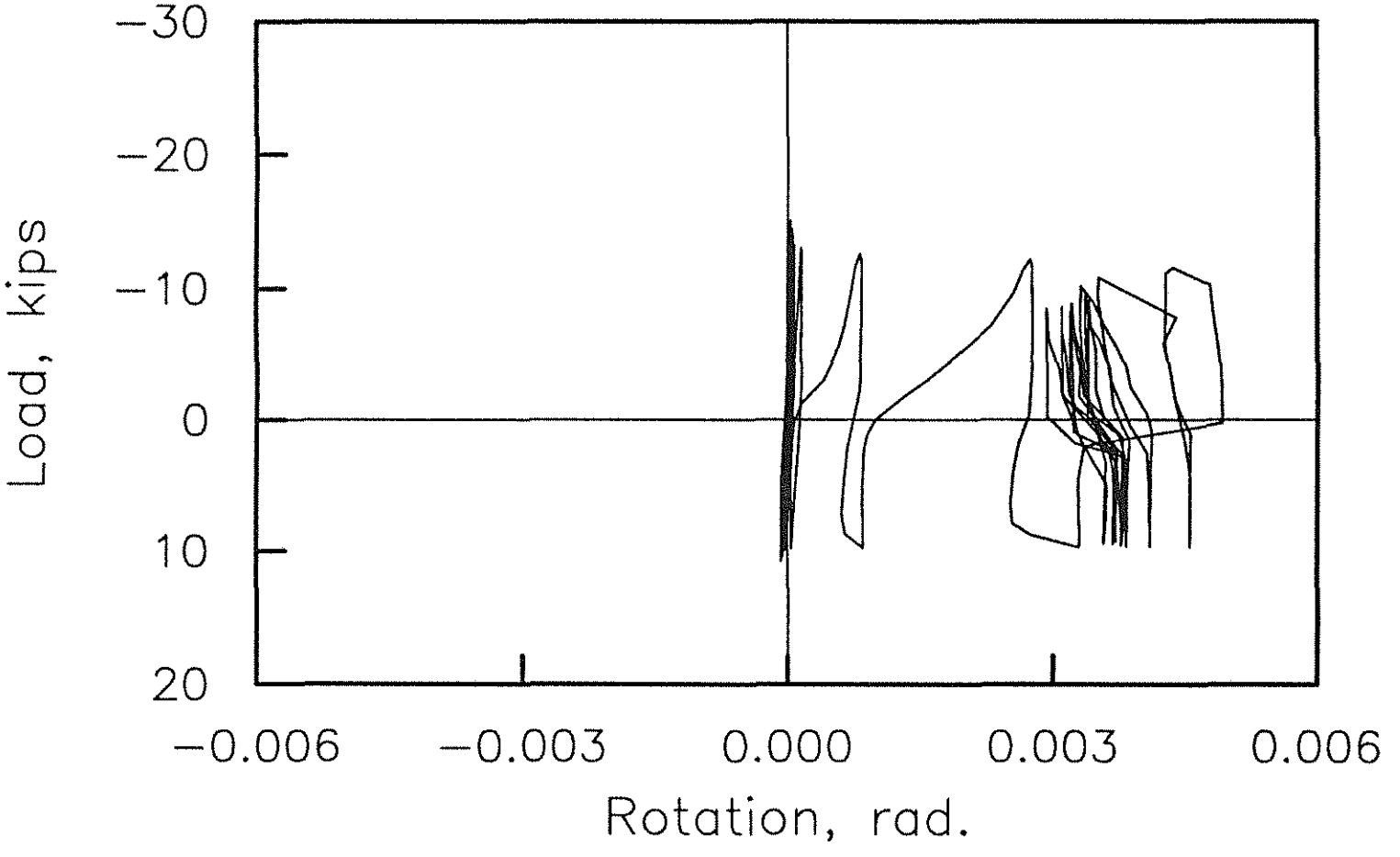

Fig. 2.14(a) Load versus Column Rotation (LVDT #9 & #10), Beam H-1

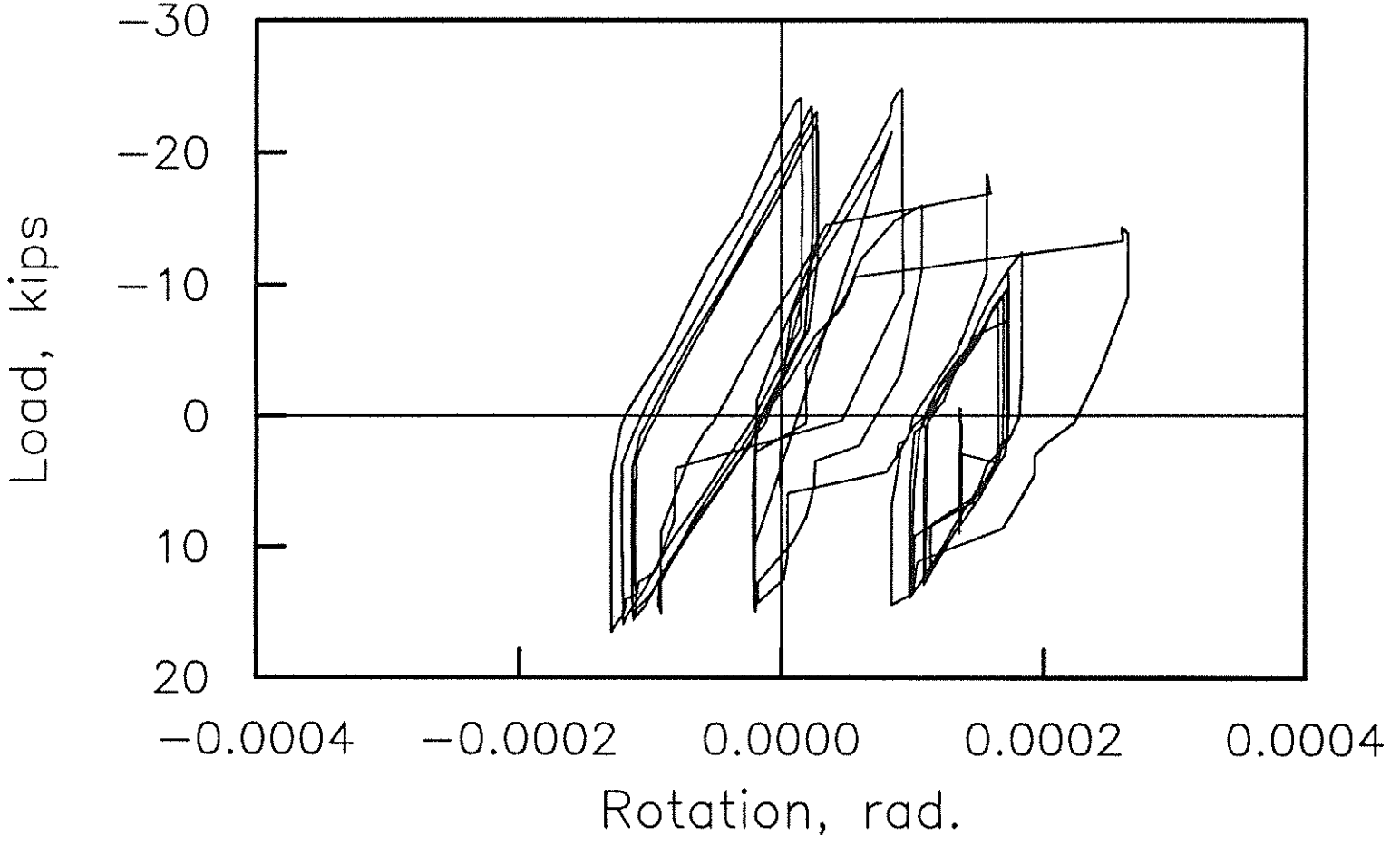

Fig. 2.14(b) Load versus Column Rotation (LVDT #9 & #10); note change of scale relative to Fig. 2.14(a), Beam H-2

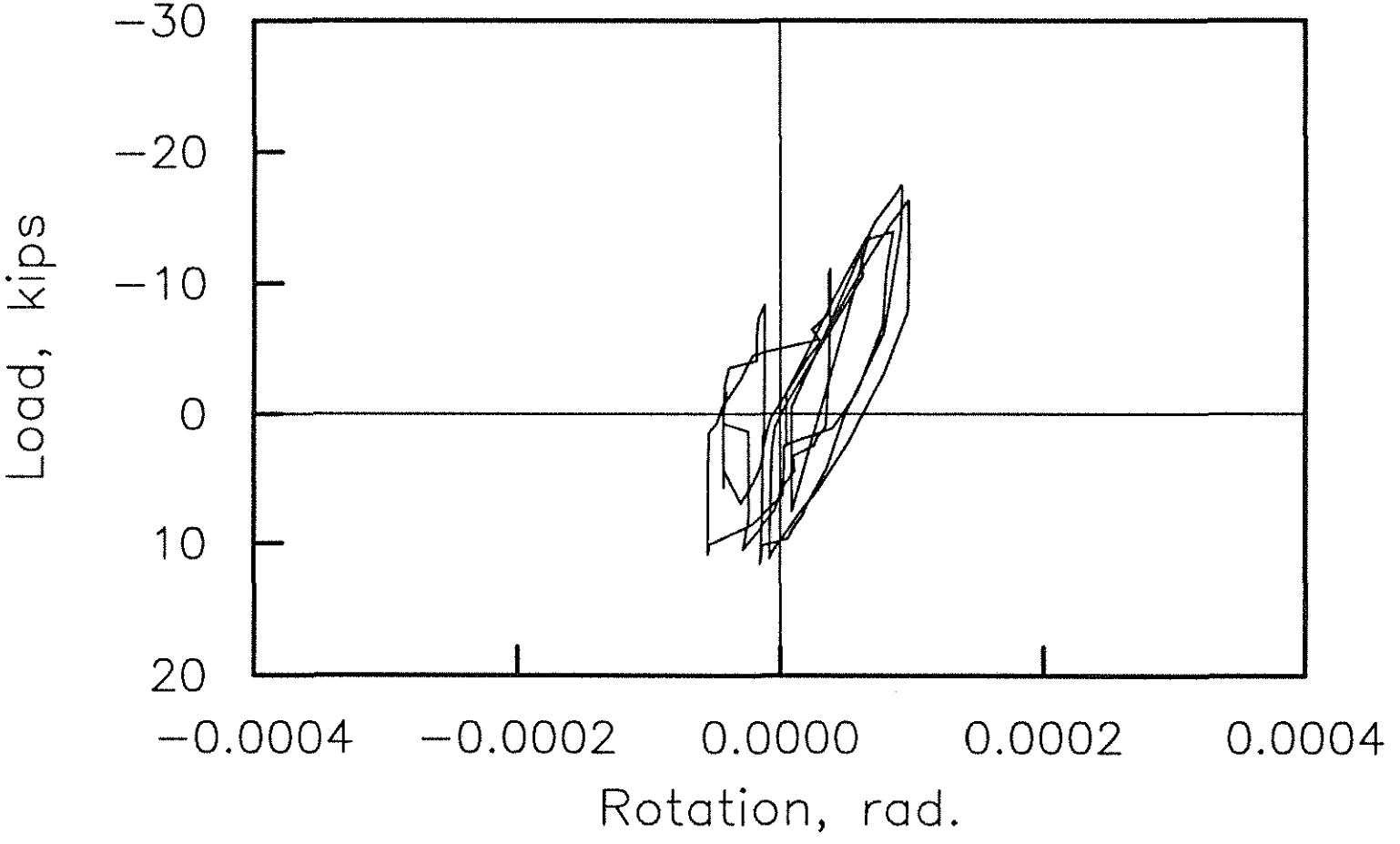

Fig. 2.14(c) Load versus Column Rotation (LVDT #9 & #10); note change of scale relative to Fig. 2.14(a), Beam H-3

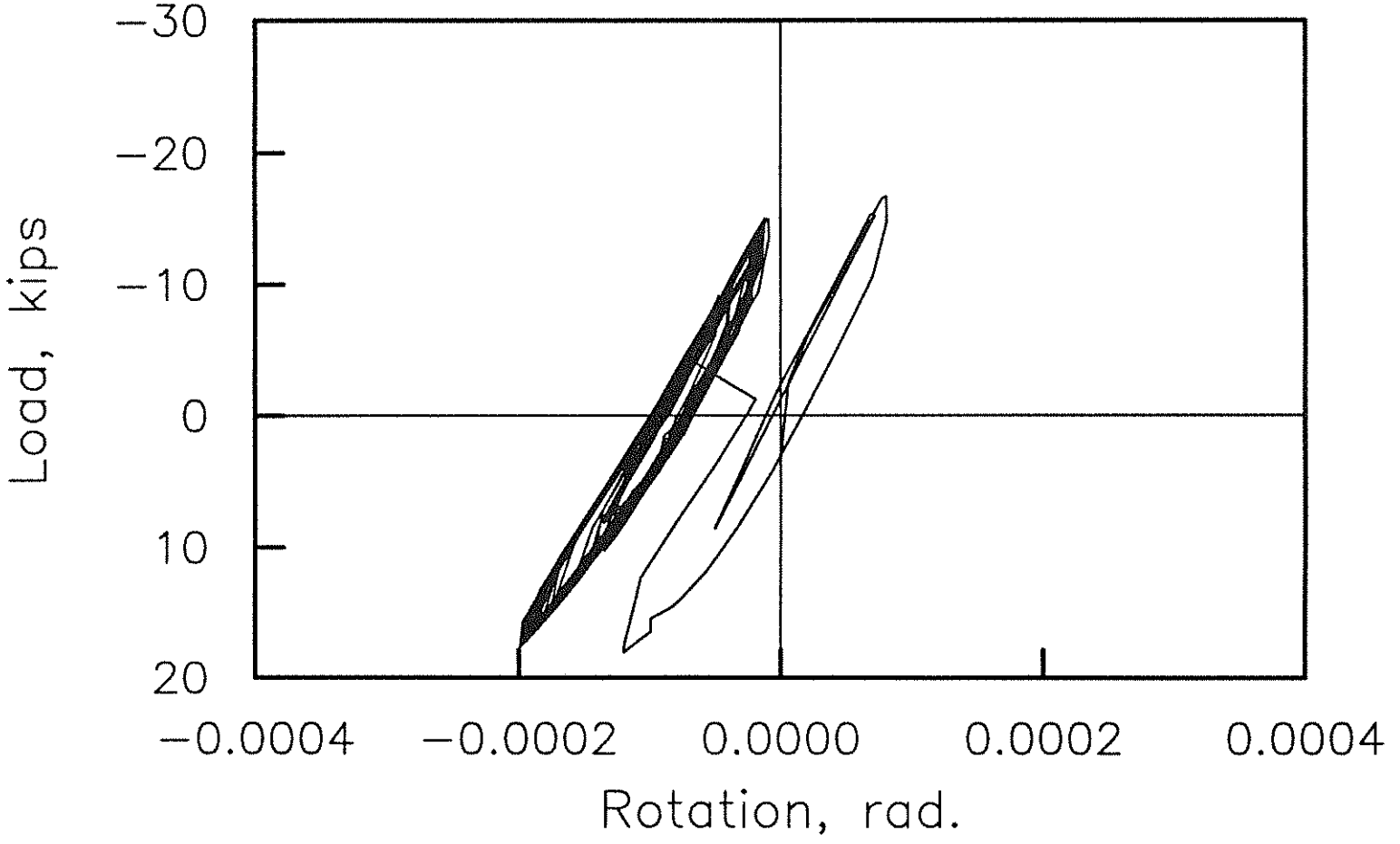

Fig. 2.14(d) Load versus Column Rotation (LVDT #9 & #10); note change of scale relative to Fig. 2.14(a), Beam H-4

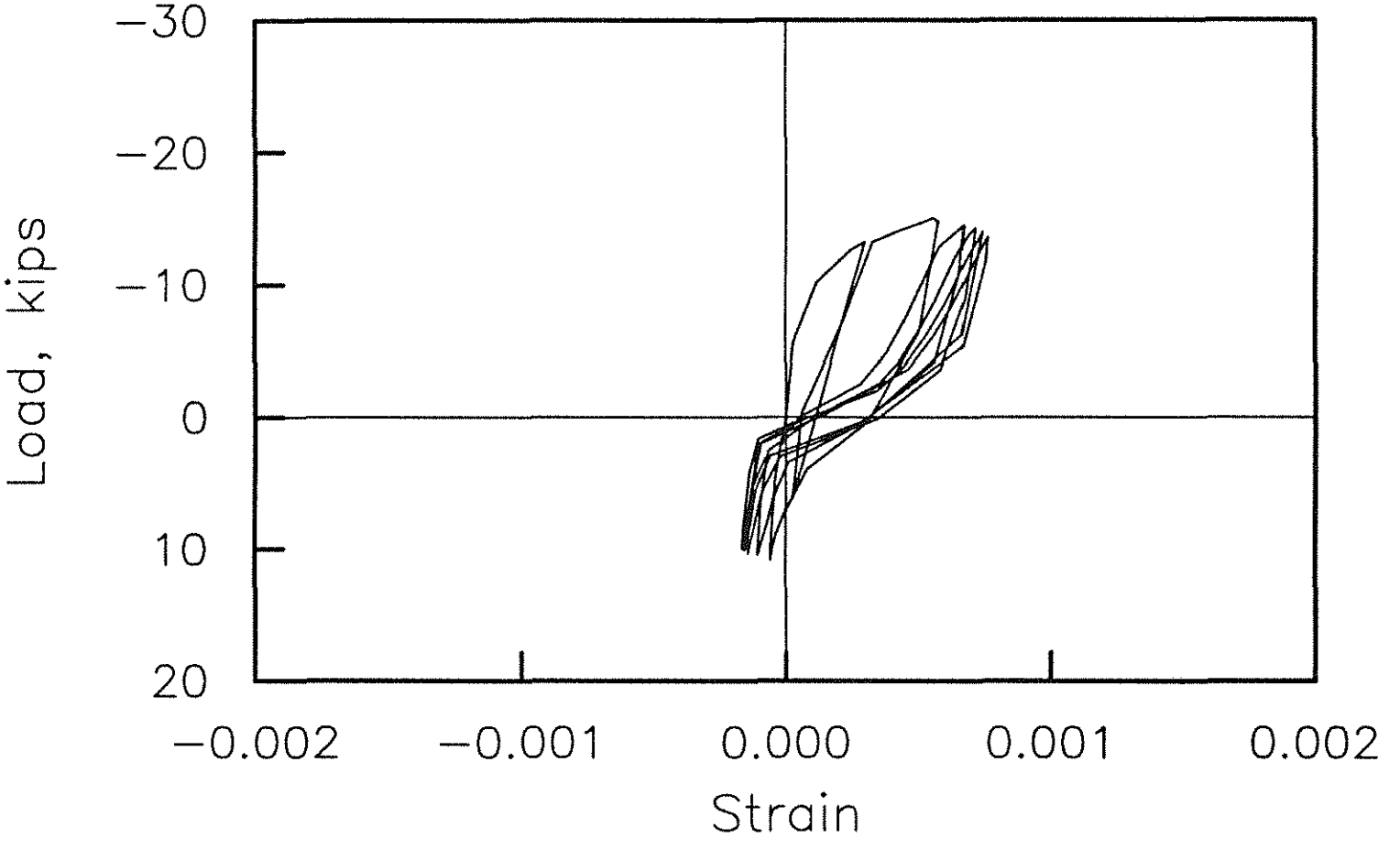

Fig. 2.15(a) Load versus Strain for the beam flexural reinforcement located within the column; first five cycles (Gage #5), Beam H-1

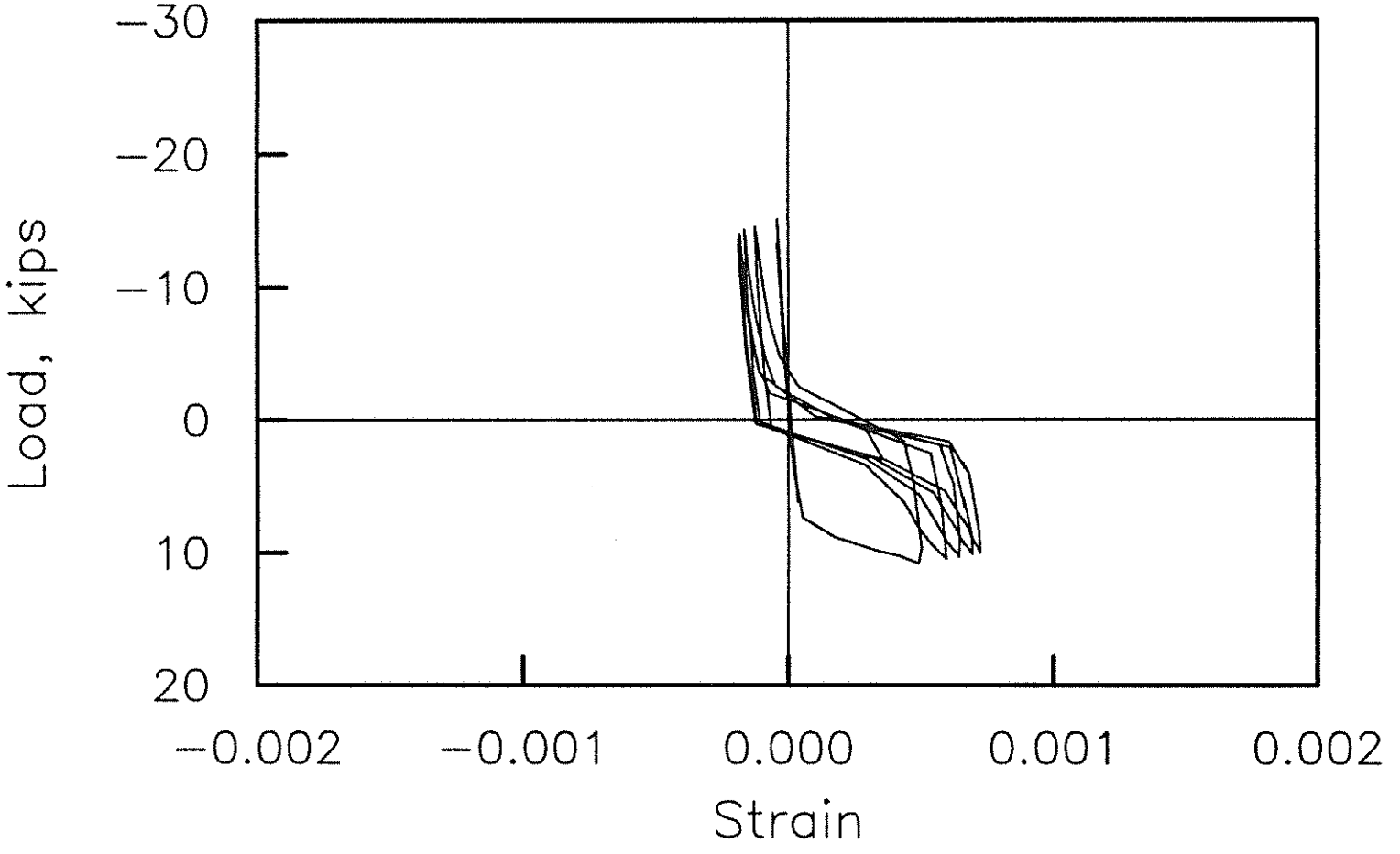

Fig. 2.15(b) Load versus Strain for the beam flexural reinforcement located within the column; first five cycles (Gage #6), Beam H-1

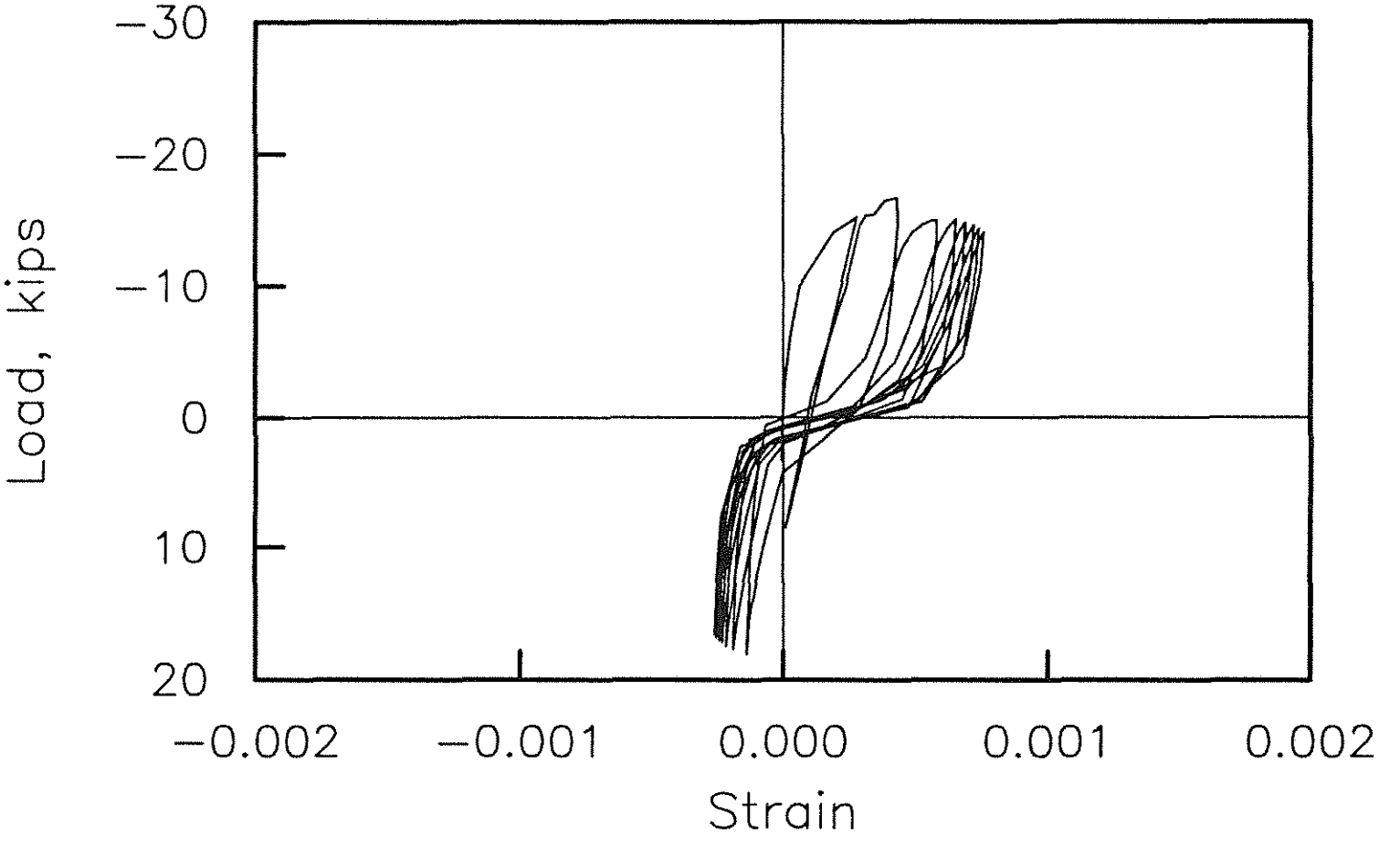

Fig. 2.16(a) Load versus Strain for the beam flexural reinforcement located within the column; first seven cycles (Gage #5), Beam H-4

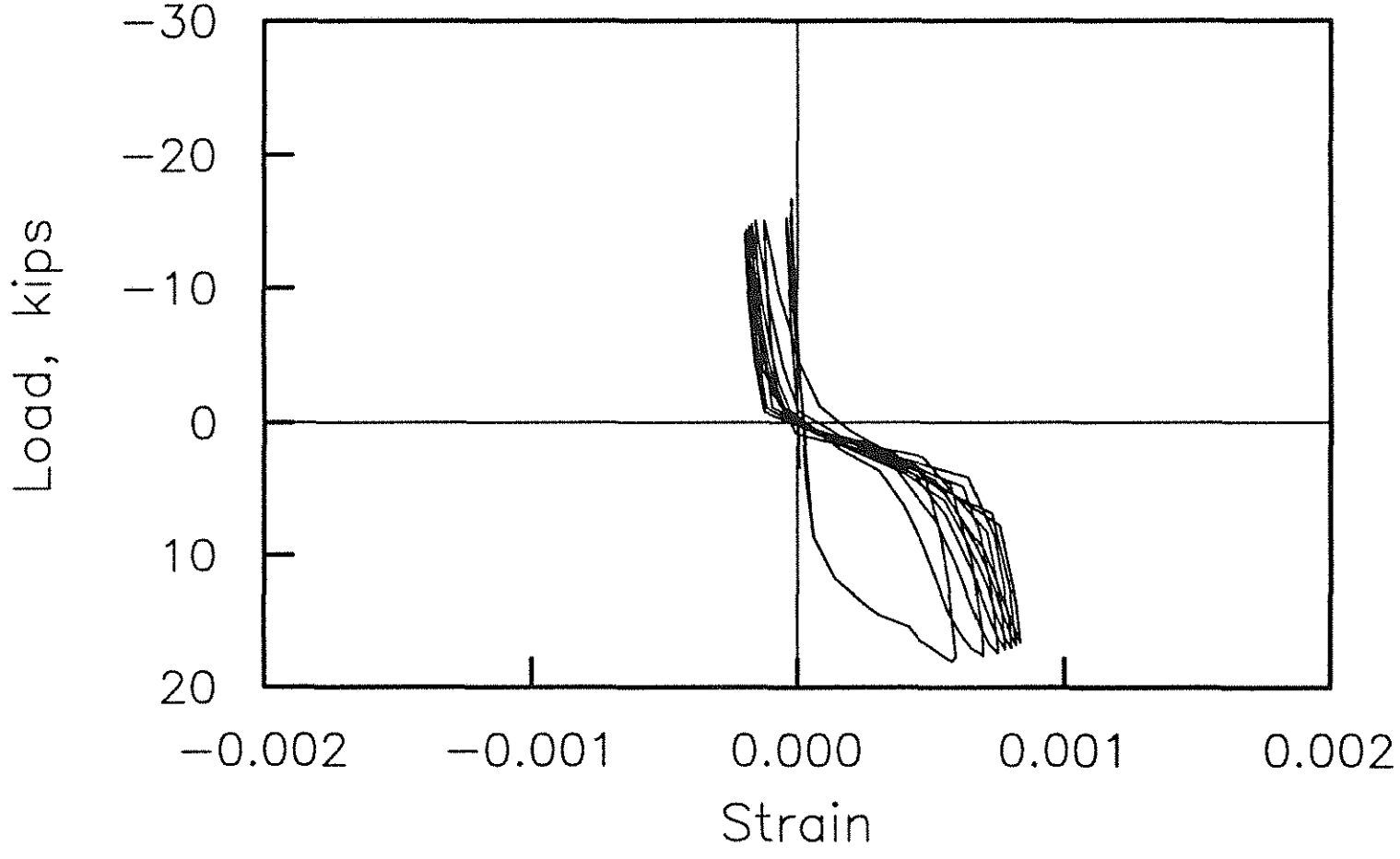

Fig. 2.16(b) Load versus Strain for the beam flexural reinforcement located within the column; first seven cycles (Gage #6), Beam H-4

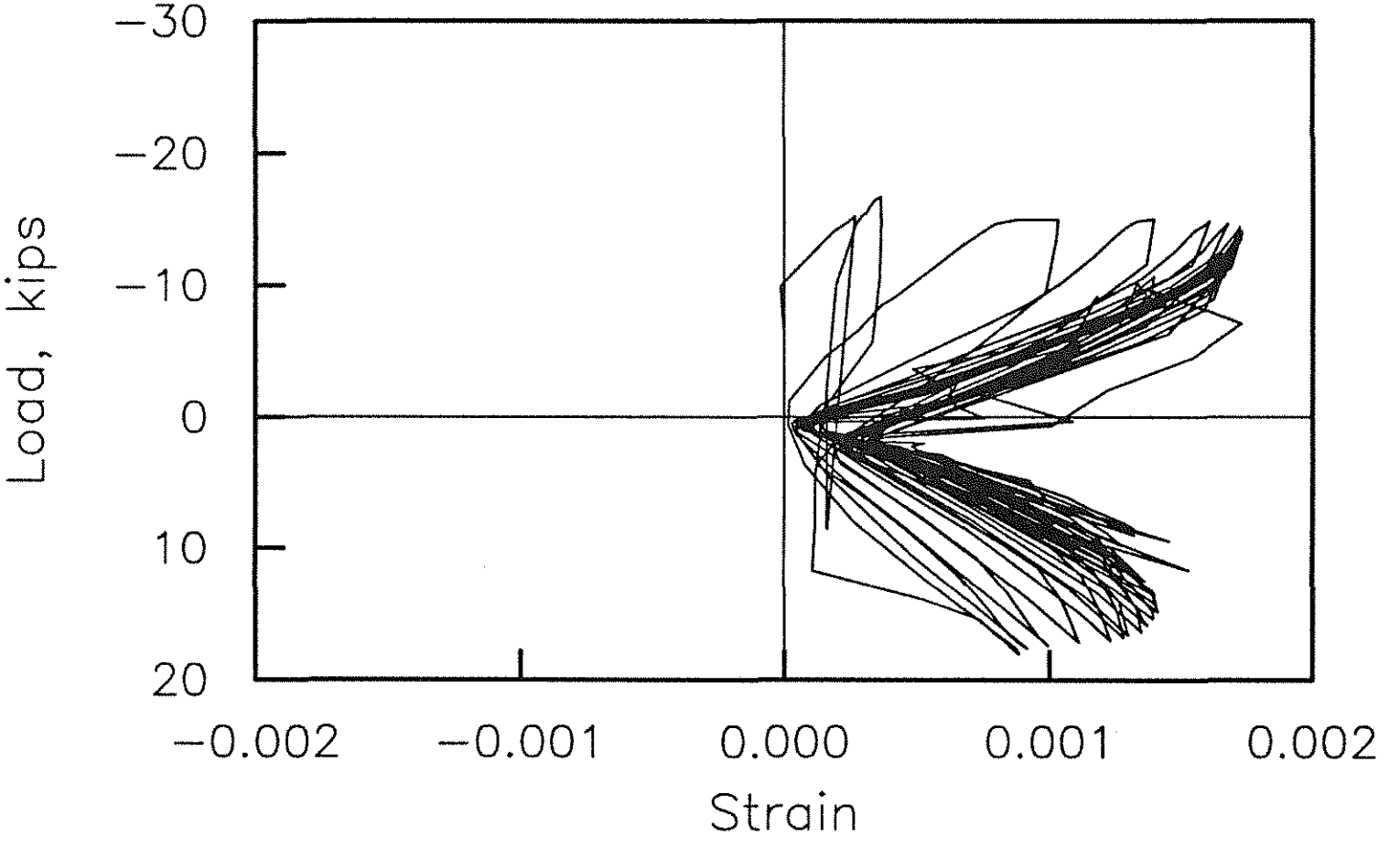

Fig. 2.17(a) Load versus Strain for the beam stirrup located d from the column face (Gage #11), Beam H-4

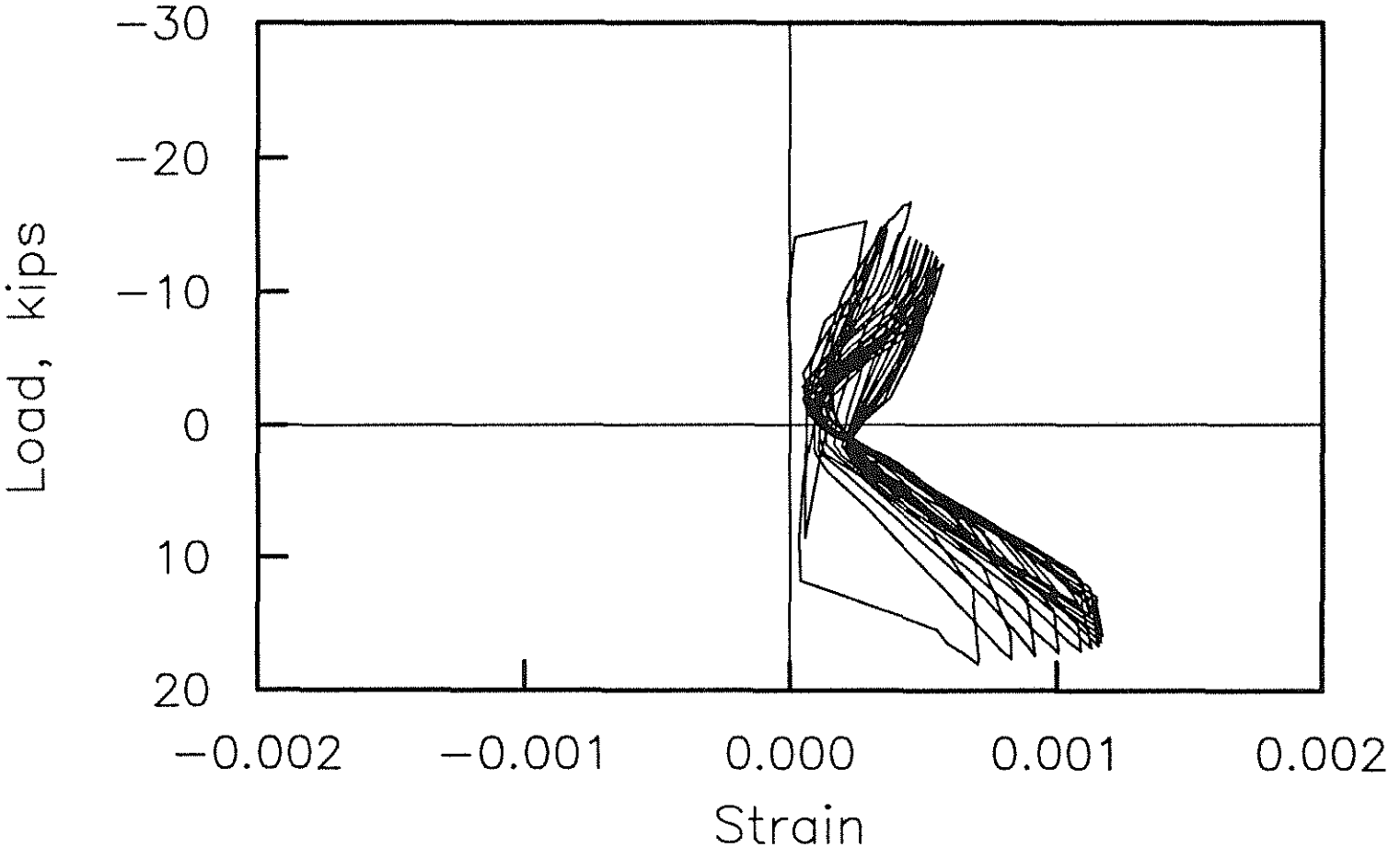

Fig. 2.17(b) Load versus Strain for the beam stirrup located d plus one stirrup from the column face (Gage #12), Beam H-4

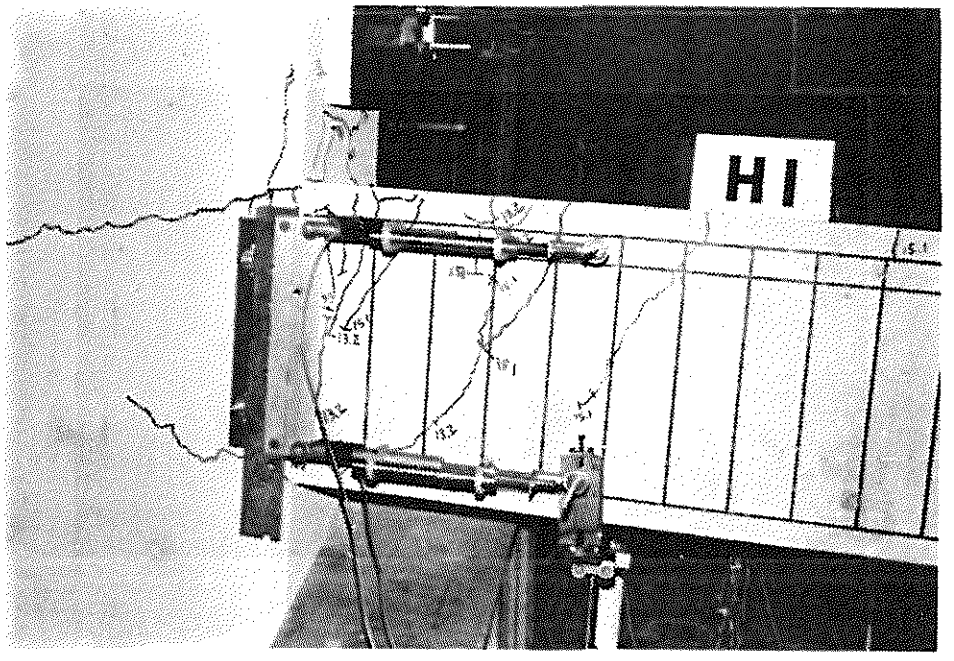

Fig. 2.18(a) Initial Crack Pattern, Beam H-1

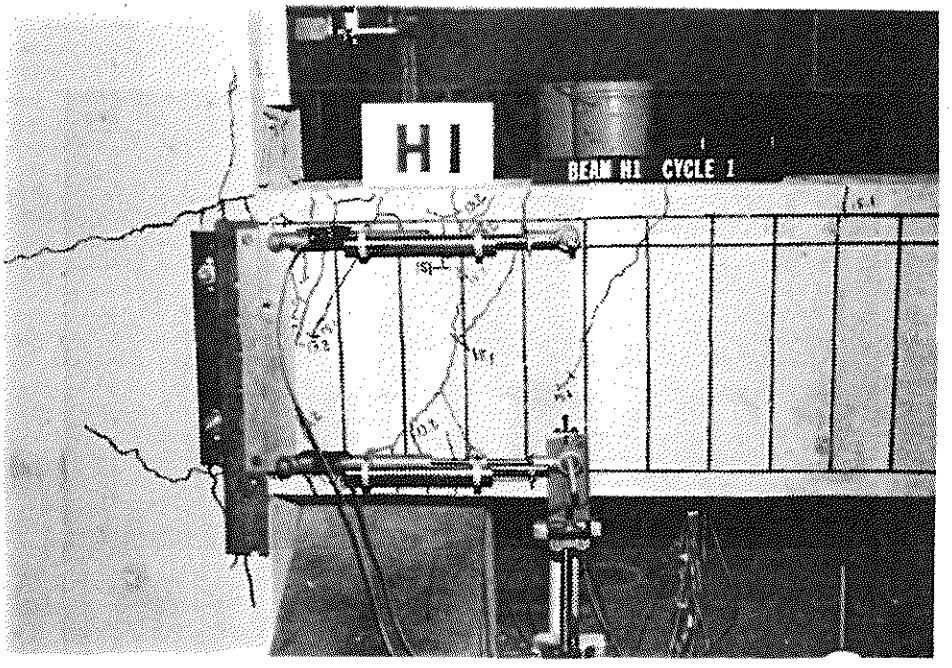

Fig. 2.18(b) Crack Pattern at the End of Cycle #1, Beam H-1

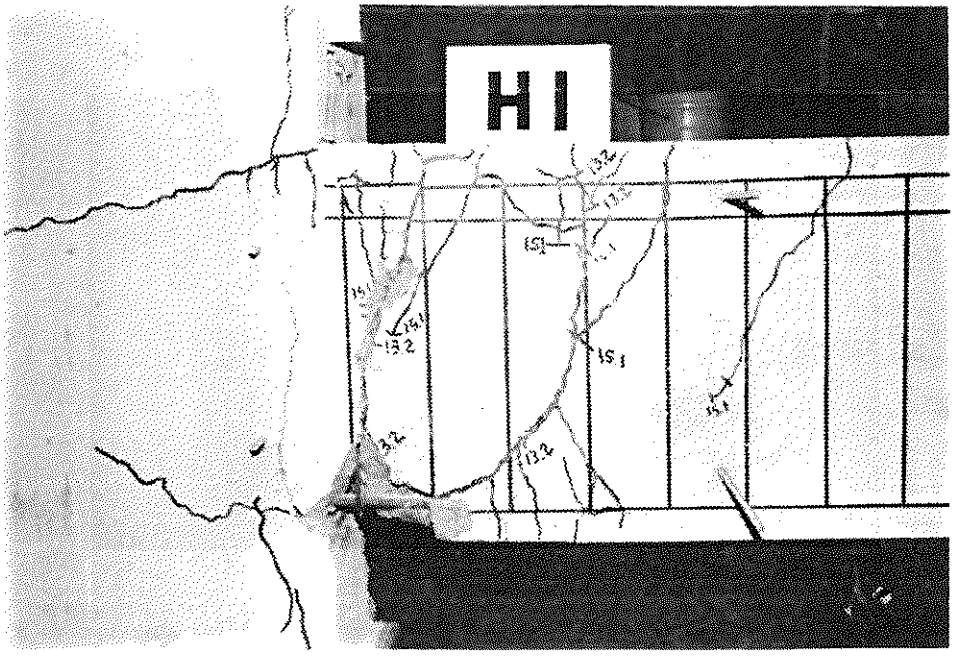

Fig. 2.18(c) Final Crack Pattern, Beam H-1

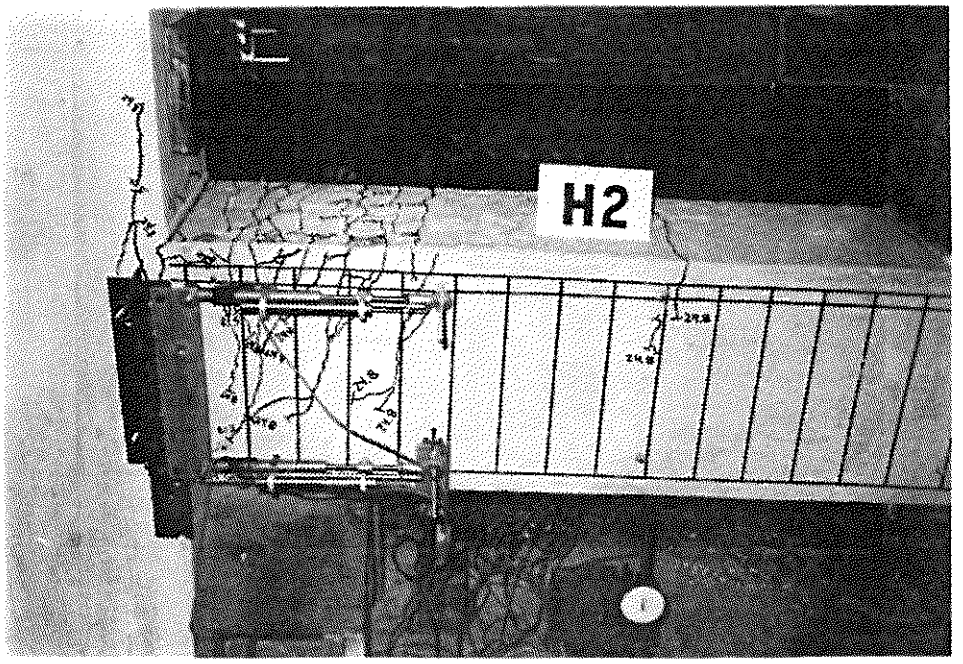

Fig. 2.19(a) Initial Crack Pattern, Beam H-2

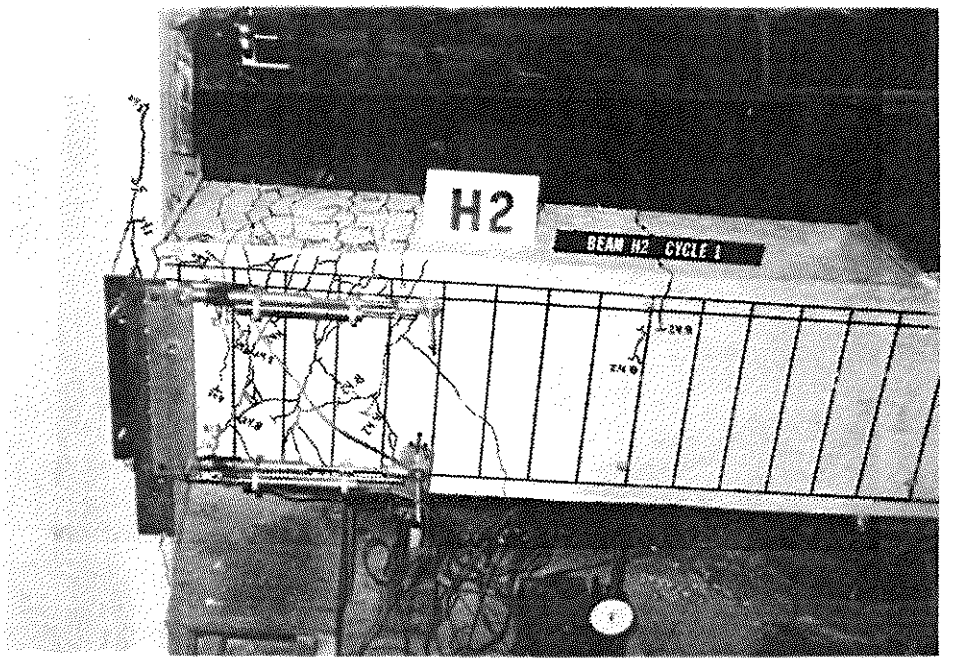

Fig. 2.19(b) Crack Pattern at the End of Cycle #1, Beam H-2

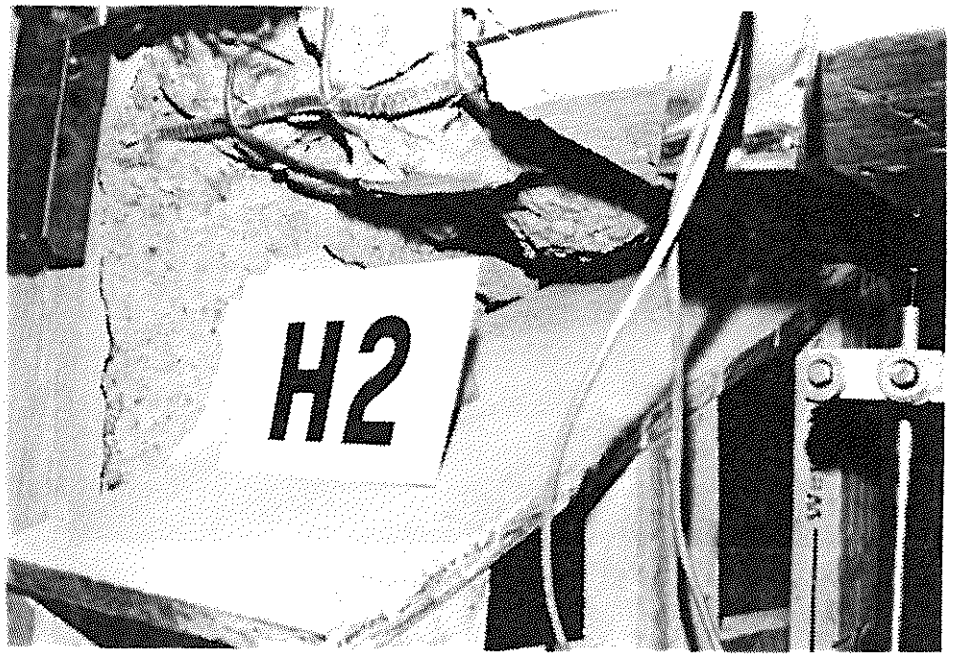

Fig. 2.19(c) Buckled Flexural Reinforcement, Beam H-2

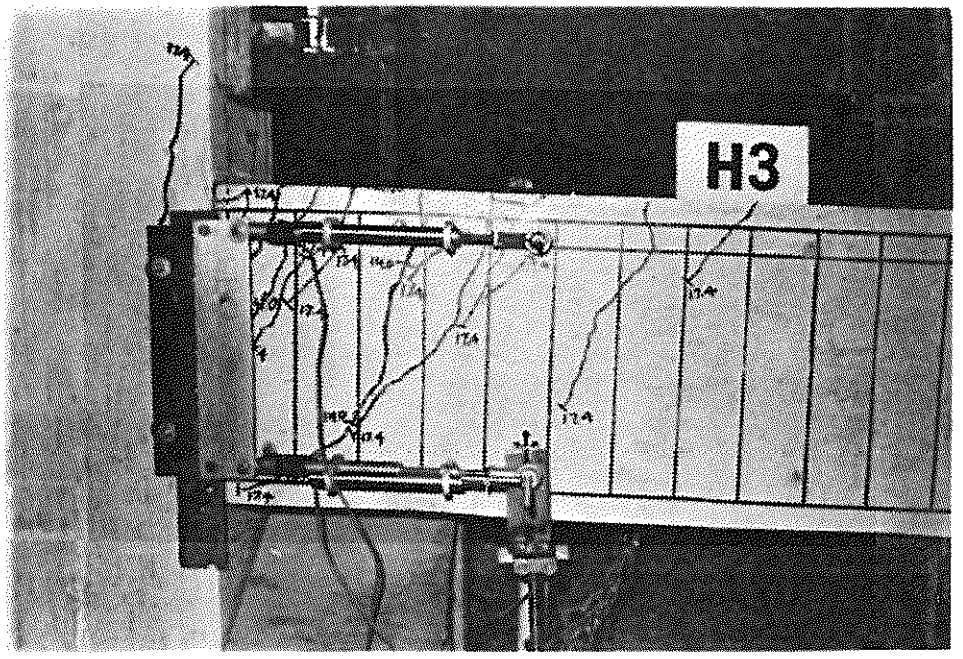

Fig. 2.20(a) Initial Crack Pattern, Beam H-3

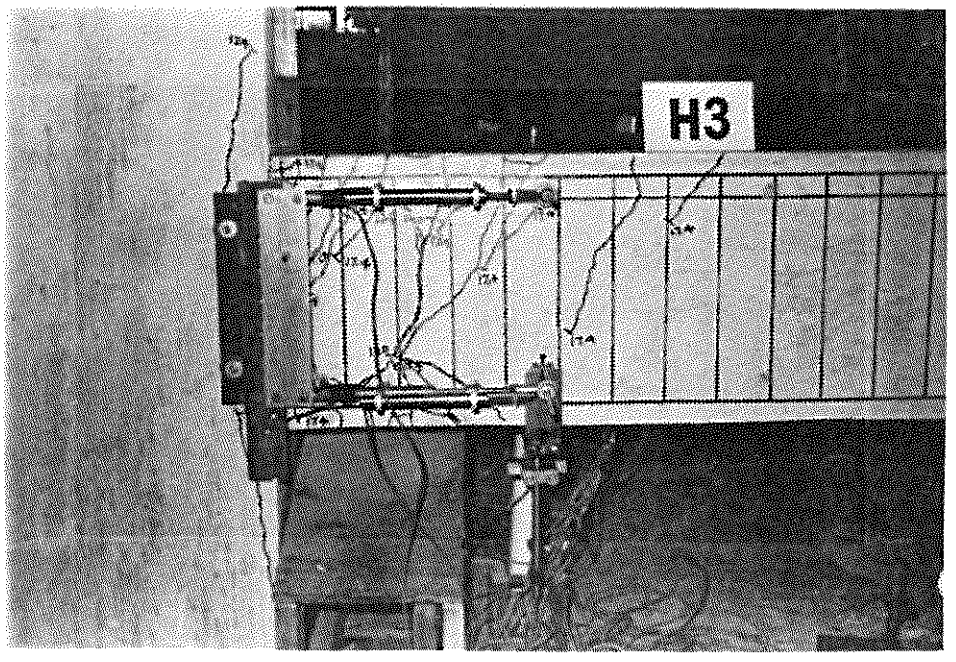

Fig. 2.20(b) Crack Pattern at the End of Cycle #1, Beam H-3 (near side)

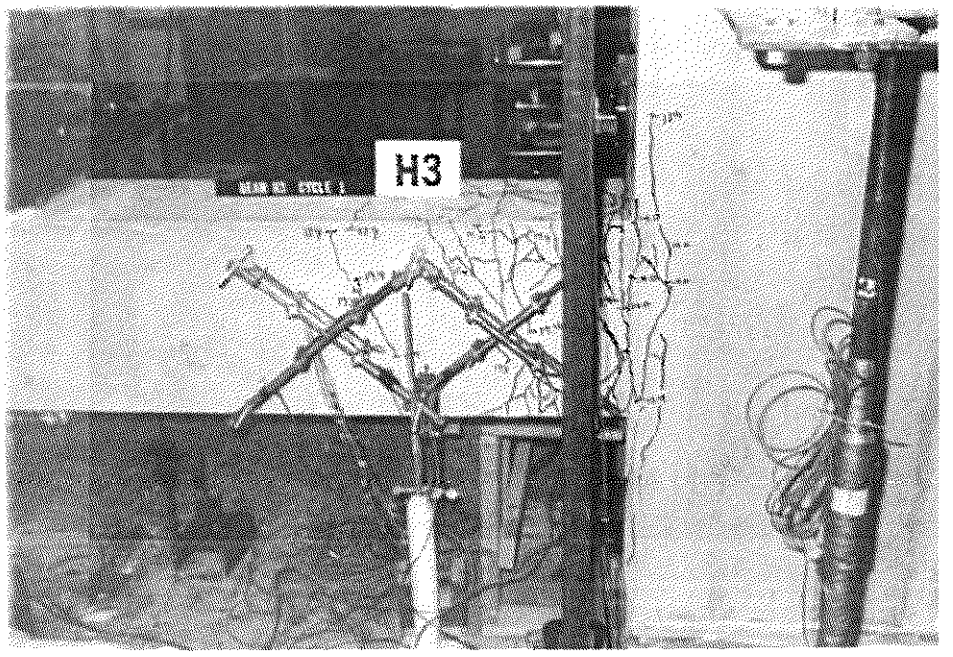

Fig. 2.20(c) Crack Pattern at the End of Cycle #1, Beam H-3 (far side)

Fig. 2.20(d) Concrete Spalling at the End of Cycle #5, Beam H-3

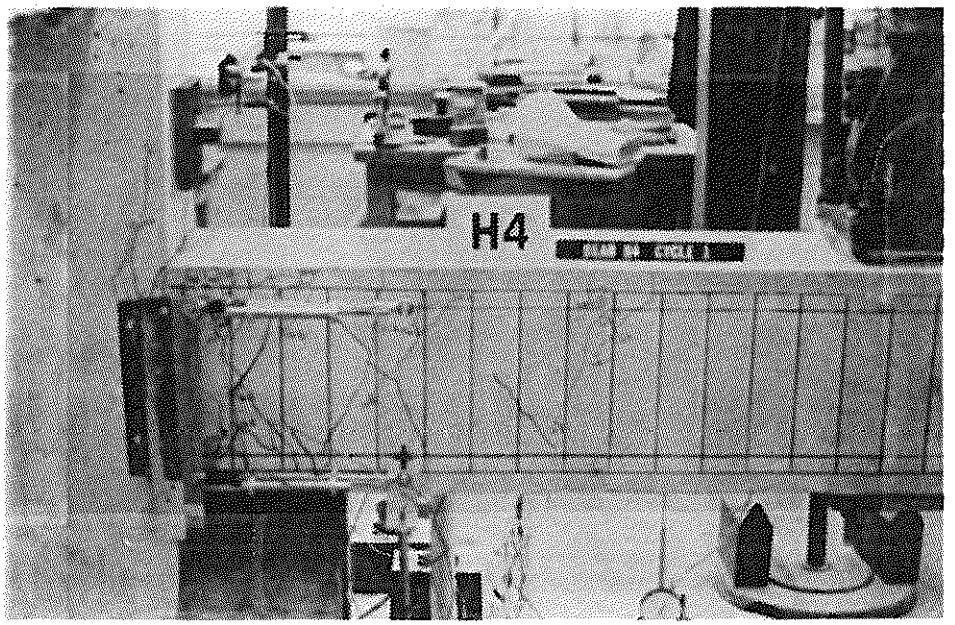

Fig. 2.21(a) Crack Pattern at the End of Cycle #1, Beam H-4

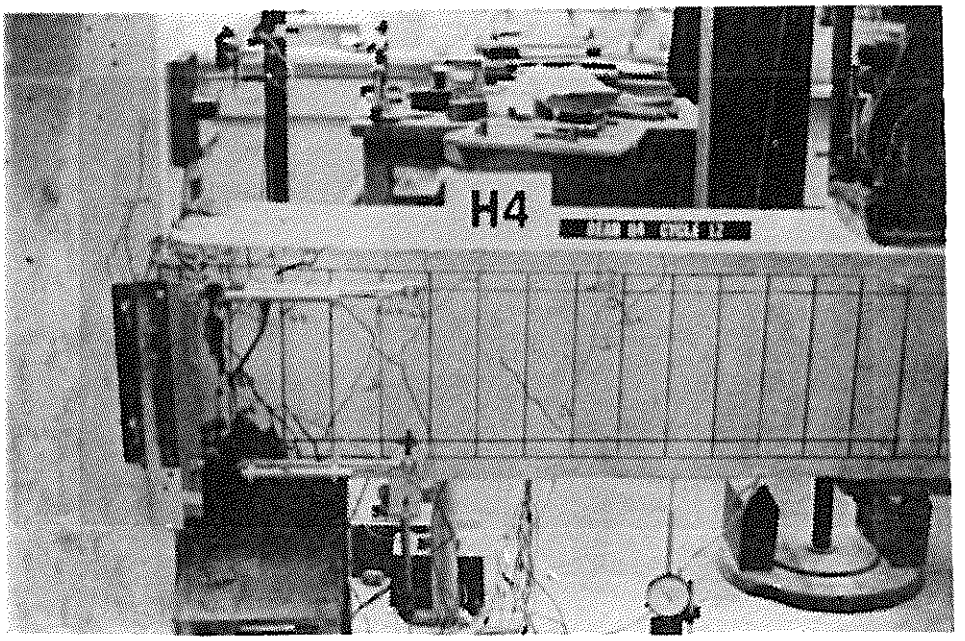

Fig. 2.21(b) Crack Pattern at the End of Cycle #12, Beam H-4

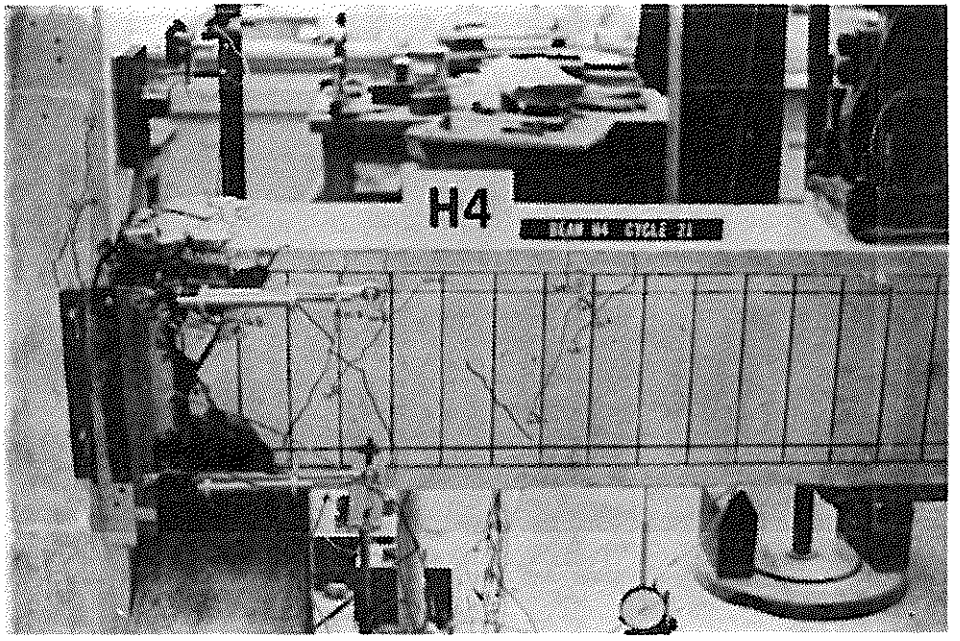

Fig. 2.21(c) Final Crack Pattern, Beam H-4 (near side)

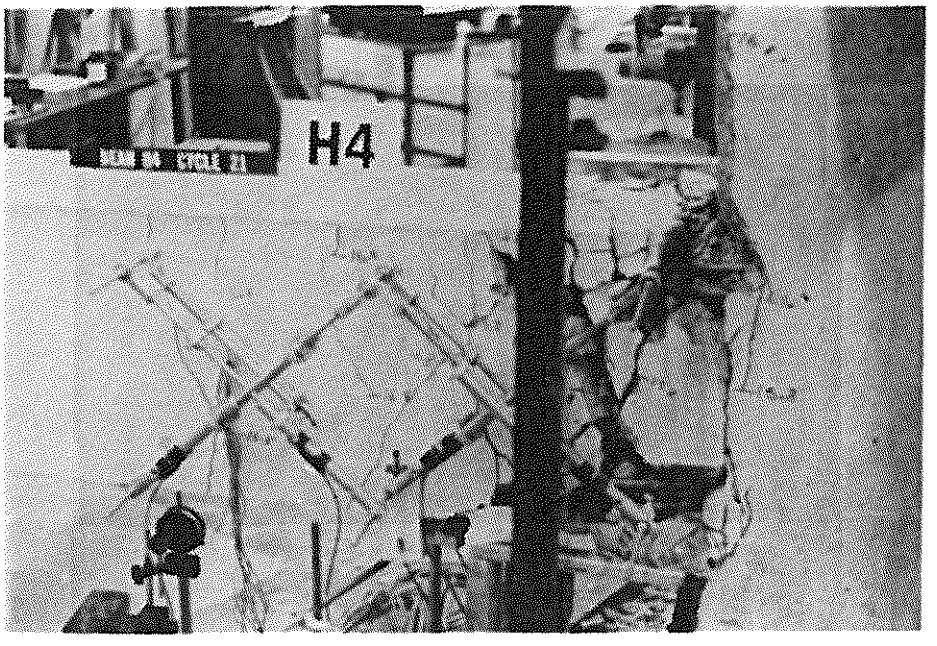

Fig. 2.21(d) Final Crack Pattern, Beam H-4 (far side)

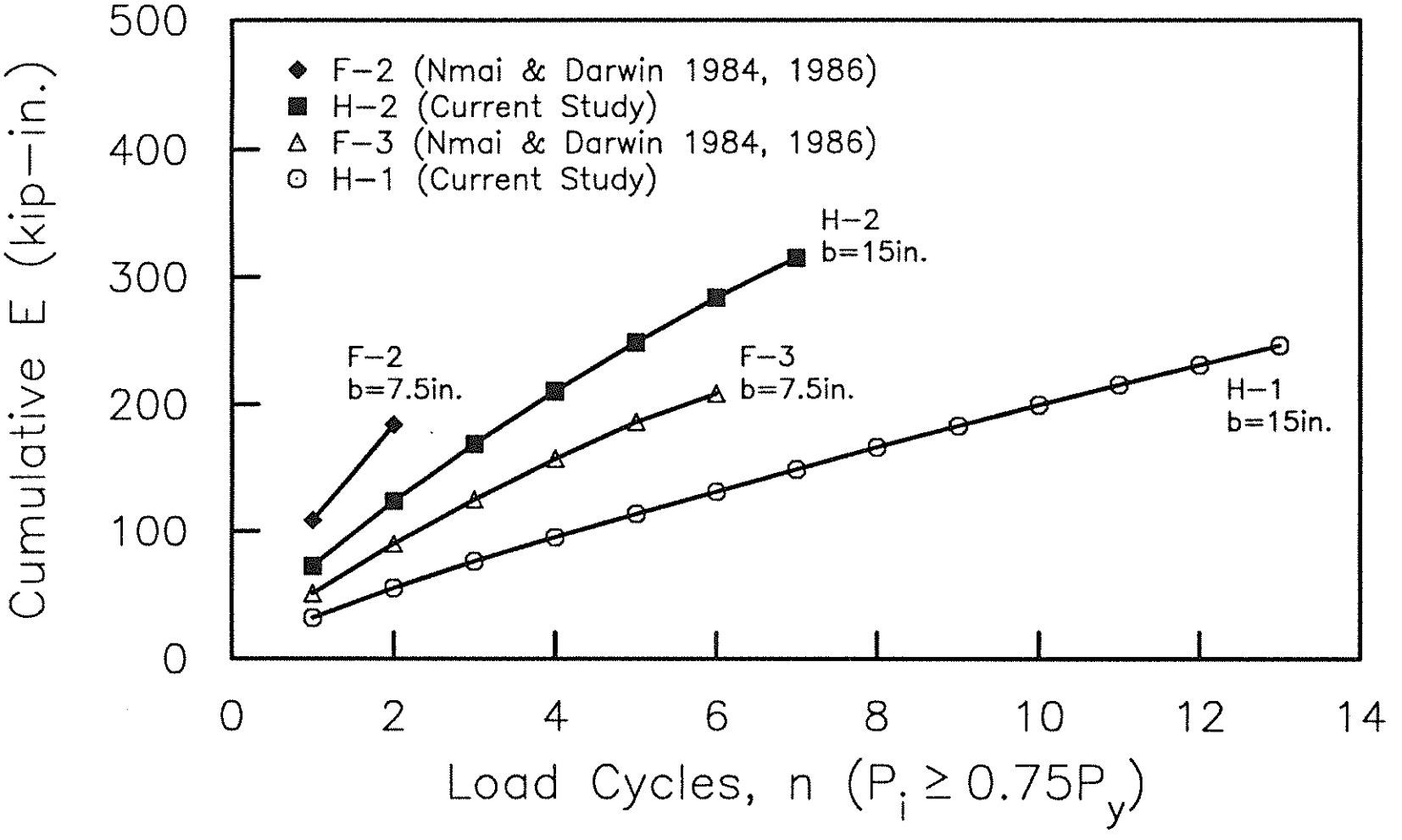

Fig. 3.1 Cumulative Energy Dissipation Capacity versus Load Cycles for specimens F-2, F-3, H-1, and H-2

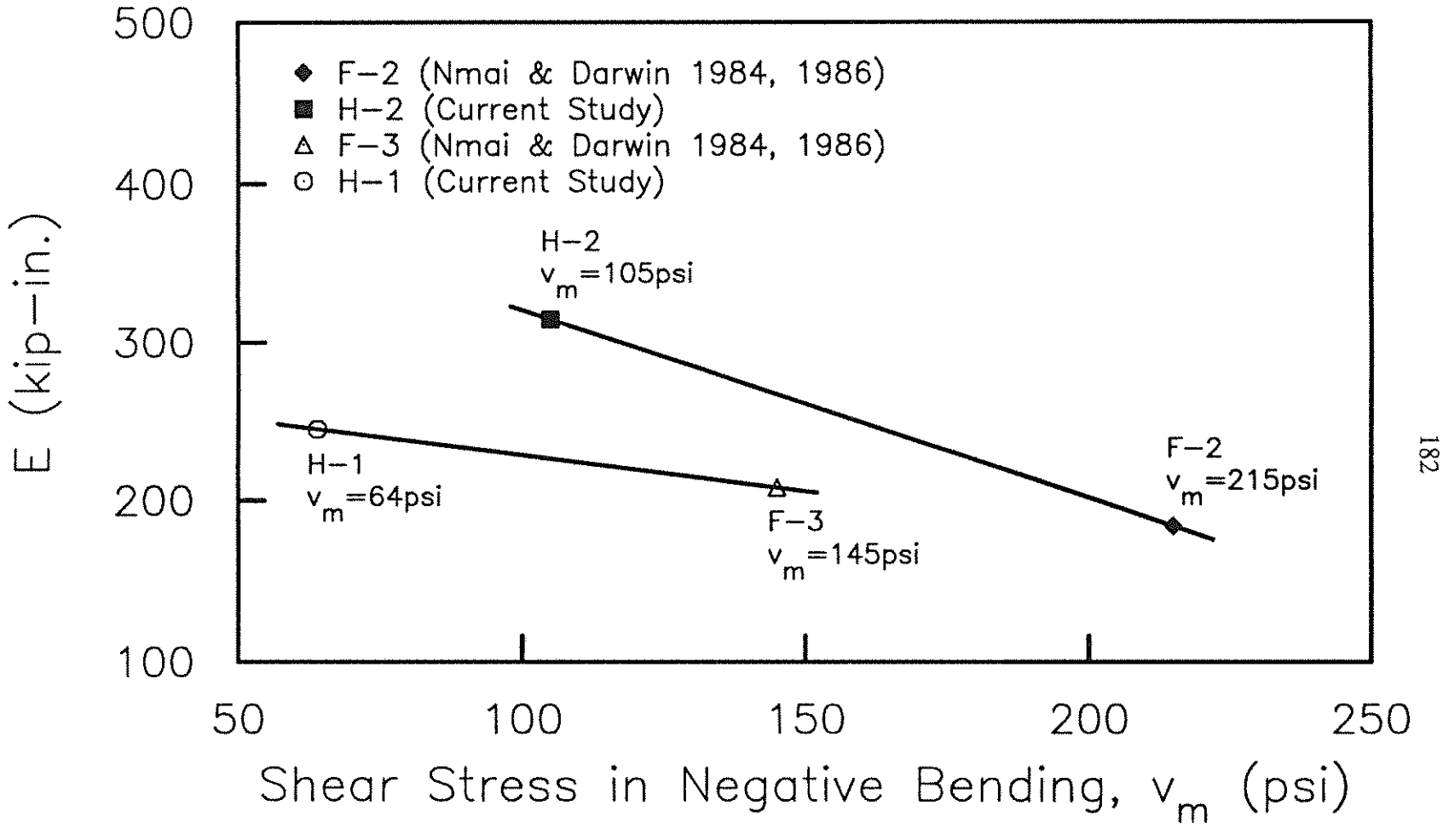

Fig. 3.2 Energy Dissipation Capacity versus Shear Stress in Negative Bending for specimens F-2, F-3, H-1, and H-2

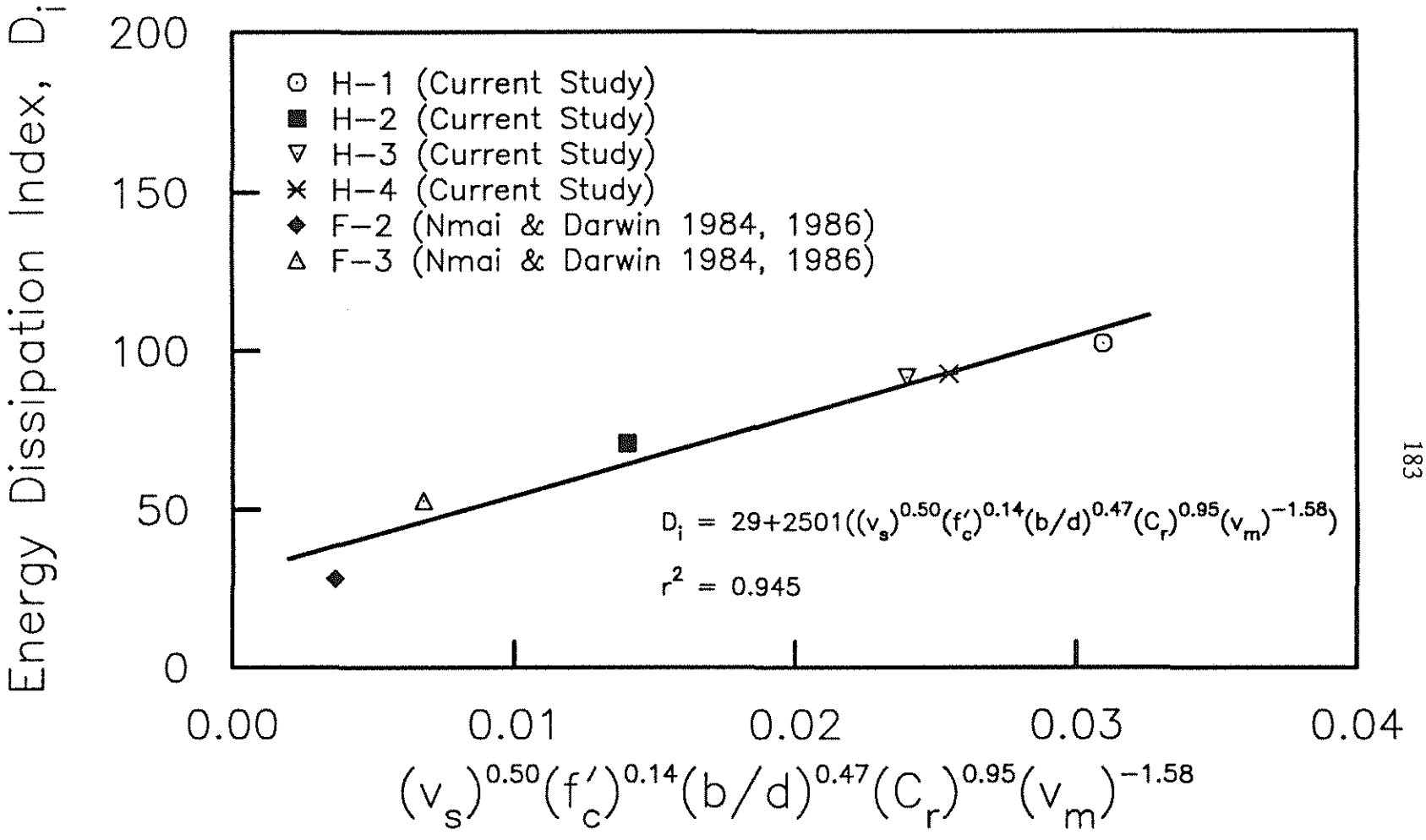

Fig. 3.3 Energy Dissipation Index versus $(v_s)^{0.50}(f'_c)^{0.14}(b/d)^{0.47}(C_r)^{0.95}(v_m)^{-1.58}$ for specimens F-2, F-3, H-1, H-2, H-3, and H-4

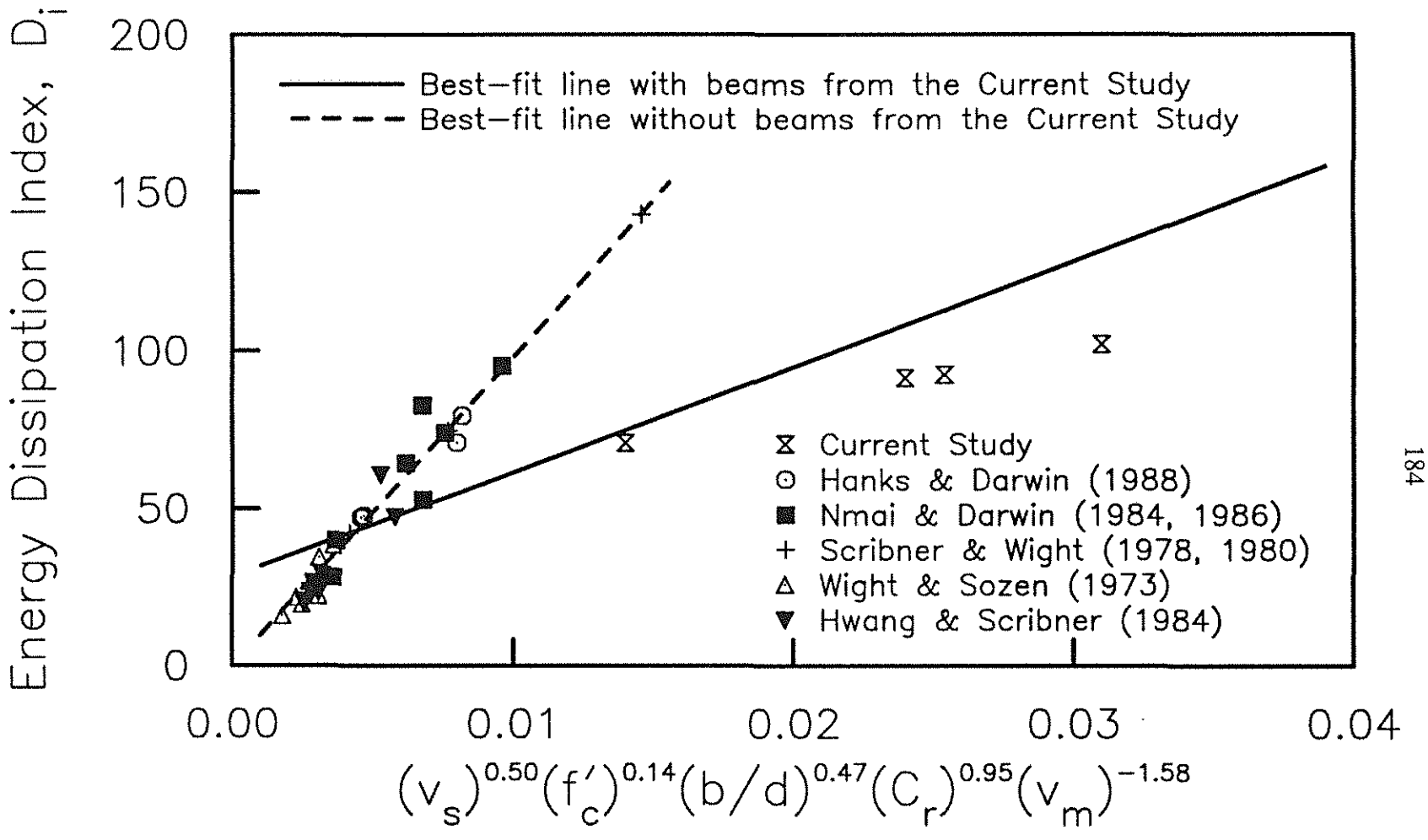

Fig. 3.4 Energy Dissipation Index versus $(v_s)^{0.50}(f'_c)^{0.14}(b/d)^{0.47}(C_r)^{0.95}(v_m)^{-1.58}$ for specimens tested in this study and those analyzed by Hanks & Darwin (1988)

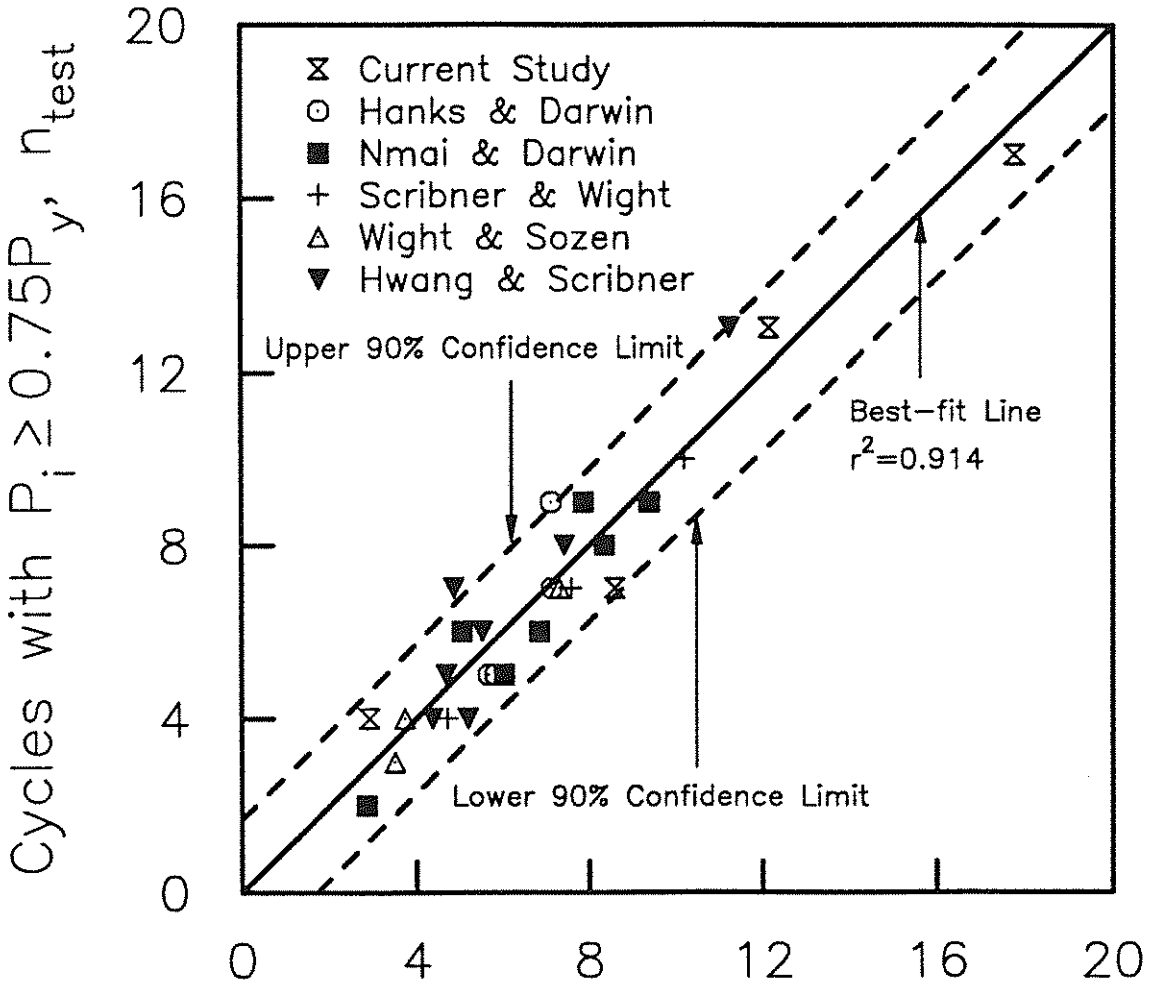

$$n_{pre} = 8.17 - 1.89\frac{v_m}{\sqrt{f'_c}}\left[1 + \left(\frac{A'_s}{A_s}\right)^2\right] + 0.80\frac{v_s}{\sqrt{f'_c}} + 16.74\left(\frac{A'_s}{A_s}\right) + 1.43\left(\frac{b}{s}\right) - 2.10(\mu_{rms})$$

Fig. 4.1 Test versus predicted cycles with $P_i \geq 0.75P_y$ for the specimens in Table 4.1 (Eq. 4.6)

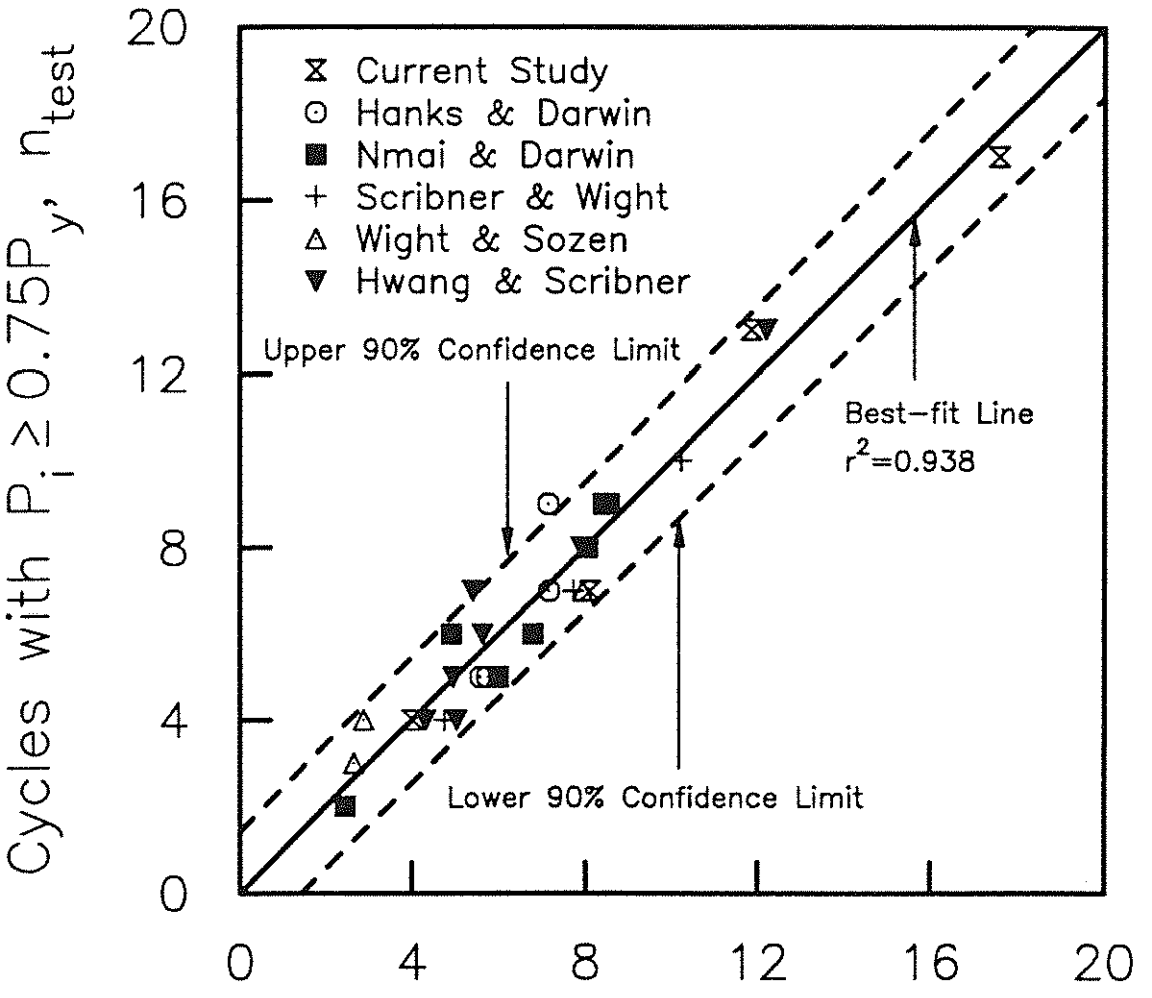

$$n_{pre} = 3.75 - 2.06\frac{v_m}{\sqrt{f'_c}}\left[1 + \left(\frac{A'_s}{A_s}\right)^2\right] + 0.85\frac{v_s}{\sqrt{f'_c}} + 67.55\left(\frac{A'_s}{A_s}\right)^{0.20} + 14.53\left(\frac{b}{s}\right)^{0.20} - 55.07(\mu_{rms})^{0.15}$$

Fig. 4.2 Test versus predicted cycles with $P_i \geq 0.75P_y$ for the specimens in Table 4.1 (Eq. 4.7)

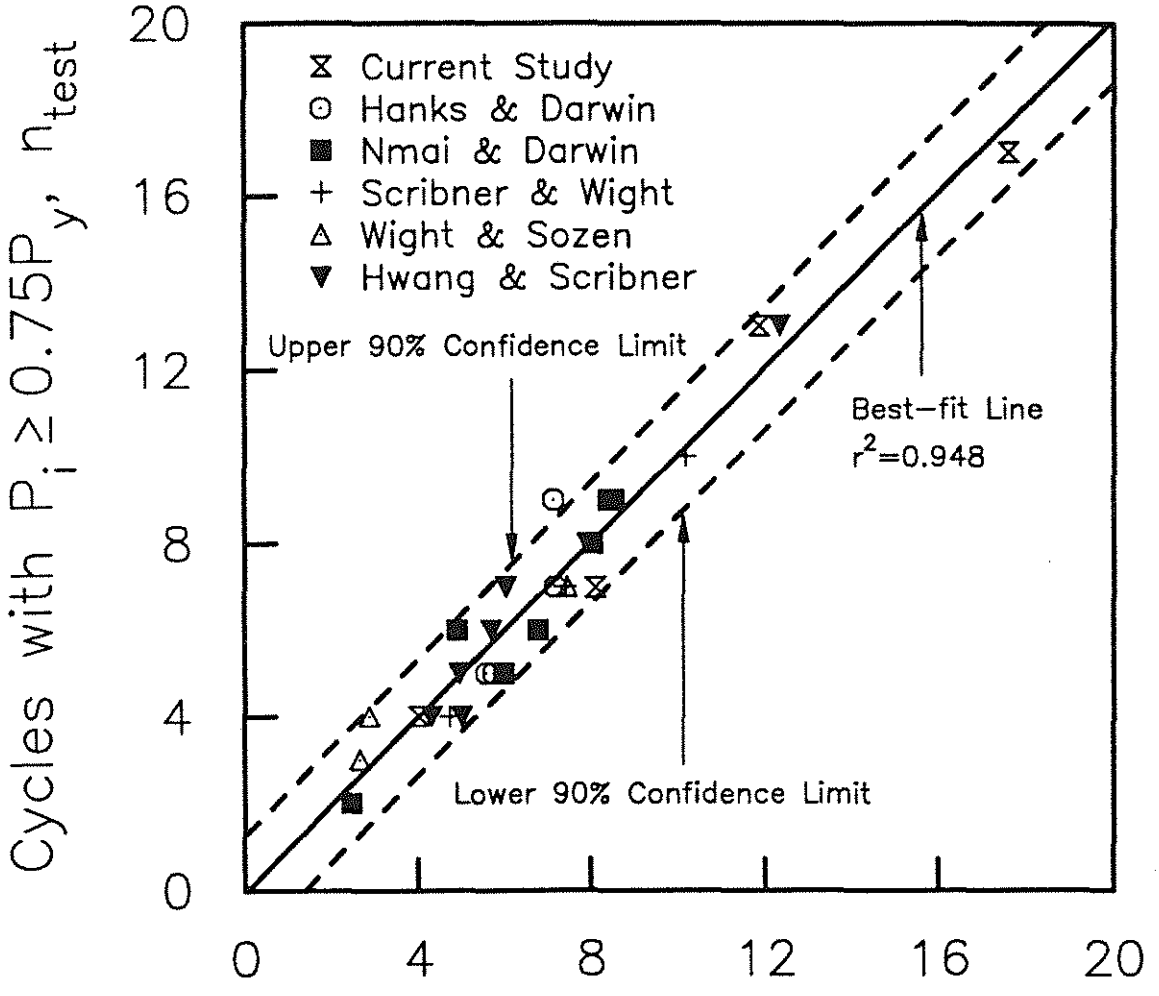

$$n_{pre} = 3.75 - 2.06\frac{v_m}{\sqrt{f'_c}}\left[1 + \left(\frac{A'_s}{A_s}\right)^2\right] + 0.85\frac{v_s}{\sqrt{f'_c}} + 67.55\left(\frac{A'_s}{A_s}\right)^{0.20} + 14.53\left(\frac{b}{s}\right)^{0.20} - 55.07\left(\mu'_{rms}\right)^{0.15}$$

Fig. 4.3 Test versus predicted cycles with $P_i \geq 0.75P_y$ for the specimens in Table 4.1 (Eq. 4.9)

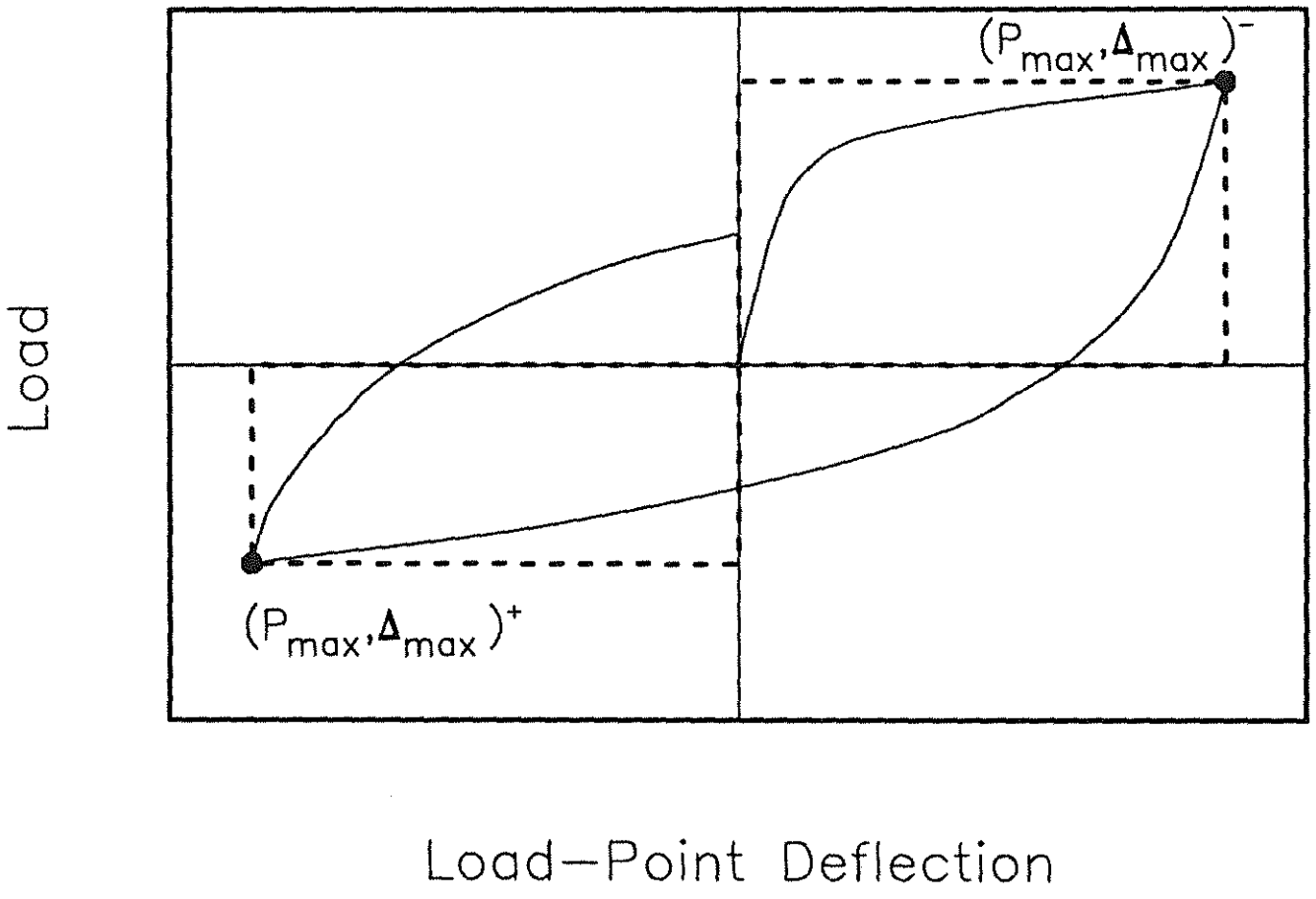

Fig. 4.4 Load versus Load-Point Deflection for specimens with different amounts of positive and negative moment reinforcement

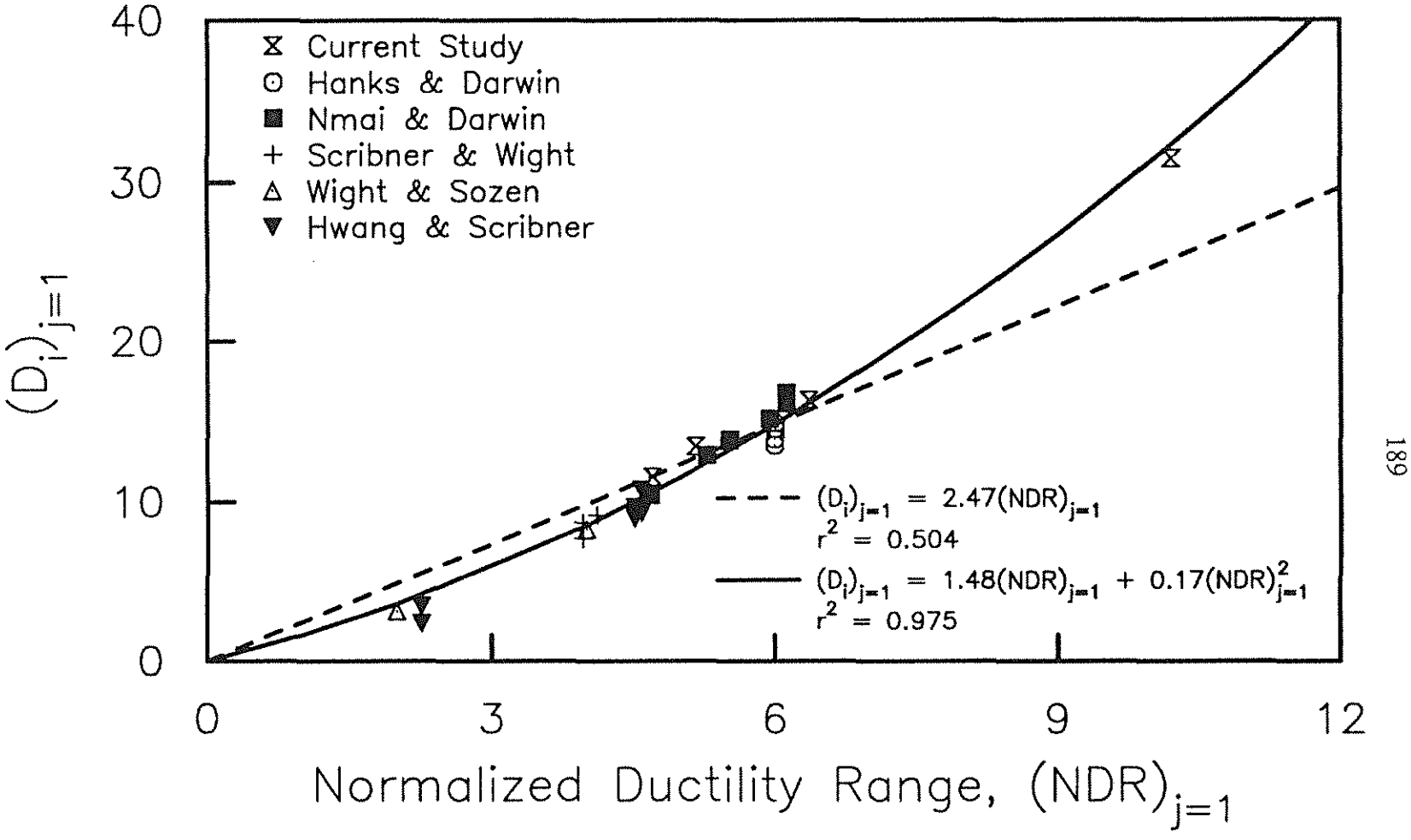

Fig. 4.5(a) $(D_i)_j$ versus $(NDR)_j$ for the specimens in Table 4.3 surviving one cycle with $P_i \geq 0.75P_y$

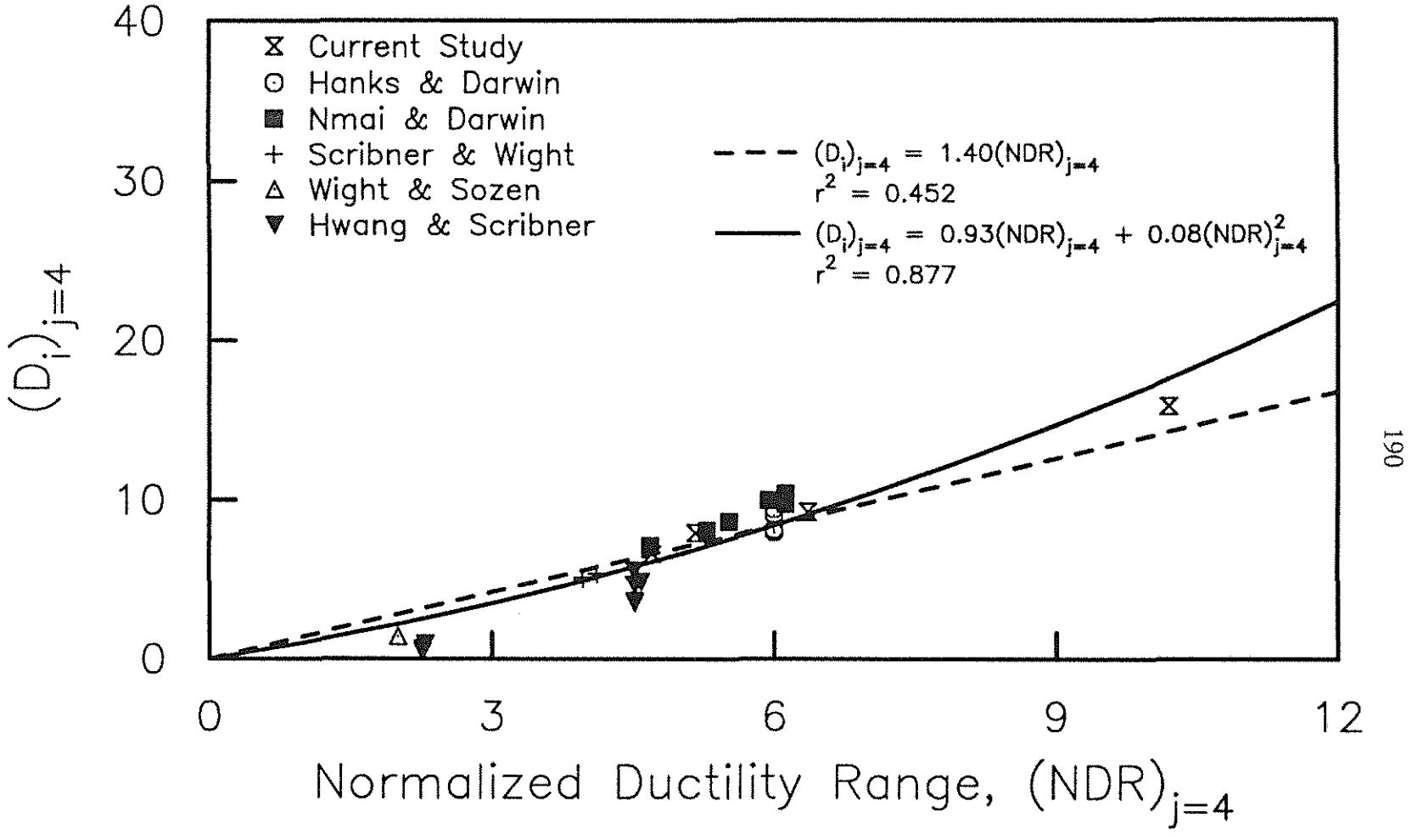

Fig. 4.5(b) $(D_i)_j$ versus $(NDR)_j$ for the specimens in Table 4.3 surviving four cycles with $P_i \geq 0.75P_y$

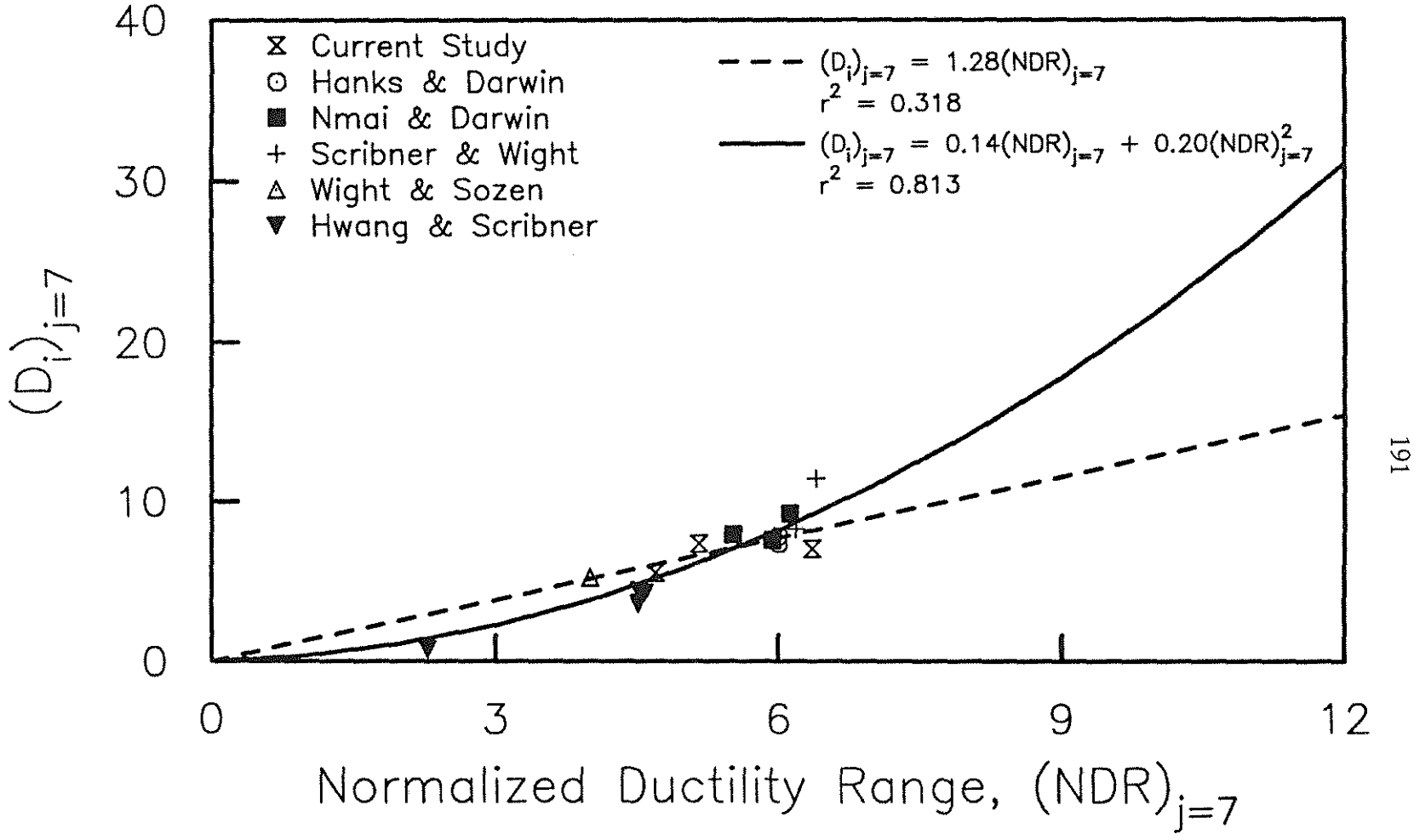

Fig. 4.5(c) $(D_i)_j$ versus $(NDR)_j$ for the specimens in Table 4.3 surviving seven cycles with $P_i \geq 0.75P_y$

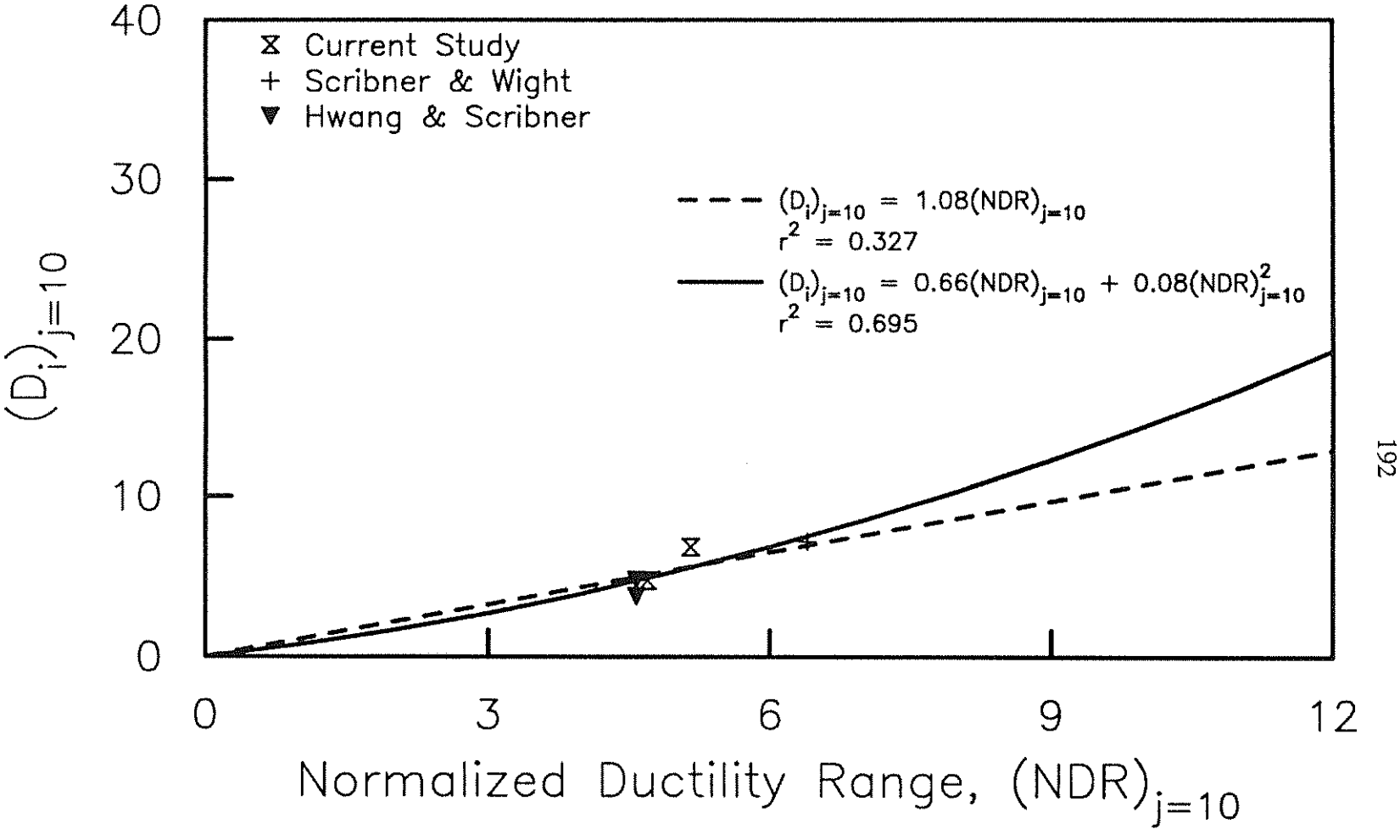

Fig. 4.5(d) $(D_i)_j$ versus $(NDR)_j$ for the specimens in Table 4.3 surviving ten cycles with $P_i \geq 0.75P_y$

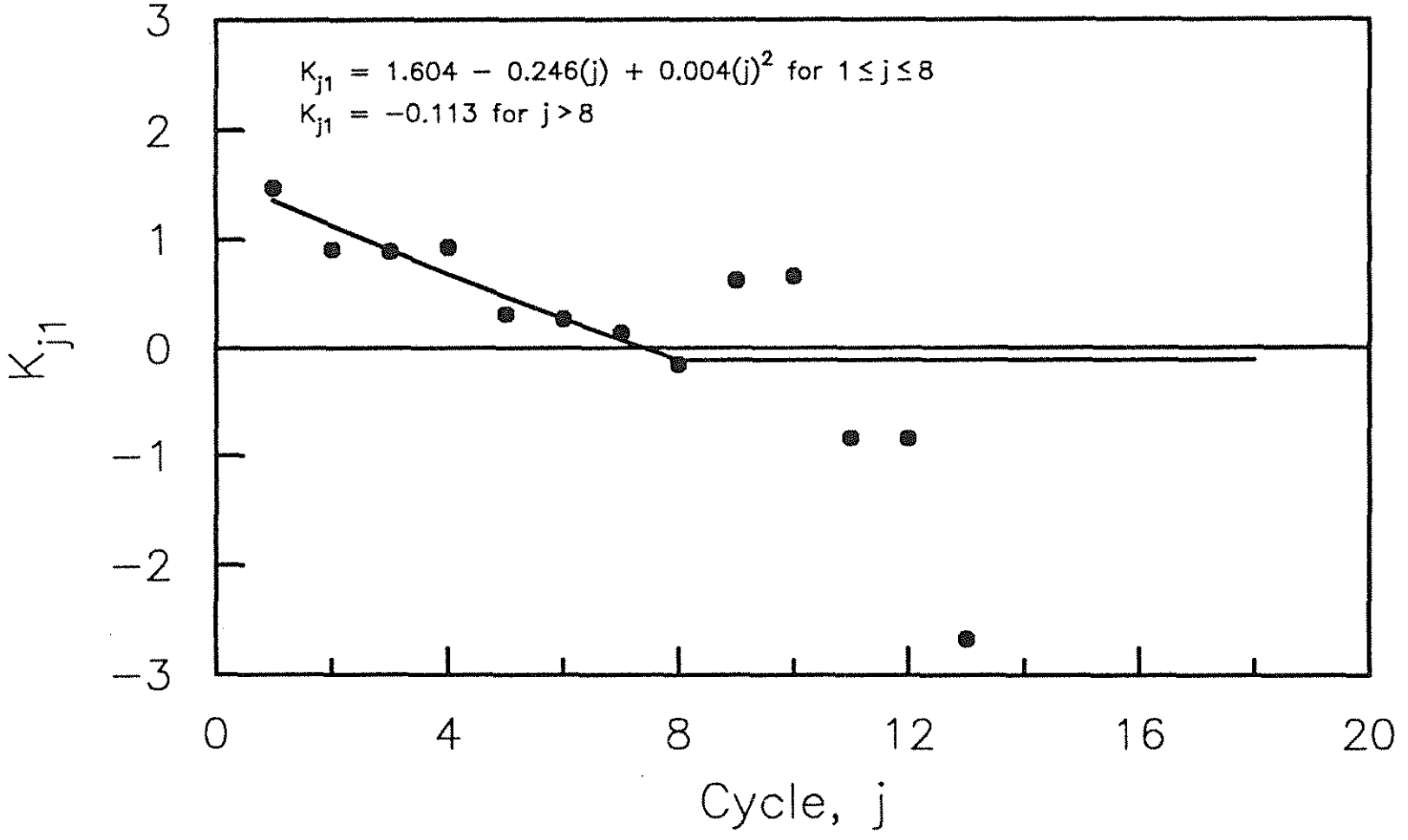

Fig. 4.6 K_{j1} as a function of Cycle

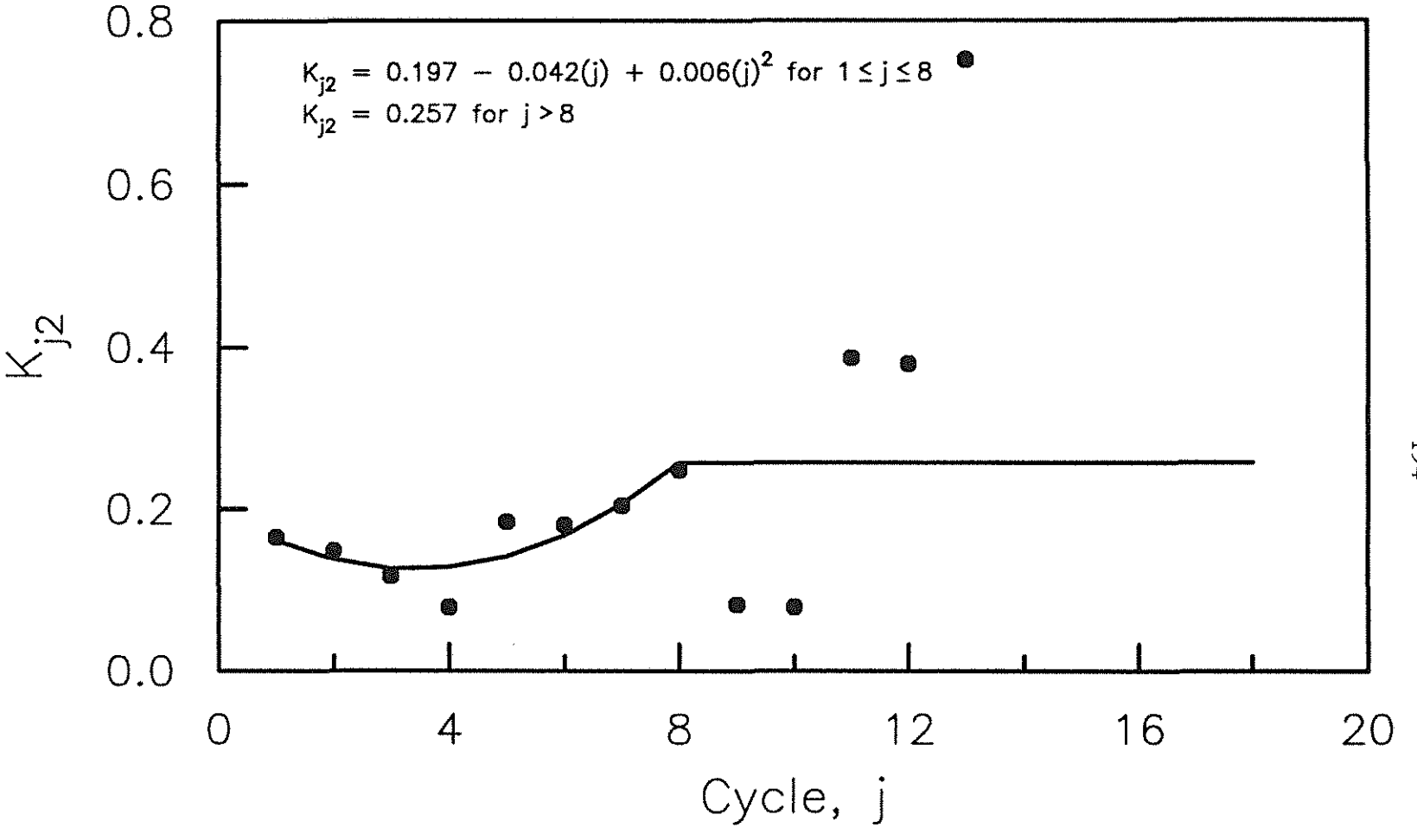

Fig. 4.7 K_{j2} as a function of Cycle

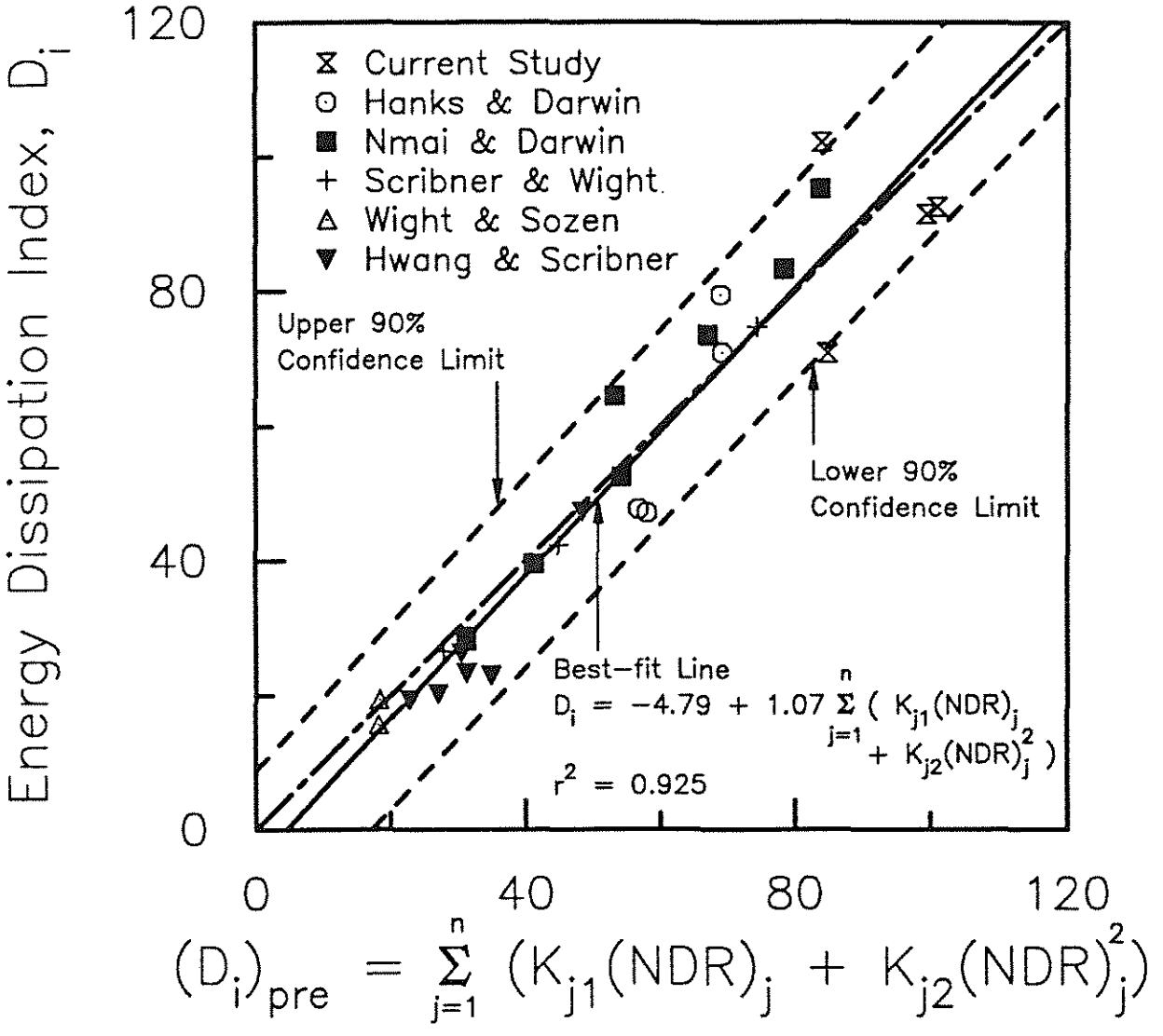

Fig. 4.8 Test versus predicted (NDR formulation) Energy Dissipation Index for the specimens in Table 4.4

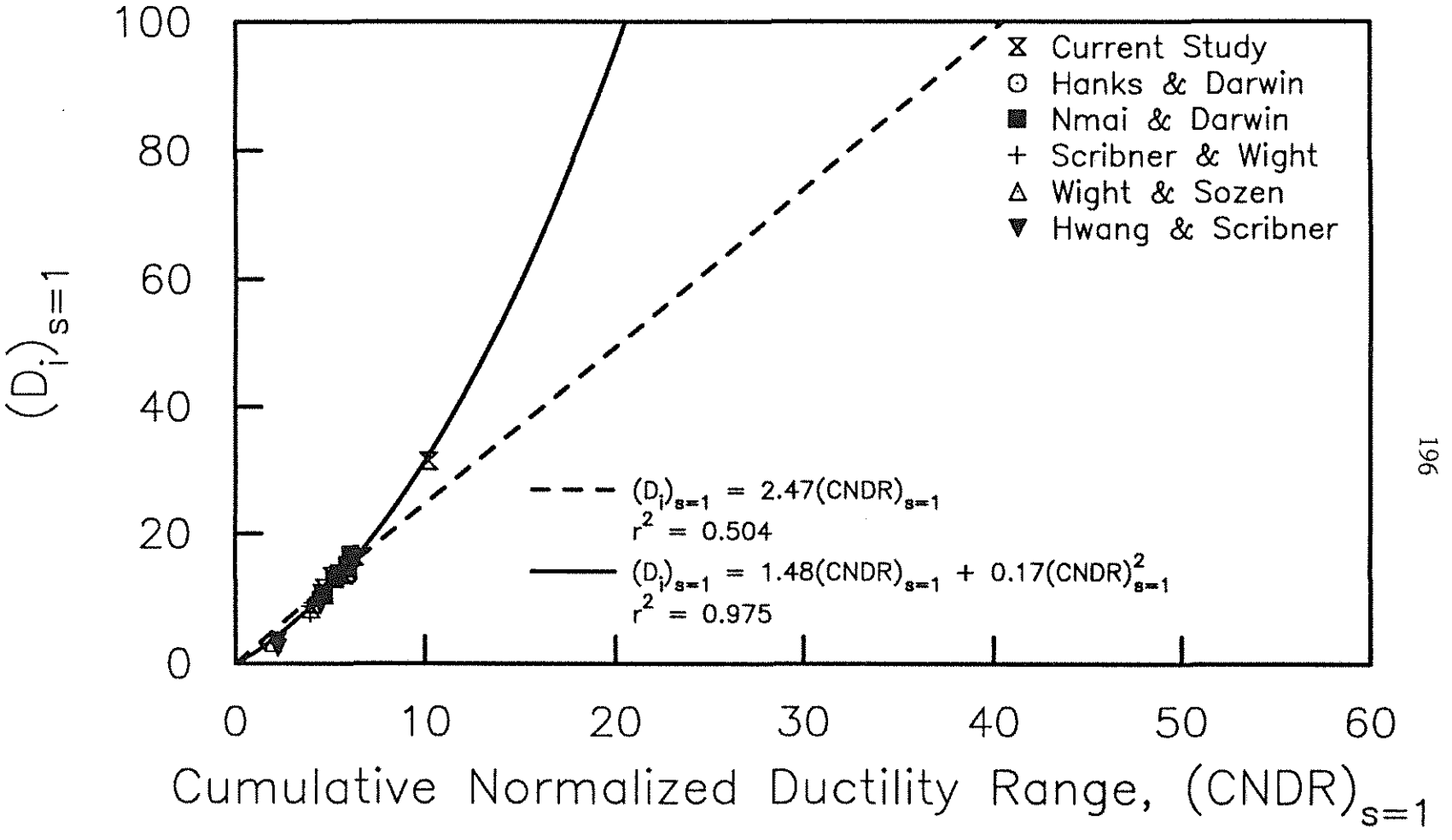

Fig. 4.9(a) $(D_i)_s$ versus $(CNDR)_s$ for the specimens in Table 4.5 surviving one cycle with $P_i \geq 0.75P_y$

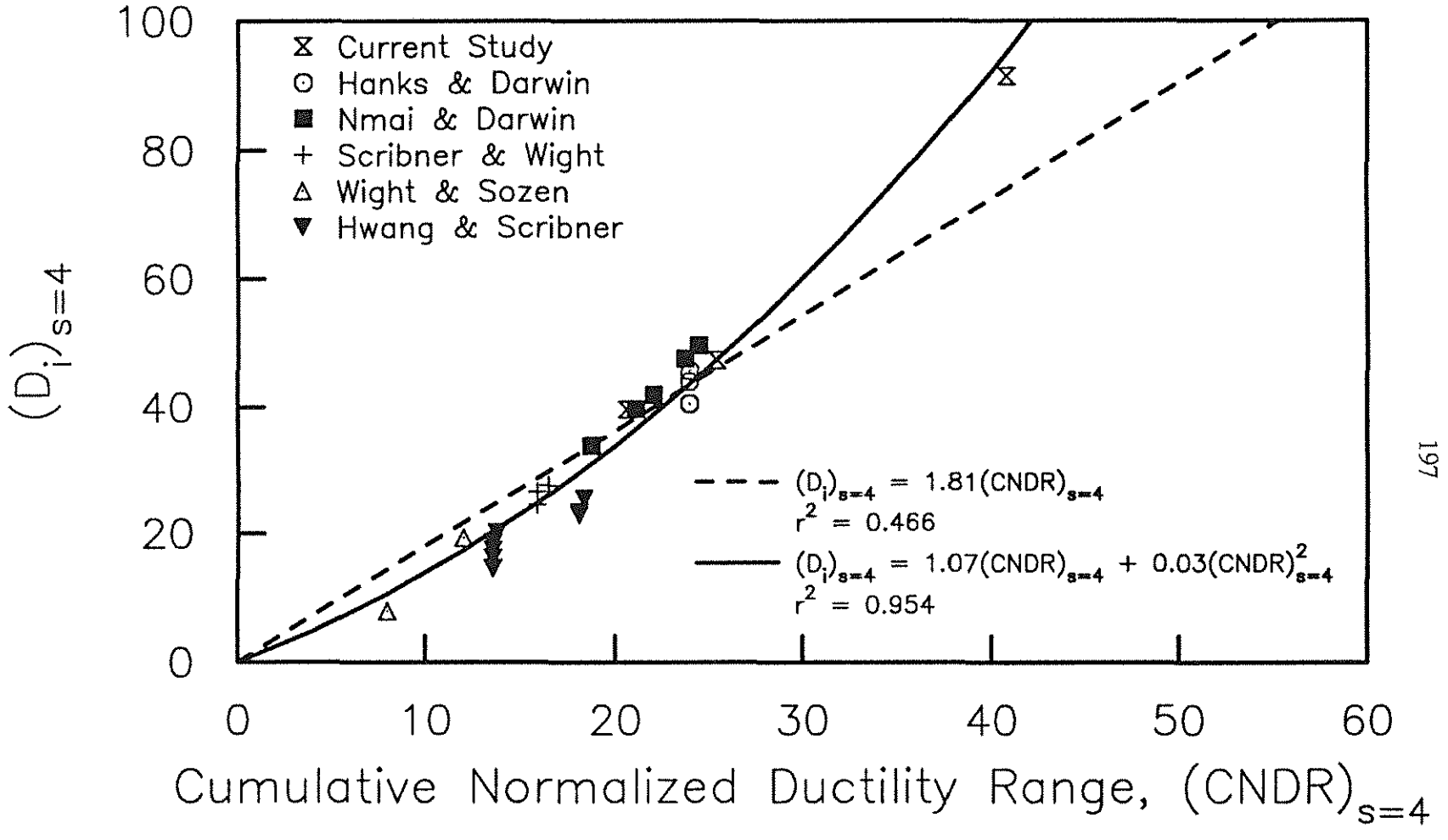

Fig. 4.9(b) $(D_i)_s$ versus $(CNDR)_s$ for the specimens in Table 4.5 surviving four cycles with $P_i \geq 0.75P_y$

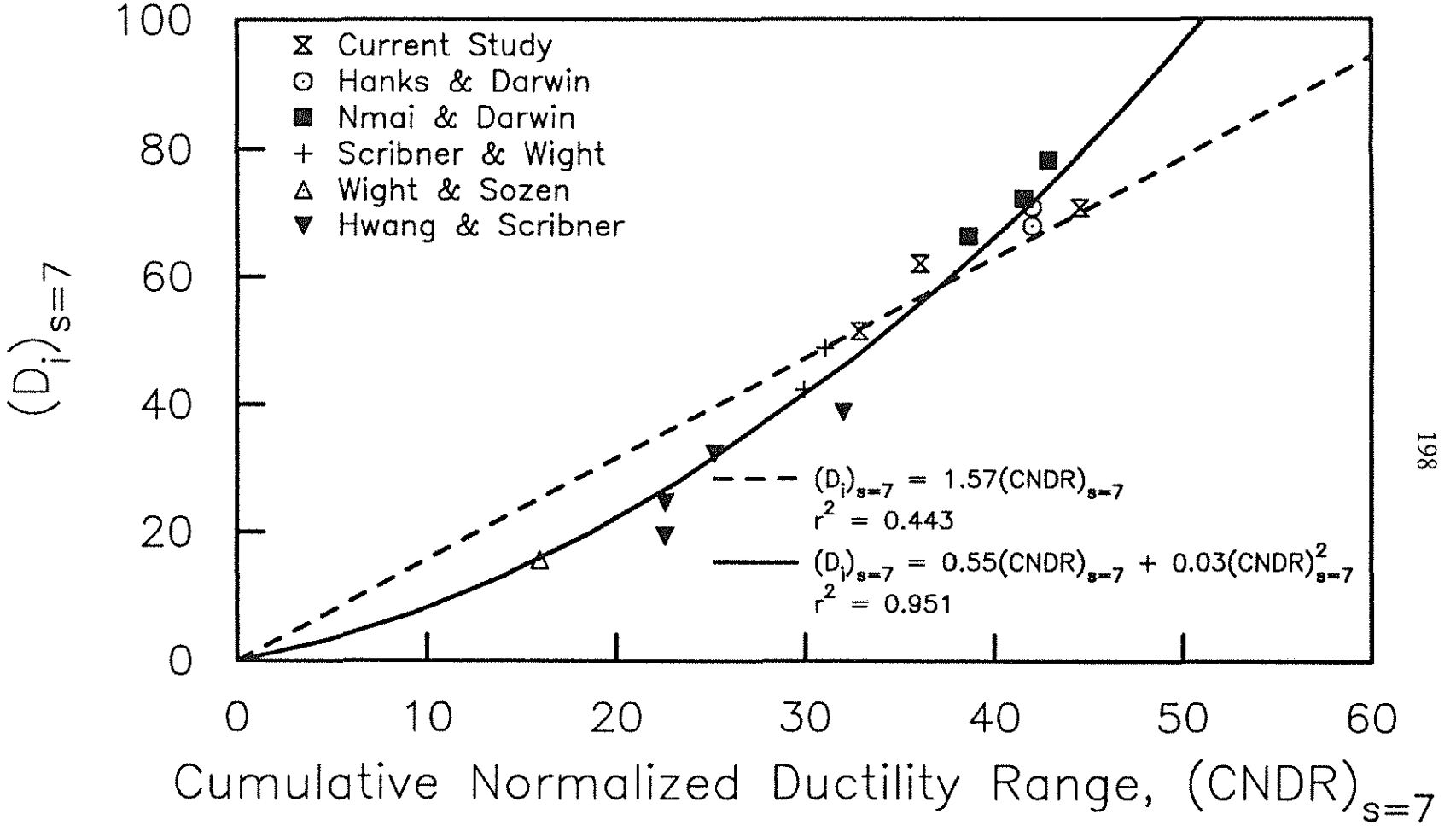

Fig. 4.9(c) $(D_i)_s$ versus $(CNDR)_s$ for the specimens in Table 4.5 surviving seven cycles with $P_i \geq 0.75P_y$

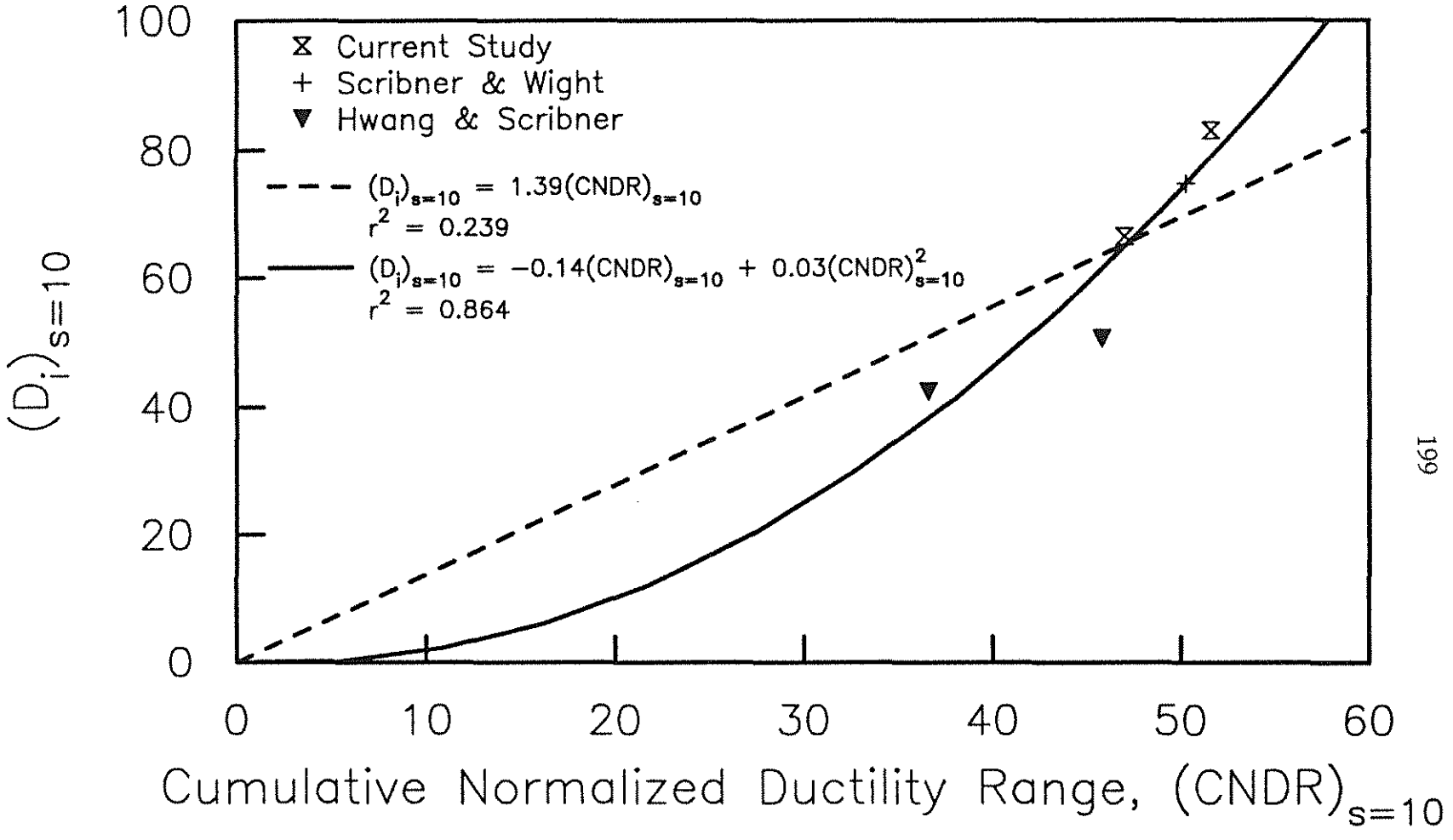

Fig. 4.9(d) $(D_i)_s$ versus $(CNDR)_s$ for the specimens in Table 4.5 surviving ten cycles with $P_i \geq 0.75P_y$

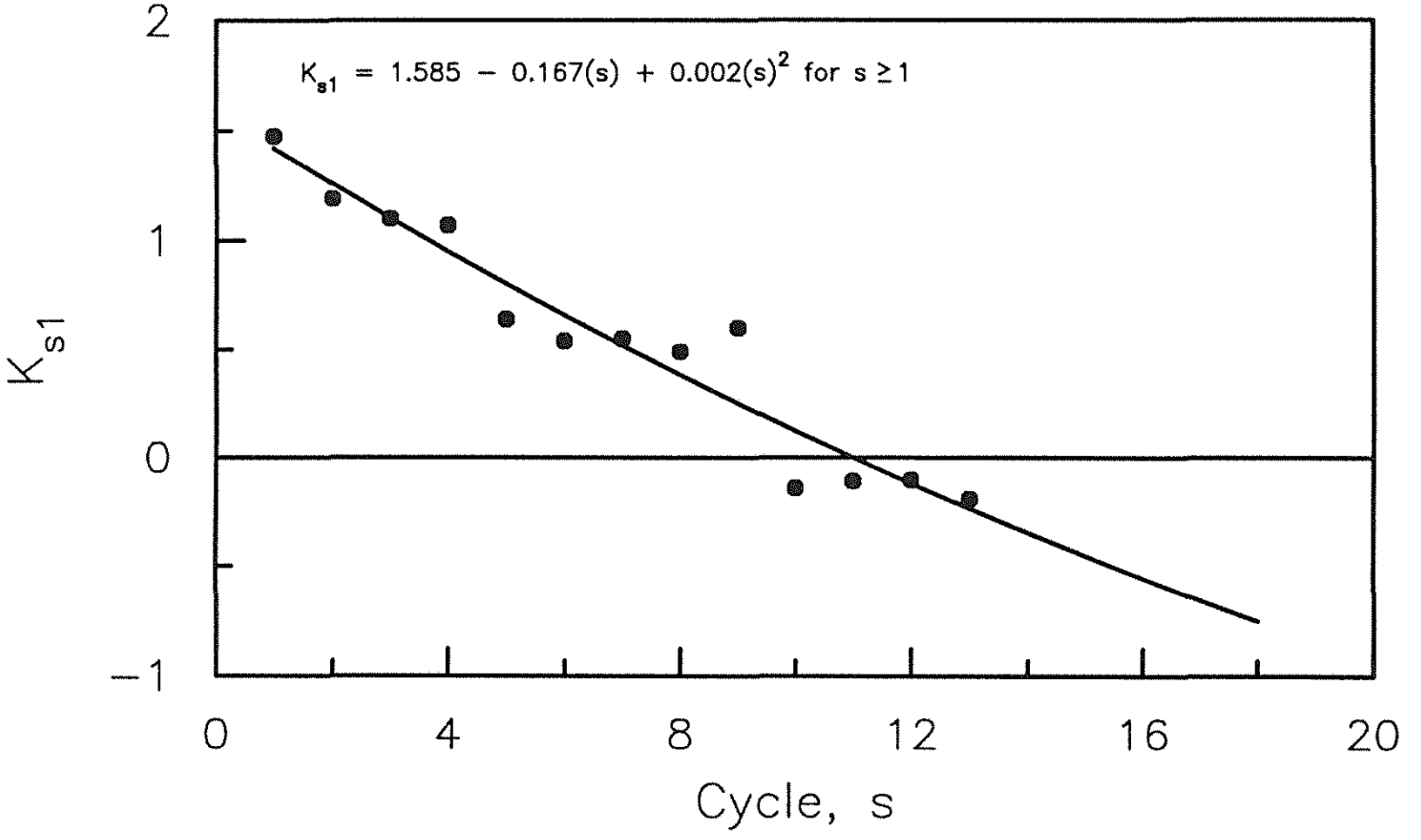

Fig. 4.10 K_{s1} as a function of Cycle

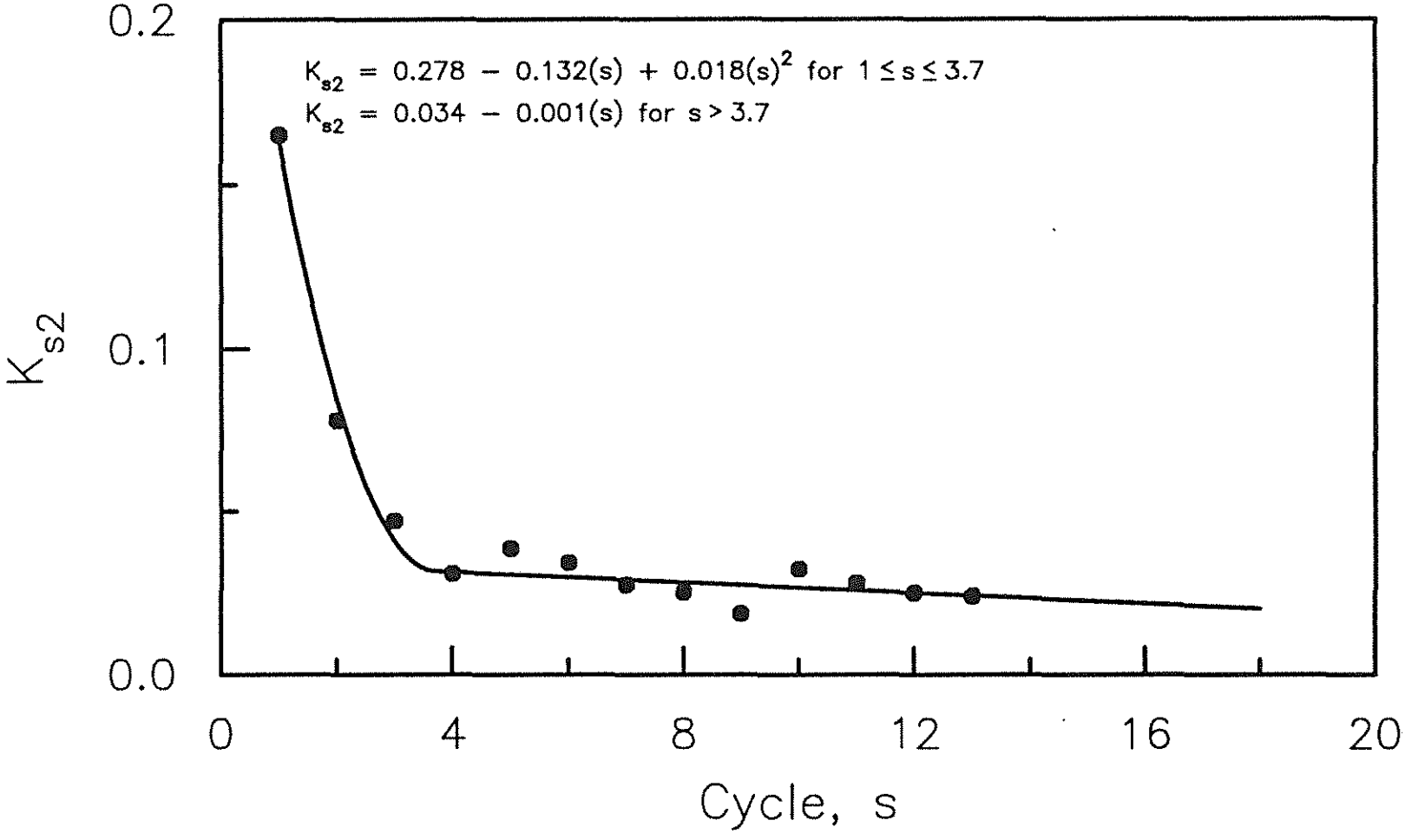

Fig. 4.11 K_{s2} as a function of Cycle

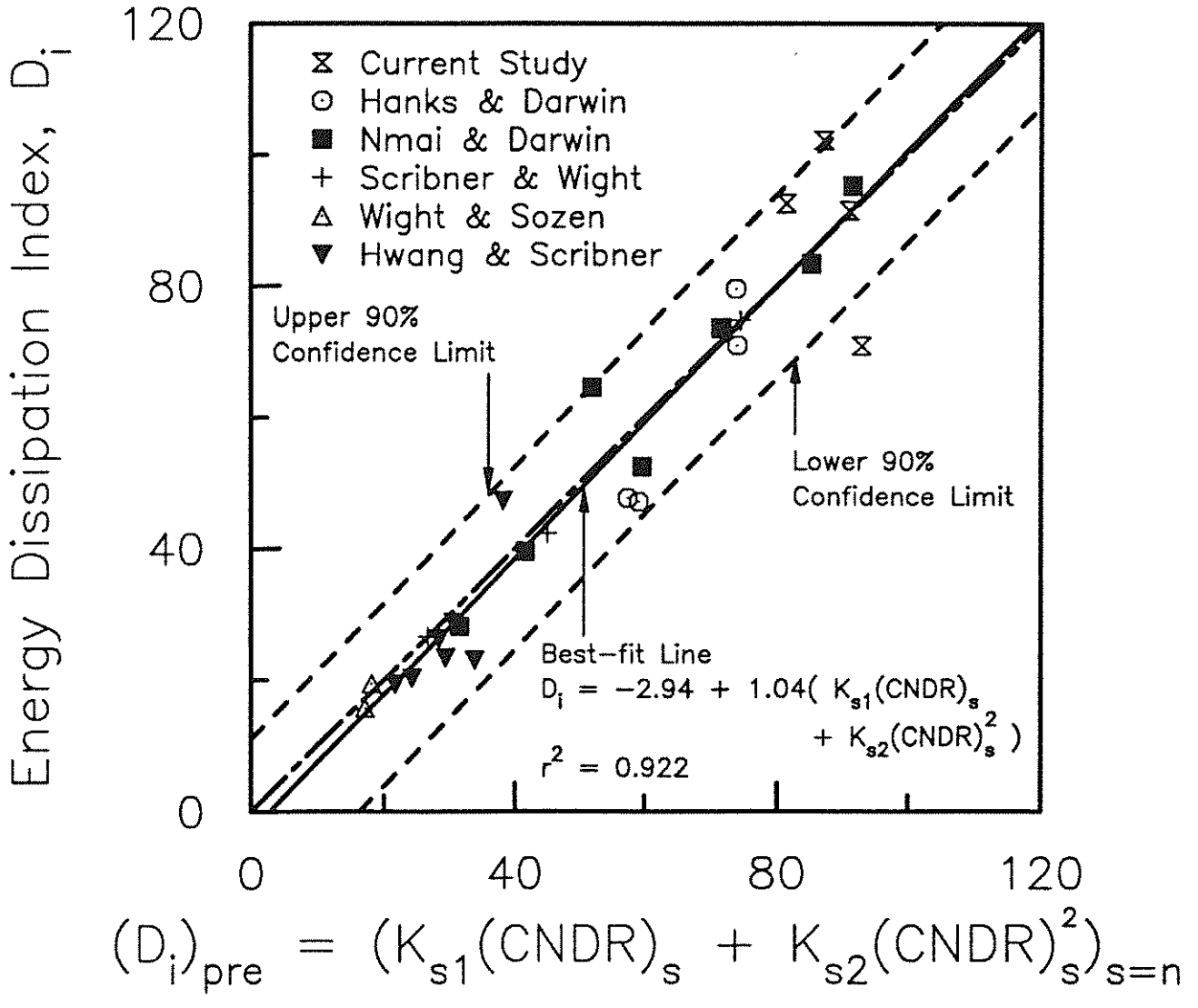

Fig. 4.12 Test versus predicted (CNDR formulation) Energy Dissipation Index for the specimens in Table 4.6

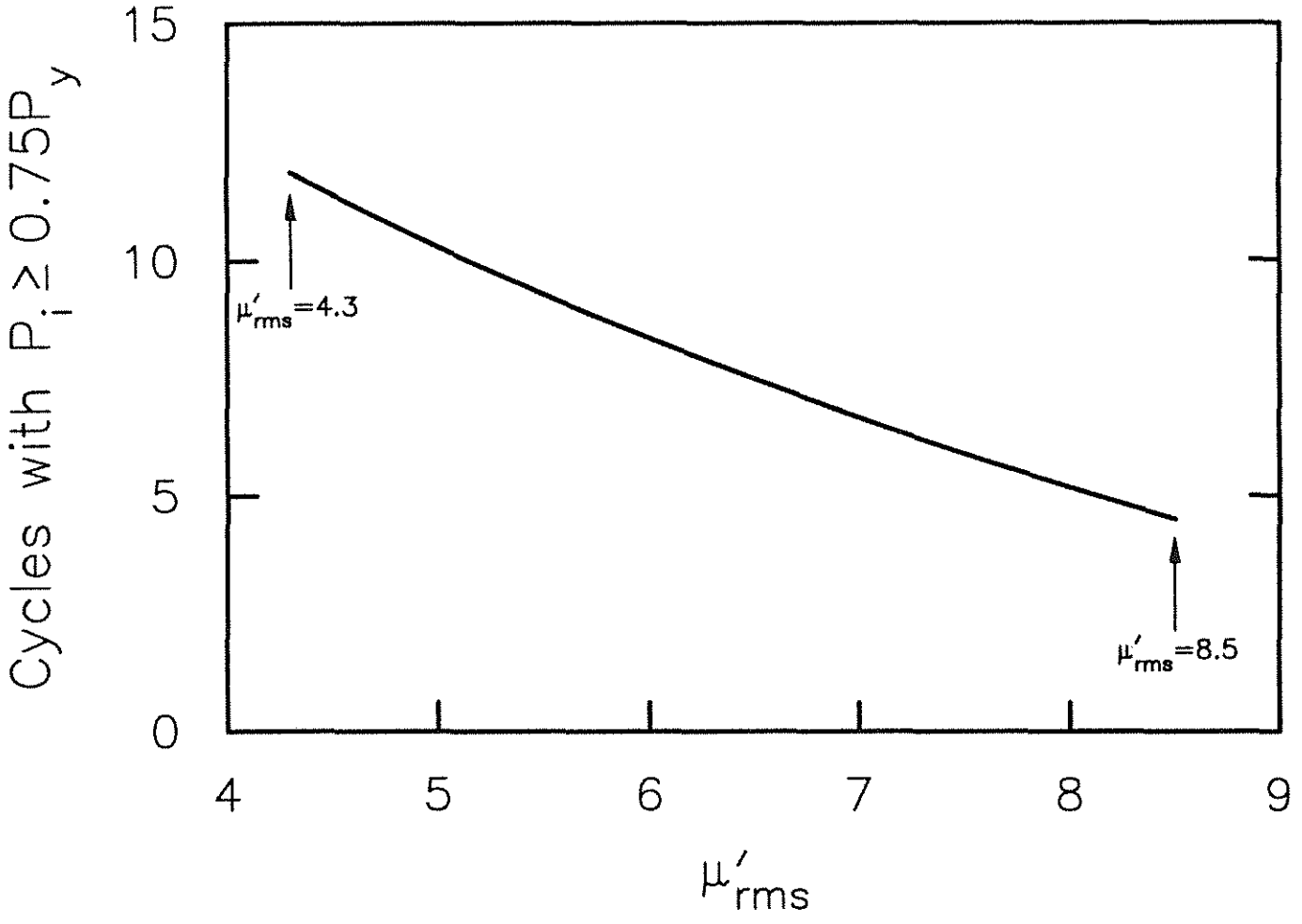

Fig. 5.1 Predicted cycles with $P_i \geq 0.75P_y$ versus μ'_{rms} for a beam with the design parameters of Beam H-1 from the current study

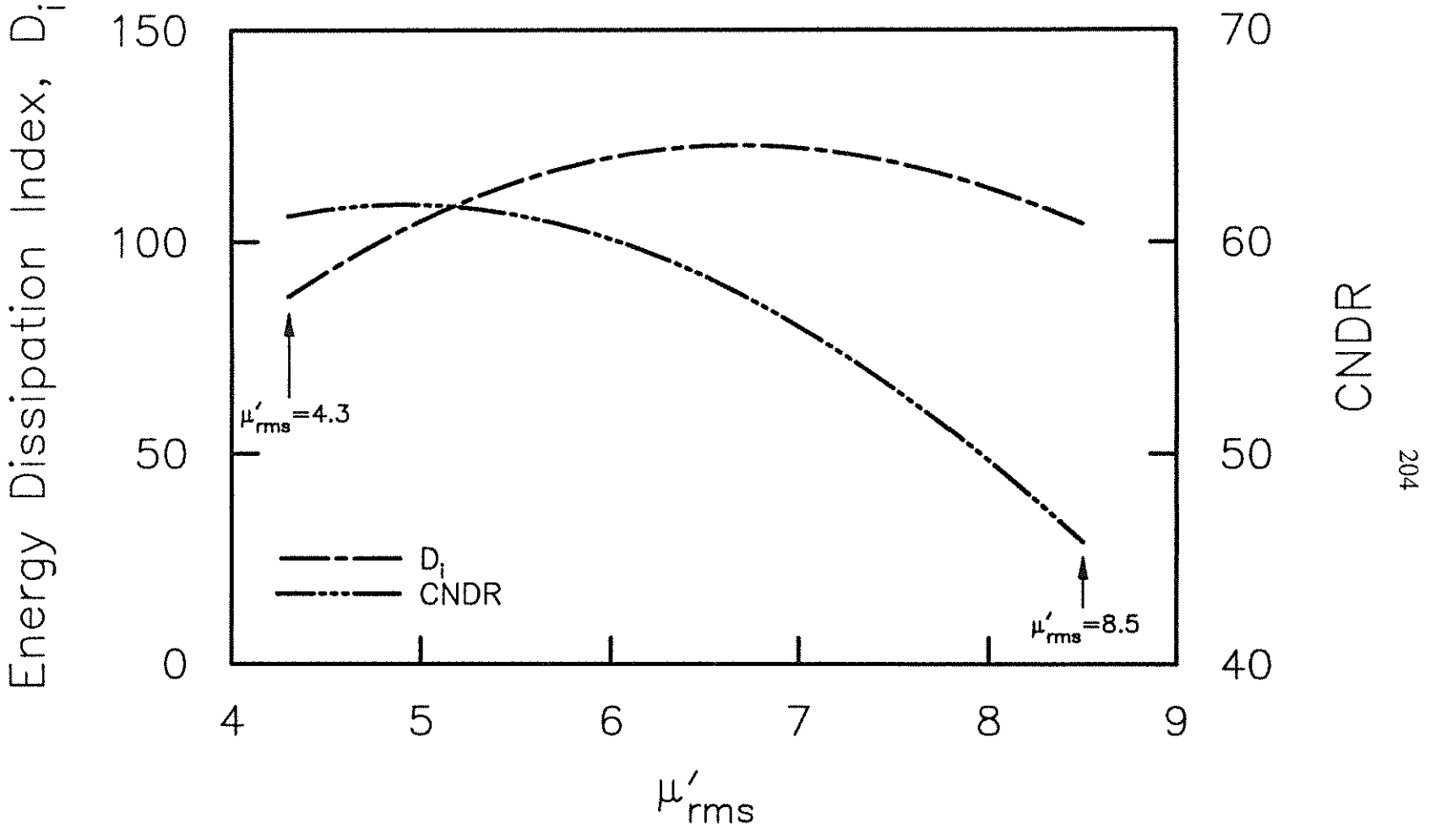

Fig. 5.2 Predicted Energy Dissipation Index versus μ'_{rms} and CNDR versus μ'_{rms} for a beam with the design parameters of Beam H-1 from the current study

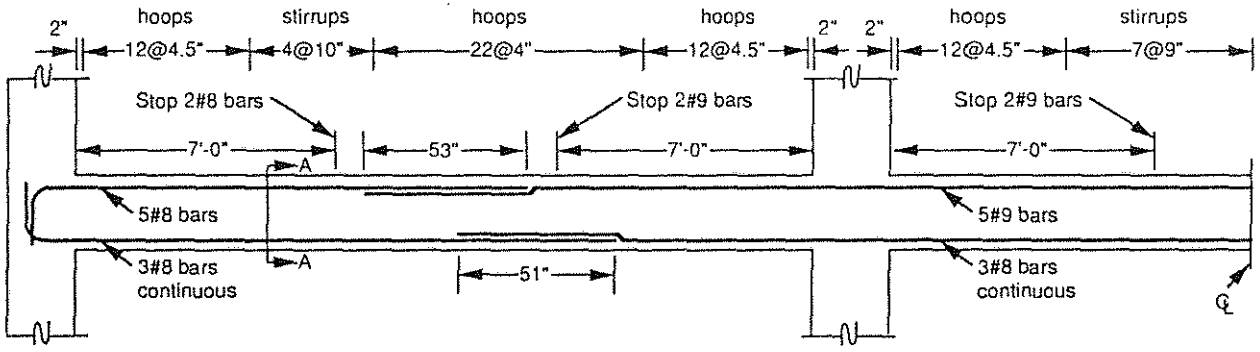

(a) Elevation

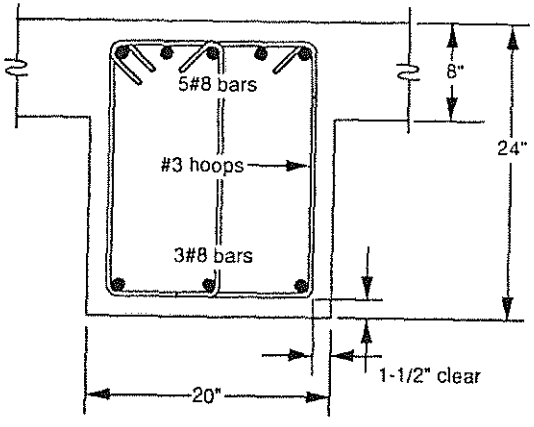

(b) Section A-A

Fig. 5.3 PCA Beam Design used in the case study (Portland Cement Association 1990)

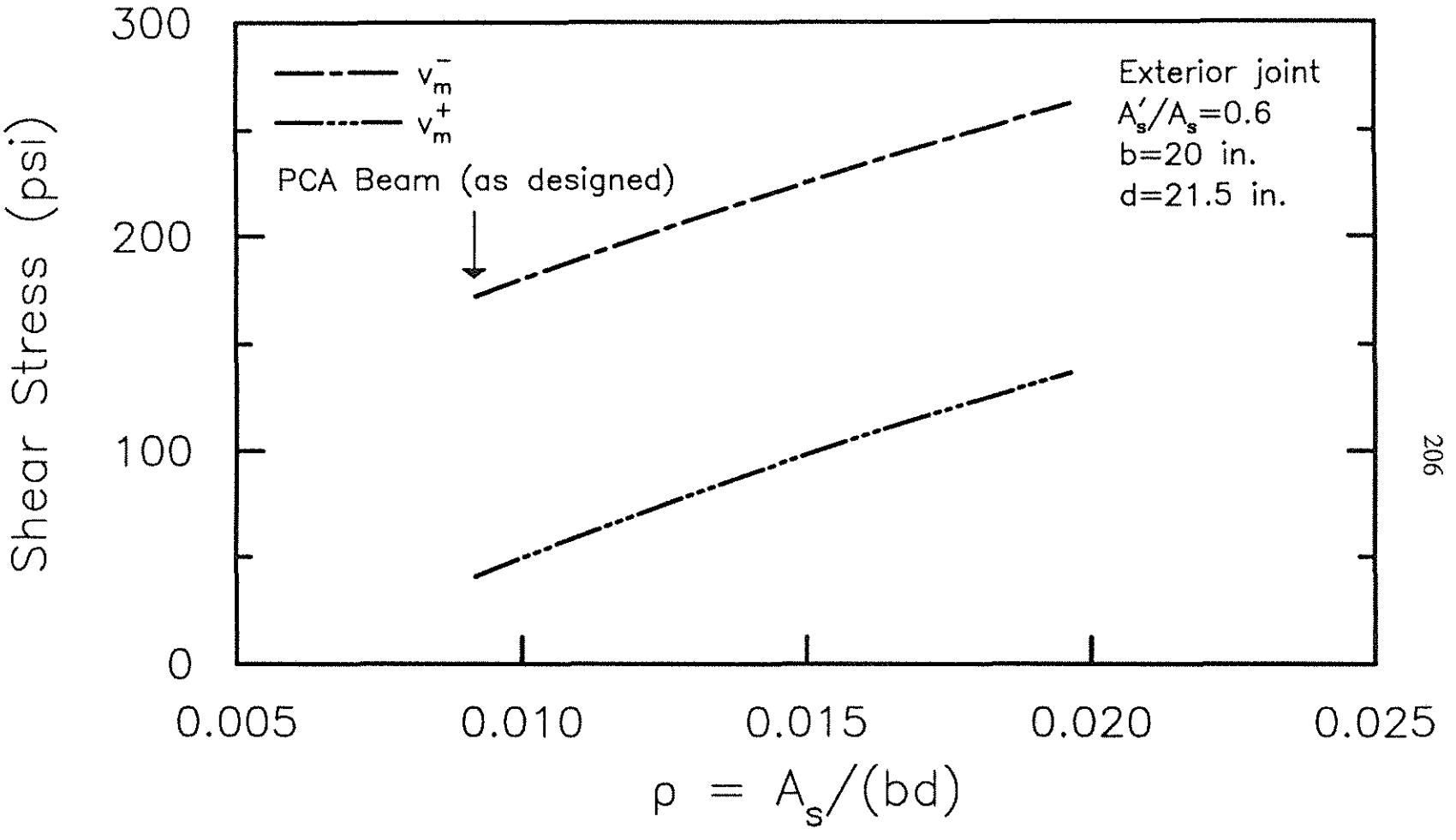

Fig. 5.4 Maximum shear stress in negative and positive bending versus ρ for the exterior joint of the beam used in the case study

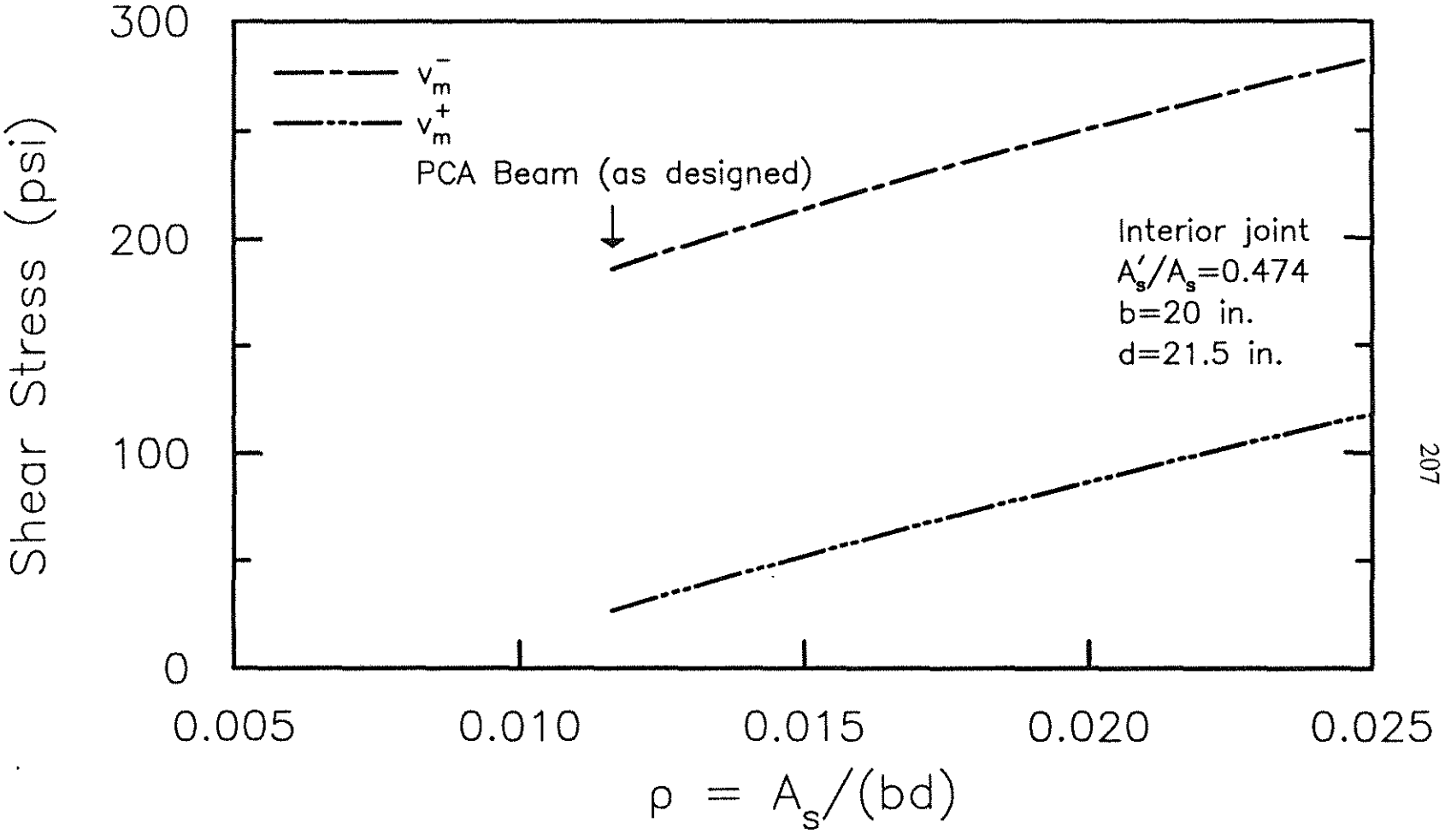

Fig. 5.5 Maximum shear stress in negative and positive bending versus ρ for the interior joint of the beam used in the case study

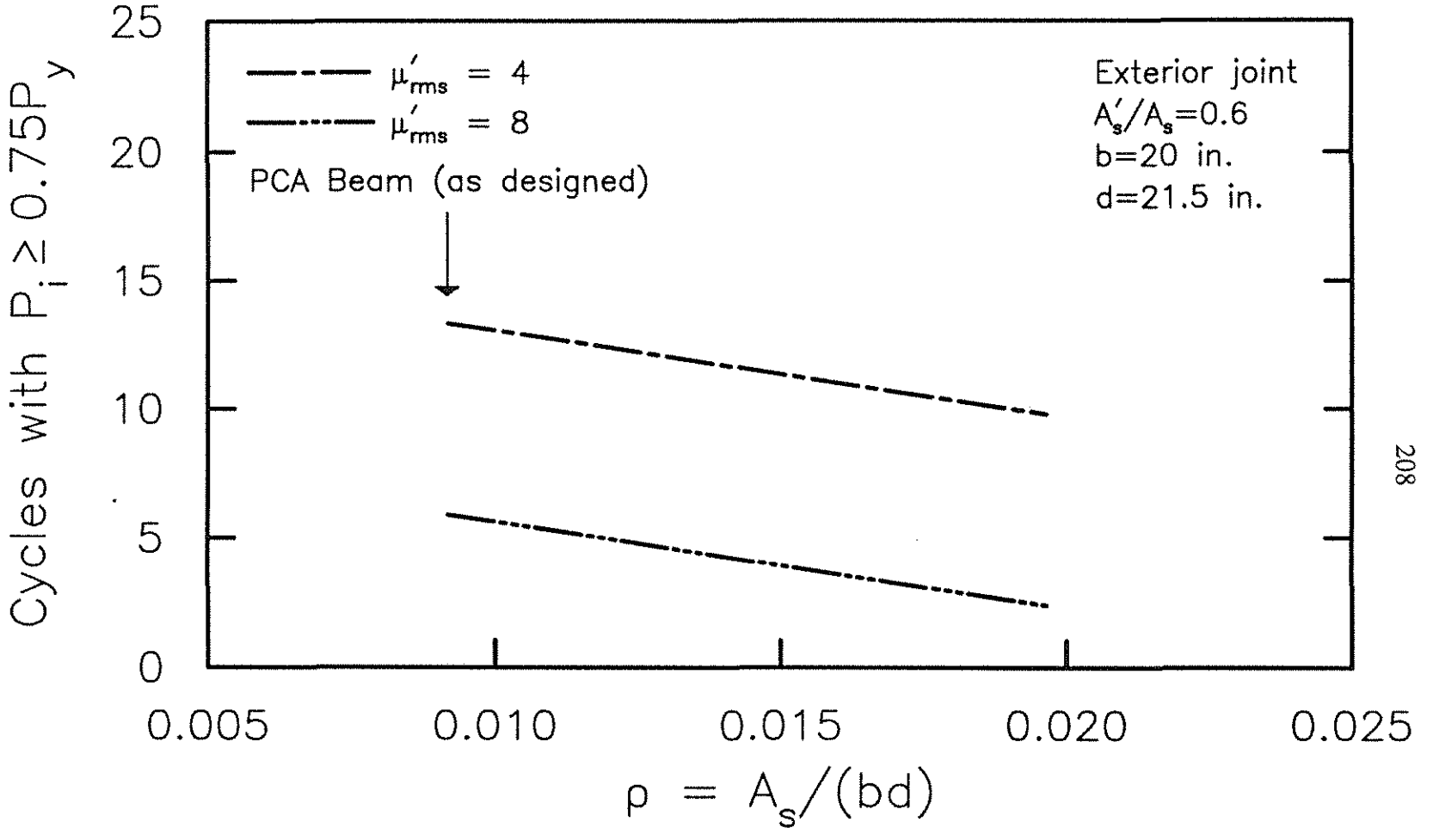

Fig. 5.6 Predicted cycles with $P_i \geq 0.75P_y$ versus ρ for the exterior joint of the beam used in the case study

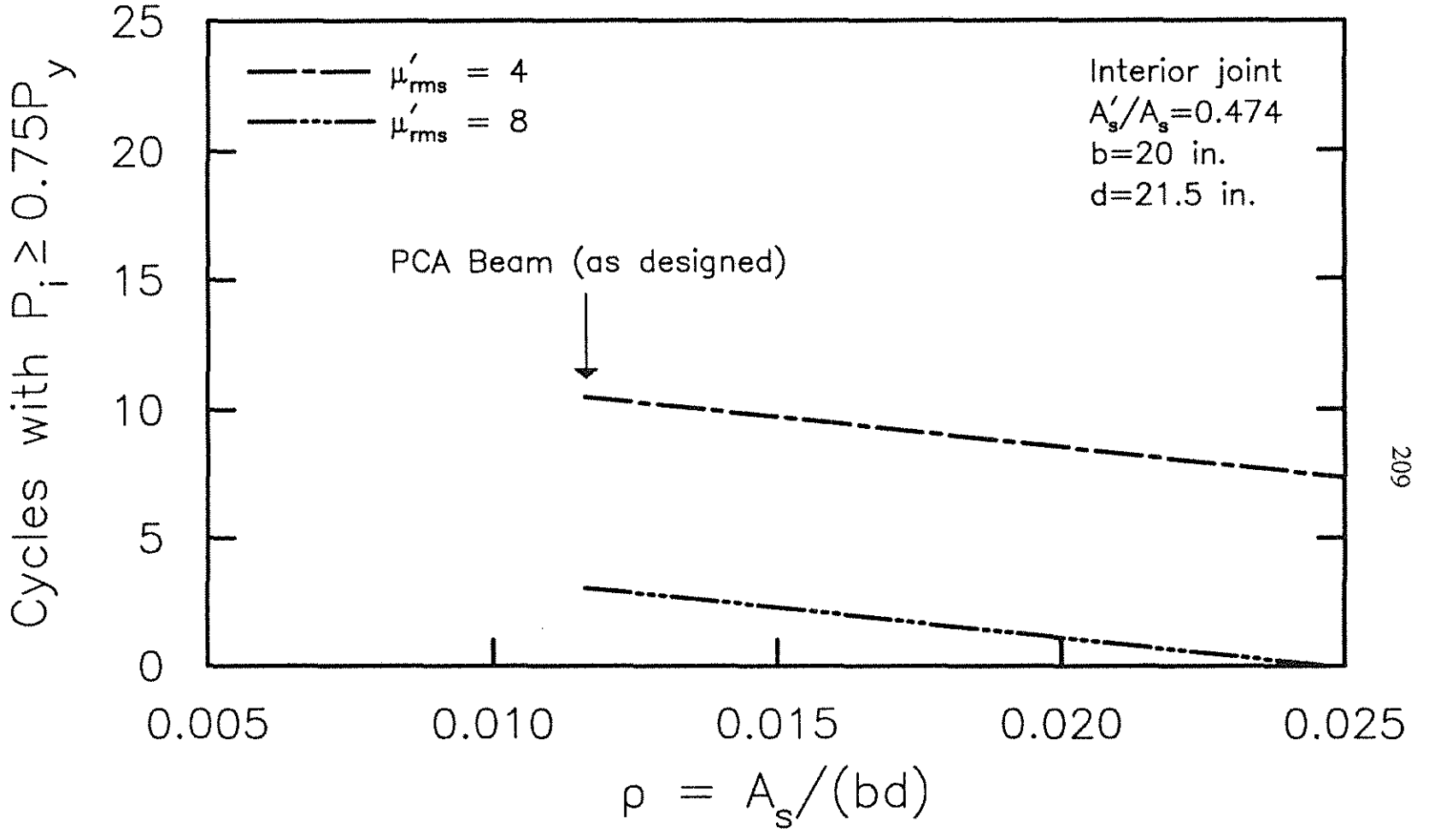

Fig. 5.7 Predicted cycles with $P_i \geq 0.75P_y$ versus ρ for the interior joint of the beam used in the case study

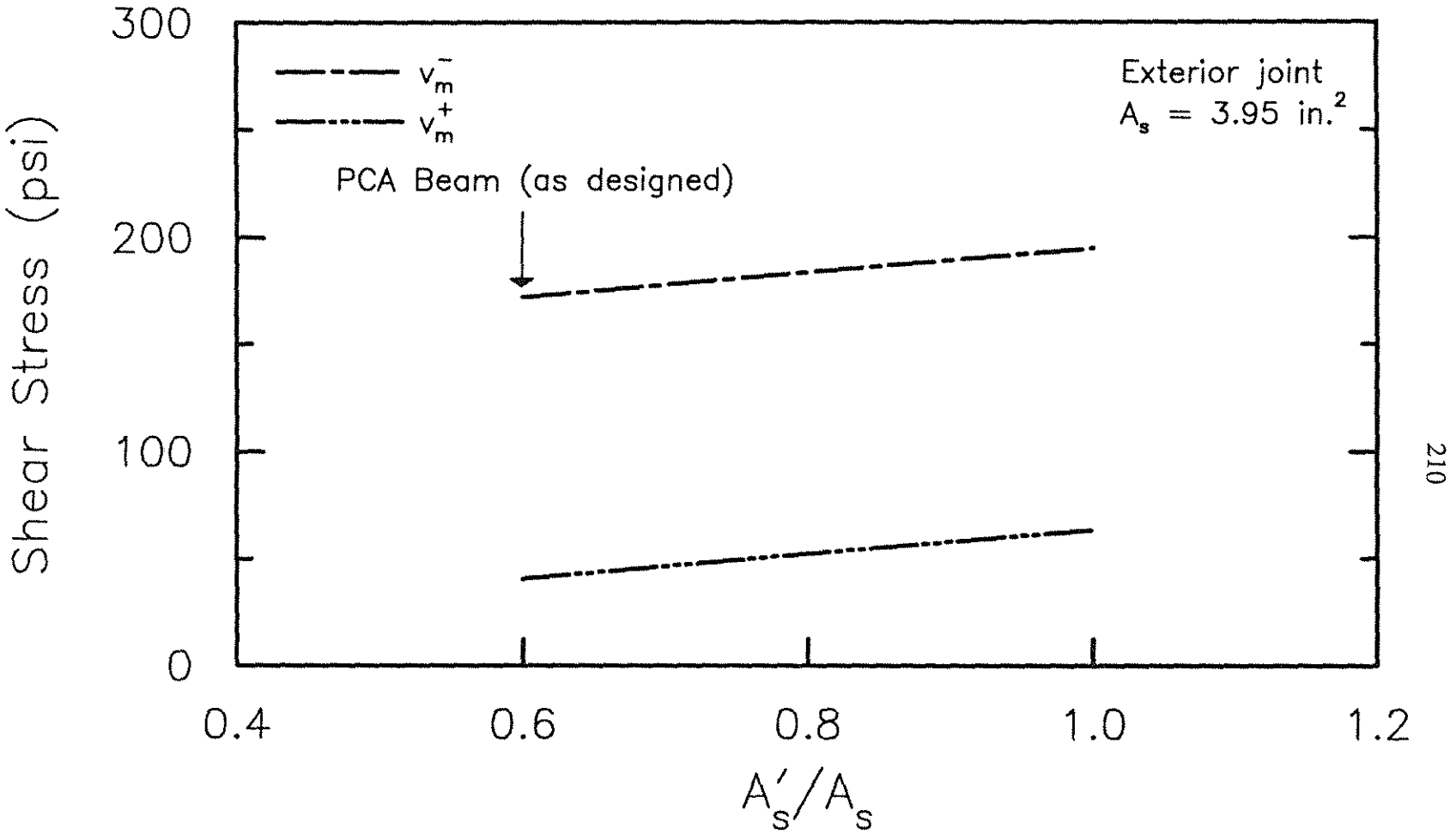

Fig. 5.8 Maximum shear stress in negative and positive bending versus A_s'/A_s for the exterior joint of the beam used in the case study

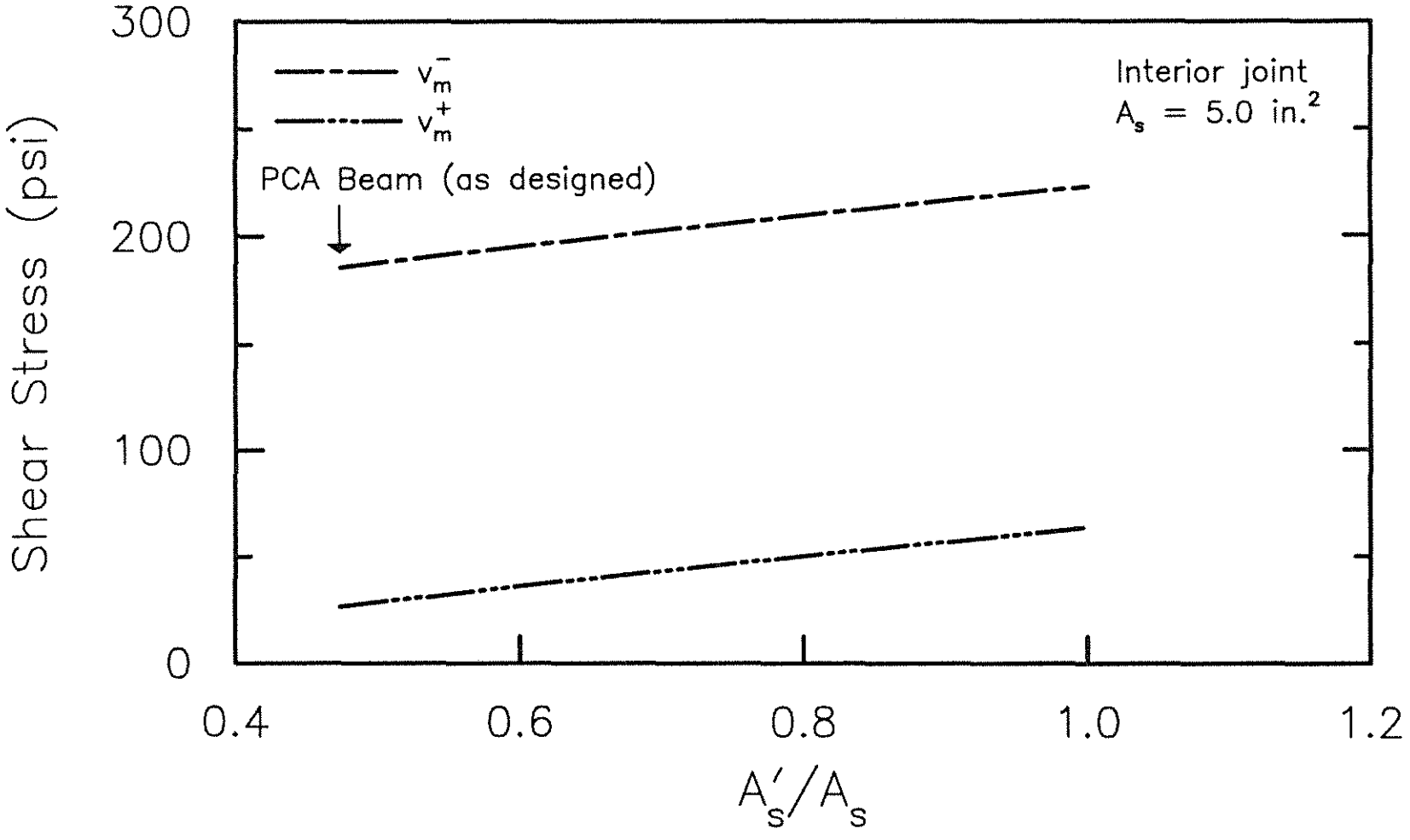

Fig. 5.9 Maximum shear stress in negative and positive bending versus A_s'/A_s for the interior joint of the beam used in the case study

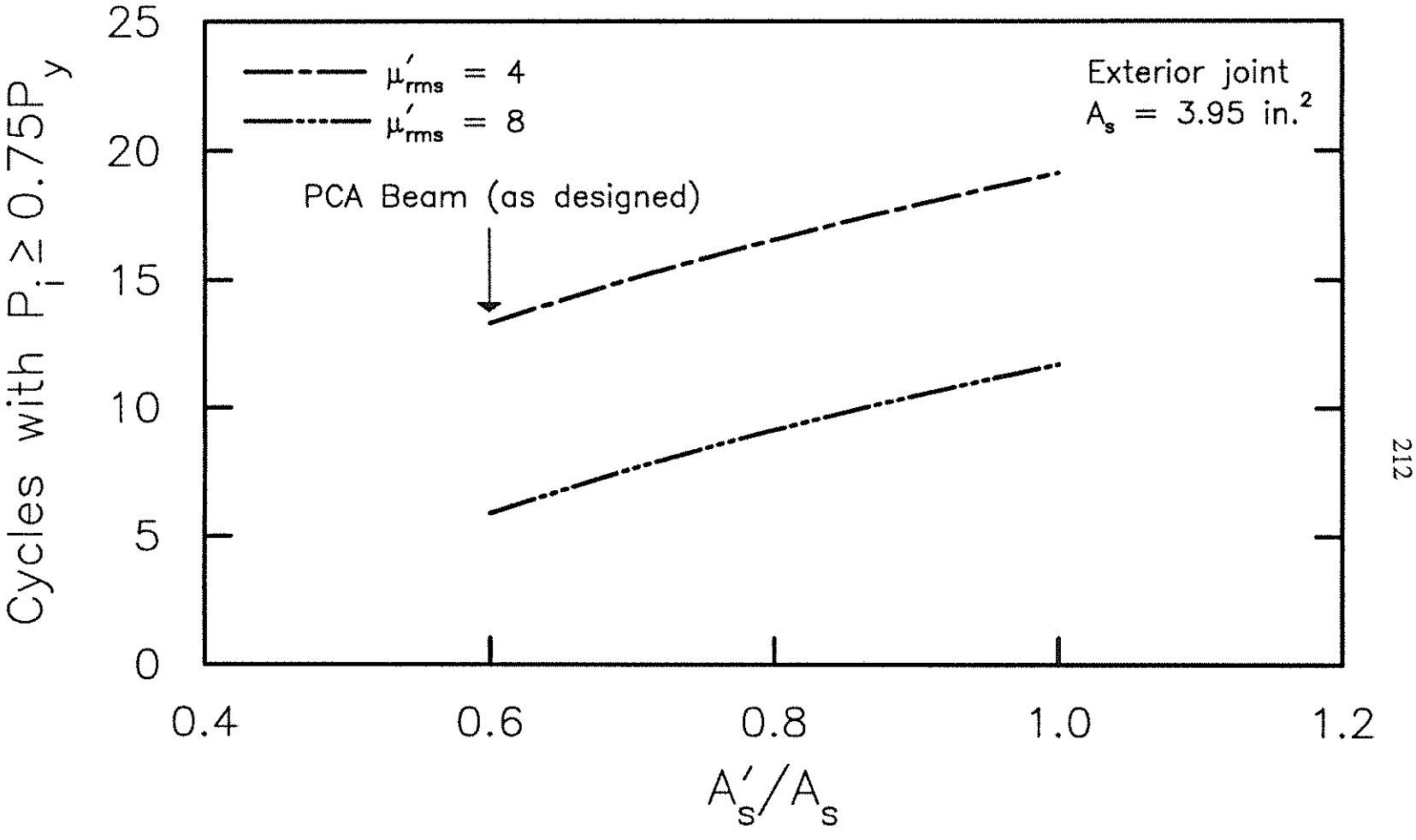

Fig. 5.10 Predicted cycles with $P_i \geq 0.75P_y$ versus A_s'/A_s for the exterior joint of the beam used in the case study

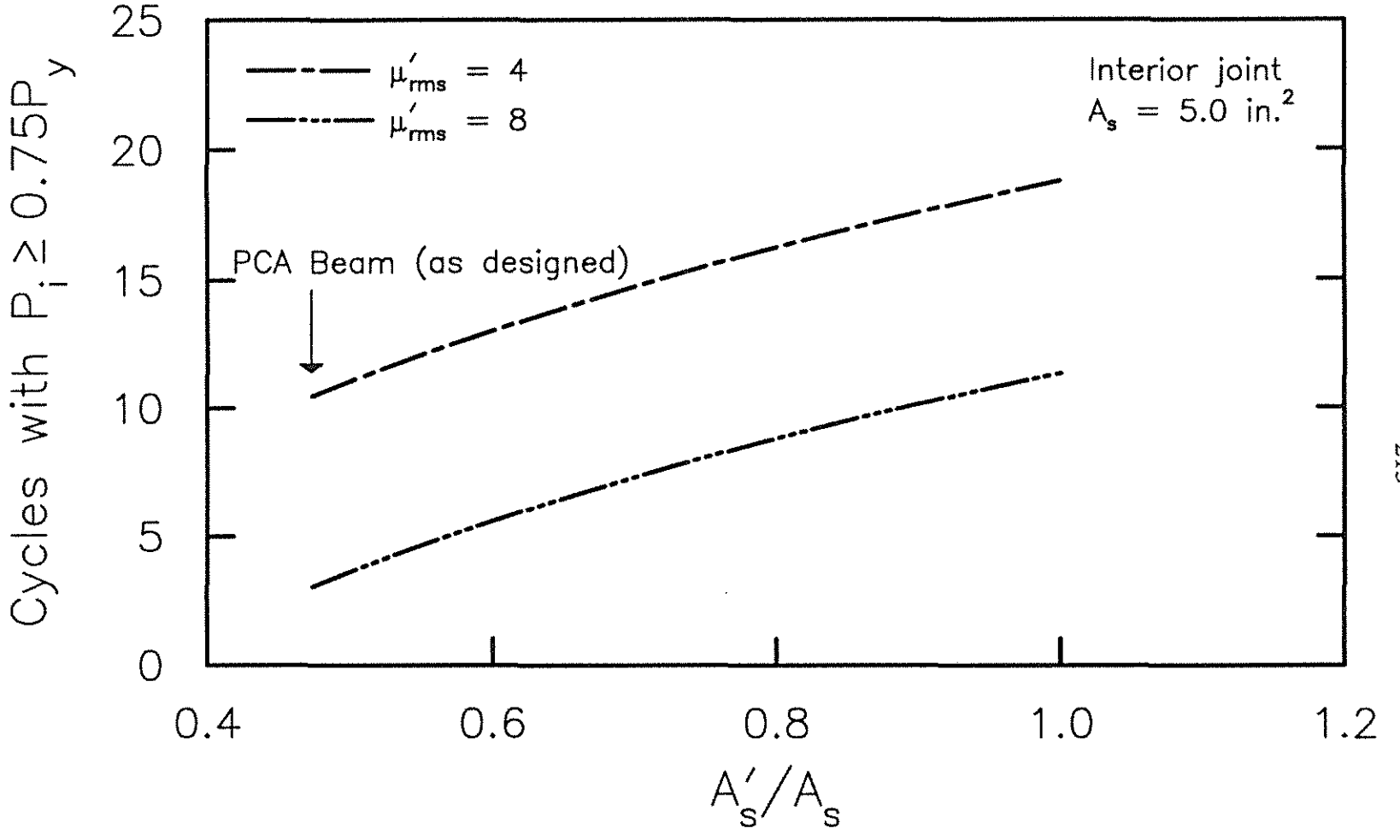

Fig. 5.11 Predicted cycles with $P_i \geq 0.75P_y$ versus A'_s/A_s for the interior joint of the beam used in the case study

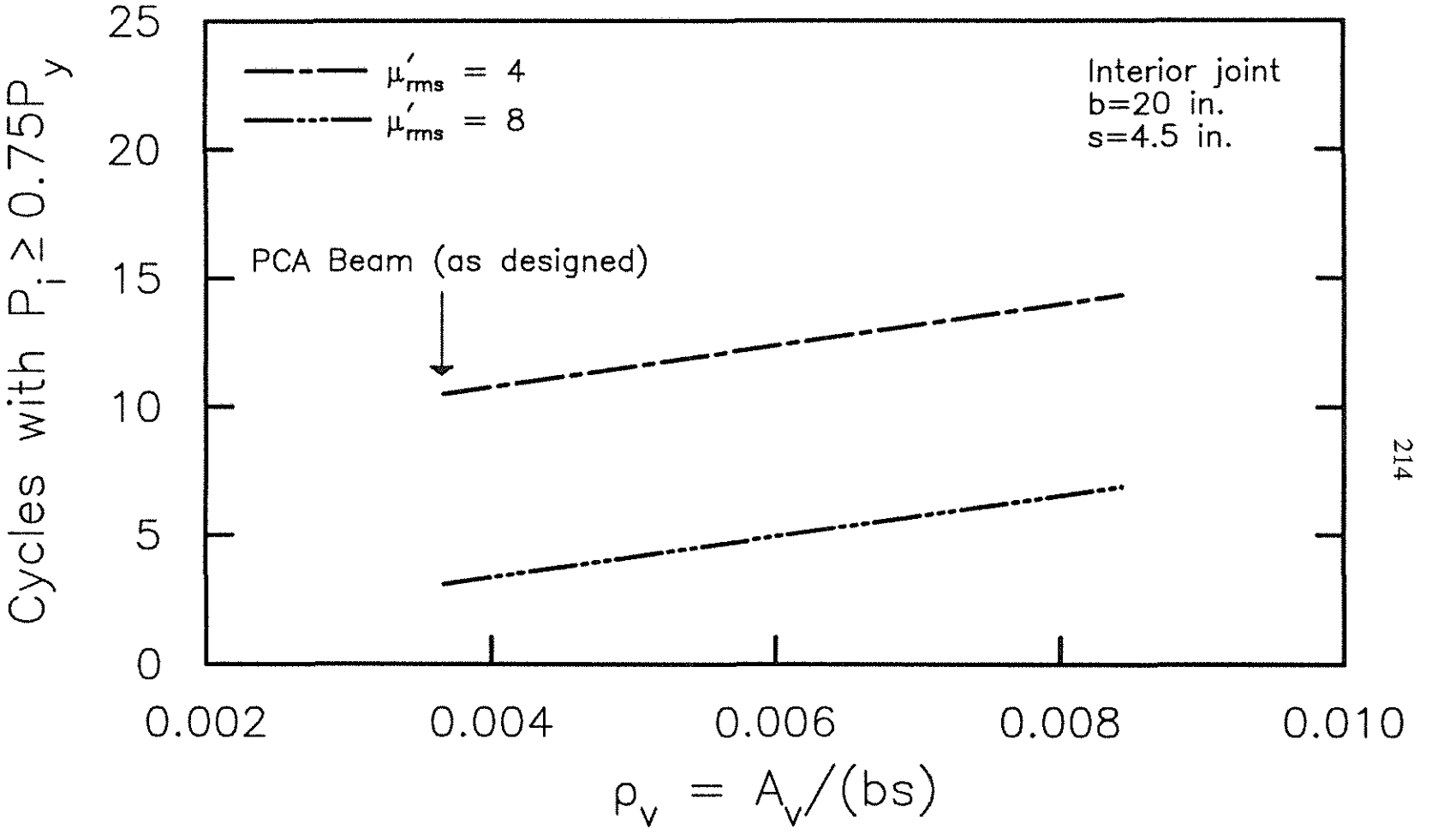

Fig. 5.12 Predicted cycles with $P_i \geq 0.75P_y$ versus ρ_v for the interior joint of the beam used in the case study (constant s); $v_s = 60{,}000\rho_v$ (in psi)

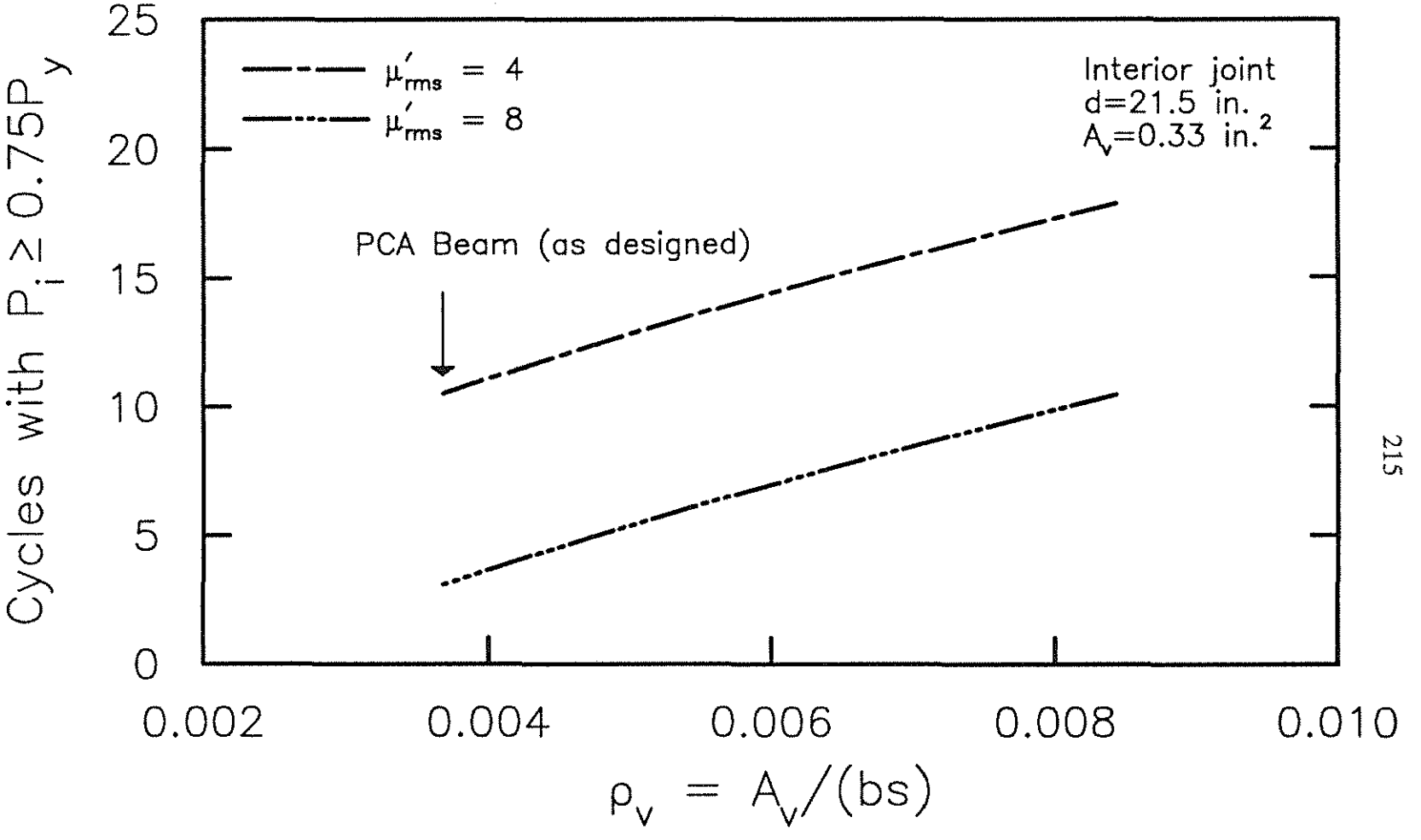

Fig. 5.13 Predicted cycles with $P_i \geq 0.75P_y$ versus ρ_v for the interior joint of the beam used in the case study (constant A_v); $v_s = 60{,}000\rho_v$ (in psi)

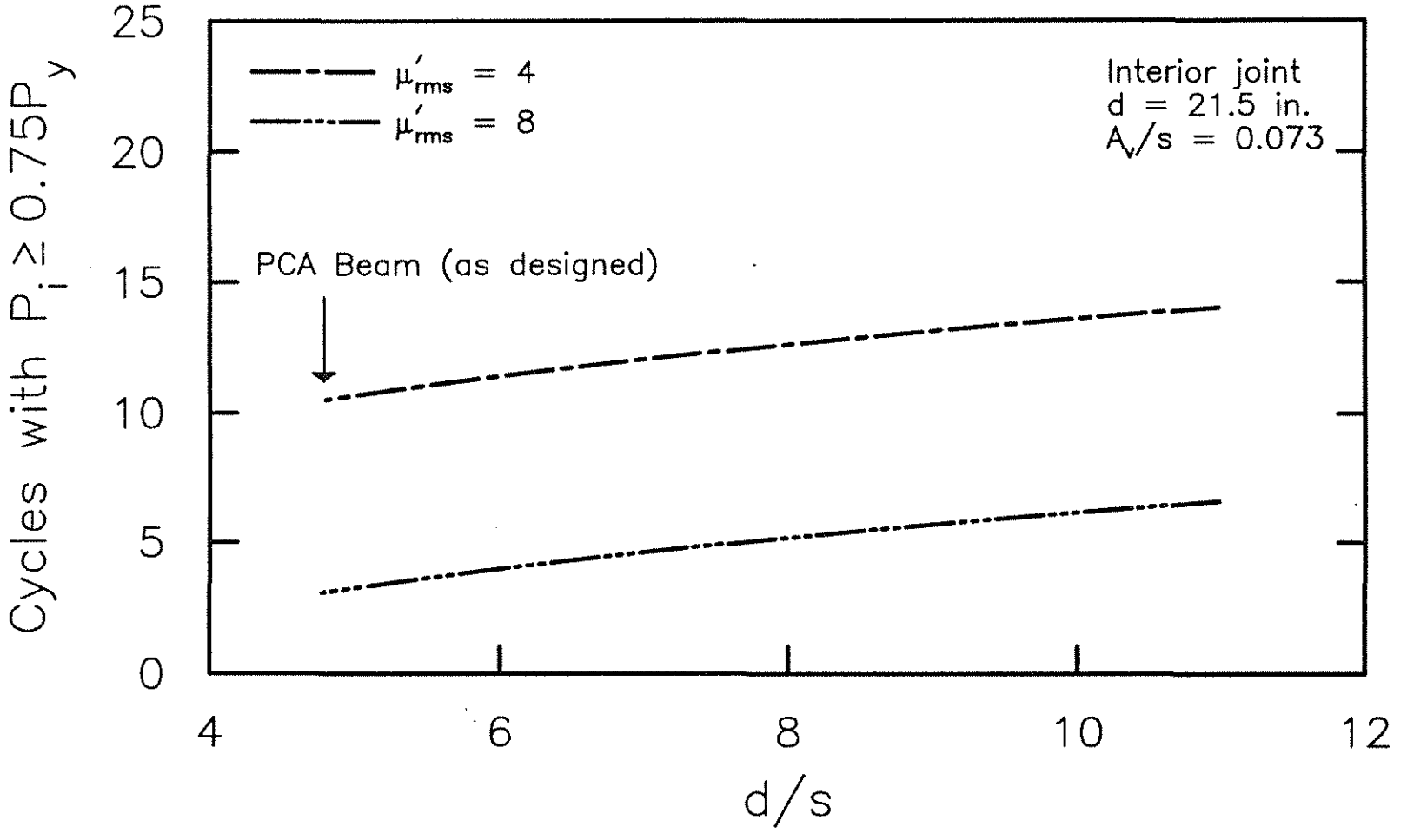

Fig. 5.14 Predicted cycles with $P_i \geq 0.75P_y$ versus d/s for the interior joint of the beam used in the case study (constant v_s)

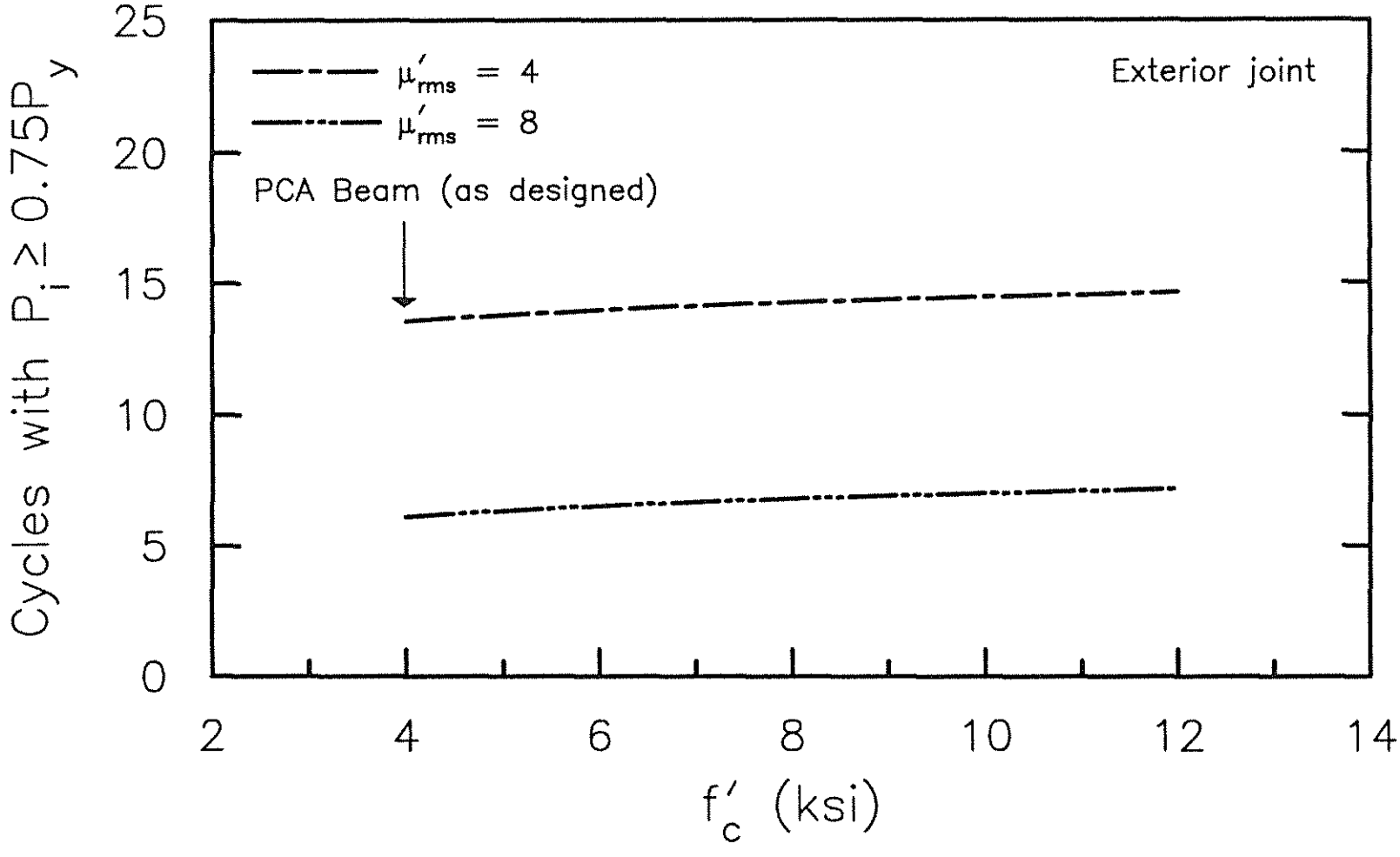

Fig. 5.15 Predicted cycles with $P_i \geq 0.75P_y$ versus f'_c for the exterior joint of the beam used in the case study

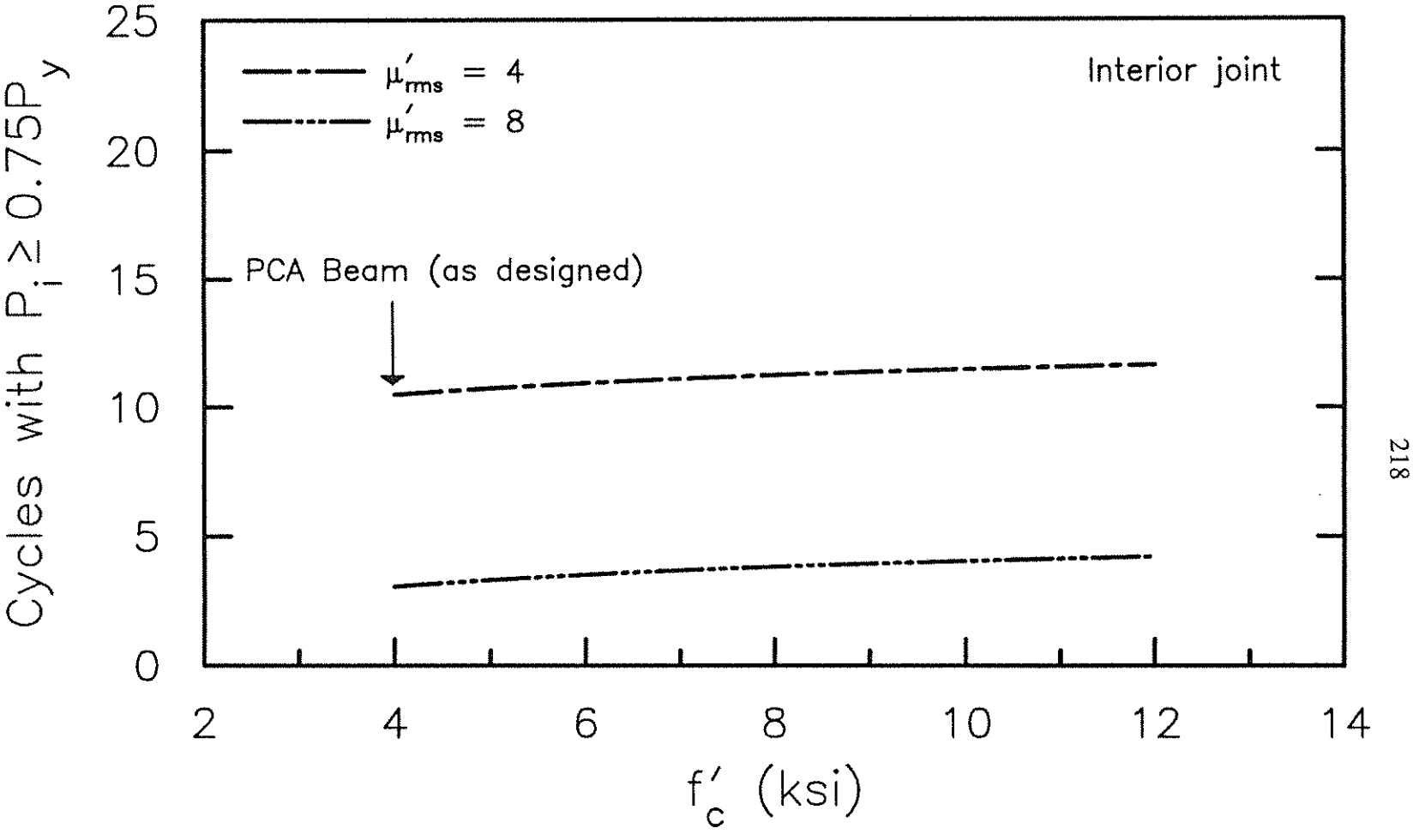

Fig. 5.16 Predicted cycles with $P_i \geq 0.75P_y$ versus f'_c for the interior joint of the beam used in the case study

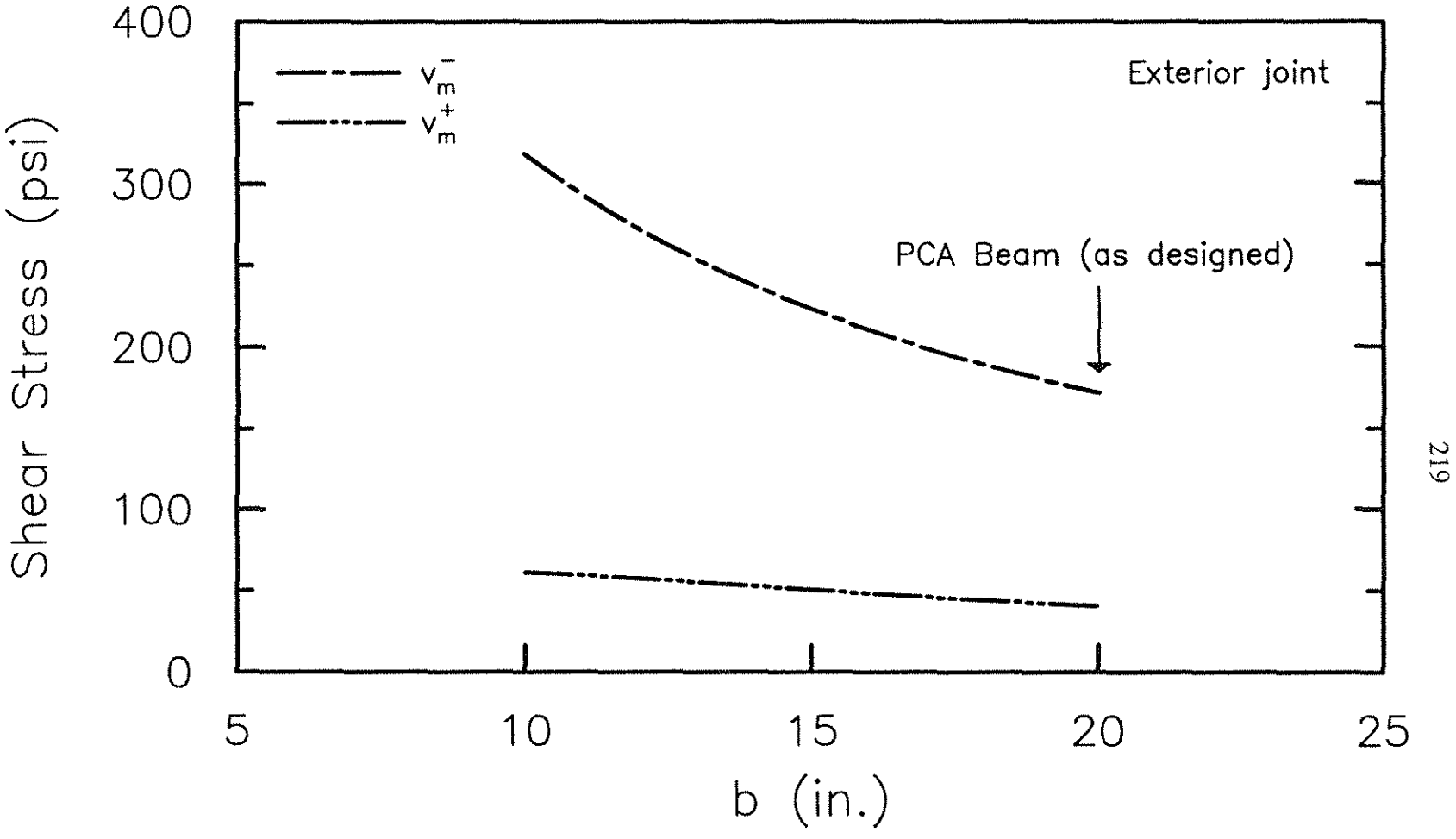

Fig. 5.17 Maximum shear stress in negative and positive bending versus b for the exterior joint of the beam used in the case study

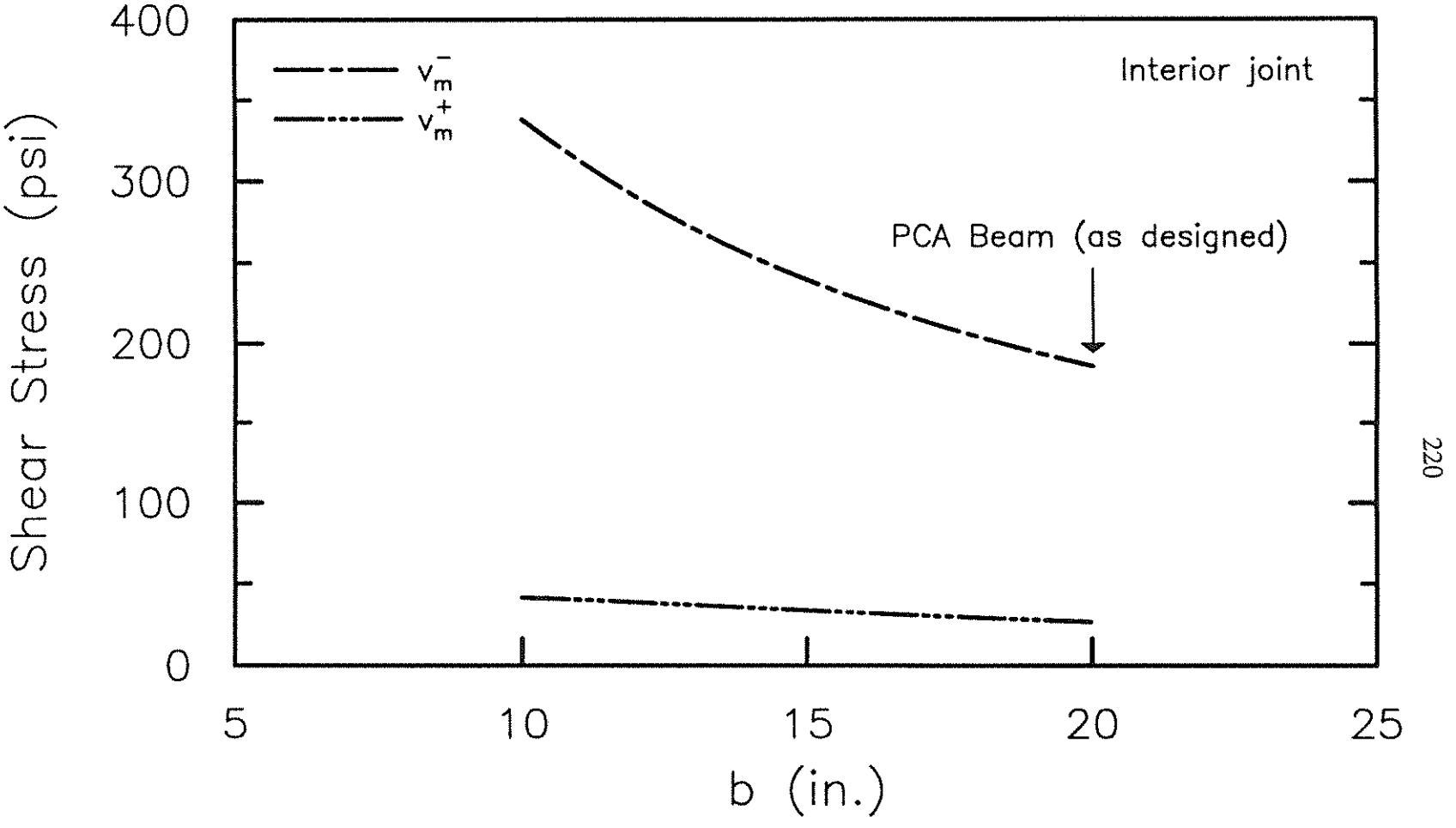

Fig. 5.18 Maximum shear stress in negative and positive bending versus b for the interior joint of the beam used in the case study

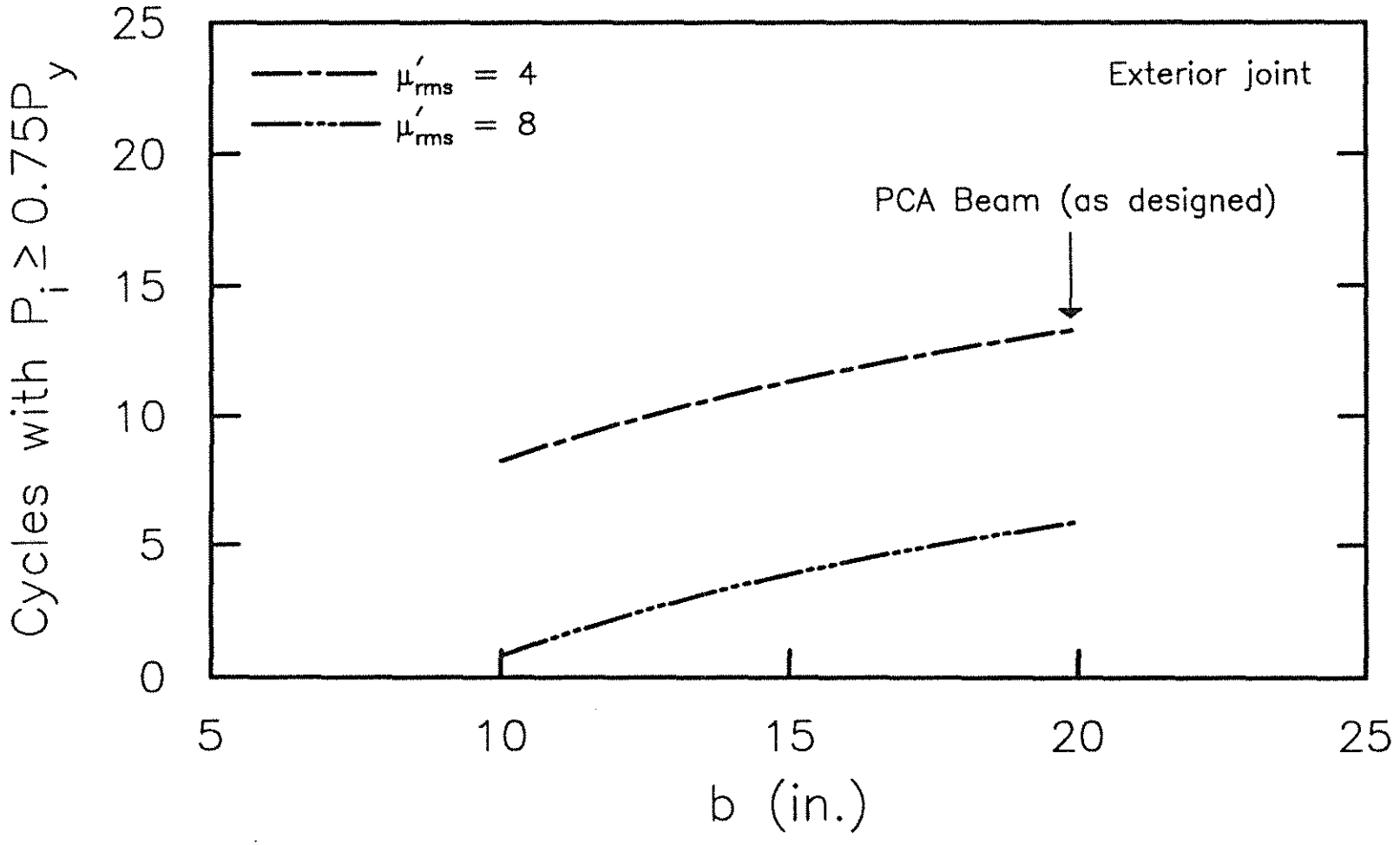

Fig. 5.19 Predicted cycles with $P_i \geq 0.75P_y$ versus b for the exterior joint of the beam used in the case study

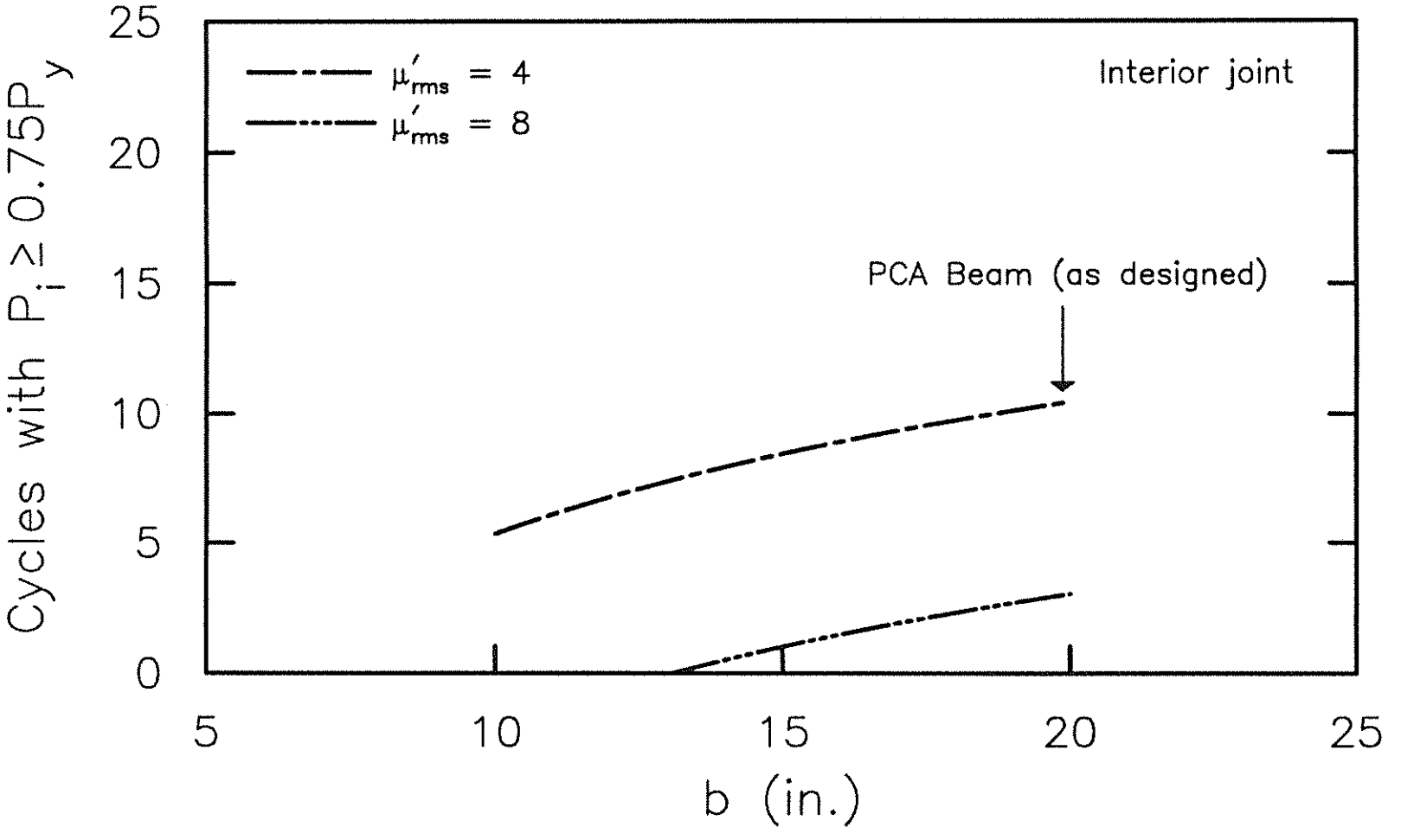

Fig. 5.20 Predicted cycles with $P_i \geq 0.75P_y$ versus b for the interior joint of the beam used in the case study

APPENDIX A

NOTATION

a = shear span

A_{core} = area of core

A_g = gross area of concrete

A_i = area of intermediate beam reinforcement

A_s = area of top reinforcing steel (negative moment reinforcement)

A_s' = area of bottom reinforcing steel (positive moment reinforcement)

A_v = total cross-sectional area of shear reinforcement

b = width of beam section = b_w

b_c = width of concrete core measured to outside of stirrups

b_w = width of rectangular beam or web width of T-beam

C_r = confinement ratio

CNDR = Cumulative Normalized Ductility Range

d = effective depth (distance from bottom of beam to centroid of top reinforcement)

d_1 = effective depth (distance from top of beam to centroid of bottom reinforcement)

d_c = depth of concrete core measured to outside of stirrup

D = diagonal dimension of region spanned by each set of diagonal LVDT's

D_i = Energy Dissipation Index = $E/[0.5P_y\Delta_y[1 + (A_s'/A_s)^2]]$

$(D_i)_j$ = contribution to D_i for the j'th cycle

E = cumulative energy dissipated for all cycles with $P_i \geq 0.75P_y$

E_i = energy dissipated during the i'th cycle

E_j = energy dissipated during the j'th cycle

f_c' = compressive strength of concrete from 6 x 12 in. cylinders

f_{vy} = yield strength of shear reinforcement

f_y = yield strength of flexural reinforcement

h = height of beam cross section

h_h = horizontal dimension of region spanned by diagonal LVDT's

h_v = vertical dimension of region spanned by diagonal LVDT's

I_E = Energy Index = $\sum E_i(K_i/K_y)(\Delta_i/\Delta_y)^2 = \sum E_i(P_i/P_y)(\Delta_i/\Delta_y)$

I'_E = Modified Energy Index = $I_E[1 - (d/a)]$

I_{EN} = Normalized Energy Index = $\sum [E_i/(P_y\Delta_y)](K_i/K_y)(\Delta_i/\Delta_y)^2$

$= \sum E_i(P_i/P_y^2)(\Delta_i/\Delta_y^2)$

I_w = Work Index = $\sum (P_i\Delta_i)/(P_y\Delta_y)$ for all cycles with $P_i \geq 0.75P_y$

I'_w = Modified Work Index = $I_w\,[1 - (d_c/a)][1 + (0.0005N/A_{core})]$

K_i = stiffness in the i'th cycle corresponding to the maximum displacement Δ_i

K_j = proportionality factor for the j'th cycle

K_s = proportionality factor for the s'th cycle

K_y = P_y/Δ_y

L = center to center length between two columns of a moment resistant frame

M^+ = positive moment capacity of a beam at a column face

M^- = negative moment capacity of a beam at a column face

M_{pr} = probable moment strength of a beam at the column face

n = number of cycles to failure

n_{pre} = predicted number of cycles to failure

n_{test} = number of cycles to failure obtained from experimental results

N = axial compression load

NDR = Normalized Ductility Range

P = load

P_i = maximum beam load in i'th cycle

P_{max}^+ = maximum beam load in positive bending

P_{max}^- = maximum beam load in negative bending

P_y = beam load at yielding of top flexural reinforcement

P'_y = beam load at yielding of bottom flexural reinforcement

r = correlation coefficient

r^2 = coefficient of determination

s = stirrup spacing

v_n = nominal shear stress = $V_n/(b_w d)$

v_m = maximum shear stress = $V_m/(b_w d)$

v_m^+ = maximum shear stress in positive bending = $V_m^+/(bd)$

v_m^- = maximum shear stress in negative bending = $V_m^-/(bd)$

v_s = stirrup stress = $V_s/(b_w d)$

v_u = factored shear stress = $V_u/(b_w d)$

V = shear force due to lateral deformation = $(M^+ + M^-)/L$

V_c = nominal shear force carried by concrete

V_n = nominal shear force

V_m = maximum shear force

V_m^+ = maximum shear force in positive bending

V_m^- = maximum shear force in negative bending

V_s = nominal stirrup shear capacity = $(A_v f_{vy} d)/s$

V_u = factored shear force

V_y = shear force at yielding of main flexural reinforcement = P_y

β = regression coefficient

γ = shear deformation = $(\gamma_1 + \gamma_2)/2$

γ_1 = first component of total shear deformation

$= [\ ((D + \Delta_1)^2 - (h_h)^2)^{0.5} - h_v\ ] / h_h$

γ_2 = second component of total shear deformation

$= [\ h_v - ((D + \Delta_2)^2 - (h_h)^2)^{0.5}\ ] / h_h$

Δ = load-point deflection

Δ_b = change in length measured with LVDT #8

Δ_i = maximum displacement during i'th cycle

Δ_{max}^+ = maximum displacement in positive bending

Δ_{max}^{-} = maximum displacement in negative bending

Δ_n = maximum load-point deflection in n'th cycle of loading

Δ_t = change in length measured with LVDT #7

Δ_y = load-point deflection at yielding of top flexural reinforcement

Δ_y' = load-point deflection at yielding of bottom flexural reinforcement

Δ_1 = change in length of diagonal measured with LVDT #3 or #5

Δ_2 = change in length of diagonal measured with LVDT #4 or #6

θ = beam flexural rotation relative to column-stub = $(\Delta_b + \Delta_t) / h_v$

μ = displacement ductility factor

μ_{rms} = root-mean-square displacement ductility factor

μ'_{rms} = modified root-mean-square displacement ductility factor

$(\mu^+)_j$ = displacement ductility factor in positive bending for the j'th cycle

$(\mu^-)_j$ = displacement ductility factor in negative bending for the j'th cycle

ρ = flexural reinforcement ratio = $A_s/(b_w d)$

ρ_v = transverse reinforcement ratio = $A_v/(bs)$

ρ_w = transverse reinforcement ratio = $A_v/(b_c s)$

ϕ = strength reduction factor

APPENDIX B

COMPUTATION OF SHEAR DEFORMATION AND BEAM FLEXURAL ROTATION RELATIVE TO COLUMN-STUB

B.1 COMPUTATION OF SHEAR DEFORMATION

The shear deformation, γ, was calculated based on measurements obtained from diagonally crossing LVDT's (Bertero, Popov & Wang 1974, Nmai & Darwin 1984, and Hanks & Darwin 1988). The total shear deformation consists of two components, γ_1 and γ_2 (Fig. B.1), given by the following expressions:

$$\gamma_1 = \frac{\left[\sqrt{(D + \Delta_1)^2 - (h_h)^2} - h_v \right]}{h_h} \qquad (B.1)$$

and

$$\gamma_2 = \frac{\left[h_v - \sqrt{(D + \Delta_2)^2 - (h_h)^2} \right]}{h_h} \qquad (B.2)$$

in which

γ_1 = first component of total shear deformation

γ_2 = second component of total shear deformation

D = diagonal dimension of region spanned by each set of diagonal LVDT's

h_h = horizontal dimension of region spanned by diagonal LVDT's
= 15.125 in.

h_v = vertical dimension of region spanned by diagonal LVDT's
= 12.75 in.

Δ_1 = change in length of diagonal measured with LVDT #3 or #5

Δ_2 = change in length of diagonal measured with LVDT #4 or #6

The shear deformation, γ, was then computed as follows:

$$\gamma = \frac{(\gamma_1 + \gamma_2)}{2} \qquad \text{(B.3)}$$

B.2 COMPUTATION OF BEAM FLEXURAL ROTATION RELATIVE TO COLUMN-STUB

The flexural rotation of the beam relative to the column-stub, θ (Fig. B.2), was computed as follows (Nmai & Darwin 1984, and Hanks & Darwin 1988):

$$\theta = \frac{(\Delta_b + \Delta_t)}{h_v} \qquad \text{(B.4)}$$

in which

Δ_b = change in length measured with LVDT #8

Δ_t = change in length measured with LVDT #7

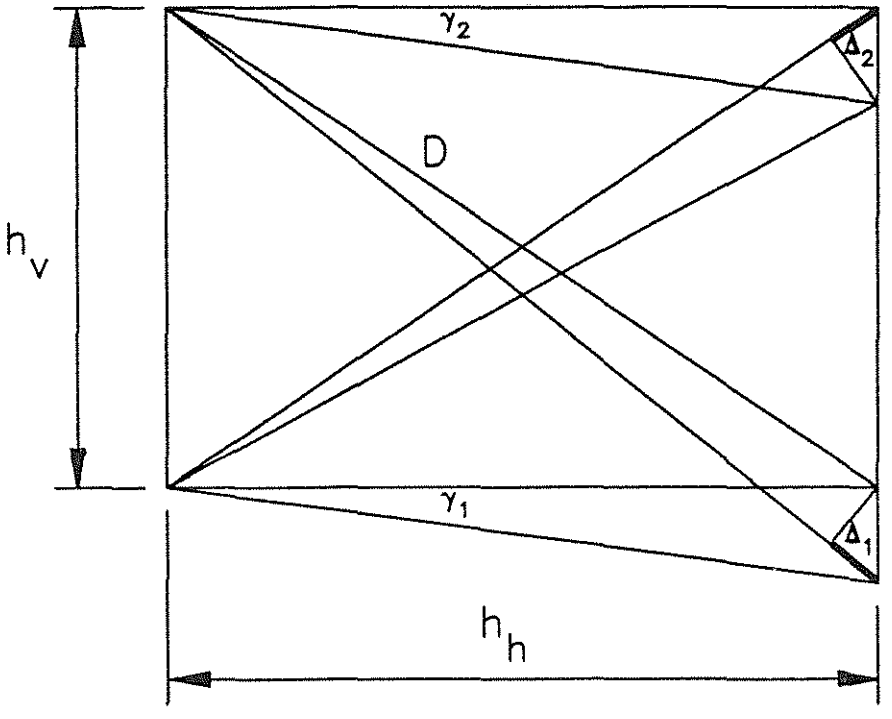

Fig. B.1 Shear Deformation Measurement

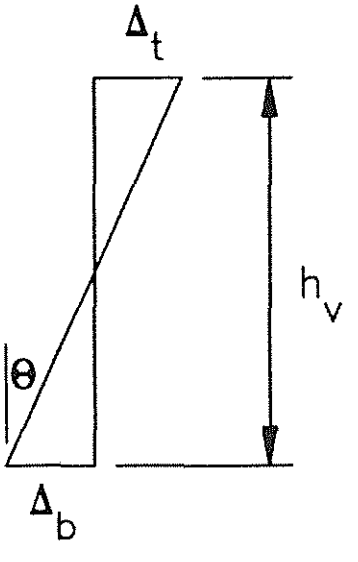

Fig. B.2 Relative Flexural Rotation Measurement

APPENDIX C

DETERMINATION OF THE ENERGY DISSIPATED PER CYCLE

In an effort to develop an improved index which takes into consideration variations in geometry and strength on the inelastic response of reinforced concrete beams, Nmai & Darwin (1984, 1986) and Darwin & Nmai (1986) proposed the Energy Dissipation Index, D_i. The Energy Dissipation Index is the ratio of a member's energy dissipation capacity (i.e. cumulative energy dissipated by a test specimen for all cycles in which the maximum load, P_i, is greater than 75% of the yield load, P_y) to a measure of the elastic energy at yield (Eq. 1.6). The Energy Dissipation Index, D_i, is numerically equivalent to the summation of individual index terms such that

$$D_i = \sum_{j=1}^{n} (D_i)_j \qquad (C.1)$$

in which n = the number of cycles with $P_i \geq 0.75P_y$. The relationship between $(D_i)_j$ and the energy dissipated in the j'th load cycle is

$$(D_i)_j = \frac{(E)_j}{\frac{1}{2}(P_y\Delta_y)\left[1 + \left(\frac{A_s'}{A_s}\right)^2\right]} \qquad (C.2)$$

and $(E)_j$ is the energy dissipated during the j'th cycle. For prototype cantilever beam specimens subjected to reversed cyclic loading, $(E)_j$, P_y, and Δ_y, are readily determined from the load versus load-point deflection plots (P_y and Δ_y are defined by discrete data points in the initial (i.e. cycle #1) hysteresis curve). $(E)_j$ is calculated by summing the area bounded by each load versus load-point deflection curve for all applicable load cycles. Several methods are available for calculating $(E)_j$. Numerical integration and "digitization" of the load-deflection curve are the two methods used

APPENDIX C

DETERMINATION OF THE ENERGY DISSIPATED PER CYCLE

In an effort to develop an improved index which takes into consideration variations in geometry and strength on the inelastic response of reinforced concrete beams, Nmai & Darwin (1984, 1986) and Darwin & Nmai (1986) proposed the Energy Dissipation Index, D_i. The Energy Dissipation Index is the ratio of a member's energy dissipation capacity (i.e. cumulative energy dissipated by a test specimen for all cycles in which the maximum load, P_i, is greater than 75% of the yield load, P_y) to a measure of the elastic energy at yield (Eq. 1.6). The Energy Dissipation Index, D_i, is numerically equivalent to the summation of individual index terms such that

$$D_i = \sum_{j=1}^{n} (D_i)_j \qquad (C.1)$$

in which n = the number of cycles with $P_i \geq 0.75P_y$. The relationship between $(D_i)_j$ and the energy dissipated in the j'th load cycle is

$$(D_i)_j = \frac{(E)_j}{\frac{1}{2}(P_y\Delta_y)\left[1 + \left(\frac{A_s'}{A_s}\right)^2\right]} \qquad (C.2)$$

and $(E)_j$ is the energy dissipated during the j'th cycle. For prototype cantilever beam specimens subjected to reversed cyclic loading, $(E)_j$, P_y, and Δ_y, are readily determined from the load versus load-point deflection plots (P_y and Δ_y are defined by discrete data points in the initial (i.e. cycle #1) hysteresis curve). $(E)_j$ is calculated by summing the area bounded by each load versus load-point deflection curve for all applicable load cycles. Several methods are available for calculating $(E)_j$. Numerical integration and "digitization" of the load-deflection curve are the two methods used

in this study and will be discussed in more detail.

For the H series beams of the current study and the G series beams tested by Hanks & Darwin (1988), discrete data points were recorded during testing and subsequently plotted to obtain relatively smooth load versus load-point deflection curves. On the average, each hysteresis curve represents twenty discrete data points. A computer program was written for a Hewlett-Packard 9825T calculator which numerically integrates the area bounded by each curve. For each specimen, the resulting value of $(E)_j$ was calculated for all cycles with $P_i \geq 0.75P_y$ (see Table 4.2).

For obvious reasons, data points used to generate load versus load-point deflection curves are not typically published, and thus, this form of numerical integration is not a viable means to calculate $(E)_j$ for specimens in other studies. However, since most experimental studies publish load-deflection curves for test specimens subjected to cyclic loading, $(E)_j$ can be determined by digitizing the load-deflection curves. This was done in the current study. The digitizing hardware consisted of an AST Premium (Model 386C) computer, NEC (Multisync Plus) monitor, and a Kurta (Series Two) digitizing tablet with an AutoCAD Standard Tablet Templet. The software used for the calculation of $(E)_j$ was AutoCad Release 9.0. Prior to digitization of the load-deflection curve, a rectangular area of known dimension (approximately 10 kip-in) was digitized on the load-deflection graph to obtain a scale factor relating dissipated energy in graph units to tablet units. Discrete data points on the load-deflection curves were digitized sequentially to form a continuous closed loop as displayed on the computer monitor. The AutoCAD command "AREA & ENTITY" was then selected and the area within the closed loop obtained (area measured in tablet units). On the average, each hysteresis loop (and rectangular area used to determine the scale factor) was digitized three times to obtain reasonably consistent measurements of area. $(E)_j$ was subsequently determined from the product of the mean area and scale factor.

The degree of agreement between the two methods of calculating dissipated energy (i.e. numerical integration and digitization) is illustrated in Table C.1 which compares the cumulative energy dissipation capacity, E, for Beams H-2 and H-3. The relatively small difference between the two values suggest that digitizing the load-deflection curves provides a reliable means with which to calculate $(E)_j$.

TABLE C.1 COMPARISON OF ENERGY DISSIPATION CAPACITY

Beam	n (Cycles with $P_i \geq 0.75P_y$)	Energy Dissipation Capacity, E (kip-in.) Numerical Integration	AutoCAD	Percent Difference
H-2	7	314.6	321.0	2.0
H-3	4	178.3	178.98	0.4

The energy dissipated per cycle, $(E)_j$, for selected specimens tested by Wight & Sozen (1973), Scribner & Wight (1978), Hwang & Scribner (1984), Nmai & Darwin (1984), Hanks & Darwin (1988), and the current study is presented in Table 4.2.